THERMAL AND FRACTURE BEHAVIOUR OF ROCKET MOTOR MATERIALS

by

KYM MARTIN IDE

B. E. (Hons.), M. Eng. Sc., Adelaide

A dissertation submitted in fulfilment of the requirements

for the degree of Doctor of Philosophy

in The University of Adelaide

March, 1997

Department of Chemical Engineering

The University of Adelaide

Adelaide, S. A. 5005

Australia

Table of Contents

Errata

Page 3 para 2 line 11 should read "effects,"

Page 7 para 2 line 10 should read "its" not "it's"
para 3 line 2 should read "is dependent" not "are dependent"

Page 12 para 3 line 3 should read "were" not "was"

Page 17 para 2 line 2 should read "hydroxy-terminated polybutadiene" not "HTPB"

Page 25 para 1 line 3 should read "in line" not "inline"

Page 26 para 1 line 9 should read "was" not "were"

Page 36 para 4 line 4 should read "methylenebis(phenyl isocyanate)" not "dimethyl di-isocyanate"

Page 38 para 1 line 4 should read "this ensures" not "this will ensure"

Page 38 para 2 line 3 should read "on top" not "ontop"

Page 46 para 2 line 3 should read "on top" not "ontop"

Page 48 para 3 sentence 4 should read "The specimens were loaded into the Instron by clamping in the usual manner (see Figure 11) and the hysteresis ratios generated from the calculated stress-strain data by adhering to the experimental method described in the section titled Hysteresis Energy Loss Measurements."

Page 65 para 2 sentence 2 should read "The effect of ageing on the thermal expansion coefficient of the insulation was inconclusive due to the large errors (10.7%) associated with the calculated values."

Page 78 para 2 line 7 should read "a HTPB" not "an HTPB"

Page 79 para 2 sentence 5 should read "Specifically, the percentage filler content of each was different and the propellant used by Kugler et al. also contained a percentage of aluminium particles, both of these factors will effect the level of binder/filler interactions observed as will the particle size differences."

Page 87 caption for Figure 36 should read "Change in Poisson's ratio for propellant, T= -20°C, 25°C and 50°C"

Page 88 caption for Figure 38 should read "Change in Poisson's ratio for inhibitor, T= -20°C, 25°C and 50°C"

Page 96 para 3 line 2 should read "form" not "from"

Page 97 para 2 line 8 should read "had" not "has"

Page 125 para 1 line 6 should read "The crack tip can be seen between graticule marks 47 to 49, it is wedge shaped and has a rough surface by comparison to the cut portion."

Page 125 para 2 line 2 should read "increases" not "increase"

Page 156 para 1 line 1 should read "The crack velocities measured for the propellant/inhibitor bimaterial specimens were higher than those for the equivalent propellant specimens tested (see Figure 109)."

Page 163 para 3 line 3 delete "which"

Page 184 para 3 line 6 delete "and"

Page 184 para 3 line 7 insert "and" before "only"

Page 193 reference 53 should read "Rigbi, Z., *"The Value of Poisson's Ratio of Viscoelastic Materials"*, Applied Polymer Symposia, No. 5, 1967, pp 1-8."

Page 193 reference 54 should read "Buswell, J. H., Dodds, J. S. and Tod, D. A., *Studies of Composite Propellant Mechanical Properties"*, Paper No. 28, (Proc) Technology Workshop, WTP-4: Energetic Materials and Propulsion Technology, TTCP, DSTO Salisbury, 18-19 April. 1996."

Page 195 reference 92 should read "Orowan, E., *"Fracture and Strength of Solids"* in Repts. Prog. Phys., Vol 12, 1948, pp 185-232."

Abstract

The thermal and fracture behaviour of the polymeric materials employed in the manufacture of the PICTOR rocket motor has been studied for inclusion into a finite element analysis approach to service life prediction. Both as-received and aged specimens were tested at each of three temperatures and strain-rates, including an ambient, sub-zero and elevated temperature. The materials were aged by subjecting them to various thermal loads (accelerated ageing, thermal cycle and thermal shock) designed to expose them to conditions similar to that experienced by a rocket motor during its service life.

The change in the thermal expansion behaviour of the propellant, inhibitor, epoxy and insulation was investigated. Values of thermal expansion coefficient for both the unaged and aged inhibitor and propellant were found to diverge over the range of test temperatures, the consequence may be the development of a stress state capable of causing crack initiation and/or propagation in either material or at a bondline during thermal loads.

The fracture behaviour of the propellant and a propellant/inhibitor bimaterial specimen was found to be similar. The bimaterial specimen failed in the propellant adjacent to the propellant/inhibitor bondline. The deterioration of the mechanical properties of the propellant depended on the severity of the thermal loads. In each case the accelerated aged specimens became harder and more brittle whilst the thermally cycled and thermally shocked specimens were only marginally affected. A marked decrease in hysteresis ratio, critical stress and critical strain, an increase in crack velocity and a distinct difference in the mechanism of crack growth was observed for the accelerated aged specimens. This deterioration will have a significant impact on the modelling process with its inclusion yielding greater accuracy in predictions of rocket motor service life.

At –40°C the inhibitor specimens exhibited glass-like behaviour due to the proximity of the glass transition temperature. The stiffened inhibitor underwent brittle failure at substantially increased stress levels. The accelerated aged inhibitor was hardened without becoming more brittle and as such the critical stress increased above that of the unaged specimens. The deterioration of the inhibitor as a result of thermal cycling and thermal shocking was marginal. A much more severe set of ageing conditions would be required to cause a substantial degradation in mechanical properties.

Declaration

This work contains no material which has been accepted for the award of any other degree or diploma in any university or other tertiary institution and, to the best of my knowledge and belief, contains no material previously published or written by another person, except where due reference has been made in the text or where common knowledge is assumed.

I give consent to this copy of my thesis, when deposited in the University Library, being made available for loan and photocopying if accepted for the award of the degree.

Kym M. Ide

Acknowledgments

The author wishes to acknowledge the generosity of Dr Peter Preston (Chief Weapons Systems Division) for granting permission and the Defence Science Technology Organisation for the support to undertake this course of study.

Joint supervision for this project was by Dr Sook-Ying Ho (Head of Rocket Technology, Weapons Systems Division) and Dr David Williams (Dept. of Chemical Engineering/Adelaide University). I wish to thank them for their time and effort in providing invaluable guidance, support and the resources required. Special mention must go to Dr Ho for providing the opportunity to perform the work within the Rocket Technology Group's program of research.

Many thanks to the following people for their contribution to this work:

The propellant material used in this study was manufactured by Mr Brian Hamshere, Mr Alan Starks and Mr John Symes.

The inhibitor material was manufactured by Mr Mark Champion. Mr Jim Bulley provided valuable assistance with the manufacture of the epoxy and insulant specimens.

The specimens of propellant used in the testing were machined by Mr Don Ashton and Mr Henry Gare.

Mr Tony Ferschl assisted with the program to expose specimens to the thermal loads.

The staff of WSD/DSTO many of whom made important contributions to the progress of the work.

The specimens of inhibitor and epoxy were machined ready for testing by Mr Brian Mulcahy. Mr Brian Mulcahy and Mr Bruce Ide fabricated various items of the experimental apparatus and, despite my best efforts otherwise, kept everything in working order.

Mr Ian Brown of the Department of Mechanical Engineering for the loan of the stereo microscope.

Dr Darren Miller for helpful discussions during the work and preparation of this thesis.

The helpful staff of the Department of Chemical Engineering made working there a very enjoyable experience.

I would like to thank my friends and family for support and encouragement. In particular my wife, Mandy, for her patience and understanding during this time. Her support made all the difference.

Chapter I
Introduction

The design and manufacture of dependable, high performance solid rocket motors is a mature technology, however, deterioration during prolonged storage results in a marked change in ballistic performance. A major reason for the change in ballistic performance is the formation of cracks in the propellant which create extra surface area for burning, resulting in an increased burning rate and the production of excess combustion gases.[1] It is therefore important to know when the deterioration has reached a level whereby the rocket motor fails to perform adequately or it has become unsafe and therefore should be replaced. At this point the rocket motor is regarded to have reached the end of its service life, a term defined as that length of time from the date of manufacture that an explosive assembly (eg., propulsion unit) of a missile system will continue to safely and reliably meet all service requirements for storage, performance and operational use. Service life is determined by assessing when the rocket motor may fail any of these requirements.

Terminology employed in the field of solid rocket motor propulsion has become specialised with terms evolving to describe the unique materials and specific components, simplifying the sometimes complex descriptions. As a result some specific terms will be employed in this thesis. The *propellant* is an energetic material and on firing expansion of the combustion gases produces the rocket motor thrust. *Inhibitors* and *insulants* are non-energetic materials, the former prevents the spread of propellant burning while the latter provides thermal protection of the rocket motor case. An expanded definition of terms and a sketch of a typical rocket motor is provided in Appendix A.

In the past, service life programs have involved a cycle of annual inspection and testing designed to ascertain the extent of deterioration in the in-service rocket motor.[2] A testing program normally includes routine mechanical and chemical tests as well as the determination of ballistic performance from static firing of a number of in-service rocket motors, drawn from batch lots, with rejection of batches if the inspection motors fail the performance specification. The destructive testing employed in this approach is costly and the method may not provide reliable information on the cause of the failure of any particular rocket motor.

More modern methods for service life are being developed which are based on predicting the capacity of the rocket motor to maintain structural integrity under the conditions of service. The methods are based, in part, on the computation of a rocket motor's mechanical behaviour in response to a series of applied stresses or temperature variations (referred to as "thermal loads") by using finite element analysis (FEA). A novel feature of the modelling process being developed by the Defence Science Technology Organisation (DSTO) will be the ability to apply criteria for crack initiation and propagation based on the values of stress and strain computed throughout the rocket motor. The propagation of the crack will be dynamically modelled allowing the growth and direction of the crack to be followed. Currently, the capability for this within FEA is extremely limited and to achieve an accurate modelling program requires an extensive understanding of the fracture mechanisms involved. The size of the crack and the rate at which it propagates can then be used in the service life analysis of the rocket motor.

This analysis will not only provide a greater understanding of the reasons for rocket motor failure but also lead to more accurate and confident assessments of rocket motor service life. The analysis, does however, require considerable data input into the model which pertains to the mechanical behaviour of the rocket motor under the conditions of service. For the FEA to

produce accurate predictions of fracture a detailed knowledge of the fracture process in the materials employed in the rocket motor is required. As well as the mechanical property data obtained from material characterisation tests, an understanding of the mechanisms of crack growth and the conditions under which the cracks propagate is required. Due to the non-linear viscoelastic nature of the rocket motor materials it is also essential to include the effect of time and temperature on the crack growth behaviour. It follows that tests to determine crack growth should be carried out after subjecting specimens to conditions which simulate those experienced by the rocket motor in service.

The thermal loads to which the rocket motor may be subjected are diverse. In service the platform, eg ship or aircraft, from which a missile is launched may experience, dry desert, cold artic or humid tropical conditions. The conditions to which a rocket motor may be exposed as part of that missile system, may include long-term storage in a magazine, periods on a launcher prior to firing or packaged for transport. In a magazine the rocket motor's temperature will fluctuate between a daytime maximum and night time minimum, referred to as a diurnal cycle. On the launcher or packed for transport the rocket motor may be exposed to either very hot or sub-zero temperatures for significant periods of time. The rocket motor may not necessarily be fired, indeed most rocket motors will reach the end of their service life after a long period of storage and perhaps having been exposed to a series of diverse environmental conditions. Deterioration in rocket motor performance will result from the environmental effects to which it is subjected over time, on the materials of construction.

The joint effect of time and temperature is to cause chemical and mechanical changes in the rocket motor's materials, a process referred to as ageing. The diversity of thermal loadings that the rocket motor is subjected to during service cause variations in the rate and extent of material ageing. At elevated temperatures the rate of oxidation is increased, whilst at sub-zero

temperatures these reactions are slowed. At low temperatures ambient moisture may be absorbed, which will react with and plasticise the polymer compounds. The ageing process will result in both damage to the material in the form of binder/filler debonding (or "dewetting") and increased cross-linking in the binder.[3,4] These cause a degradation in the mechanical properties of the materials which in turn increases the likelihood of material cracking or bondline failure occurring. This investigation will focus on the deterioration of the rocket motor materials' mechanical properties which occurs as a result of chemical changes during ageing; there will be no emphasis on the chemical reactions taking place.

As the temperature in the environment rises and falls, heat is transferred to and from the rocket motor causing thermal gradients in the rocket motor components. Each material employed in the rocket motor has a unique value for thermal expansion coefficient which varies with temperature. Hence, the differing amounts of expansion and contraction in each material will produce thermally induced strains and an associated thermal stress field which has the potential to cause cracking within any of the rocket motor materials when it reaches a sufficient magnitude.

Cracking in the propellant/inhibitor system (referred to as the charge) is of greatest concern as the presence of cracks in the propellant or at the propellant/inhibitor interface increases the surface area for burning which subsequently decreases the burn time and creates an excess quantity of combustion gases. This may result in a failure of the motor to achieve minimum performance targets (such as minimum burn time, thrust, impulse or any number of other criteria). In the extreme case the excess combustion gas may cause over-pressurisation and rocket motor case failure.

Thermally induced strains generate high stress levels at the bondline (or interface) of two materials with widely differing thermal expansion coefficients. The integrity of the bond needs to be maintained however this stress condition has the potential to cause crack initiation and propagation. As the temperature transients continue the associated stress fields may be capable of causing a crack to extend in length with time.

During the service life of the rocket motor, damage caused by thermal loads and material ageing leads to a degradation of the mechanical properties of the polymers. This deterioration with time must be included in any finite element analysis of a rocket motor to obtain accurate results on which to base predictions of service life.

Smith and Liu[5] studied crack propagation in a solid propellant, the mechanism of growth was observed as a blunt-growth-blunt process. Liu[6] investigated the consequences of damage on crack growth behaviour by studying a "pre-damaged" solid propellant at ambient temperature. These authors did not explore the effect of ageing on the fracture behaviour of the materials. Also, the question remains as to the effect of ageing and temperature on the fracture behaviour in the inhibitor and at the propellant/inhibitor interface.

In this study the effect of material ageing, which results from the service life type thermal loadings, on the fracture behaviour of propellant, inhibitor and at the bondline of these two materials, will be investigated over a wide range of temperatures and strain-rates.

The rocket motor chosen to be examined in this study is the PICTOR, which is a case bonded rocket motor employing a cast composite propellant and inhibitor. To understand the effect of temperature on the fracture behaviour of the materials, the thermal expansion coefficient and glass transition temperature of the polymeric materials used in the manufacture of the PICTOR rocket motor will be measured. As the materials age the debonding and/or rehealing at the

polymer matrix/filler interface may produce a measurable change to the thermal expansion coefficient. Changes to the thermal expansion coefficient of the materials caused by ageing will be important as it may affect the level of stress and hence the likelihood of crack propagation. Surprisingly, there have been no studies reported in the literature on the effect of material ageing on the thermal expansion coefficient in composites.

The transition from a glassy, elastic material behaviour to a rubbery, elastomeric one occurs at the glass transition temperature. The change in glass transition temperature as a result of ageing will affect the mechanical behaviour of the material in a region close to that transition temperature. A temperature at which a material may have previously behaved elastomerically may now lie in the glassy region and this will have a significant effect on the damage resulting from the thermal strains and hence the fracture behaviour. It is therefore necessary to measure the thermal expansion coefficients and glass transition of aged rocket motor materials by exposing them to service life type conditions.

Values of thermal expansion coefficient are fundamental inputs to finite element modelling (FEM). However, current strategies for FEM do not routinely include the variation of thermal expansion coefficient with temperature or ageing. When included more accurate stress and strain values can be determined leading to improved model predictions.

It is essential that accurate values of Poisson's ratio, ν, are used in a finite element analysis as small changes in Poisson's ratio may cause large variations in the calculated stresses. Many workers have devised techniques in an attempt to accurately determine Poisson's ratio.[7,8] The most common problems are susceptibility to gross errors from gauges losing contact with the specimen and the effect of the test chamber media on the behaviour of the material being

studied. In this study, a technique has been developed for measuring the axial and lateral strains present in viscoelastic materials.

For metals Poisson's ratio is approximately 0.33, for incompressible materials the value is 0.5. Nearly incompressible elastomers have Poisson's ratios slightly less than 0.5 and the addition of particulate fillers, such as in those materials employed in the PICTOR rocket motor, further reduces the Poisson's ratio. Examination of the change in Poisson's ratio with increasing strain provides an understanding of the mechanisms and extent to which they cause damage in particulate filled polymers. When strained, debonding of the binder and filler leads to the formation of vacuoles and a subsequent reduction in Poisson's ratio, this relationship will be expanded upon in the Literature Review. The PICTOR materials are viscoelastic in nature hence the value of Poisson's ratio is also time, strain and temperature dependent. (For example, the polymer matrix will become stiffer as it's temperature approaches the glass transition, causing the material to behave more elastically). This strain dependency is related to the formation of damage in the material.

For particulate composites, such as the propellant, the damage caused by dewetting during straining of the material is critical. The level of binder/filler interactions are dependent on the strain and will be evident from the extent of the non-linear variation in Poisson's ratio. The effect of damage and its extent may be taken into consideration by examining the changes in Poisson's ratio as the material is strained. Ideally, the values of Poisson's ratio should be measured under conditions reflecting the typical strain-rates and temperatures seen by the rocket motor in service.

A study of the mechanisms of crack growth and their response to strain-rate and temperature variations is necessary for a greater understanding of fracture behaviour. Cracking in fibre

reinforced composites is well documented however our understanding of the mechanisms present in particulate composites, such as propellants, is incomplete due to the often unique nature of the materials. Crack growth behaviour may also be significantly affected if a material has aged due to the thermal loads to which it has been subjected. Knowledge of the effect of temperature and strain-rate on the crack mechanism in unaged and aged propellant, inhibitor and along the interface of a bimaterial specimen of propellant and inhibitor bonded together as in the charge is incomplete.

A criterion for crack initiation is firstly applied to the FEA results of the rocket motor. Once crack initiation is achieved another criterion is required which describes the conditions under which the crack will propagate. Most criteria which have been proposed are unable to adequately account for material hysteresis. One successful criterion introduced by Kinloch and Tod[1] was later modified by Ho and Tod.[3] The critical strain energy release rate (or fracture energy), G_c, is a criterion that applies equally to elastic and inelastic materials and is independent of the test geometry and loading conditions. Fracture energy provides a measure of the energy that is required for a crack to propagate under the conditions of stress and strain in the motor. However, there are no studies in which fracture energy of propellants or inhibitor materials at elevated and sub-ambient temperatures have been reported.

OUTLINE OF THESIS

This thesis will discuss the way in which ageing, temperature and strain-rate affect the thermal and fracture properties of the polymeric components in the PICTOR rocket motor. Chapter II will review the studies in the literature which deal with the effects of ageing on the thermal expansion coefficient and glass transition temperature of all the materials. Then the methods for measuring Poisson's ratio in elastomers will be reviewed with reference to their ability to

detect damage as the specimen is strained. The literature available which details the mechanism of crack growth and the effect of ageing on it will be reviewed. Lastly, literature discussing the relationship of ageing to the propensity of fracture in a viscoelastic material will be reviewed. The experimental methods employed in this study will be discussed in Chapter III. The details of the thermal mechanical analysis of the PICTOR materials and an improved image analysis technique for digital edge location which was developed to measure the strain in tensile specimens of the PICTOR rocket motor materials will be outlined. Methods used to measure the hysteresis energy losses and study crack propagation in specimens of propellant, inhibitor and the propellant/inhibitor bimaterial will be detailed. Lastly, the experimental method for measuring fracture energy will be summarised.

In Chapter IV the thermal expansion coefficient and glass transition temperature measurements of aged materials will be discussed. Followed by a discussion of an improved method based on video image analysis to determine the effect of strain on the Poisson's ratio of the PICTOR materials and how it is related to the accumulation of damage in the material. The effect of strain-rate and temperature for unaged and aged specimens of propellant, inhibitor and bimaterial propellant/inhibitor on the hysteresis energy losses occurring when the specimens are cyclically loaded will be discussed. The details of image analysis to determine the effect of temperature and strain-rate on the fracture mechanism in aged and unaged materials will be discussed. The mechanical behaviour of aged and unaged materials at various strain-rates and temperatures will be discussed with particular reference to the values of critical stress and strain determined. Finally, the fracture energy of the propellant and inhibitor at various temperatures will be compared. In Chapter IV data will be presented in plots located at the end of each section. The conclusions in Chapter V will highlight the relationship between ageing, mechanical degradation and the mechanism of crack propagation in materials employed in

rocket motor construction. The understanding gained will be described in terms of the consequences for and improved accuracy of finite element analysis of rocket motors. The references contained in the thesis are presented in a bibliography.

Chapter II
Literature Review

THERMAL BEHAVIOUR

Studies of the chemical changes occurring in a solid rocket motor propellant during ageing are common.[9-14] It is known that oxidative cross-linking and hydrolytic chain scission in the binder are the typical ageing processes. Decomposition of the AP causes a weakening of the bond at the binder/filler interface and the particles may dewet resulting in propellant softening. As the propellant continues to age increased cross-linking between the binder main-chains may cause the material to harden and become brittle. The harder propellant has an increased modulus and lower strain capacity.

The materials which comprise the other componentry of the rocket motor will also age however studies of the effect of ageing on the inhibitor, epoxy and insulation materials is meagre.[15,16] This investigation will concentrate on the effect ageing has on the mechanical properties of the PICTOR rocket motor materials, without emphasis on the chemical reactions.

Physical ageing is a property of glassy polymers and can be described as the time-dependent, asymptotic collapse of free volume trapped inside the entangled chain segments of the macromolecules.[17] It arises when the polymer exists in a non-equilibrium state below the glass transition temperature. The mobility of chain segments below the glass transition temperature is not quite zero. With time, the material approaches equilibrium through conformational rearrangements of the macromolecular chains. Subsequently whilst in the non-equilibrium state the thermal expansion coefficient below the glass transition will be lowered. In this study the susceptibility of the materials employed in the PICTOR rocket motor to the physical ageing processes described above will be investigated.

Differences in the thermal expansion coefficients of the rocket motor materials result in thermal stresses during temperature transients which may cause fracture. Changes in the thermal expansion coefficient and glass transition temperature on material ageing may have a significant effect on the mechanism and propensity for crack propagation. It is surprising then that no studies of the relationship between thermal expansion coefficient and ageing of composite materials have been identified in the literature.

Nielsen[18] describes in general terms the behaviour of composites consisting of a binder having a much larger thermal expansion coefficient than the rigid filler. Firstly, the thermal expansion coefficient of the composite will be lower than that of the pure polymer due to the presence of the filler. More importantly, he reports that at the interface of the binder and filler particles strong tensile forces, capable of causing binder/filler dewetting, may result from the mismatch of the coefficients of thermal expansion.

Hardening or softening of the binder as the material ages will cause changes in the level of stress at the interface and subsequently the likelihood of dewetting. Ho and Tod[19] reported that the main mechanisms present during ageing of rubbery composite propellants was debonding and/or rehealing at the polymer matrix/filler interface. Thus binder/filler dewetting during ageing may cause a measureable change to the overall thermal expansion coefficient.

A change in the slope of the thermal expansion curve plotted against increasing temperature for a particular material occurs in the glass transition region. The glass transition temperature, T_g, is identified in this region. As the specimen temperature increases through this region the material behaviour will change from a glassy, elastic state to a rubbery, elastomeric one. Eisele[20] reported how a variety of chemical and physical changes to the polymer may affect the value of T_g. The temperature of glass transition is generally only slightly affected by the

addition of a filler. He also noted that with increased cross-linking the mobility of the polymer backbone is reduced causing an increase in the glass transition temperature. The influence of side chains and their mobility on the glass transition temperature is characterised by an increasing glass transition temperature for stiff side chains and a decrease in glass transition temperature for flexible side chains. Plasticisers, such as moisture, act similarly to flexible side chains, sliding between the polymer chains increasing the free volume and decreasing the glass transition temperature. Some of the changes reported by Eisele may be present during material ageing, resulting in a variation of the glass transition temperature. If the glass transition temperature varies the mechanical behaviour of the material in a temperature range close to that of glass transition will be affected. A temperature at which a material may have previously behaved elastomerically may now lie in the glassy region.

POISSON'S RATIO

Poisson's ratio is a fundamental material property needed for finite element analysis. The simplest definition of Poisson's ratio describes the relationship between the strain caused by a tensile load and the resultant lateral contraction of the specimen. The FEA code calculates lateral stresses in response to an applied axial load from the value Poisson's ratio input. The value of stress calculated is extremely sensitive to minor variations of Poisson's ratio,[21] therefore the input of accurate values is essential. Due to the viscoelastic nature of the materials employed in the PICTOR rocket motor it is also important to ascertain the time, temperature and non-linear effects on the variation of Poisson's ratio as the material is strained. Few studies have been conducted which examine the change in Poisson's ratio for viscoelastic materials. In fact very little data exists on the effect of strain, temperature and strain-rate on the change in Poisson's ratio.

The dependence of Poisson's ratio on strain is related to the change in specimen volume. The expression relating volume change with the axial and lateral strain in a body under tension is written as:

$$V_f = V_0(1+\varepsilon_A)(1-\varepsilon_{L1})(1-\varepsilon_{L2}) \quad \text{.....(1)}$$

where V_f is the final volume, V_0 is the original volume, ε_A is the axial strain, ε_{L1} is the lateral strain in one direction and ε_{L2} is the lateral strain in the perpendicular direction. The definition of Poisson's ratio is expressed as:

$$\nu = -\frac{\varepsilon_L}{\varepsilon_A} \quad \text{.....(2)}$$

where for an isotropic material $\varepsilon_{L1} = \varepsilon_{L2} = \varepsilon_L$.

Substituting equation (2) into equation (1) and expanding (the second and third order terms are ignored as they are negligible) leads to:

$$\Delta V/V_0 = \varepsilon_A - 2\nu\varepsilon_A \quad \text{.....(3)}$$

where ΔV is the volume change.

Rearranging this expression gives:

$$\nu = \tfrac{1}{2}\left(1 - \frac{\Delta V}{\varepsilon_A V_0}\right) \quad \text{.....(4)}$$

Thus for an incompressible material, where there is no volume change, $\Delta V/V_0 = 0$ implying that $\nu = 0.5$. For compressible materials, where $\Delta V/V_0 \neq 0$, Poisson's ratio decreases from 0.5 as

volume change and strain increase. The volume change in compressible materials has been studied using gas dilatometry and values of Poisson's ratio obtained from the above equation.

Smith[22] observed the non-linear variation in Poisson's ratio of a polyvinyl chloride (PVC) filled with glass beads. He measured a decrease in Poisson's ratio from approximately 0.5 at low strain to 0.25 at a strain level of 0.4. Smith found that three distinct types of interactions at the binder/filler interface were evident in plots of Poisson's ratio against extension ratio. First, at low strain there is little or no binder/filler debonding or vacuoles formed and the polymer behaves similar to an unfilled one. As strain increases a critical point is reached at which the binder/filler bonds begin to break, with subsequent deviation from linearity. There is an onset of dewetting with a significant increase in specimen volume as vacuoles form in the polymer matrix and a subsequent loss of reinforcement. The result is that Poisson's ratio decreases at an increasing rate, dependent on the rate of vacuole formation, until the filler particles become completely debonded from the polymer matrix.

Similar results were obtained by Yilmazer and Farris[23] (and Anderson and Farris[24]) who employed a gas dilatometer to monitor the mechanical behaviour of polyurethane elastomers filled with various fractions of glass beads by measuring specimen volume change. Unfilled polymers were found to have minimal volume change on straining as did composites at low strain, prior to dewetting. As the strain increased the non-linear behaviour of the polymers was found to be strongly affected by the separation of filler and binder. Mechanical reinforcement of the composite was observed to decrease as a result of the formation and growth of vacuoles when the filler particles dewetted. Yilmazer and Farris proposed an equation relating stress, strain and volume change. The inclusion of material dilatation allowed the stress-strain data for the specimens tested to be predicted.

The relationship for Poisson's ratio derived (see Equation 2) from elastic laws only applies at low strain levels in a viscoelastic material. Many alternative definitions for large deformations have been proposed;[25] however, these usually convey very little meaning in any physical sense and are not applicable for FEA codes.

The definition of Poisson's ratio adopted in this study is expressed as:

$$\nu(\varepsilon,t) = -\frac{\varepsilon_L(\varepsilon_A,t)}{\varepsilon_A(t)} \quad \text{.....(5)}$$

where $\nu(\varepsilon,t)$ is the Poisson's ratio as a function of the applied strain and time, $\varepsilon_L(\varepsilon_A,t)$ is the lateral strain as a function of the axial strain and time and $\varepsilon_A(t)$ is the applied axial strain as a function of time.

Poisson's ratio as defined above conveys an easily recognised physical meaning and is the standard expression employed in finite element analysis codes, as such it is more useful than other definitions. Since direct measurements of the change in both axial and lateral strain with time were recorded, the dependence of Poisson's ratio on non-linear material behaviour is included.

The more precisely Poisson's ratio can be measured the greater the accuracy of the results from the finite element model. This has proved to be a difficult task, particularly at extremely low values of strain and is usually associated with large experimental errors. Many methods have been devised to directly measure axial and lateral strain or the volumetric change of the specimen enabling the variation in Poisson's ratio to be determined. The advantages and disadvantages of some methods and the results reported will be described here.

Kugler, Stacer and Steimle[26] discussed an optoelectronic system for simultaneously measuring axial and lateral contractions for simple extensions. Axial strain was measured by calculating the change in distance between light beams reflected from contrasting stripes printed on the specimen surface. Lateral strain was obtained by measuring the quantity of light passing either side of the specimen's edges from a light source placed on the opposite side of the specimen from the detector unit. Any lateral expansion or contraction altered the quantity of light detected, thus allowing a measure of lateral strain. This would imply that only one value of lateral strain is obtained at any time and that it is an average over the gauge length. Thus the test does not account for non-uniform lateral expansion and contraction over the gauge length.

The tests Kugler, Stacer and Steimle conducted were on a polyurethane filled with glass beads and a HTPB type composite propellant. The variation of Poisson's ratio in response to stress relaxation and simple extension, was reported. It was concluded that errors in the measured width of the specimens caused the greatest errors in Poisson's ratio because the error in the measurement was the same order of magnitude as the size of the filler particles. Thus using the specimen edges in the measurement of lateral strain, as compared to values obtained from the middle of the specimen, can be a source of gross errors.

Laufer et. al.[7] employed a liquid dilatometer to measure Poisson's ratio in unfilled and filled polybutadiene elastomers using water as the contacting medium (the filler was 35% asbestos powder). They found that the Poisson's ratio of both the filled and unfilled polymers varied linearly and were not significantly different up to 14% strain. It was concluded that no dewetting occurred in the filled elastomer to this point and therefore its behaviour will be identical to the unfilled polymer. The difficulty with this technique is that the liquid used in the dilatometric device may affect the specimen to be tested. The liquid may cause swelling and subsequent changes to the mechanical properties, although Laufer[7] reported no observable

effect on the materials chosen after immersion for 20-30 minutes. However, both the inhibitor and propellant used in this study are affected by water. Gas dilatometers may provide a solution to this, however, they are sensitive to gas expansion or contraction with ambient temperature changes and thus require expensive control systems.

Fedors and Hong[25] employed sets of knife edge gauges, which helped delineate longitudinal extension and lateral contraction due to the elongation during uniaxial testing. The gauges measuring lateral contraction contacted the specimen's edges and were fixed in space relative to the longitudinal movement of the specimen. The knife edge did not continually measure contraction at the same point on the gauge length. Thus if the contraction of the material takes place non-uniformly over the gauge length this will not be accounted for in the lateral strain measurement. A general concern with the use of contact type gauges is their lack of ability to maintain contact with the specimen at the same position on the specimen over the test. This is especially true for viscoelastic materials which are capable of sustaining high strains to rupture. The variation of Poisson's ratio for a variety of unfilled polymer composites were reported only up to an axial strain of approximately 3%.

Urayama et. al.[8] used a video camera to record the extension process, they measured the Poisson's ratio in polyvinyl alcohol (PVA) gels. The extensions were derived by measuring the movement of two points marked on the specimen as viewed from the record on a video monitor. A comparison was made between gels swollen by a variety of solvents. It was found that a poor solvent produced a low Poisson's ratio value (0.338), whilst good solvents gave values in the range 0.453 to 0.485.

Techniques for measuring strain which rely on a device maintaining contact with the surface of the specimen are susceptible to non-uniform dimensional changes and edge effects. The liquid

in a dilatometer may affect the specimen's mechanical behaviour and gas equipment is costly. The approach taken by Urayama et. al. of measuring the movement of a grid marked onto the specimen's surface has considerable advantages over other methods and the technique will be enhanced in this study. Video records of uniaxial testing can be digitised to computer and image analysis performed to calculate strain directly from the marked grid without contacting the specimen. Measurements can be performed to high extensions and the points at which each end of a gauge length is defined cannot change thereby allowing the uniformity of specimen elongation and contraction to be easily monitored.

FRACTURE BEHAVIOUR

A crack propagating in a structural component of a rocket motor can have a significant effect on the integrity of that component. To predict the likelihood and rate of cracking we firstly need to understand the mechanisms present during crack growth. In the following section a review of the current position, with particular emphasis on the unique nature of cracking in a composite propellant, is presented.

A significant insight into the mechanism of crack extension in a filled polymer has been achieved by the use of acoustic imaging, x-ray imaging, photographic and video records. Smith, Mouille and Liu[27] studied an inert propellant, the composition of which they believed would simulate a live propellant. Tension, relaxation and crack propagation tests on biaxial specimens were carried out at two crosshead speeds (2.54 $mm.min^{-1}$ and 12.7 $mm.min^{-1}$) at each of three test temperatures (−54°C, 22°C and 74°C). Photographic records showing the propagation mechanism for a sharp (25 mm) edge crack were presented. It was concluded that the mechanism was clearly defined and involved near tip blunting accompanied by the formation of a stretch and/or damage zone ahead of the crack at the free surface. Crack growth

was achieved by a resharpening of the blunted crack tip probably by a coalescence of voids ahead of the crack with the main crack front. It was noted that whilst the test temperature had a significant effect on the load level and rate of crack growth, the strain-rate did not. The load and crack growth response was found to be quite different at the sub-zero temperature to that above zero whilst the behaviour at the above zero temperatures was quite similar. It was conjectured that the binder was much stiffer at the sub-zero temperature even though the glass transition temperature for the pure binder was −101°C, this resulted in the substantially different behaviour observed. Whilst the rate of crack growth varied the mechanism was, interestingly, observed to be the same for all of the test temperatures. The mechanism propounded in this study was contrasted with that observed in earlier studies by the same authors,[28] where tests were also conducted using inert propellants. It is interesting to note that severe crack blunting seen in the earlier tests did not occur here. The authors concluded that this resulted from a much stronger resistance to dewetting in the simulated propellant.

Liu[29] recorded the local fracture processes near the crack tip in an inert solid propellant by employing high energy real-time X-ray imaging. He tested both edge-cracked and centre-cracked sheet specimens by incremental straining the specimens 5% at a crosshead speed of 50 $mm.min^{-1}$. The energy of X-rays emitted from a source is absorbed by the fracture processes present during crack propagation. A X-ray detector placed on the opposite side of the specimen to the source produces an X-ray image of the energy absorbed by the cracking specimen. This was processed to create a visual image which could be recorded to videotape. A region of high X-ray absorption (ie., the area of highest damage) was seen as a dark area, whereas a region of low damage and low absorption produced a light/white area, in between were 256 levels of gray. The mechanism of crack growth was described as including crack-tip blunting, resharpening and a zigzag direction for crack growth. More specifically, microcracks

generated in the failure or damage zone ahead of the crack tip increase in number with increasing applied strain. The large microcracks coalesce with the main crack tip leading to crack extension. Depending on the severity of the damage in the failure zone the main crack can grow a short distance into the zone or it can grow a distance approximately equal to the failure zone in length.

It is well known that the mechanical behaviour of inert propellants can be substantially different from that exhibited by a live propellant. By substituting an AP filler with an inert material the effect on the binder/filler interactions may be significant. The following workers studied the crack growth in live propellants.

Yeh, Le and Liu[30] investigated the crack growth behaviour in a centrally cracked biaxially stressed composite propellant specimen. They monitored the crack extension during the experiment with a video camera, recording the images onto videotape. The raw experimental data, including crack length and load as a function of time, was used to calculate the instantaneous crack growth rate and associated stress intensity factor. Three crosshead speeds (0.25 $cm.min^{-1}$, 2.5 $cm.min^{-1}$ and 25 $cm.min^{-1}$) were used and two different initial crack lengths (2.5 and 5 cm). It was concluded that the critical load for crack initiation decreased as the initial crack length was increased. They found that a power law relationship existed between the stress intensity factor and the crack growth rate which is consistent with the theoretical results obtained by Schapery[31] and Knauss[32] in their studies of the fracture in linear viscoelastic materials.

In a study by Smith and Liu[5] a series of tensile tests were conducted on edge cracked (25 mm) biaxial stressed solid propellant specimens (203×51 mm) of two thicknesses (2.54 mm and 12.7 mm) which were glued to aluminium grips. Two crosshead speeds (2.54 $mm.min^{-1}$ and

12.7 $mm.min^{-1}$) were employed at each of three test temperatures (–54°C, 22°C and 74°C). Tensile and relaxation tests were also conducted on two thicknesses of uncracked specimens and no significant thickness effect was observed.

Smith and Liu photographed the crack growth during each test, the mechanism was observed as a blunt-growth-blunt-growth process. The process was described as highly non-linear with voids forming in the damaged zone ahead of the crack during blunting followed by growth during which the crack resharpened. It was found that in a global sense the crack grew in a plane normal to the direction of extension. However, the crack path was locally undulating with growth accomplished by the crack tip connecting with voids ahead of it.

A clear difference between the low temperature and above zero testing in the curves of load versus extension was reported by Smith and Liu. The low temperature tests suggested a much stiffer response, with much greater values of initial modulus, while the curves at 22°C and 74°C showed very similar responses. At the elevated temperatures the value of maximum load per unit specimen thickness was higher for the thin specimen which was attributed to the larger and greater number of voids possible in the thicker specimen. The reverse was observed at –54°C with the thicker specimen exhibiting higher maximum load per unit thickness and classic brittle failure across the specimen. The absence of crack blunting at the low temperature was ascribed to binder stiffening producing a transverse constraint at the crack tip which caused the material to behave as a single phase continuum.

Material ageing during service life caused by the thermal loads affects the mechanical and fracture properties of the rocket motor components. It is therefore important to have an understanding of the mechanism of crack growth in aged materials.

Liu[6] endeavoured to investigate the consequences of damage on crack growth behaviour by studying a "pre-damaged" solid propellant. Thin sheet specimens were stretched to 15% strain and then unloaded to 0% strain to simulate the damage caused by thermal loads. A 2.54 cm horizontal crack was then cut in the centre of the specimen with a razor blade. The specimen was strained and an acoustic imaging system was employed to examine the effect of pre-damage and to help explain the growth mechanisms. From the acoustic imaging data of the cracking specimen an iso-intensity plot of the damage field was generated. The results showed an extensive amount of damage was induced in the specimen by the prestraining and that it was uniformly distributed throughout. This was seen to indicate that the damage process is dominated by damage nucleation and that the number of microvoids increases with the strain level.

Liu also compared specimens of both pre-damaged and virgin specimens with and without cracks. The presence of a crack in the specimen caused a redistribution of the stresses and subsequent modification of the distribution of damage. Larger damage zones with higher damage intensities were seen ahead of crack tips in pre-damaged specimens. It was concluded that pre-damage in a specimen may induce different material response and crack growth behaviour as compared to a virgin specimen. The mechanism of crack growth in both pre-damaged and virgin specimens was found to be a process whereby the crack tip sharpened temporarily by coalescing with voids in the damaged zone ahead of the crack and then blunted as microcracks grow to form voids in the damage zone. The crack growth mechanism was described as one of stop-grow-stop while the crack tip geometry was one of blunt-sharp-blunt. It was concluded that the crack growth behaviour was a highly non-linear process that occurred in both pre-damaged and virgin specimens.

The need to characterise the effect of thermal loads on the rocket motor materials is considerable. However, no studies have been located in the literature which discussed the effect of material ageing on the crack growth mechanism. It should be noted that the study by Liu[6] is useful for examining the qualitative effect of damage on the crack growth mechanism but is not adequate when considering the damage caused by material ageing from thermal loads as the extent of this type of damage has not been quantified in relation to crack growth. Also, Liu did not study the effect of temperature and strain-rate on the pre-damaged material which especially in the case of temperature has been described as significant.[5]

No studies detailing the crack growth mechanisms in the inhibitor or at bondlines in bimaterial composite specimens were located. However, Liu[33] states that similar mechanisms and basic damage modes will be found to apply to most highly filled polymeric materials. The damage mechanisms in the inhibitor and propellant/inhibitor bimaterial specimens will be reported here.

While authors[5,6,27-29] reported the fracture process as highly non-linear in nature a number calculated a stress intensity factor and related it to the crack velocity in an attempt to produce a crack propagation criterion. As stress intensity factors are derived from the assumptions of linear elastic fracture mechanics (LEFM) their interpretation when dealing with non-linear fracture mechanics is not clear.[34] A criterion which includes the effects of non-linear viscoelastic material behaviour is required. The development of such a criterion is outlined below.

To supply a crack propagation criterion for non-linear materials, one of the first such approaches was to modify the relationship between the stress intensity factor and the crack propagation rate. Langlois and Gonard[35] expressed the opinion that the power law relationship between stress intensity factor and crack propagation rate developed by Schapery,[36,37,38]

appeared to be inadequate for the correct representation of crack propagation in viscoelastic materials. An improvement was attempted by explaining the values of the parameters employed in the expression more inline with viscoelastic behaviour. However, they based their theoretical development on linear cumulative damage theory and the concept of a failure area. The modified law was verified by calculating the stress intensity factor and crack propagation rate from uniaxial tests conducted on polyurethane and carboxy-terminated polybutadiene propellants at several temperatures and strain-rates. They concluded that the modified law was more successful at accounting for experimental results than the law proposed by Schapery.

Gledhill and Kinloch[39] proposed the development of a unique crack propagation criteria for fracture in propellants which also accounted for the thickness of the specimen and was applicable over a wide range of temperatures. Double-base propellant specimens manufactured from nitrocellulose/nitroglycerin in a compact tension geometry were strained in an Instron tensile testing machine at a variety of temperatures (from –60°C to 20°C). From the load-time data the load at crack propagation and the value of stress intensity factor were determined. By assuming linear-elastic behaviour in the bulk and that plastic behaviour in the specimen is limited to a zone surrounding the crack, it was considered that the plane-strain and plane-stress components of the experimentally determined stress intensity factor could be separated. A linear relationship between the plane-stress component of the stress intensity factor, K_{c2}, and the yield stress was observed, which was highly dependent on temperature. (The temperature dependence was considered to be a reflection of the viscoelastic and plastic energy-dissipative mechanisms that occur at the crack tip.) This linear relation was proposed as a unique failure criterion, independent of temperature for this propellant. From an expression relating the plastic zone radius to the slope of the curve of K_{c2} against yield stress, the critical radius of the plastic zone for crack propagation could be calculated.

Kinloch and Gledhill[40] extended their work reviewed above by interrelating the measured values of stress intensity factor with temperature and rate effects by using the Williams-Landel-Ferry relation for viscoelastic materials. They discussed the usefulness of the stress intensity factor approach for stress controlled fracture events and noted that an alternative approach based on an energy balance would be more appropriate when a critical strain or energy requirement must be met. However, from the conclusion they made regarding the temperature dependence of K_{c2} being a reflection of the energy dissipation near the crack tip, it would appear that an energy based criterion is more appropriate here. The value of fracture energy for the completed tests were calculated from the relationship between stress intensity factor and fracture energy derived from linear elastic fracture mechanics, this relationship does not apply in the case of non-linear viscoelastic material behaviour.

Devereaux[41] studied crack propagation in circumferentially notched cylindrical specimens of composite modified cast double-base propellant using the J-integral technique. The specimens were tested at a variety of strain-rates in a tensile testing machine with data collection via computer and high speed film. The J-integral is a measure of the rate of decrease in potential energy as the crack propagates. However, its derivation assumes that the plastic deformation in the specimen is confined to a region surrounding the crack tip and material unloading occurs along the same path on the stress-strain curve as the loading. The criterion for crack propagation is that the onset of crack growth occurs at a critical level of J-integral, J_c. Devereaux concluded that to extend this approach to highly non-linear propellant formulations would drive the analytical technique to its furthest limit. The task would be difficult due to the requirement for analytical solutions which included the non-linear viscoelastic material behaviour in the near tip stress fields surrounding the crack.

The studies reported above all assumed that elastic behaviour applied in the bulk of the composites and that the non-linear behaviour is limited to a small plastic zone near the crack tip. This approach has been successfully applied to extruded double-base propellants which are more brittle and have a lower strain to failure than present day composites. However, this is not always an appropriate approach as many rubbers exhibit significant internal energy dissipation outside the region in the immediate vicinity of the crack tip, bulk inelasticity. The development of the concept of fracture energy, G_c, as a failure criterion from an energy balance approach is reviewed below.

Griffith[42] originally conjectured that the work done to extend a crack by the external load and the energy stored in the bulk of the specimen was converted to surface free energy. The following equation was formulated:

$$\frac{\partial}{\partial a}(F-U) \geq \gamma \frac{\partial A}{\partial a} \quad \text{.....(6)}$$

where F is the external load, U is the stored energy, γ is the surface free energy and ∂A is the increase in area associated with an increment of crack length ∂a.

The surface free energy term was replaced by G_c which encompasses all the energy losses at the crack tip and is referred to as the fracture energy, the criterion for fracture becomes:

$$\frac{1}{b}\frac{\partial}{\partial a}(F-U) \geq G_c \quad \text{.....(7)}$$

since $\partial A = 2b\partial a$ is the area created as the crack extends (where b is the thickness) G_c is the energy required to increase the crack by unit length in a specimen of unit thickness.

An early study by Rivlin and Thomas[43] on cross-linked rubbers extended the work of Griffith. The rubber vulcanizates possessed high energy losses in the region surrounding the crack tip but were non-linear elastic in the bulk. A number of solutions for the work and potential energy terms of the equation for fracture were derived for different test piece geometries. One solution was for the single edge notch (SEN) specimen:

$$-U = k_1 a^2 b W_i \quad \text{.....(8)}$$

where W_i is the strain energy per unit volume of the uncracked SEN specimen and k_1 is a proportionality constant related to the size of the area over which the strain energy is reduced to zero following insertion of the crack.

Test pieces were extended in tensometers and observed using low powered microscopes. The cracked specimens were coloured with ink and the instant of crack propagation was determined as the moment when fresh uninked rubber first appeared. The critical value of input strain energy density (denoted W_{ic}) was calculated from the area under the stress-strain curve up to the strain at which the crack first propagated, the critical strain, e_c. The fracture criterion was expressed as:

$$G_c = 2k_1 a W_{ic} \quad \text{.....(9)}$$

(Rivlin and Thomas[43] used the quantity T, the energy of tearing).

Values of tearing (or fracture) energy for three types of rubber were calculated. It was concluded that where the shape and disposition of the cut are such that the change in stored elastic energy resulting from an increase in crack length can be calculated from known elastic characteristics of the rubber, the force required for tearing could be calculated from the characteristic fracture energy.

Marom, Harel and Rosner[44] studied a terpolymer of butadiene with AP and aluminium particle fillers. The test specimens were cut into a "trouser" geometry with an initial crack of 20 mm length inserted by a razor blade. A series of pen marks along the length of the test specimen were used to enable calculation of the extension ratio. The tests were carried out at a crosshead speed of 5 cm/min. The crack propagation was followed by marking the load versus time printout as the crack advanced passed each pen marking. A series of tests were performed on propellants stored at a constant temperature of 60°C and plots of fracture energy against age were produced.

The fracture energy was calculated by Marom, Harel and Rosner using the expression derived by Rivlin and Thomas[43] which is based on the input energy of the applied load. The fracture energy was found to increase slightly initially and then consistently decrease with ageing period. They concluded that the long-term result of ageing would be an increase in the rate of oxidation which destroys the adhesion between the binder and filler particles and degrades the polymer chains resulting in the decreased fracture energy observed. It was suggested that the slight initial increase in fracture energy on ageing was the result of a drop in the binder/filler bond strength due to the oxidation reactions. The initial damage caused being restricted to the binder/filler interface thus eliminating the energy dissipating crack front mechanism, before spreading into the polymer matrix and resulting in the expected decrease in fracture energy. The authors did not study the effect of strain-rate and temperature on the fracture energy nor other ageing conditions.

Kinloch and Tod[1] observed that modern rubbery propellants exhibit pronounced mechanical hysteresis when loaded and unloaded and that only a fraction of the input strain energy is recovered. This recovered strain energy will be the only energy available for crack propagation. They went on to develop a fracture criterion based on the energy balance

approach which took into account the bulk inelastic behaviour of composite propellants (which is equally applicable to other materials exhibiting this behaviour).

The equations derived by Rivlin and Thomas[43] for the calculation of the tearing energy were adapted by Kinloch and Tod to give the fracture energy in SEN and "trouser" test specimens of propellant by substituting the critical recoverable strain energy density, W_{rc}, for the critical input strain energy density.

For a SEN specimen the equation is expressed as:

$$G_c = \frac{2\pi a W_{rc}}{(1+\varepsilon_c)^{1/2}} \quad \text{.....(10)}$$

where G_c is the fracture energy, a is the initial crack length, W_{rc} is the critical recoverable strain energy density and ε_c is the critical strain. The critical recoverable strain energy density and critical strain are those values measured at the onset of crack propagation.

Kinloch and Tod determined the values of critical recovered strain energy density for use in the equation for fracture energy from experiments on a HTPB/AP type propellant. Uncracked SEN and "trouser" specimens were tested at 20°C and an initial strain-rate of 0.01 min^{-1}. The specimens were subjected to constant load testing for a variety of loading and unloading times from which a stress-time history was developed. The recovered strain energy density was determined from the integral of the unloading stress-strain curves and an empirical relationship between W_r and strain, loading and unloading time was generated.

Crack propagation tests in the SEN specimens were conducted by introducing a small sharp crack (2 mm) after it had been held under constant load for 30 minutes. The legs of the "trouser" test specimen were extended at a constant rate and the load required to propagate

the crack was recorded. The crack growth was monitored by a video camera and crack velocity calculated by replay of the recorded image.

Kinloch and Tod presented the fracture energy as a function of crack velocity and concluded that fracture energy increased with crack velocity due to the increasing extent of plastic deformations and bond rupturing occurring in the region around the crack tip. There was reasonable agreement between the fracture energy values determined for both the SEN and "trouser" test specimens. This shows that the fracture energy is indeed a criterion which is independent of specimen geometry and loading conditions and supports the concept that it is a true material parameter.

Ho and Tod[3] using a modified fracture mechanics approach determined the fracture energy of a number of composite propellants, an elastomer modified cast double base propellant (EMCDB) and a thermoplastic elastomer propellant. They reported that the fracture behaviour of solid propellants is highly strain-rate and temperature dependent because of the viscoelastic nature of the material. Also the viscous and plastic deformations and filler particle dewetting causes bulk inelastic behaviour whereby on loading and unloading the material exhibits mechanical hysteresis and only a portion of the applied strain energy is recovered.

Specimens of the propellants were cut to SEN geometry (70×24×6 mm for the EMCDB and 70×24×9 mm for the other propellants). A sharp crack of various lengths was cut for the crack propagation tests which were conducted at four crosshead speeds (0.5, 1.0, 2.5 and 5.0 $mm.min^{-1}$). In the case of the composite propellants a number of tests were carried out on specimens that had naturally aged for between 12 and 85 months. The load at crack propagation was determined by visual inspection of the specimen under test. In order to measure the hysteresis losses, required for the calculation of fracture energy, tests were

conducted on uncracked specimens at crosshead speeds matching those used in the crack propagation tests. Each specimen was cycled to load levels which were incrementally increased until specimen rupture and the area under the force-displacement curve measured.

Ho and Tod found that a constant hysteresis ratio, h_r, was obtained from the tests for hysteresis energy loss for all the propellants studied in the range of strains where propellant failure occurred in the crack propagation tests. This allowed the relationship between hysteresis ratio and critical recovered strain energy density to be used, eliminating the need to measure the critical recovered strain energy density at a variety of loading and unloading times. The relationship was expressed as:

$$W_{rc} = W_i(1 - h_r) \quad \text{.....(11)}$$

where W_i was the input strain energy density measured in the crack propagation tests.

Hysteresis ratio was observed by Ho and Tod to be higher for more rubbery propellants and those with larger filler particles. The hysteresis ratio was found to fluctuate with propellant ageing and it was concluded that this was due to the opposing effects of dewetting/rehealing and increased cross-linking and main chain scission. An increase in hysteresis ratio was generally associated with higher values of fracture energy. The fracture energy also fluctuated with ageing and it was suggested that hysteresis plays an important role in the fracture process. It was concluded that fracture energy gave an improved indication of propellant failure than other, more simple criterion such as maximum strain.

The use of stress intensity factors as a failure criterion for composite propellant by many authors[30,35,39,40] is limited by the assumption of bulk inelasticity which does not adequately describe the non-linear viscoelastic behaviour outside the region in the immediate vicinity of the crack tip. One criterion which does account for the bulk inelastic behaviour is fracture

energy. Fracture energy can be easily calculated from data provided from hysteresis and crack propagation experiments using the modified fracture mechanics approach of Ho and Tod.[3]

There is a lack of literature available on the effect of ageing on fracture in propellant, inhibitor materials and at the bondline of composite bimaterials such as the propellant/inhibitor. Little attention has been paid to the effect of material temperature on the propensity for cracking in composites with all studies confined to ambient temperatures. An attempt to address these issues will be made in this study.

SUMMARY

As a tool in the service life assessment of the PICTOR rocket motor a finite element model can be produced. This model will calculate stresses, strains, crack initiation and propagation when the rocket motor is subjected to cyclic thermal loads. The accuracy of the model results will depend on the inclusion of extensive material characterisation under the conditions of service. The effect of time, temperature, strain and ageing on the mechanical behaviour of the materials of construction when subjected to thermal loadings will need to be determined. The materials employed in the construction of the PICTOR rocket motor have unique properties of which very little has been reported in the literature.

Values for thermal expansion coefficients and glass transition temperatures of the PICTOR materials and their dependence on temperature have not been adequately reported. The effect of ageing on these properties has also not been discussed in the literature. Without this information accurate values of thermal stresses resulting from the thermal strains are not possible.

Small changes in the value of Poisson's ratio lead to large variations in the stresses calculated by the FEA. Very little information on the effect that time and temperature has on the value of

Poisson's ratio for these materials has been recorded. An understanding of the damage processes and their extent when the material undergoes strain is required.

Some workers have reported fracture properties, such as fracture energy, crack growth mechanism and crack velocity for propellants. Although, the inclusion of inelastic material behaviour in the facture properties has been overlooked in a number of cases. The effect of temperature, strain-rate and ageing has also not been widely reported. No literature detailing the fracture of the propellant/inhibitor bondline was located. The need for hysteresis data, a description of the crack growth mechanism, crack velocity data, a measure of the propensity for crack propagation provided by the fracture energy and the effect that temperature, strain-rate and ageing has on these as the propellant, inhibitor and propellant/inhibitor interface is subjected to the thermal loads of service, necessitates the work of this study.

This study will address these issues so that the finite element analysis is able to achieve greater accuracy thus allowing better predictions of service life.

Chapter III
Experimental Method

THE PICTOR ROCKET MOTOR

The rocket motor to be investigated in this study is the PICTOR. It is an Australian research rocket motor of common design. The PICTOR rocket motor is of a case-bonded, end burning configuration. It is manufactured by first preparing a charge which consists of a cast polyurethane (Adiprene L315) beaker, filled with a composite propellant. The beaker contains 35% ammonium sulphate (AS) by weight and incorporates an anti-oxidant. The beaker is more commonly referred to as the inhibitor, its function is to inhibit the spread of combustion gases away from the burning end face of the propellant. The composite propellant consists of a hydroxy-terminated polybutadiene binder, with approximately 80% by weight ammonium perchlorate (AP) added, plus an anti-oxidant. The charge is bonded into the steel rocket motor case at the head-end with an epoxy resin adhesive, which fills a groove in the outer diameter of the charge to form a keying mechanism. The epoxy used is a mixture of 60% Epikote 828, with 40% Versamid 140 added as the curing agent. The steel casing is pre-lined before charge insertion with an ethylene propylene diene monomer (EPDM) rubber for thermal protection against the combustion gases.

For the purposes of this study, specimens of the rocket motor materials described above were required for testing. These were individually prepared as required from quality assured ingredients and in accordance with specified production methods.

The EPDM is cut to size from prepolymer sheet. Two pieces are bonded together with Chemlok 236A to give the required insulation thickness. The Chemlok 236A is allowed to air dry for 1 hour at 50°C to 60°C at which time the two pieces are brought together and the

specimen is placed in a heated press (600kPa and 155-165°C) for 2 hours. The material undergoes sulphur vulcanisation giving a cured sample from which the desired specimens can be cut to any geometry.

Epikote 828 epoxy resin and Versamid 140 curing agent were heated to 80°C for one hour prior to degassing. The epoxy and curing agent were mixed thoroughly in a 6:4 ratio and degassed before pouring into dogbone shaped teflon lined molds. The cast specimens were held at 30°C to 40°C for 16 hours to cure. Test specimens were cut or machined from the cast material and lightly polished to remove surface irregularities.

The polyurethane was mixed in a 1:1 ratio with trimethylol propane as curing agent. The components, including ammonium sulphate filler material and an antioxidant, were combined in a heated, stirred vessel and degassed. The mix was cast into teflon lined molds and held at 80°C for 16 hours to cure.

Hydroxy-terminated polybutadiene R45-M (HTPB) and ammonium perchlorate (AP) are the primary ingredients employed in the production of the PICTOR composite propellant. The HTPB and two size ranges ("coarse and fine") of AP are mixed in a heated vessel under vacuum, prior to the addition of a curing agent (dimethyl di-isocyanate) and an anti-oxidant. The mix is cast into teflon lined molds and held at 60°C for a total of 216 hours for curing.

In addition to "as-received" or unaged specimens the program called for examination of aged specimens. Selected samples were subjected to three service life type thermal loads to simulate the ageing environments commonly encountered by in-service rocket motors. A thermal shock involved holding the samples at 60°C for 16 hours after which the sample temperature was returned to 25°C. The sample was then subjected to a further 8 hours at –40°C then again

equilibrated to 25°C. This cycle was repeated 10 times to simulate the effects of diurnal cycling (see Figure 1).

To simulate ageing from long term storage in hot climates some samples were subjected to accelerated ageing conditions. This involved conditioning the samples at 64°C for a period of 16 weeks, after which a 24 hour exposure to –40°C was completed (see Figure 2). The final thermal load was long-term thermal cycling. The samples were held at 45°C for 30 days, followed by 20 days at 30°C, with equilibration at 25°C between - this hot/cold cycle was repeated five times (see Figure 3).

For all these thermal loadings the materials were first wrapped in aluminium foil and a layer of waxed paper before being placed in an air tight cylinder purged with high purity nitrogen for storage during the low temperature portion of the thermal load to prevent the absorption of moisture.

THERMAL MECHANICAL MEASUREMENTS

The thermal expansion coefficient and glass transition temperature of the materials employed in the PICTOR rocket motor were measured using a Mettler TA4000 Thermal Mechanical Analyser with low temperature attachment. The TA4000 employs an internal microprocessor to control the temperature in the unit's cell and to record the specimen's expansion and contraction in response to temperature change. Data analysis was performed by TA72.2 software on an IBM compatible computer linked to the TMA controller. The analysis software can calculate instantaneous or average thermal expansion coefficients and the glass transition temperature from the recorded data.

By utilising liquid nitrogen in the low temperature attachment dewar a temperature range of −100°C to +300°C can be achieved. High purity nitrogen gas was continually supplied to the TMA test cell in order to give an inert atmosphere and prevent condensation during sub-ambient testing, this will ensure reproducible test conditions.

Samples for testing in the TMA were necessarily small due to the test cells confines. The dimensions of each sample were approximately 3.5 mm on each side. Once the sample was located on the cell pedestal a cover glass was placed ontop of it to prevent probe penetration into samples softened by heating. A measurement of the glass cover's thermal expansion coefficient showed that it was negligible in comparison to the polymer specimens over the range of test temperatures.

A heating and cooling rate of 2°C.min^{-1} was chosen in order to simulate those found in common environmental thermal loadings. Tests on each sample consisted of cooling from ambient temperature to −60°C followed by heating to 75°C and final recooling to ambient. The heating/cooling cycle was repeated, providing four measurements of thermal expansion. The temperature range encompasses that employed in modelling thermal loading of full-scale rocket motors. Prior to and after each set of measurements the sample weight and dimensions were recorded in order to detect any effect of heating/cooling on the sample.

POISSON'S RATIO MEASUREMENTS

The variation in Poisson's ratio with strain was measured for all of the polymeric materials employed in the PICTOR rocket motor. In addition a composite propellant employing polypropylene glycol (PPG) as the binder was tested. The PPG propellant was included as its mechanical properties are different from the HTPB type propellant and a useful comparison can be made on the applicability of the method to a variety of composite binder types.

The standard propellant specimen was a rectangular bar. The cast propellant was machined into rectangles of 100×8×8 mm and aluminium tabs of dimensions 30×10×10 mm were glued to each end to provide a hard surface for gripping in the Instron tensile testing machine (see Figure 4). The minimum amount of epoxy resin required was used to secure the propellant specimen to the aluminium tabs. In all specimens the material failure occurred near the centre of the gauge length, not adjacent to the glued ends.

The inhibitor and insulation specimens were cut using a dogbone die (ASTM D412[45]) and the epoxy was cast into dogbone shaped molds[45] and then finished by milling to a thickness of 3 mm.

A high resolution Super-VHS video recorder in combination with a S-VHS Charged Couple Device (CCD) camera recorded the extension and contraction of a fine grid marked onto the surface of each specimen. To enable the greatest precision a high contrast grid was required. This was achieved by spraying a thin coat of matte black paint onto the specimen surface and allowing it to dry. Onto the black background a grid was ruled using a metallic silver ink pen. Care was taken to produce sharp line edges.

The video camera was fitted with a standard 50 mm focal length lens which was modified by fitting a number of tubes, totalling 12 mm in length, onto the rear of the lens in order to extend the focal length. The extension tubes have the effect of dramatically decreasing the minimum focusing length of the lens thus allowing the camera to be placed very close to the specimen. A highly magnified image is achieved without the need for a zoom lens, which inevitably have large minimum focussing lengths, requiring large distances between specimen and camera. A small grid was drawn in the central portion of the specimen away from the edges and was

magnified to fill the entire screen as recorded by the VCR. The positioning of the grid in the bulk of the specimen reduces the edge effects.

A LED which was activated on machine start was included in the frame of view of the camera to allow precise identification of the test start.

The CCD camera had a resolution of 500 horizontal lines which when combined with the S-VHS video recorder, capable of recording to a resolution of 425 lines, gave superior images to normal video thus allowing greater accuracy, for a minimal extra cost. A digital frame numbering device allowed accurate identification of the time between events on the video record. This system numbers each individual complete video frame, which are normally recorded at a speed of 25 frames per second. Playback could be paused allowing one of the two separate recorded fields which make a completed frame to be viewed individually, thus providing a resolution of up to 50 frames per second. Hence, events recorded can be precisely timed.

Each test consisted of extending the specimen at constant crosshead speed in the Instron tensile testing machine until failure. The expansion and contraction of the grid on the test specimen would be recorded to video tape. The applied load was also recorded by computer linked to the Instron load cell via an analogue to digital converter. Three slow crosshead speeds, which are relevant to service-life strain-rate conditions, were chosen (1, 2 and 5 $cm.min^{-1}$ for propellants, 0.5, 1 and 2 $cm.min^{-1}$ for inhibitor, epoxy and insulation). The two sets of crosshead speeds were required as the propellants and the non-explosive material specimens had differing gauge lengths, the result was equivalent strain-rates for each respective test. The maximum strain level obtained just prior to failure and the time taken to achieve this were used to calculate the average strain-rate, $\dot{\varepsilon}$, for each test.

All materials were first tested at ambient temperature (25°C). The HTPB type composite propellant and the inhibitor materials were additionally tested at elevated (50°C) and sub-ambient temperatures (–20°C). Some difficulty in obtaining measurements of strain was experienced at the sub-ambient temperature. Formation of condensation on the specimen caused bright areas to be visible on what should have been an otherwise dark background. This tended to obscure the gridlines making accurate measurements difficult. The choice of –20°C as the sub-ambient temperature alleviated the problem (in comparison to the previously chosen test temperature of –40°C). The use of high purity air free CO_2 as the cooling medium and maintaining tight seals on the conditioning chamber also helped.

For analysis the VCR was connected to a PC via a video frame grabber card. The replayed images were captured to computer and stored as 256 level grey scale "tiffs" (tagged image format files) of 768×576 pictures elements (or pixels) in dimension. These stored images were analysed using the NIH Image Analysis program. Using a 10 pixel wide "measure tool" the dimensional changes of the grid as the specimen is elongated were measured. The measuring tool functions as a ruler, a straight line is drawn across the image from point to point between which a distance (in pixels) is returned as a result. The result can also be calibrated to any standard unit of measurement. The tool additionally outputs the average of the grey levels from the pixels across its width against the distance along the length of the measuring tool, at intervals of one pixel. Since the difference between the black background and the high intensity ink gridline is many grey levels, this step in grey values can be used to conveniently locate the edge of the gridline. A line edge is used to define one end of the gauge length, since it is one-dimensional its position will remain constant relative to the changes in the specimen resulting from the applied strain.

A digital image edge locater algorithm, known as the Moment Preserving Method,[46,47] will locate the edge of the gridline on the image to sub-pixel accuracy ($\frac{1}{100}^{th}$ of a pixel). When calibrated the line edge could be located to ±0.0008 mm. Once the line edge locations are known the distances between line edges in the grid can be calculated. As the grid expands axially and contracts laterally the changes in the distance between gridline edges allows a calculation of the strain for each analysed image. Four axial measurements of grid expansion and five lateral measurements of grid contraction, obtained from each video frame analysed, were averaged to provide the axial and lateral strains. Although the choice of longer axial gauge lengths would reduce the error present in the measurement, the use of multiple gauge lengths provides a test for the uniformity of the expansion in the specimen, similarly for lateral contraction. Figure 5 shows an image from the video record of a test on a propellant specimen and the gauge lengths over which the strain calculations were measured. Ten images were captured and analysed from each test from the initial conditions to just prior to specimen rupture.

The maximum error expected in the value of Poisson's ratio is approximately ±2%, (by considering the precision achieved in the measured value of strains obtained from gridline edge location via the "moment preserving method"). Accuracy is affected by any lack of definition in the line edge and will have a deleterious effect on the value of Poisson's ratio calculated at low levels of axial strain. Great care was required in the application of the grid, particularly for the composite propellant which contains a high level of filler particles which results in an irregular surface finish even for milled specimens. The result of this was that in some instances at very low strain levels lack of line definition effected the value of Poisson's ratio obtained such that the value calculated was greater than 0.5, the theoretical maximum, these erroneous values have been omitted.

In addition to the rectangular specimens some HTPB type propellant was machined into cylinders of 100 mm length and 8 mm diameter. The aim of testing cylindrical and rectangular specimens was to examine the effect of specimen geometry on the variation of Poisson's ratio measured (see Figure 6). The values of Poisson's ratio calculated for both the cylindrical and rectangular shaped bars agrees, implying that the variation is governed by material considerations and is independent of the specimen geometry chosen.

HYSTERESIS ENERGY LOSS MEASUREMENTS

Measurement of hysteresis energy loss was performed on specimens of propellant, inhibitor and a combined propellant and inhibitor bimaterial specimen. The specimens were all prepared by first casting the mix into rectangular molds of dimensions 300×190×60 mm. A number of slabs of propellant and inhibitor were cast to a depth of 45 mm to allow for shrinkage during curing and wastage from machining. After curing the slabs were milled into specimens of dimension 125×40×10 mm, ready for the hysteresis tests. These dimensions will also be employed for the specimens in the crack propagation tests.

The propellant/inhibitor bimaterial sample was prepared by casting a layer of inhibitor material into the mold to a depth of 22 mm and allowing it to cure. After curing, the slab of inhibitor was removed from the mold, degreased and replaced with the bottom of the cast material ready to accept the propellant layer. The propellant was cast within 7 days of inhibitor casting to ensure a strong bond between the two materials. The propellant was cast to a depth of 22 mm and the mold was returned to the oven in order for the propellant to cure. After curing the propellant/inhibitor slab was milled into specimens of dimension 125×40×10 mm. The propellant/inhibitor specimens each consisted of 20 mm high propellant and 20 mm high inhibitor layers.

To study the hysteresis behaviour of aged materials a quantity of the prepared specimens were placed in thermal conditioning chambers and aged according to the three thermal loads described previously.

The specimens were prepared for testing in the Instron tensile testing machine by bonding them to grips made of mild steel (see Figure 7). The mild steel grip was prepared prior to specimen bonding by lightly linishing the face to which the specimen was to be bonded, followed by thorough degreasing. The specimen was bonded to the grip with a thin layer of epoxy resin. The specimen was located centrally in the face of each grip by alignment with a centreline marked onto the grip. A system of pins and threaded clamps were employed to overcome any slack in the coupling between the specimen and the Instron load cell.

The Instron load cell is connected to a computer via an analogue to digital converter for recording the load via software. Loads of known weight are used to calibrate the collection software and convert the incoming signal into a load in kilograms. After balancing the load cell a negative offset equal to the combined weight of the grip and specimen was applied to the load recorded in software.

The hysteresis loop was applied with the Instron's cycling capability. An example of the load against time recorded during a series of hysteresis cycles is illustrated by the main curve plotted in Figure 8. The inset curve shows the crosshead movement, at the maximum extension the crosshead reverses direction and returns to the zero position. The hysteresis loading cycle (or loop) was repeated three to five times at each strain level. At the end of each unloading stage a negative load resulted due to material compression. The specimen was allowed to relax for a period of five to ten minutes between each loop during which time the load measured returned to zero. The maximum extension was increased after each completed set of loops until the

material suffered a gross deformation or fractured. A set of hysteresis loops from low strain to material fracture was recorded for each of three crosshead speeds (0.2, 0.5 and 1.0 $cm.min^{-1}$) and three temperatures (–40°C, 25°C and 60°C).

The S-VHS camera and VCR setup as described for the Measurement of Poisson's Ratio was employed to record selected tests of hysteresis specimens. The specimen to be videorecorded was coated with a thin layer of matte black paint and after drying high intensity ink lines were ruled onto the specimen surface. The lines served as gauge markings with strain in the specimen calculated from the variation in the distance between the line edges. Hence, for each crosshead speed employed a corresponding strain-rate was calculated. The image analysis method for calculating the strain and strain-rate was outlined in the Measurement of Poisson's Ratio section above. Comparison between painted and non-painted specimens revealed no difference in the measured load, inferring that the layer of paint does not affect the results.

Once the strain-rate of each test is known it is a simple procedure to convert the load against time data recorded by the collection software to a graph of stress against strain. A schematic representation of the stress against strain measured during a hysteresis cycle is shown in Figure 9. The shaded area represents the hysteresis strain energy density, H, and the area under the unloading curve the recovered strain energy density, W_r. The input strain energy density, W_i, is the sum of these two:

$$W_i = W_r + H \quad \text{.....(12)}$$

The hysteresis ratio is calculated as:

$$h_r = \frac{H}{W_i} = \frac{W_i - W_r}{W_i} \quad \text{.....(13)}$$

CRACK PROPAGATION MEASUREMENTS

Fracture tests were performed on specimens of propellant, inhibitor and a combined propellant/inhibitor bimaterial. The dimensions of the fracture specimens were the same as those used in the hysteresis tests (they will be referred to as "horizontal bar" type specimens). The specimen geometry was chosen so that the 125 mm length would provide a sufficiently long distance to follow the propagating crack and allow ample data to be recorded for calculating the crack velocity. A similar test specimen geometry and gripping method were used in the crack propagation study of Liu.[29]

For the propellant/inhibitor bimaterial sample, the slab of inhibitor was removed from the mold after curing and a 10 mm length of teflon tape was applied to one of the bottom edges of the slab. This would create a non-stick surface for the layer of propellant later cast ontop and provided a sharp, thin, pre-made crack between the two materials. After curing the propellant/inhibitor slab was machined, with care taken to ensure that the edge containing the teflon tape was retained at one end of the milled specimen. The propellant/inhibitor samples each consisted of a 20 mm high section of propellant and 20 mm high section of inhibitor with the teflon tape acting as an initial crack between the two layers.

To study the crack propagation behaviour of aged materials a quantity of the prepared specimens were placed in thermal conditioning chambers and aged according to the three thermal loads described previously.

Just prior to bonding the propellant or inhibitor specimens to the grips a cut 10 mm in length was inserted in the centre of one end of the specimen with a razor blade to provide the initial sharp crack. The specimens were then bonded to the mild steel grips (see Figure 10) with a light layer of epoxy resin. The mild steel grip was prepared prior to specimen bonding by

lightly linishing and then degreasing the face to which the specimen was to be bonded. The specimen was located centrally in the face of each grip by alignment with a centreline marked onto the grip.

The Instron load cell was connected to a computer via an analogue to digital converter where the load was recorded by data collection software. Loads of known weight were used to calibrate the signal from the load cell. A collar was slid over the Instron universal joint to restrict specimen motion to uniaxial only. After balancing the load cell a negative offset equal to the combined weight of the grip and specimen was applied to the load recorded by the software.

Three crosshead speeds were employed (0.2, 0.5 and 1.0 $cm.min^{-1}$) which corresponded to the speeds employed in the hysteresis energy loss tests. The crosshead was set in motion and the progress of the crack was recorded onto videotape.

The same video apparatus as used in the measurement of Poisson's ratio was again employed to record the progress of the crack. The standard camera lens and extension tubes were, however, replaced with a travelling microscope. The use of the microscope allowed a much higher degree of magnification enabling a recorded image which captured the crack opening in detail and precise identification of the onset of crack propagation. At the high magnification employed, particles of dirt present on the lenses in the imaging system were detected as darkened spots on the image, it is important to note that these are not specimen imperfections. The S-VHS VCR recorded the signal from the digital frame numbering device onto each frame of the videotape record and a LED placed in the field of view of the camera allowed the precise moment of the test start to be identified. The travelling microscope and camera tracked the progress of the crack as it propagated through the specimen. The distance the travelling

microscope moved was measured by a micrometer fixed into the mount. A graticule which was internally fitted into the microscope enabled the calculation of the crack length. The time taken for the crack tip to pass from a designated graticule mark to the same mark after the stage had been shifted a known distance along the crack path, was calculated from the difference in the respective frame numbers of the videotape. It was then a simple matter to calculate the crack velocity.

The onset of crack propagation was precisely identified and the difference in frame numbers from test start to the instant of crack tip advance was used to calculate the critical strain. Fracture tests were performed on all types of aged and unaged specimens, and the critical strain and stress determined.

FRACTURE ENERGY MEASUREMENTS

The modified fracture mechanics method outlined by Ho and Tod[3] was employed to measure the fracture energy of the PICTOR propellant and inhibitor. Standard SEN specimens were machined from unaged slabs of propellant and inhibitor, the preparation of which has been described previously. The propellant specimens measured 100×25×5 mm and inhibitor 100×25×1 mm. Firstly, the hysteresis ratio for each material at a crosshead speed of 0.5 $cm.min^{-1}$ and at each of –40°C, 25°C and 60°C was measured using uncracked specimens. The specimens were loaded into the Instron by clamping in the usual manner and the hysteresis ratios generated from the calculated stress-strain data by adhering to the experimental method described in the section titled Hysteresis Energy Loss Measurements.

To measure fracture energy a sharp crack of 5 mm length was inserted into a number of SEN specimens prior to clamping in the Instron tensile testing machine. Analogue to digital conversion and collection of the load data as well as video recording the crack test to

determine the instant of crack propagation has been described previously. The critical input strain energy density is determined by calculating the area under the stress-strain curve of the fracture test to the instant of crack propagation (the critical strain level). The critical recovered strain energy density can then be obtained from the expression:

$$W_{rc} = W_i(1 - h_r)$$

The fracture energy of a SEN specimen is then calculated from the expression given by Kinloch and Tod[1] (which was derived from the equation of Rivlin and Thomas[43]):

$$G_c = \frac{2\pi a W_{rc}}{(1+\varepsilon_c)^{½}}$$

Tests for fracture energy were conducted on the propellant and inhibitor at a crosshead speed of 0.5 cm.min^{-1} and at –40°C, 25°C and 60°C, which corresponds to those conditions used in the hysteresis tests.

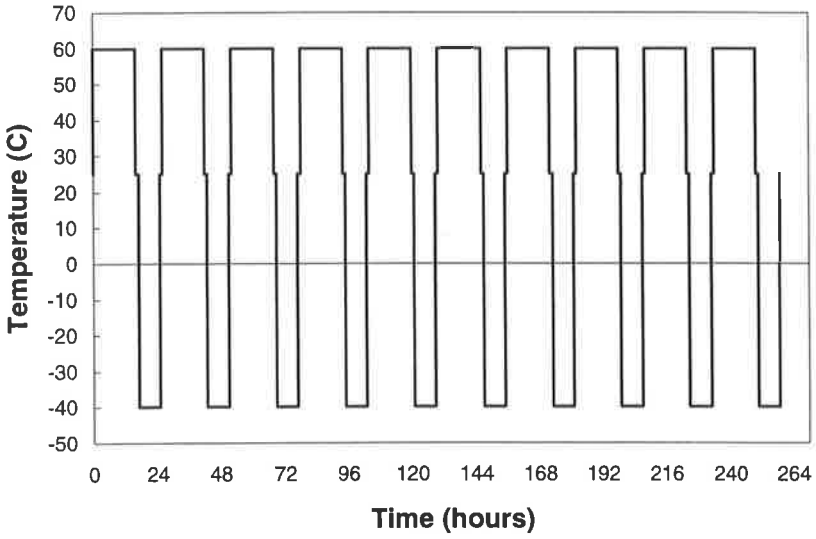

Figure 1 Temperature conditions for thermal shock

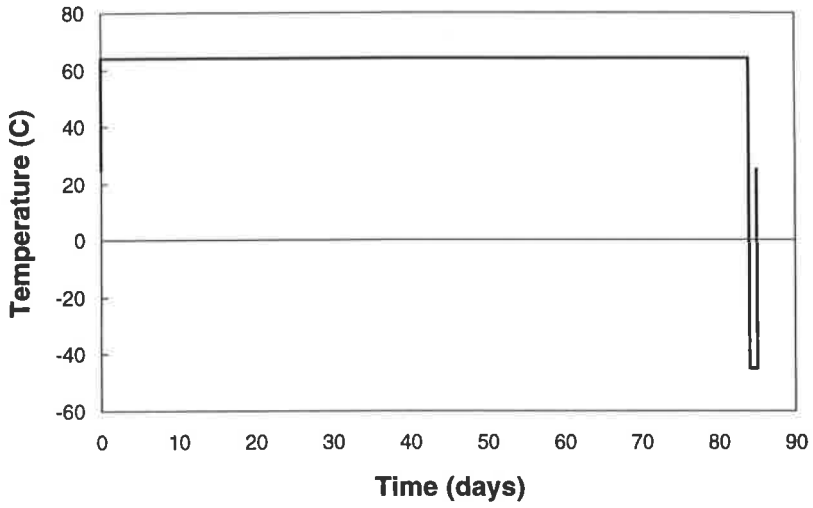

Figure 2 Temperature conditions for accelerated ageing

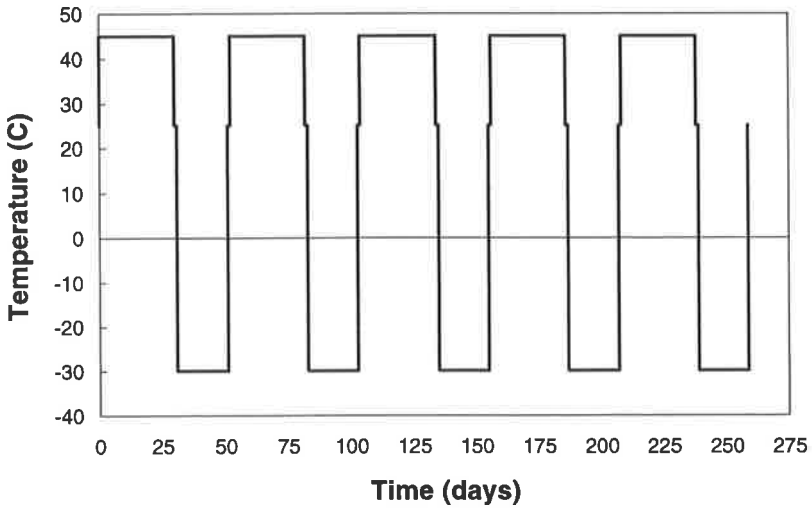

Figure 3 Temperature conditions for thermal cycle

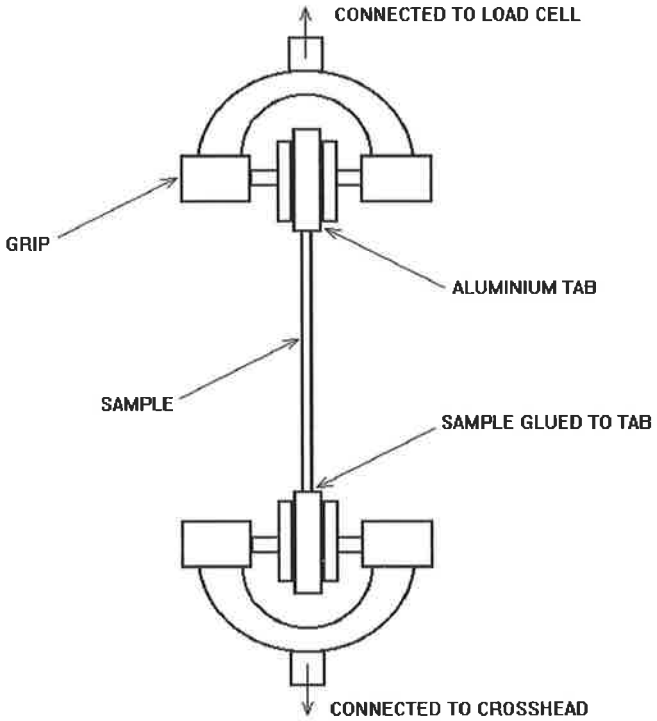

Figure 4 Specimen geometry and application of grips for measurement of Poisson's ratio

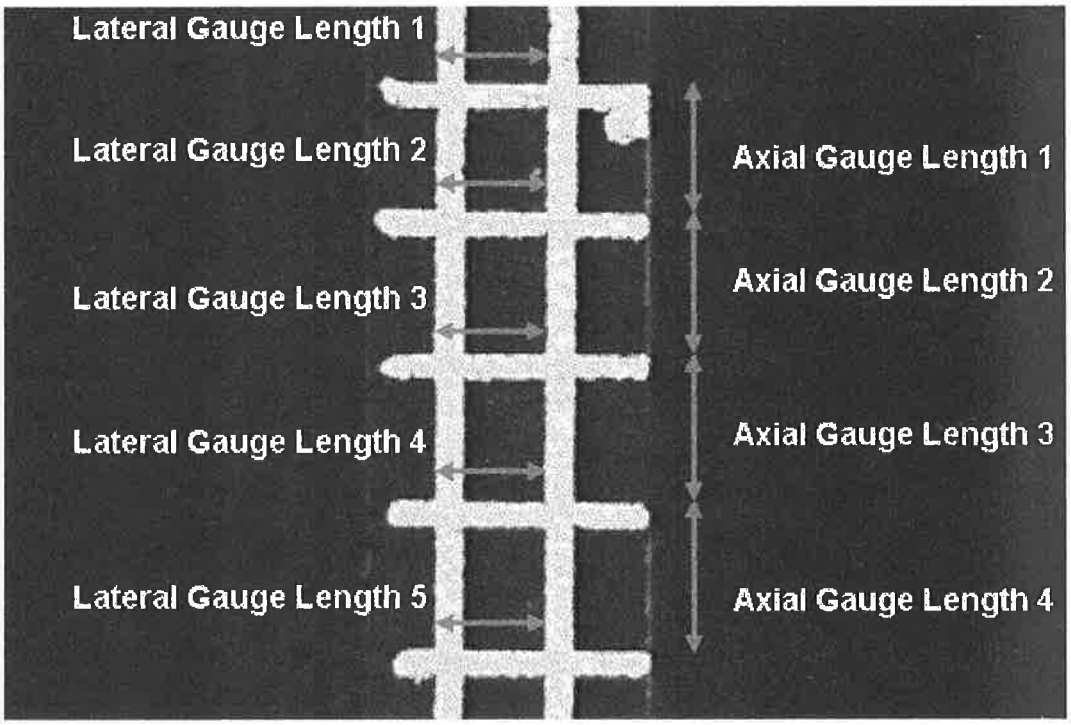

Figure 5 Image of propellant specimen from video record showing gauge lengths

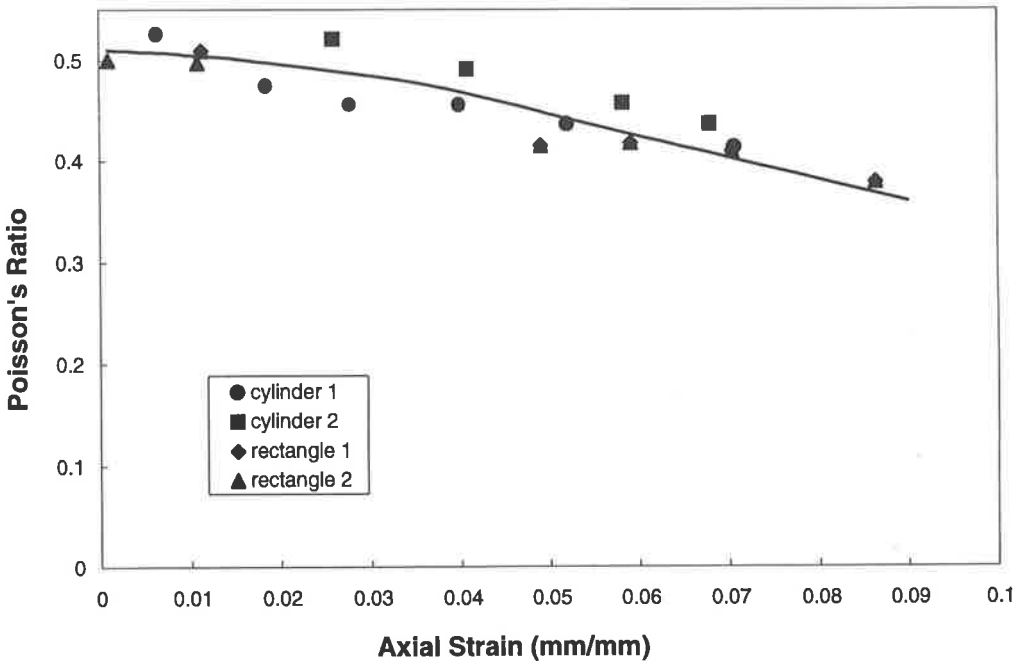

Figure 6 Change in Poisson's ratio for different propellant specimen geometries, T=25°C

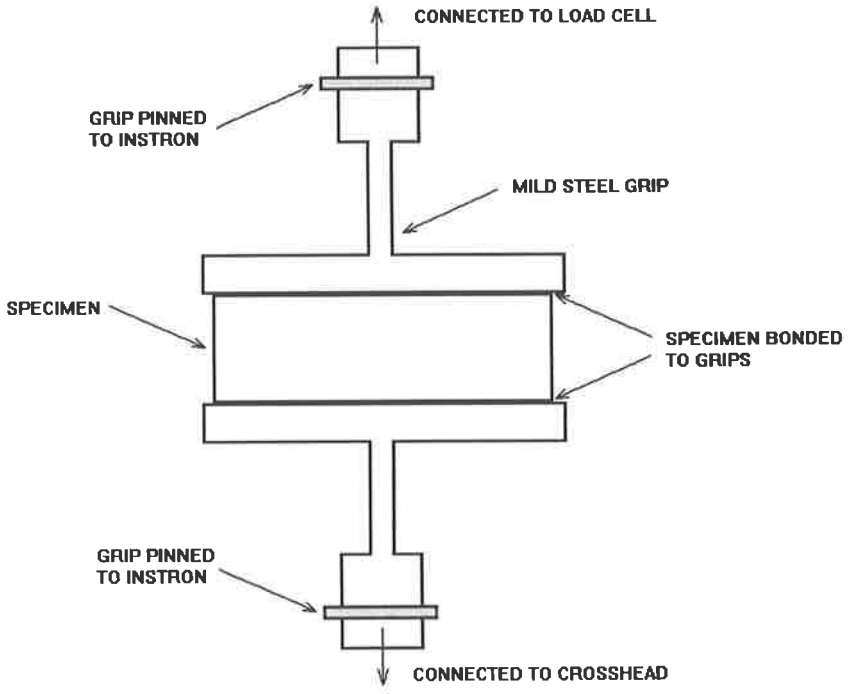

Figure 7 Sample geometry and grip application for hysteresis energy loss test

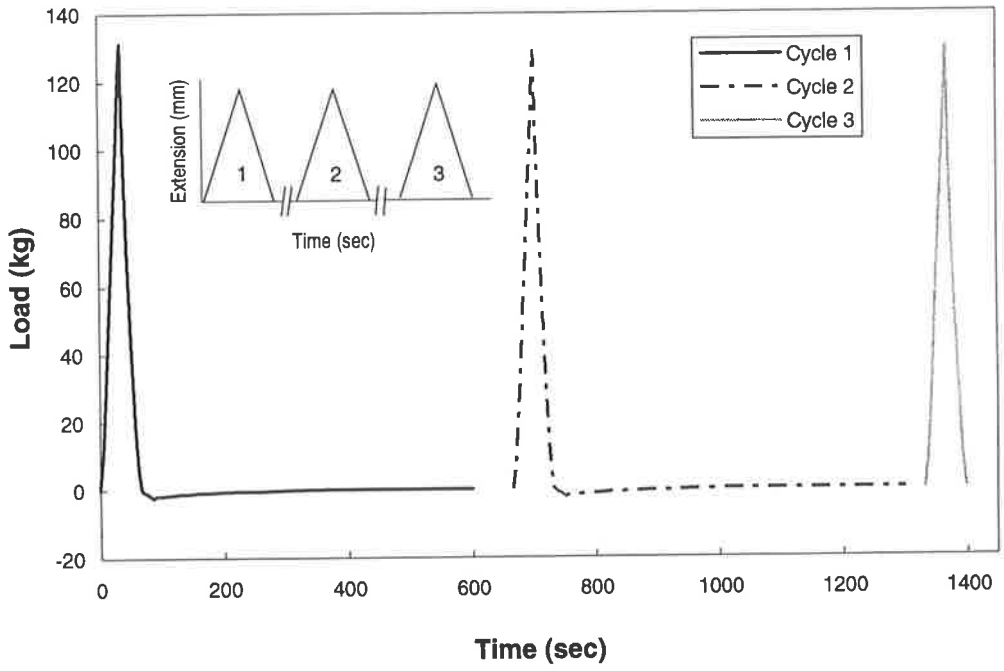

Figure 8 Load against time for propellant hysteresis, T= –40°C (unaged, $\dot{\varepsilon} = 0.00077\ s^{-1}$)

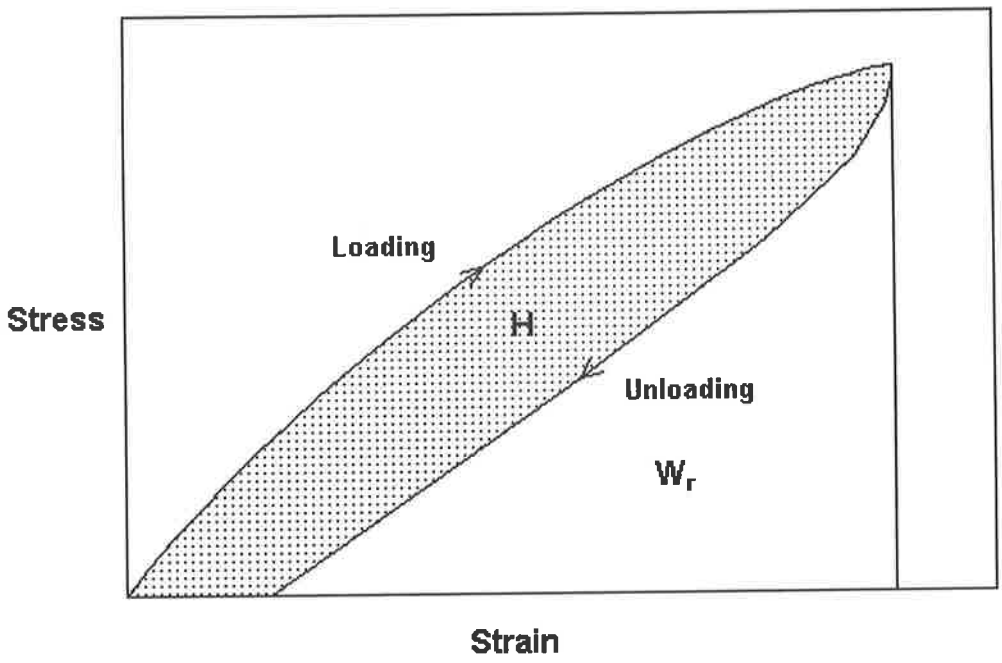

Figure 9 Hysteresis curve showing strain energy densities

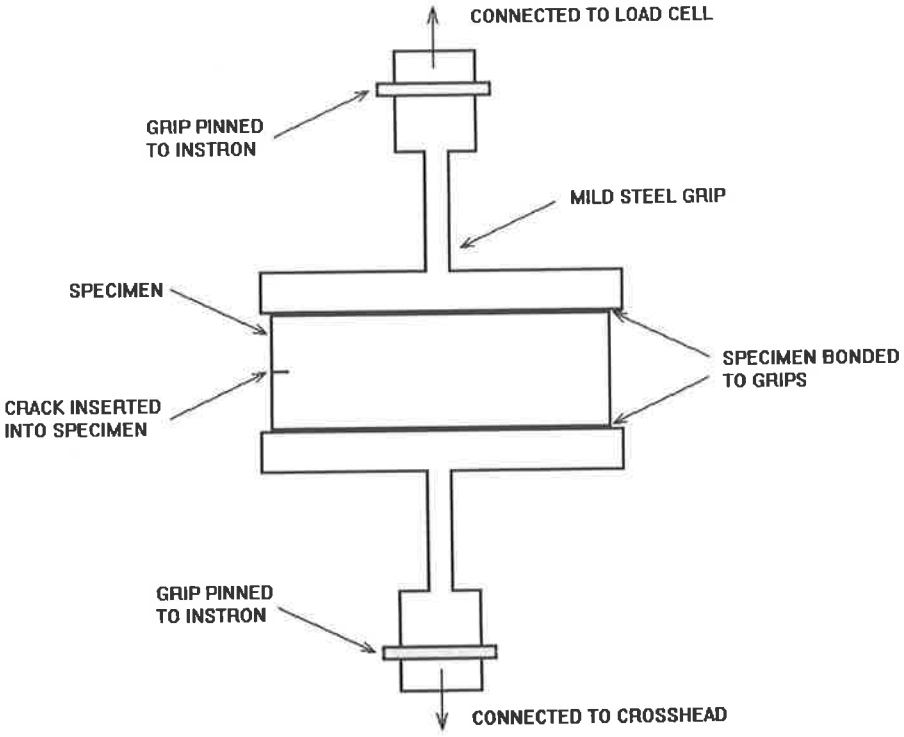

Figure 10 Sample geometry and grip application for crack propagation test

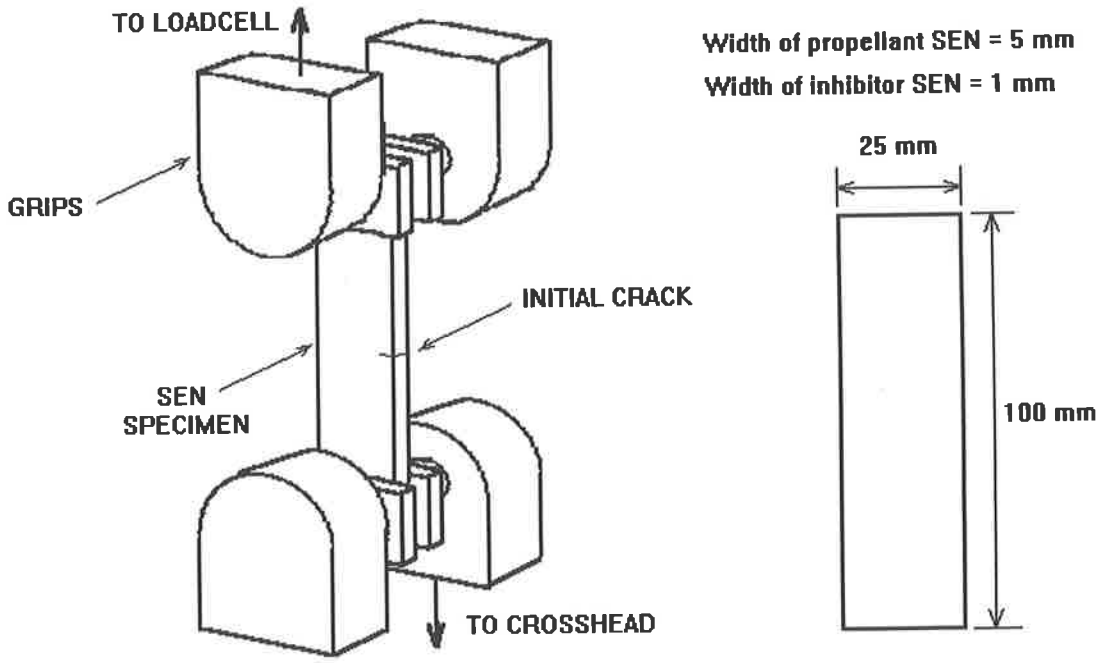

Figure 11 Dimensions and application of grips for SEN specimens

Chapter IV
Results and Discussion

THERMAL EXPANSION

Divergent values of thermal expansion coefficient for the individual materials employed in the PICTOR rocket motor will cause thermal stresses to arise in those rocket motor components consisting of two materials bonded together. Differences in the thermal expansion of each material will occur during temperature gradients associated with thermal loads. The thermal expansion coefficient of each material is also a function of temperature and temperature gradients in the bulk of the material will result in thermal stresses. In a particulate material there will be a large difference in the thermal expansion coefficients of the binder and filler, resulting in thermal stresses at the binder/filler interface as the material temperature rises or falls.

These thermal stresses are capable of causing crack initiation and propagation in the bulk or at the interface between two materials. A greater divergence in the values of thermal expansion coefficient for materials subjected to ageing will lead to increased stress gradients. Hence, an investigation of the thermal behaviour and the effect of ageing on this behaviour for the materials employed in the PICTOR rocket motor was conducted.

In the first instance specimens of all materials were prepared for thermal mechanical analysis and a number of heating and cooling runs performed on each to determine the repeatability of the expansion results. The thermal expansion results in repeated tests of propellant and inhibitor were in very good agreement. The average deviation in the absolute value of the thermal expansion between initial and repeat results for the propellant was 6% (Figure 12

shows a comparison for two heating runs). Figure 13 shows a cooling run for the inhibitor material, the average error in the thermal expansion for inhibitor was 2%.

The standard deviation of the instantaneous thermal expansion coefficients, calculated over the temperature range of the tests for the insulation was 10.7% (see Figure 14). By comparison the standard deviation of the thermal expansion coefficients over the range of test temperatures employed was 10.4% for the propellant, 3.3% for the inhibitor and 6.5% for the epoxy.

In the first heating run conducted on the epoxy, an unexpected contraction of the specimen occurred from 59°C to 64°C (see Figure 15). After heating, the specimen was subjected to a cooling run, under TMA control, and a repeat heating run was performed. During the second heating run the specimen did not exhibit any contraction. This procedure was repeated several times on unaged (ie., "as received") specimens of epoxy from different production batches and in each case some contraction of the specimen occurred during the first heating run only. Two repeat heating runs on an unaged specimen of epoxy is shown in Figure 16.

The behaviour exhibited in the initial run of the unaged epoxy is consistent with that expected due to the influence of a small amount of absorbed moisture. The weight and dimensions of each epoxy specimen was recorded prior to loading into the TMA for testing. When re-weighed on completion of the test an average weight loss of approximately 2% was noted, however no change in specimen dimensions were recorded. Therefore, the moisture present does not have a detectable effect on the swelling of the epoxy. The moisture present was liberated during the first heating run.

A sheet of epoxy resin was placed in an oven at 60°C for a period of three days. It was then placed in a humidity chamber containing a saturated solution of barium chloride which provides an atmosphere in the chamber of approximately 90%RH for a temperature range of

20°C to 30°C. At various times specimens cut from the sheet were tested to determine the extent on the thermal expansion behaviour of moisture absorption.

Runs 1, 2 and 3 were performed on the specimen after the 72 hours storage at 60°C. The significant portion of the results from these runs are highlighted in Figure 17 (the experiments were conducted over the temperature range −60°C to 70°C). No contractions are present, hence any absorbed moisture was liberated by preheating the specimen. The resulting thermal expansion curves were identical (the result from run 3 was not plotted). The specimen was then placed into the humidity chamber for 15 days, prior to retesting.

A contraction of the specimen at 41°C in run 4 can be seen. On release of moisture from the epoxy the specimen stops expanding. After some time, the moisture liberation ceases and the specimen begins to expand again. Run 5 was conducted immediately and while no contraction was observed, the resulting curve shows a slightly higher thermal expansion than those of runs 1 and 2. This would tend to indicate that not all the intermolecular moisture was released during run 4 (this was confirmed from the measurement of the moisture content of the specimen, which fell only from 1% w/w prior to run 4 to 0.9% w/w after run 5) and that it contributes to the total thermal expansion of the specimen.

Similar behaviour was observed after continued storage in the humidity chamber. Run 6 shows a decrease in the expansion above 45°C and the thermal expansion in Run 7 (conducted immediately) was greater than that in run 2 due to the contribution of the moisture present.

The moisture absorbed by the epoxy may cause swelling and plasticise the polymer, leading to a reduction of the mechanical properties.[48,49,50] The consequence of swelling may be increased internal stresses which can contribute to material failure.[49] The effect of absorbed moisture

exhibited here indicates that care should be taken to ensure effective sealing to prevent exposure of the rocket motor components to atmospheric air.

It should be noted that the other polymers employed in the PICTOR rocket motor did not exhibit any effects due to absorbed moisture during the experiments, nor did the weight or dimensions of the specimens vary from those before testing.

All materials were tested to examine the extent of material isotropy. It may be that the direction of casting or inhomogenities may influence the isotropic nature of some materials. Knowledge of a materials isotropic behaviour or otherwise will become critical when modelling the thermal expansion of the rocket motor. Non-isotropic materials will require that the Poisson's ratio in each of the two perpendicular and the lateral direction be known. For isotropic materials, however, the resultant contractions in the two lateral directions from the longitudinal expansion will be equal, thus only one value of Poisson's ratio is required.

Three specimens of each material were prepared for TMA. Each of the three specimens were tested across axes perpendicular to one another. It was noted that the epoxy, inhibitor and propellant exhibit the same characteristic expansion regardless of the specimen orientation as prepared from the cast material. Figure 18, Figure 19 and Figure 20 show a comparison of these materials for the three axial orientations during various heating and cooling runs. The materials can be considered isotropic over the range of test temperatures and stresses.

The insulation material was found to be of a non-isotropic nature. Figure 21 shows that the lateral and longitudinal thermal expansion measurements vary. The lateral tests were carried out with the adhesive bondline between the two sheets of insulation orientated parallel to the direction of the expansion measurement, whereas the longitudinal test measured the expansion perpendicular to the bondline. The presence of the bondline at the different orientations can be

seen to affect the value of thermal expansion measured. It acts to constrain expansion in the longitudinal direction as compared to that in the lateral direction. When bonded into the rocket motor casing the orientation of the insulation is such that only longitudinal expansion and contraction will be critical to rocket motor performance under thermal loading. Therefore only the longitudinal expansion and contraction will be measured in this study.

The susceptibility of the materials employed in the PICTOR rocket motor to physical ageing was tested. Physical ageing is the time-dependent, asymptotic collapse of free volume trapped inside the entangled chain segments. When a material susceptible to physical ageing is quenched to a temperature below its glass transition there will be no clear transition on slowly reheating the material to above the T_g. While the material is held below the glass transition temperature the trapped free volume will collapse at a very slow rate, the possibility exists for moisture absorption into the free volume before the material reaches an equilibrium state. Specimens of propellant, inhibitor and insulation were placed in an oven at 25°C and a specimen of epoxy at 90°C, for 20 minutes. The TMA cell was equilibrated 20°C below the glass transition temperature of the material to be tested. The specimen was quickly moved from the oven to the TMA cell to quench it and then subjected to a slow heating run. For the conditions of the tests performed here none of the materials exhibited the artifacts associated with physical ageing, all had a clear transition point in the expansion curve.

The instantaneous thermal expansion coefficient was calculated as the slope of the tangent to the material's thermal expansion curve at each temperature. The thermal expansion coefficients at 10°C intervals over the range –45°C to 65°C were calculated from tests performed on aged and unaged specimens.

The coefficient of thermal expansion of a composite polymer filled with particles having a much lower thermal expansion coefficient will be reduced relative to that of the unfilled polymer.[18] The extent of the difference between the thermal expansion coefficient of unfilled HTPB and propellant can be seen in Figure 22. The rule of mixtures was employed to calculate an approximate value for the thermal expansion coefficient of the ammonium perchlorate (and ammonium sulphate) particles at each temperature. The more rigid AP particles have a much lower coefficient of thermal expansion which cause the overall thermal expansion coefficient of the propellant to be much reduced compared to the unfilled HTPB. Similar behaviour can be seen from the addition of ammonium sulphate (AS) particles to the polyurethane in Figure 23. The overall thermal expansion coefficient of the inhibitor is decreased as compared to the pure polyurethane.

The difference in the thermal expansion coefficients of the pure polymers and the filler particles will result in the development of stresses in the binder matrix and at the binder/filler interface as the material temperature changes during the thermal loadings. The expansion/contraction of the binder is greater than the filler per degree temperature change. When the composite contracts the binder material strained between the filler particles may fail or the binder/filler bond may fail, resulting in dewetting of the filler particle.[18] It is noted that the difference in the thermal expansion coefficient of the HTPB and propellant (HTPB+AP) is almost constant across the entire test temperature range. Whilst there is a minor difference between the thermal expansion coefficient of the polyurethane and inhibitor at low temperature, it is significant at the higher temperatures. The thermal expansion coefficient of the AS particles is roughly constant over the temperature range.

The difference in thermal expansion coefficients between materials that are bonded together will result in a stress discontinuity at the interface of the two materials when thermal loadings

cause strain in the materials, with the potential to cause bondline cracking. A comparison of the thermal expansion coefficients for the unaged polymeric materials employed in the PICTOR rocket motor is presented in Figure 24. The figure shows that the effective difference in thermal expansion coefficients of the various materials after accounting for errors, is significant. The epoxy resin had the lowest thermal expansion coefficients ranging from 44.4 to 86.9 μm/m/K, whilst the insulation the highest ranging from 187.9 to 233.6 μm/m/K.

Of particular interest is the difference between the thermal expansion coefficients of the propellant and inhibitor. The thermal expansion coefficient of the propellant varied with temperature from 90.2 to 124.8 μm/m/K and the inhibitor's from 58.9 μm/m/K at –45°C to 163.5 μm/m/K at 65°C. It can be seen from Figure 24 that the difference in the thermal expansion coefficient of the propellant and inhibitor was greatest at the lower and upper bounds of the temperature range and therefore when the temperature of the two materials approach these limits the stress discontinuity across the interface will be maximised. When subjected to environmental conditions which cause the temperature in the rocket motor to increase the inhibitor expands at a higher rate than the propellant and a compressive stress forms at the interface. As the temperature decreases from ambient to sub-zero the propellant will tend to contract a larger amount per degree of temperature than the inhibitor, a tensile stress will develop at the interface. The presence of the tensile stress provides a loading state which may be capable of causing crack initiation and/or propagation at the bondline.

The inhibitor will behave in a glasslike manner at –45°C (see Table 1) compared to that at ambient temperature, more specifically, the modulus will be increased and the strain to failure decreased.[18] Hence, the stress levels arising in the inhibitor in response to the thermal strain will be significantly increased. This may increase the propensity for cracking at the interface.

Another important interface is that of the epoxy and inhibitor, if this bond fails the charge may no longer be adequately fixed to the rocket motor casing. At sub-zero temperatures the thermal expansion coefficient of the two materials was quite close, whilst a substantial difference occurs at high temperature. Again tensile stresses which develop in response to thermal strains may provide enough energy to cause crack initiation and/or propagation. The stress in the epoxy will be influenced by the fact the material is below the glass transition temperature for the entire range of temperatures seen here (see Table 1).

The thermal expansion coefficient, modulus, specific heat and many other properties all undergo an abrupt change at the glass transition temperature. The glass transition temperatures of all the materials were calculated from the curves of thermal expansion versus temperature and are shown in Table 1. Over the range of test temperatures studied the epoxy was below the glass transition, whilst the propellant and inhibitor materials were above it. The epoxy will behave in a brittle, glassy manner and the inhibitor, propellant and insulation in a flexible, rubbery manner for most temperatures in the range of interest.

During prolonged thermal cycling the materials will age. The chemical changes within the material, for example, oxidation and increased cross-linking may affect the thermal expansion behaviour and the glass transition. Changes in a material's thermal expansion behaviour may affect the magnitude of stresses arising from the strains associated with thermal loading and ultimately the propensity for crack propagation.

The glass transition temperature of the propellant increased slightly after the accelerated ageing due to increased cross-linking between the binder chains.[20] A graph of the thermal expansion behaviour for accelerated aged propellant compared to that of unaged propellant is shown in

Figure 25. The change in the glass transition temperature is indicated by the guidelines, which show the position of the transition for each specimen.

The effect of both the thermal shock and thermal cycle loadings on the glass transition temperature of the propellant was negligible. No literature detailing the chemical reactions present during these thermal loads was located, hence no evidence for increased cross-linking exists. Ageing resulting from thermal cycling and shock will include similar processes and it can be assumed that some additional cross-linking will occur. However, only a minimal amount of additional cross-linking is likely to have occurred during the thermal cycle and thermal shock due to the limited periods at elevated temperature in comparison to accelerated ageing. The minor change in glass transition temperature observed could not be attributed to any particular cause as it falls within the range of error for the measurement.

The glass transition temperature of the inhibitor increased when the material was subjected to accelerated ageing, again this was most likely caused by increased cross-linking in the binder chains of the material. Differences in the glass transition temperature after the material was subjected to the thermal shock and thermal cycle are not significant, the values remained almost constant.

The glass transition temperature of the insulation has not changed significantly after the material was subjected to the thermal loadings. The temperature employed in the accelerated ageing test is significantly below the specified cure temperature of EPDM (155-165°C), there appears to be no further vulcanisation occurring when the material was exposed to the accelerated ageing conditions.

It can be seen that the glass transition temperature of the epoxy increases beyond 70°C (the upper temperature of the range used for these tests) after being subjected to accelerated

ageing. This results from increased cross-linking of the epoxy chains caused by continued curing reactions.[20] For the thermal cycle and thermal shock the glass transition temperature increased very slightly. The limited time spent at an elevated temperature during each of these cycles allows only a minor increase in the cross-linking.

Table 1 Glass transition temperatures of aged materials

	T_g Propellant	T_g Inhibitor	T_g Insulation	T_g Epoxy
Unaged	–75.5°C	–42.7°C	–47.8°C	58.8°C
Accelerated Ageing	–73.4°C	–40.2°C	–48.0°C	>70.0°C
Thermal Cycle	–75.0°C	–42.3°C	–47.6°C	59.9°C
Thermal Shock	–75.8°C	–42.8°C	–47.4°C	60.1°C

The thermal expansion coefficients of all the aged and unaged materials are plotted against temperature in Figure 26 to Figure 29. The thermal expansion coefficients plotted are an average value calculated from tests performed on several specimens of aged materials.

Figure 26 shows the results for the epoxy specimens. The difference in the thermal expansion coefficients of the accelerated aged and the unaged epoxy was negligible, except below –20°C were the thermal expansion coefficient for the accelerated aged epoxy is slightly greater than that of the unaged epoxy. The thermally shocked epoxy displayed thermal expansion coefficients greater than that for the unaged material over the entire range of temperatures. Whilst the epoxy that was thermally cycled has similar values of thermal expansion coefficient to the unaged material over most of the temperature range, the values were greater above 40°C.

In Figure 27 the thermal expansion coefficients of the aged inhibitor specimens can be seen to be negligibly different from those of the unaged material. However, the accelerated aged

specimens have values of thermal expansion coefficient which increase at temperatures above 20°C. As a consequence of ageing the difference between the values of thermal expansion coefficient for the inhibitor and epoxy was reduced at temperatures above 20°C. The maximum difference in the thermal expansion coefficient of the unaged inhibitor and epoxy was 81.3×10^{-6} K^{-1} at 50°C, whereas after thermal cycling the maximum difference was reduced to 57.3×10^{-6} K^{-1} at 65°C (with lesser reductions for the other aged materials). This will affect the level of the strain discontinuity occurring at the bondline of these materials during thermal loadings, which in turn influences the propensity of crack initiation and propagation.

The variation in the thermal expansion coefficient for the aged and unaged insulation material is displayed in Figure 28. The effect of ageing on the thermal expansion coefficient of the insulation was inconclusive due to the large errors associated with the calculated values.

In Figure 29 we can see the effect of ageing on the values of thermal expansion coefficient for the propellant. The thermal expansion coefficient for the accelerated aged propellant does not vary greatly from that of the unaged material. The thermal expansion coefficient of the thermally shocked and thermally cycled materials do not varying from those of the unaged propellant at temperatures above 10°C. Below 10°C these specimens have decreased thermal expansion coefficients as compared to the unaged propellant. Figure 30 shows the thermal expansion coefficients for the thermally shocked propellant and inhibitor. The difference in the values of the thermal expansion coefficient at –45°C for the propellant and inhibitor has been reduced from 31.3×10^{-6} K^{-1} for the unaged specimens to 4.4×10^{-6} K^{-1} for the thermally shocked specimens. The consequence of this will be discussed later in conjunction with the discussion of the hysteresis behaviour and mechanical properties of the thermally shocked propellant specimens.

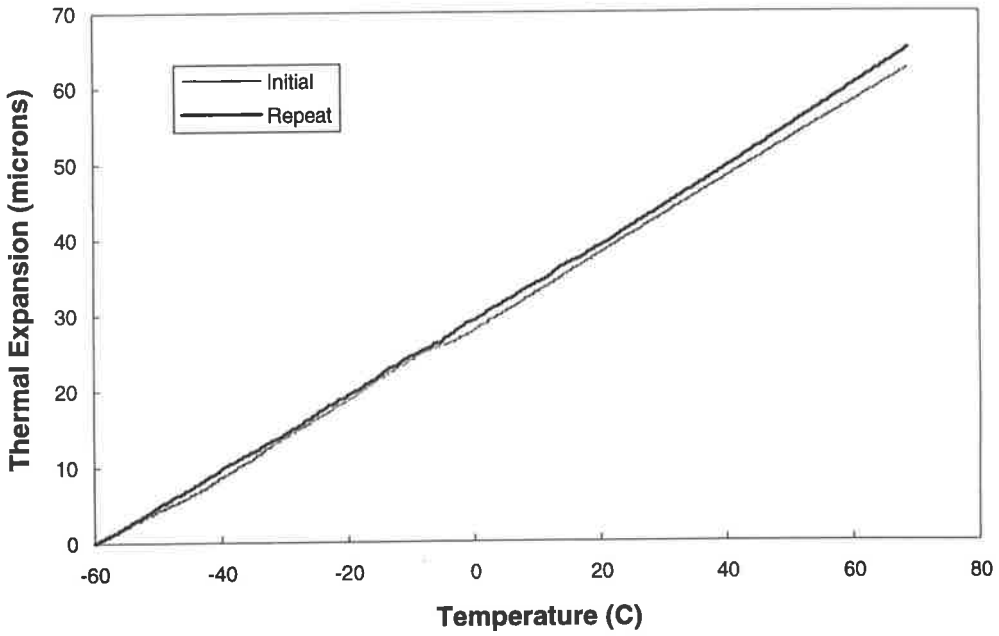

Figure 12 Repeatability of thermal expansion for propellant

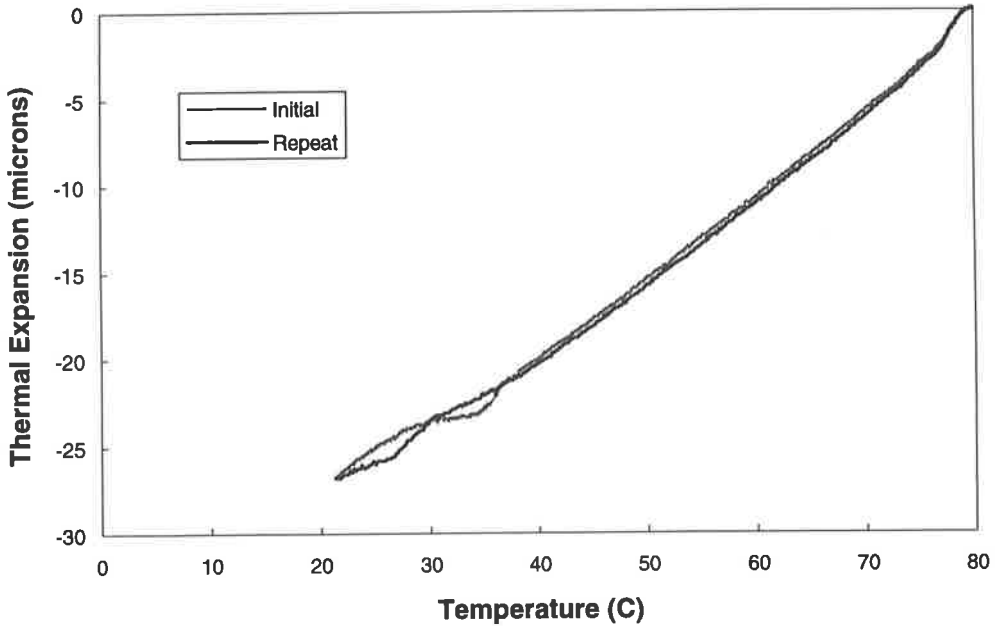

Figure 13 Repeatability of thermal expansion for inhibitor

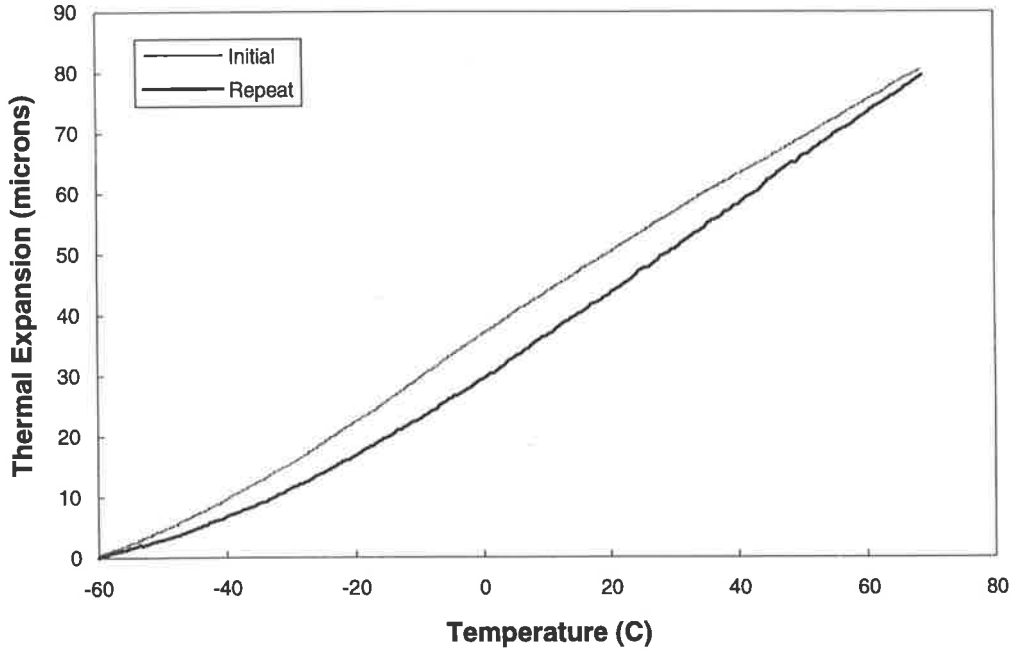

Figure 14 Repeatability of thermal expansion for insulation

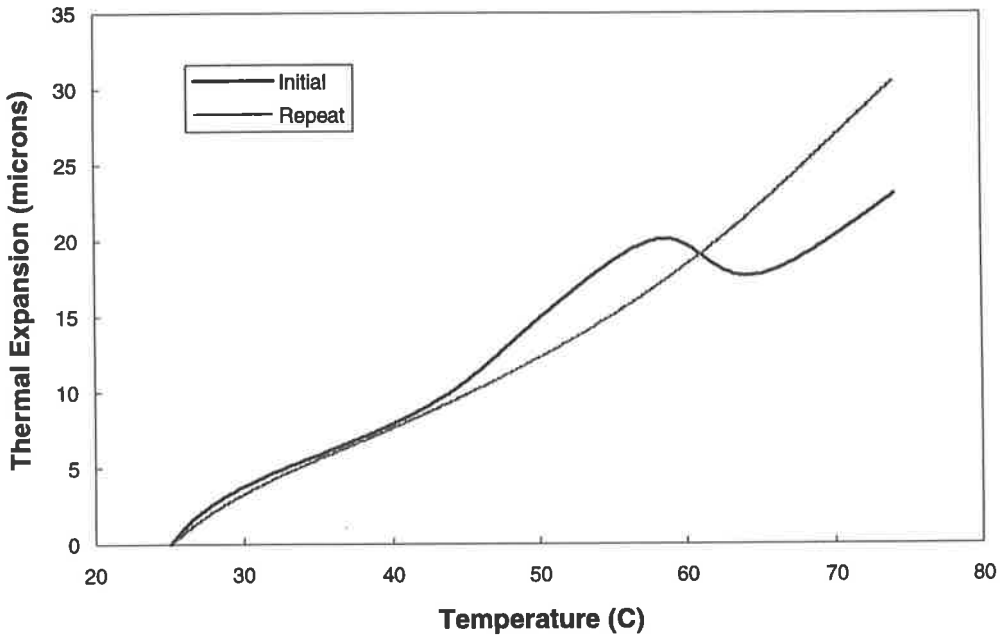

Figure 15 Effect of water during initial epoxy runs

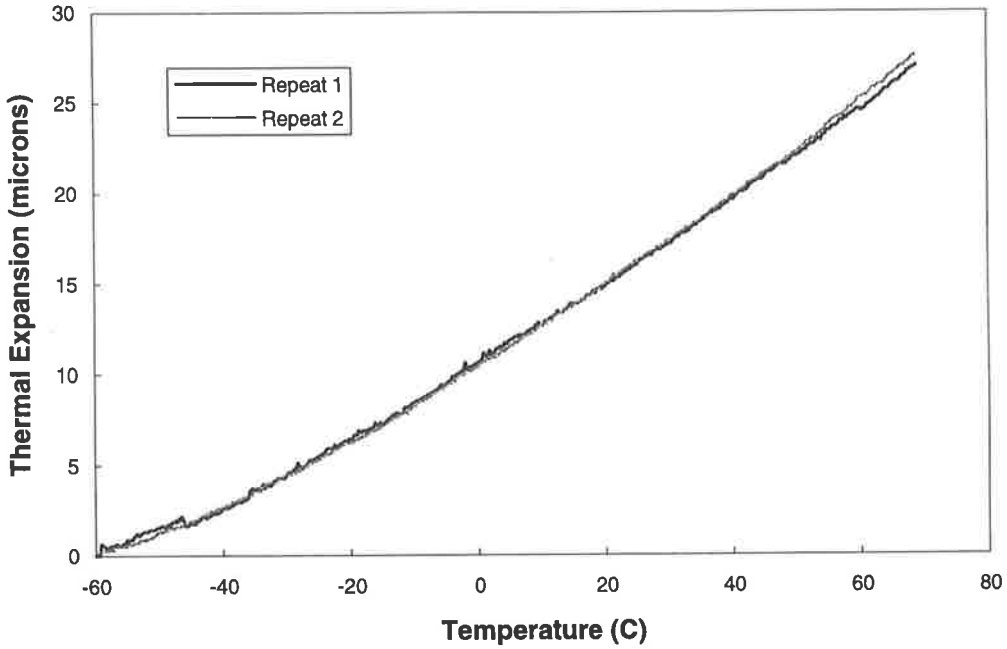

Figure 16 Repeatability of thermal expansion for epoxy

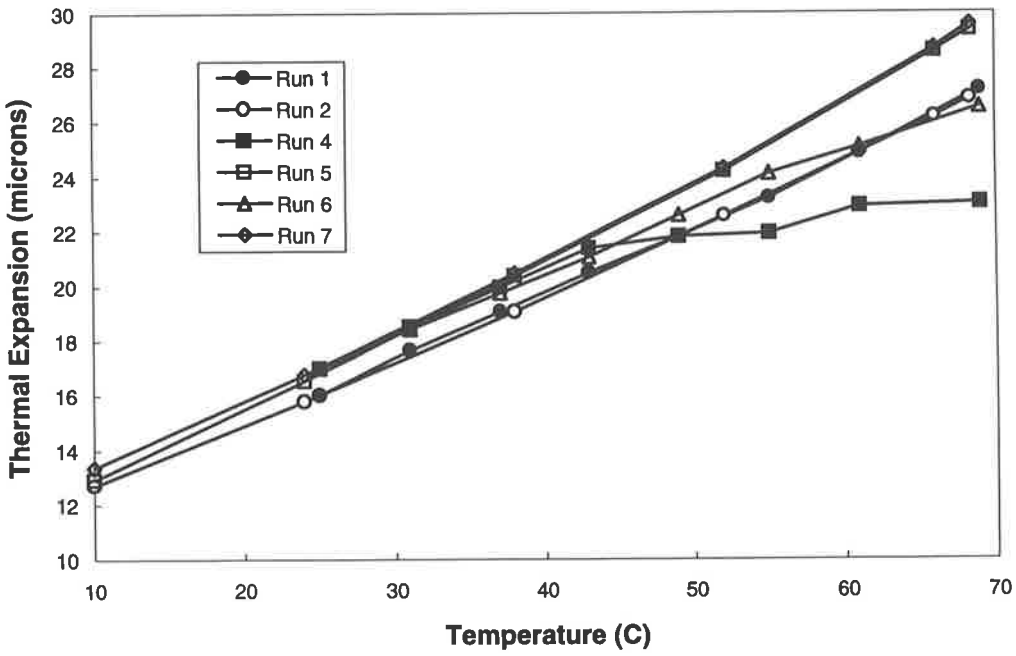

Figure 17 Effect of humidity on epoxy

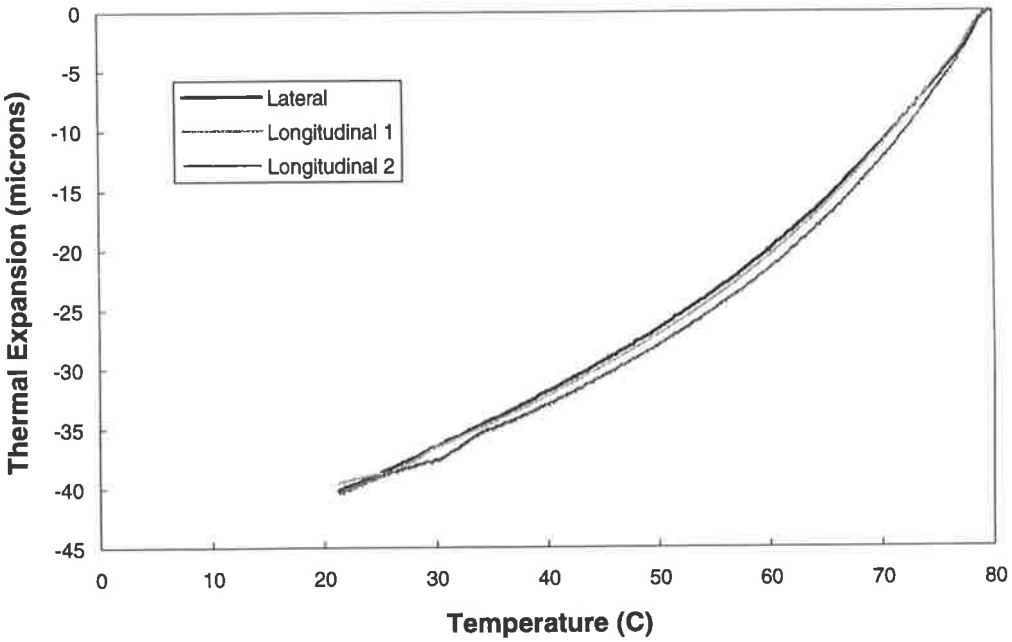

Figure 18 Isotropic nature of epoxy

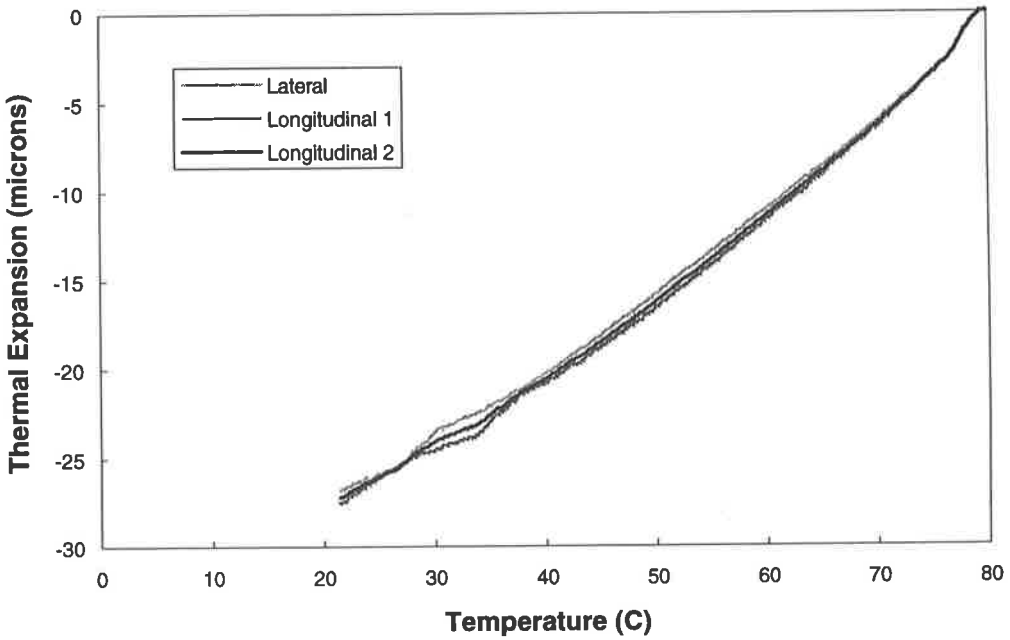

Figure 19 Isotropic nature of inhibitor

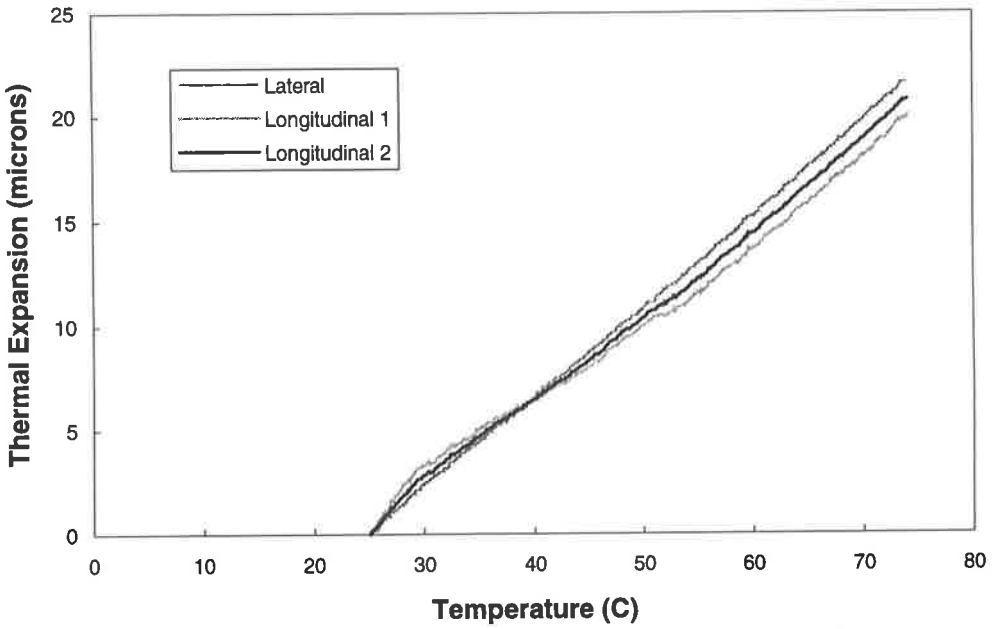

Figure 20 Isotropic nature of propellant

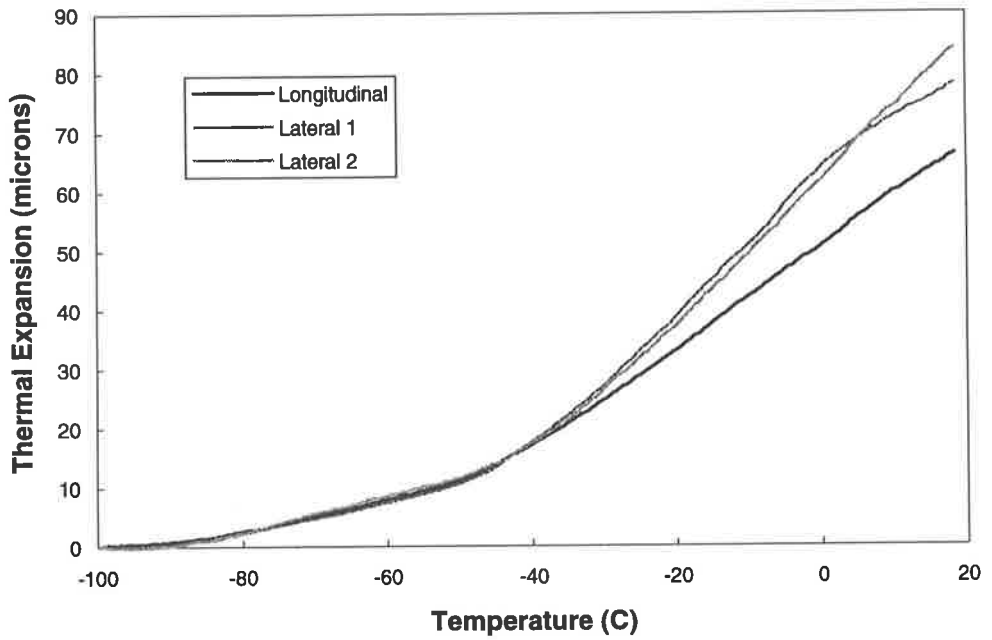

Figure 21 Isotropic nature of insulation

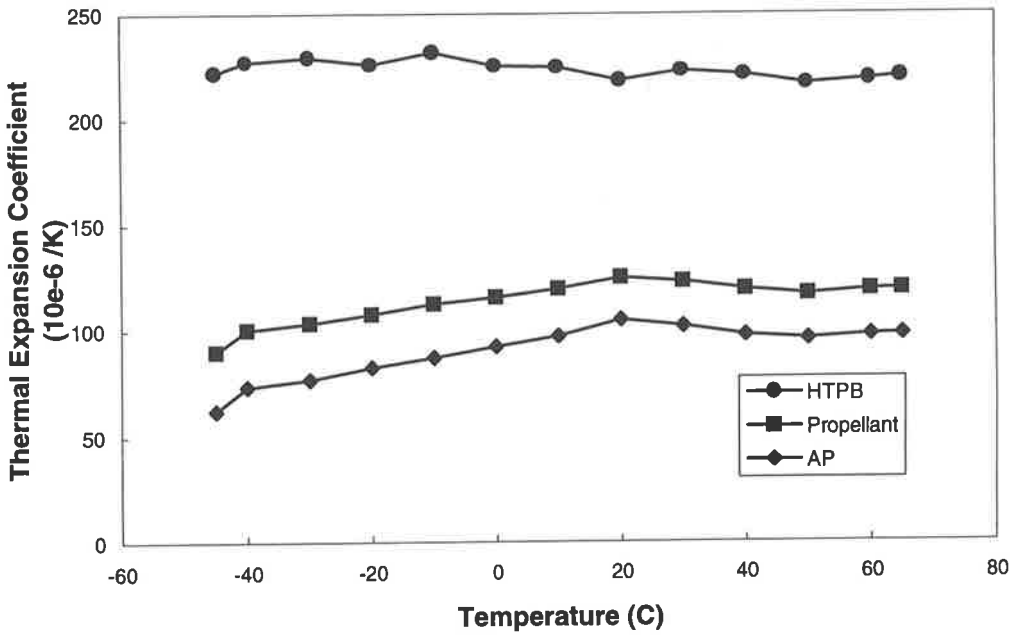

Figure 22 Effect of ammonium perchlorate filler in HTPB

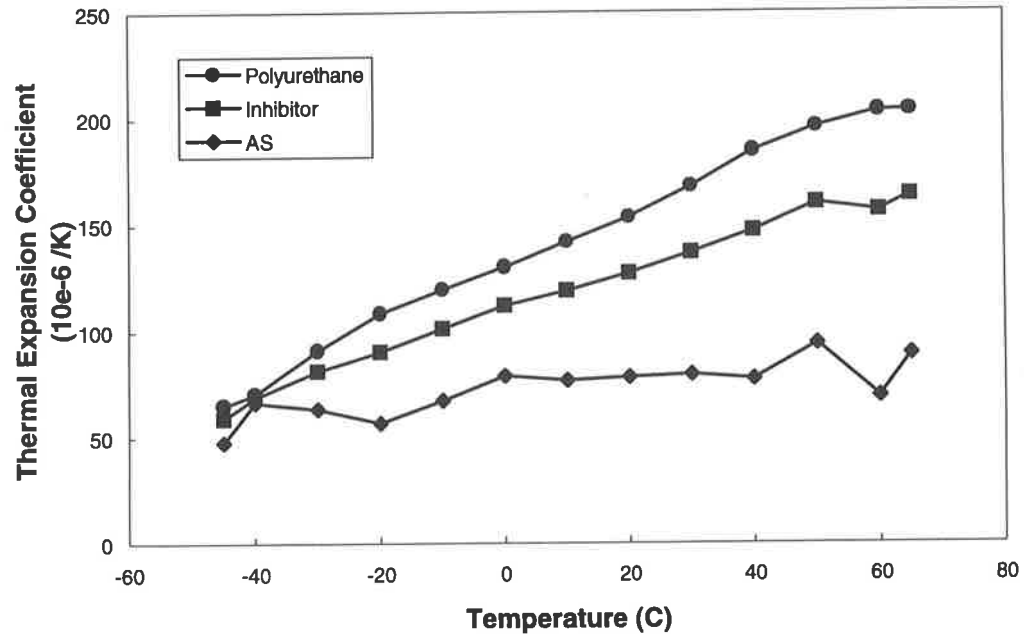

Figure 23 Effect of ammonium sulphate filler in polyurethane

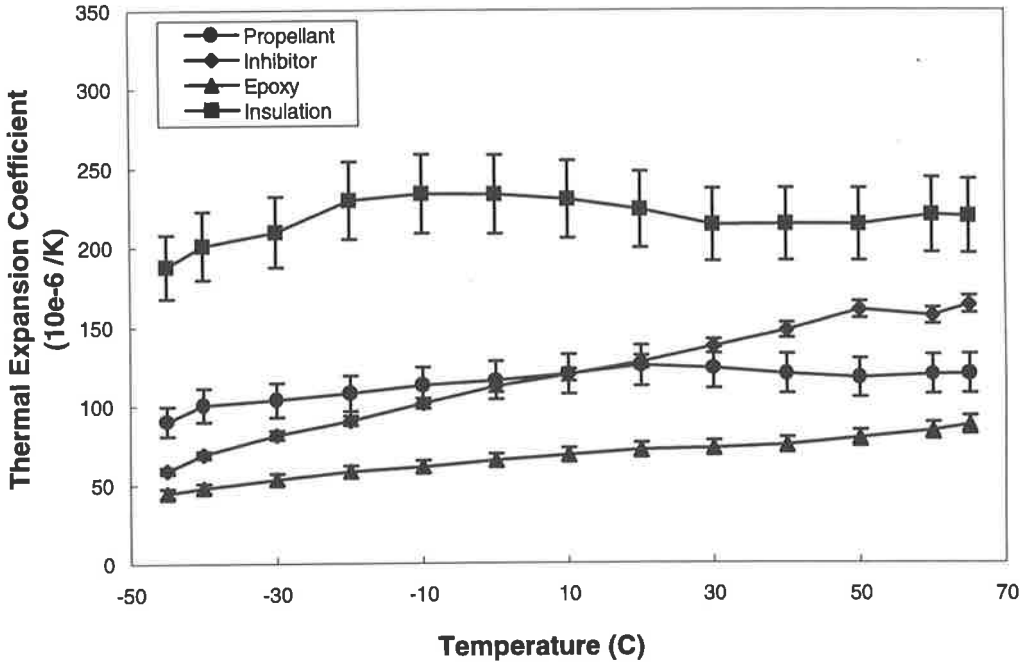

Figure 24 Comparison of thermal expansion coefficients for unaged materials

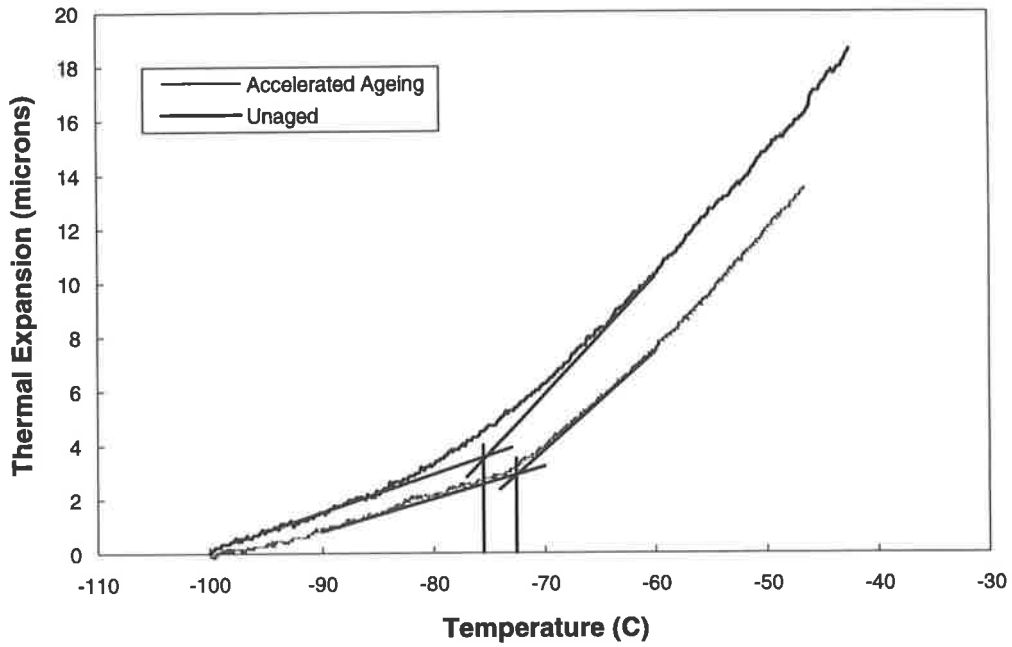

Figure 25 Effect of ageing on the glass transition temperature of propellant

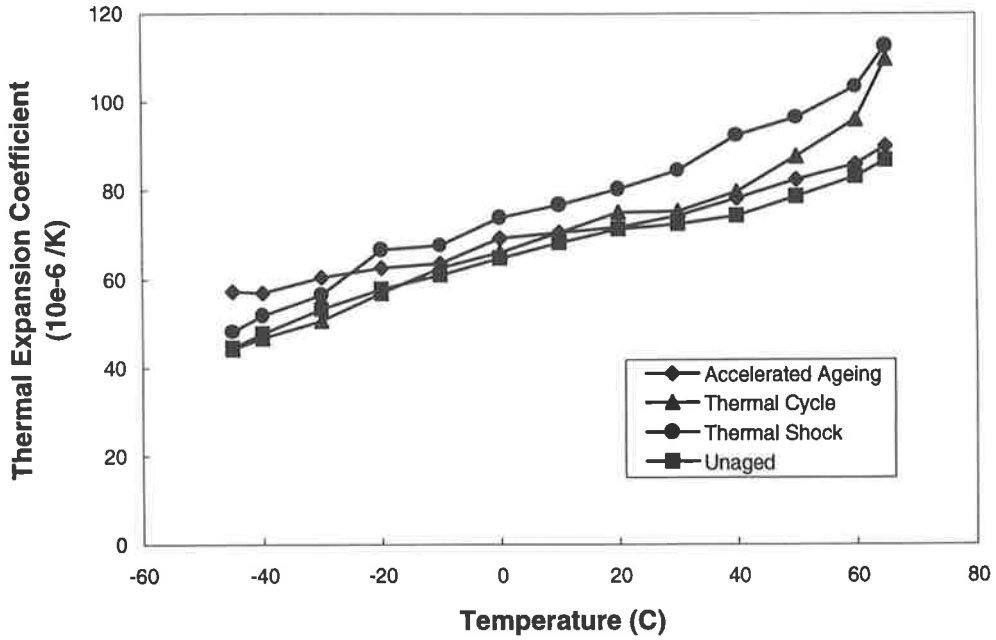

Figure 26 Effect of ageing on the thermal expansion coefficient of epoxy

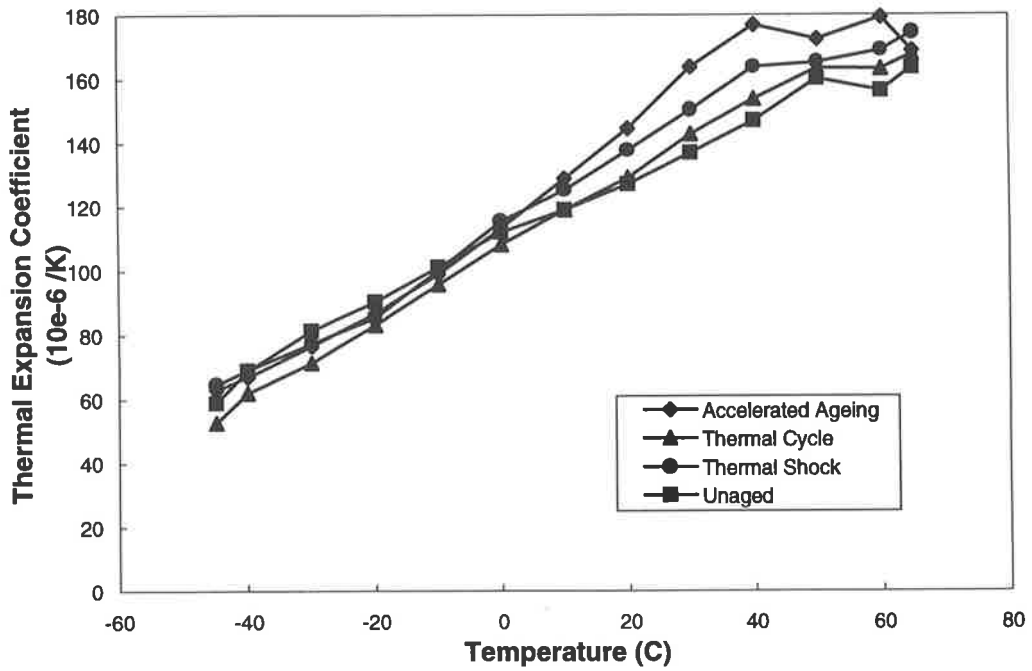

Figure 27 Effect of ageing on the thermal expansion coefficient of inhibitor

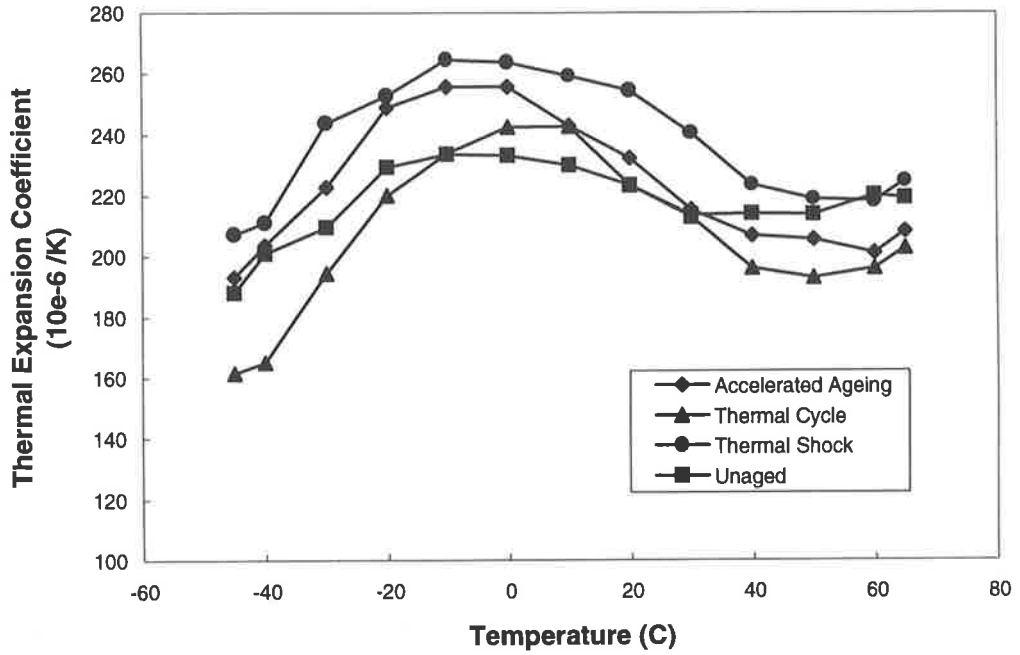

Figure 28 Effect of ageing on the thermal expansion coefficient of insulation

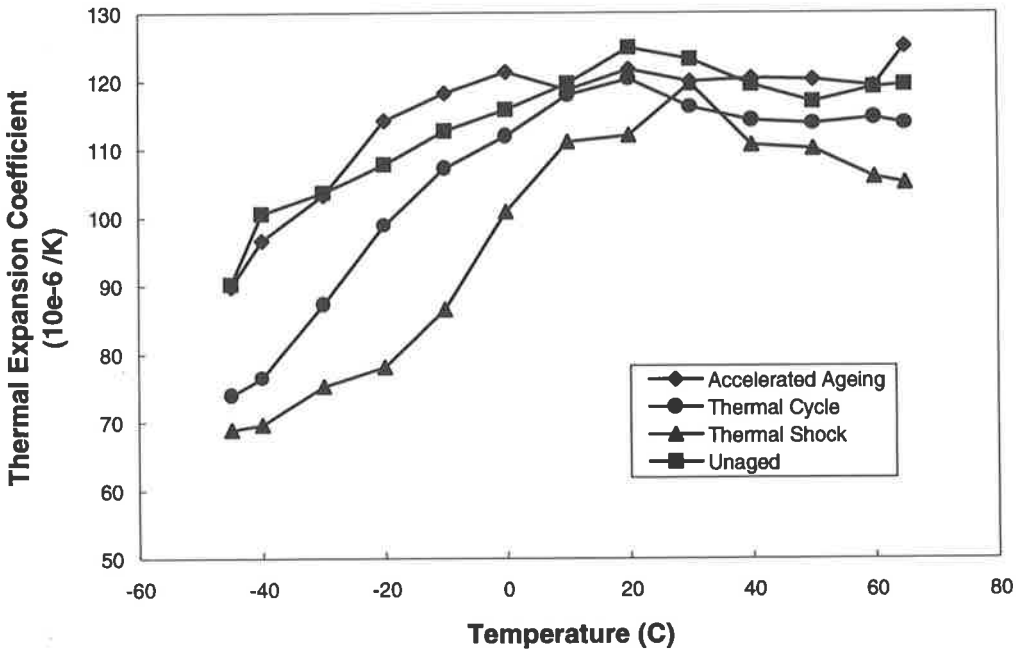

Figure 29 Effect of ageing on the thermal expansion coefficient of propellant

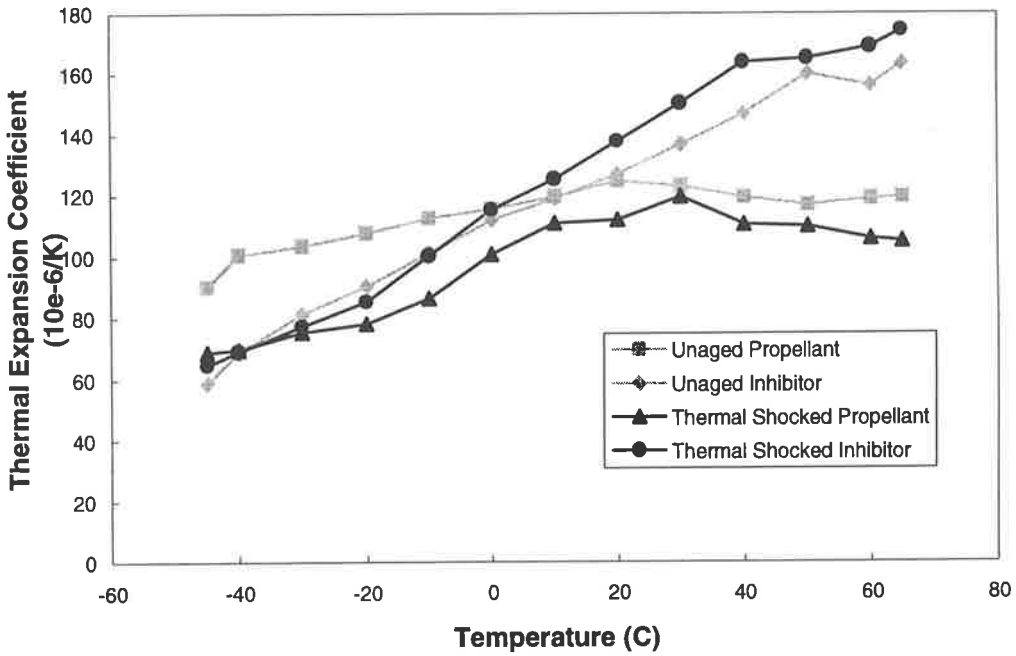

Figure 30 Comparison of thermally shocked propellant and inhibitor

POISSON'S RATIO

The polymers and particulate filled composite materials employed in the PICTOR rocket motor are viscoelastic in behaviour and exhibit values of Poisson's ratio which are time, strain and stress dependent. Interactions at the binder/filler interface in the composite materials result in the formation of vacuoles which grow with increasing strain. The significance of the relationship between volume increase and Poisson's ratio at each strain level to FEA was discussed in the Literature Review. By monitoring the effect of strain and temperature on the value of Poisson's ratio the importance of the binder/filler interactions and its influence on the material behaviour can be identified. The change in Poisson's ratio with increasing axial strain for the materials employed in the PICTOR rocket motor was measured at various temperatures and strain-rates using an image analysis technique.

An example of values for axial strain calculated from analysis of each image captured (ten in all) over the period of the test is plotted in Figure 31. It indicates that the values of strain calculated from the four gauge lengths present on the specimen from each image captured during a test of inhibitor are in good agreement. The gauge lengths span the longitudinal length of the specimen and therefore it can be concluded that the elongation of the specimen was uniform over this length. The change in axial strain with time was linear, hence the strain-rate during the test corresponds to the slope of the line. Similar behaviour was observed for the other materials tested.

Figure 32 shows the lateral strain measured from the images captured and analysed from the same experiment. The contraction of the specimen varied non-linearly but uniformly over the set of gauge lengths. This response when combined with the corresponding measurements of axial strain leads to a non-linear variation in Poisson's ratio. The same non-linear response was

observed in the results of lateral strain against time for the propellant and insulation. The variation in the lateral strain for the epoxy was linear.

The variation of Poisson's ratio with axial strain for specimens of propellant is shown in Figure 33. (For each plot values of Poisson's ratio were determined from the set of images captured off the videotape record between very low strain and just prior to specimen rupture). The line of best fit for the data of three tests, two at a strain-rate of 0.004 s^{-1} and one at 0.01 s^{-1} are shown. The strain-rates used in this study were not significantly different in magnitude, hence, the variation of Poisson's ratio as a function of strain-rate was not detectable. The Poisson's ratio data obtained from the two tests at 0.004 s^{-1} show that the method produces repeatable results. The value of Poisson's ratio was initially 0.499 at 0.2% strain but at 1% strain the value had dropped to 0.497, it began to noticeably decrease when the strain reached 1.5% and was 0.29 at 11.3%. The non-linear decrease in the Poisson's ratio observed in Figure 33 is evidence that damage resulting from dewetting occurs at higher strain levels. Particle dewetting which has previously been reported as the dominant mechanism causing non-linear viscoelastic response in propellants[51,52] will result in an increase in volume due to the formation and growth of vacuoles.

Smith,[22] Yilmazer and Farris[23] and Anderson and Farris[24] observed that the non-linear material behaviour of PVC and polyurethanes filled with glass beads was related to three types of interaction at the binder and filler interface; little or no binder/filler debonding at low strain, the onset of dewetting at a critical value of strain corresponding to vacuole formation and growth and complete separation of the filler from the polymer matrix. The values of Poisson's ratio measured decreased at an increasing rate until the filler and binder became completely debonded.

In Figure 33 the initial portion of the curve (up to 1.5% strain) is the response of the material due to molecular straining within the polymer network, no significant binder/filler interactions occur in this region and Poisson's ratio remains relatively constant.[22] The relationship between the variation in Poisson's ratio and volume was expressed in Equation 4. A comparison of the decrease in Poisson's ratio can be made with the increase in specimen volume against strain which is plotted in Figure 34. The initial portion of the curve correlates with that of the change in Poisson's ratio observed, very little increase in specimen volume occurs, whilst the elongation was 1.6% the increase in volume was limited to only 0.16%.

With increasing strain the value of Poisson's ratio decreases significantly below 0.5, this agrees with the large increase in specimen volume exhibited from 2 to 9% strain. In this region interactions at the binder/filler interface result in the formation voids which grow rapidly causing the volume to increase at an increasing rate. In the last portion of the curve, just prior to specimen rupture, the change in Poisson's ratio and specimen volume becomes a linear relationship with the level of axial strain. The specimen ruptures at 12% strain, where the Poisson's ratio has decreased below 0.3. Rigbi[53] noted that Poisson's ratio for an HTPB propellant falls with strain and does so at rates increasing with the rate of extension and that this applied more so to those materials with more prominent viscous characteristics.

The sensitivity of Poisson's ratio to volume changes resulting from the extent of binder/filler interactions was employed in an investigation into the effect of coating filler particles with a bonding agent in a composite propellant. Buswell, Dodds and Tod[54] measured the difference in Poisson's ratio of HTPB/AP propellants with and without the bonding agent Bobba 8 (an aziridine complex) using a Farris dilatometer. For both propellant formulations the value of Poisson's ratio was observed to decrease non-linearly in response to the applied strain, similar to the trend observed in this study. At the higher strain levels the value of Poisson's ratio fell to

0.35 for tests conducted at 20°C. However, the propellant containing the bonding agent had a higher strain to failure due to the increased strength of the binder/filler adhesive bond.

A comparison can also be made with the data of Kugler et. al.[26] who measured Poisson's ratio in a HTPB/AP propellant (see Figure 35), using an optoelectronic system. It is observed that the change in Poisson's ratio in the data of Kugler et. al. follows a similar trend to the data acquired in this study. As the strain level increased the damage occurring at the binder/filler interface causes a non-linear variation in the Poisson's ratio. The quantitative difference in the measured values of Poisson's ratio at each strain level observed in Figure 35 results from the different propellant formulations used in each study. Specifically, the percentage filler content of each was different and the propellant used by Kugler et al. also contained a percentage of aluminium particles, both of these factors will effect the level of binder/filler interactions observed.

Poisson's ratio was also measured as a function of temperature for the propellant. In Figure 36 we see that within the range of experimental error, values of Poisson's ratio do not vary significantly over the temperature range –20°C to 50°C. The sub-zero test temperature was well above the glass transition temperature of the propellant (–75.5°C) so the behaviour of the propellant tended to be flexible and rubbery. Surprisingly, the behaviour of the material over the three test temperatures was substantially the same.

A graph of Poisson's ratio against axial strain for the inhibitor is shown in Figure 37. The Poisson's ratio of the inhibitor has an initial value of 0.45 that decreases with the axial extension until the value approaches 0.2. The results presented are for two strain-rates ($0.002\ s^{-1}$ and $0.008\ s^{-1}$). Again the results are repeatable, however, the small difference in

strain-rate does not allow a conclusion to be made about the effect of strain-rate on Poisson's ratio.

Figure 38 shows the variation in Poisson's ratio versus axial strain for the inhibitor at three test temperatures. At a test temperature of −20°C the material behaviour will be approaching that of a glass-like state as the T_g of the inhibitor is −42.7°C. For the sub-zero test the material has an initial value of Poisson's ratio of approximately 0.3 and the strain at rupture was reduced to 15% compared to the above zero temperatures. The material exhibits a more glass-like behaviour, thus the level of binder/filler interactions was much increased when compared to tests where the temperature was above zero. In the range of temperatures from 25°C to 50°C the material is well above the glass transition and the specimens display similar behaviour.

To evaluate the experimental method's ability to detect differences between Poisson's ratios of two propellants with similar filler loadings but different mechanical properties, testing of a PPG/AP propellant was performed. The resulting variation in Poisson's ratio is compared with that from the HTPB type propellant and inhibitor in Figure 39. The difference in behaviour between the two propellants results from the stronger adhesive bonding between the binder and filler particles present in the PPG/AP propellant. As a result the PPG type propellant exhibits a more rubbery behaviour compared to the HTPB type, it has a lower modulus, sustains a higher strain to rupture (19% compared to 12%) and at equivalent values of axial strain the value of Poisson's ratio is higher, even though the filler loading is similar. The values of Poisson's ratio for the PPG type propellant lie between those of the HTPB/AP propellant and the inhibitor.

Evidence for the importance of the binder/filler interactions on the high strain-rate mechanical properties in different formulations of composite propellants was reported by Ho and Fong.[55]

They studied the rupture properties of a group of composite propellants formulated from various elastomeric binders (including HTPB and PPG) and AP, PETN (pentaerythritol tetranitrate) and RDX (cyclo-1, 3, 5-trimethylene-2, 4, 6-trinitramine) oxidisers. The results of Dynamic Mechanical Thermal Analysis (DMTA) tests showed evidence for the interaction between binder and filler at the bondline and indicated that stronger bonding between the binder and filler particles resulted in an increased fracture toughness, yield and maximum stress of the PPG/AP propellant compared to the HTPB/AP propellant.

Similar evidence was also presented by Ho and Fong[56] in a study of the high strain-rate fracture behaviour of two composite propellants and a cast double base propellant. The polymeric binders were HTPB and glycidyl azide (GAP) and the filler in each case was AP. Results of DMTA tests on each propellant indicated that the level of binder/filler interaction in the GAP/AP propellant was slightly greater than that in the HTPB/AP propellant.

The inhibitor has a strain to rupture of almost 90% which is approximately 10 times that of the HTPB/AP propellant. The inhibitor contains 35% filler (by weight) compared to the propellant's much higher 80% proportion, which will influence the level of binder/filler interactions. Thus the bonding between the polyurethane and AS particles is stronger than that between the HTPB and AP particles. The strength of the binder/filler bond acts to reinforce the inhibitor and as a result it sustains a higher strain to rupture; by comparison there is only weak reinforcement in the propellant.

Stacer et. al.[52] proposed a model which quantified the factors influencing the degree of non-linearity observed in highly filled composite elastomers, in terms of the binder/filler interactions. Model predictions were compared with experimental data and it was concluded that greater adhesion between the binder and filler reduced the molecular slippage during

deformation. As a result the dependence of the modulus on the strain decreased, resulting in decreased non-linearity. Hence, the decreased non-linearity seen in Figure 39 of Poisson's ratio for different combinations of binder and filler results from stronger binder/filler bonding.

The variation of Poisson's ratio for the HTPB type propellant and the inhibitor at 50°C is given in Figure 40. The behaviour exhibited does not vary greatly from that at 25°C since both materials behave in the same rubbery manner as they are well above their respective T_g values. The propellant and inhibitor's Poisson's ratios only approach the same value in the region of 3 to 3.5% strain. The inhibitor was able to sustain a higher strain to rupture, approximately 90%, whilst the propellant breaks at around 12% strain.

Results for these two materials at -20°C are shown in Figure 41. At this temperature the propellant was still well above its T_g whilst the inhibitor's behaviour tends towards the glass-like state. The strain to rupture of the inhibitor was much reduced and the two materials break at comparable levels, 11% for the propellant and 13% for the inhibitor. However, the difference between Poisson's ratio for the two materials extends over the entire range of strains.

The variation of Poisson's ratio with axial strain for the insulation, is shown in Figure 42. The material temperature was above the T_g (−47.8°C) and thus the behaviour was elastomeric in nature. At 1% axial strain the value of Poisson's ratio was approximately 0.45. As the strain increased the value of Poisson's ratio decreased. In contrast to the propellant and inhibitor the insulation, which contains no filler, can sustain very large extensions to failure. The results presented are for three rates of strain of similar magnitude. The strain-rate does not affect the values of Poisson's ratio measured.

The epoxy's glass transition temperature is 58.8°C and it therefore behaves in a glass-like manner at 25°C. This behaviour is exhibited by the material in Figure 43 where the value of Poisson's ratio increases linearly with axial strain. The range of values of Poisson's ratio is from 0.22 to 0.36, which compares with the value observed in metals of 0.33, and specimen rupture occurs at approximately 9% strain. The change in Poisson's ratio exhibited by the epoxy is comparable to the increase predicted by the "standard solid" model (a Maxwell and elastic element in parallel) wherein the internal movement of a "rigid" elastic material is accomodated by the expansion.[57] As the specimen elongates less internal movement can occur resulting in smaller increases in volume. The change in specimen volume for epoxy as calculated from Equation 3 is shown in Figure 44. The volume was found to increase with strain but at a decreasing rate which results in an increasing Poisson's ratio.

Odom and Adams[58] measured the value of Poisson's ratio for epoxy (828) up to strains of 0.5%. Whilst the Poisson's ratio of a mPDA cured epoxy varied from 0.34 to 0.38 depending on the percentage of curing agent used, the value for a MDA cured epoxy was constant at 0.38. Their method involved measuring the Young's, E, and Shear, $\mathcal{G}$, modulus of the material and calculating the Poisson's ratio from the isotropic relationship for elastic materials:

$$\mathcal{G} = \frac{E}{2(1+\nu)} \qquad \text{.....(14)}$$

Odom and Adams stated that the maximum strain level attained in their experiments was below that required for non-linear material behaviour.

Tests conducted on the epoxy and inhibitor at 25°C are shown in Figure 45. It can be seen that the epoxy fails at a significantly lower strain level than the inhibitor. The Poisson's ratio of the two materials are very different over the entire range of axial strains. At a strain of 1% the

Poisson's ratio in the epoxy will be approximately 0.26 whilst for the inhibitor it is 0.42. This difference will be significant due to the adhesive bonding between the inhibitor and epoxy.

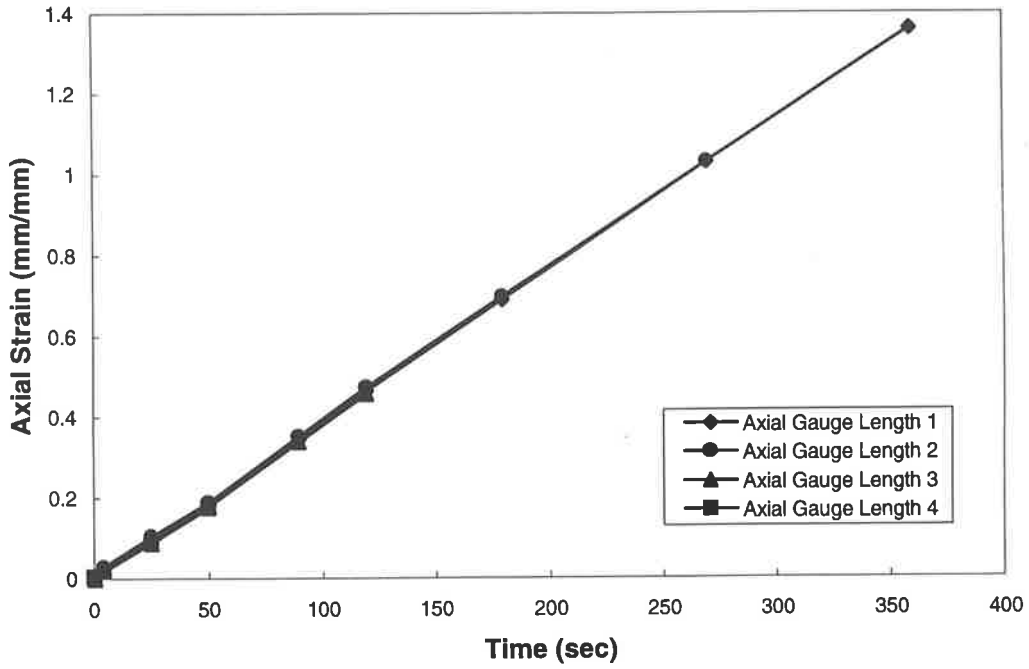

Figure 31 Change in axial strain with time for inhibitor, T= 25°C

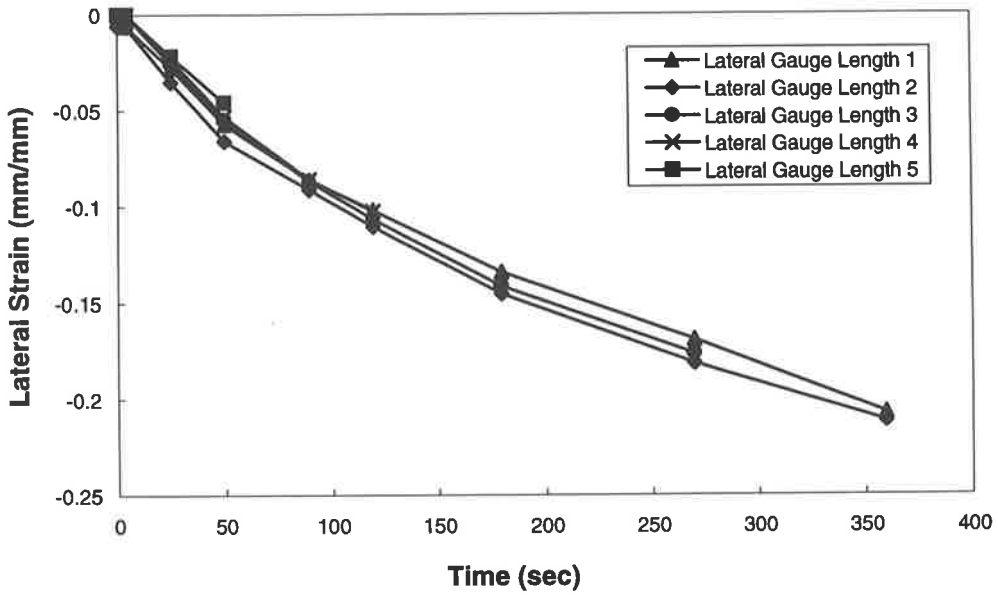

Figure 32 Change in lateral strain with time for inhibitor, T= 25°C

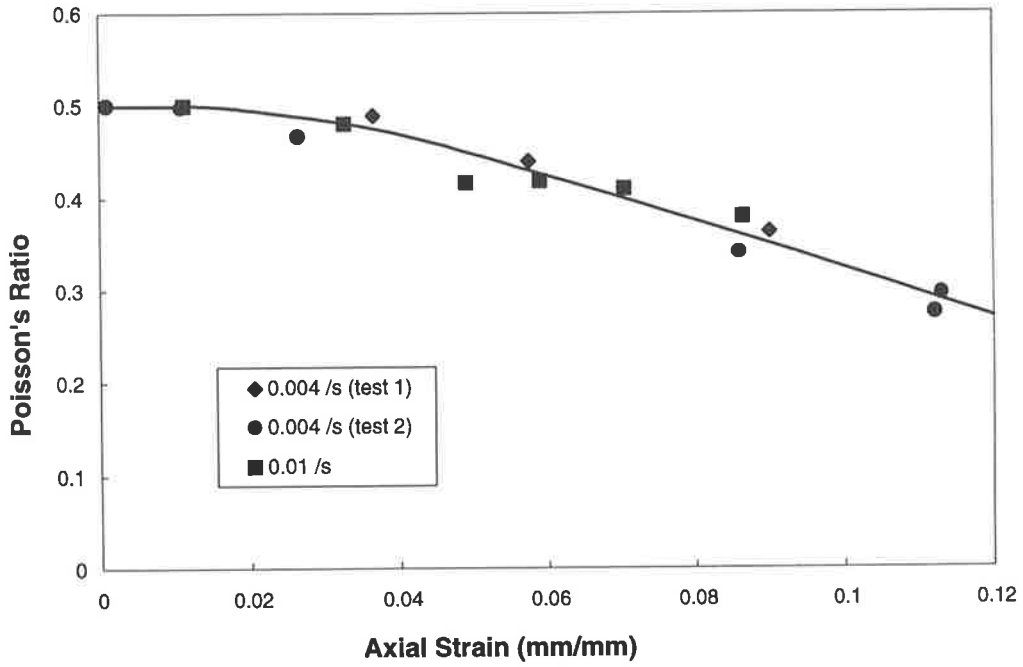

Figure 33 Change in Poisson's ratio with axial strain for propellant, T= 25°C

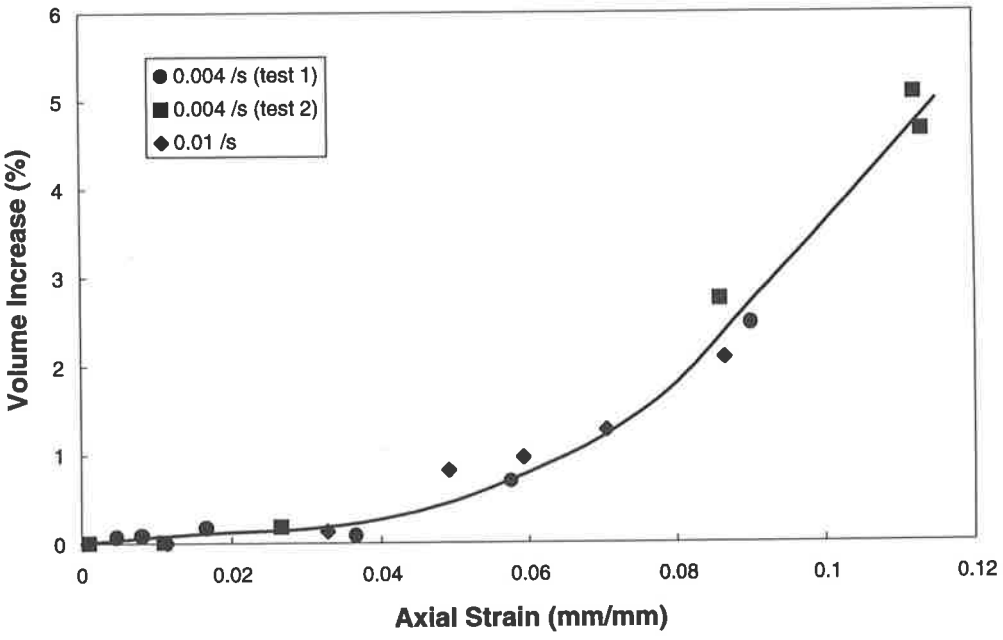

Figure 34 Volume increase with axial strain for propellant, T= 25°C

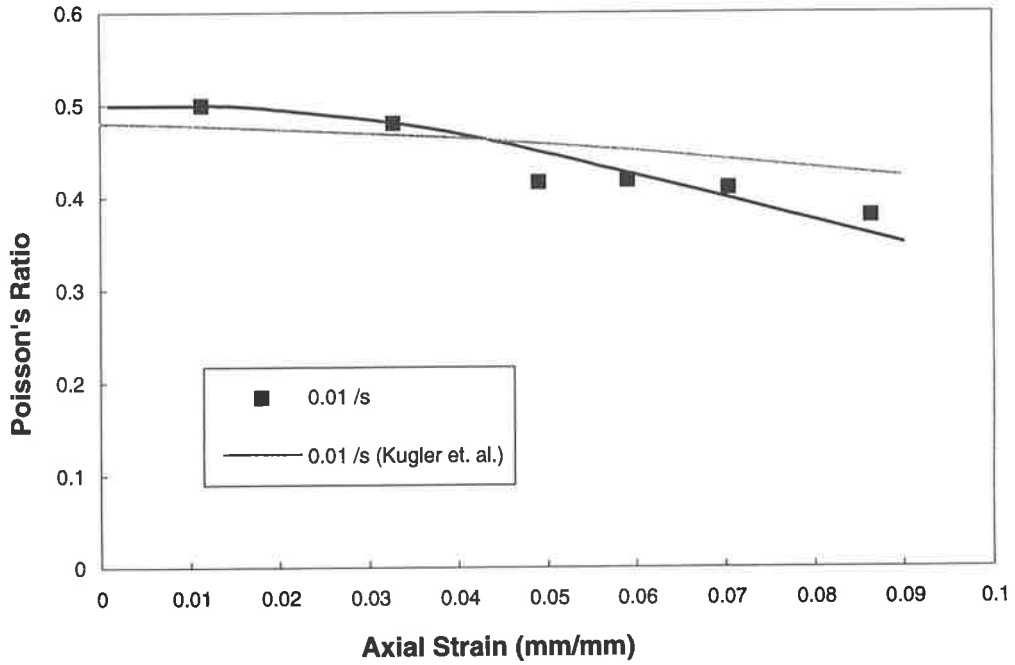

Figure 35 Comparison with the data of Kugler et al.[26] for propellant, T= 25°C

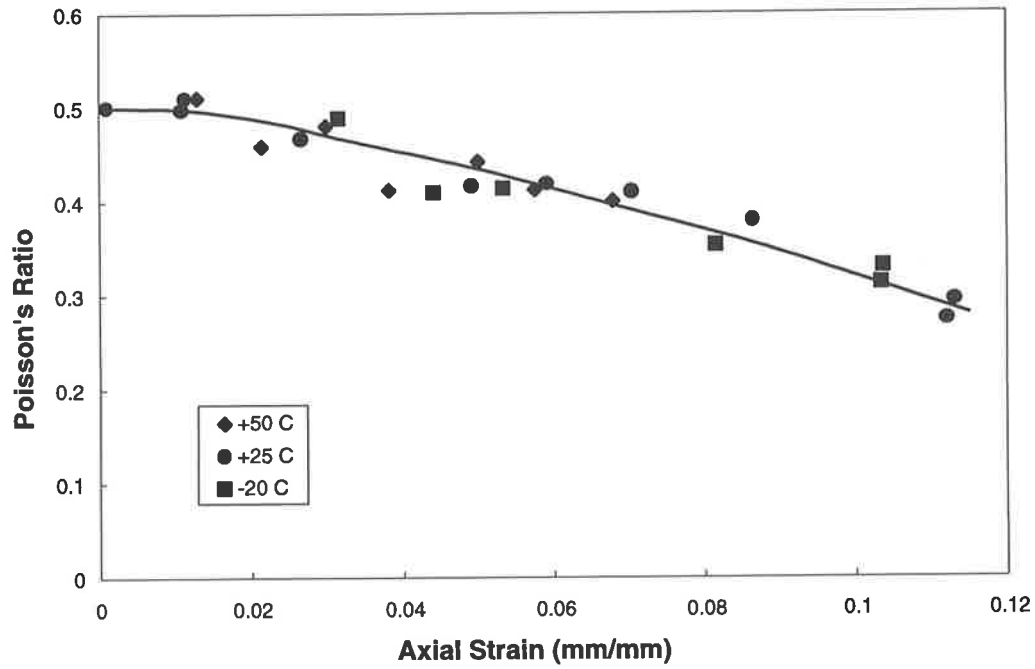

Figure 36 Change in Poisson's ratio with axial strain for propellant, T= 25°C

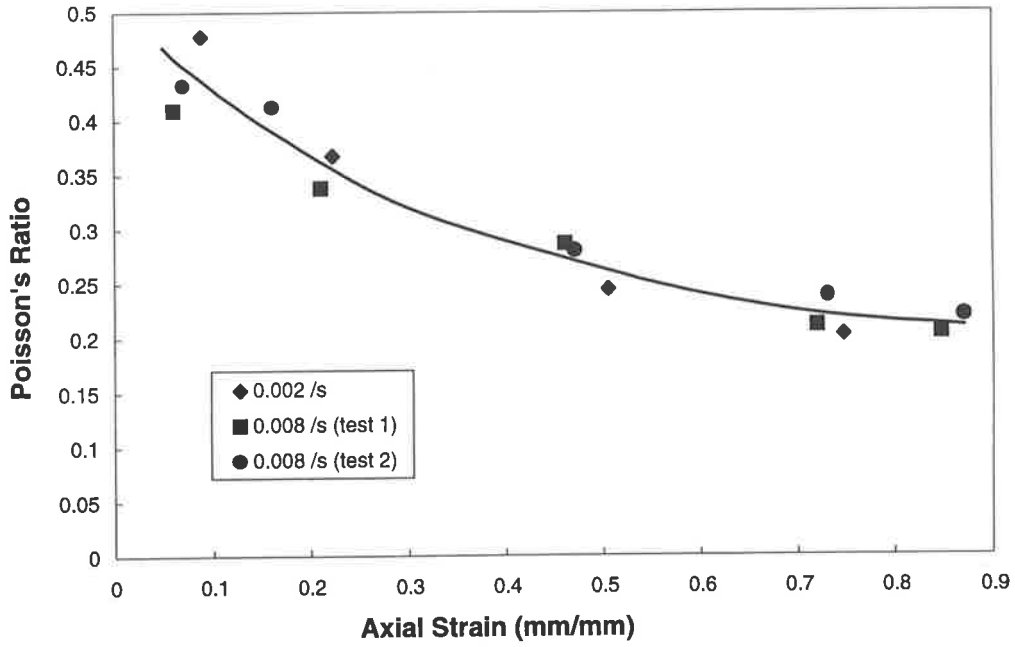

Figure 37 Change in Poisson's ratio with axial strain for inhibitor, T= 25°C

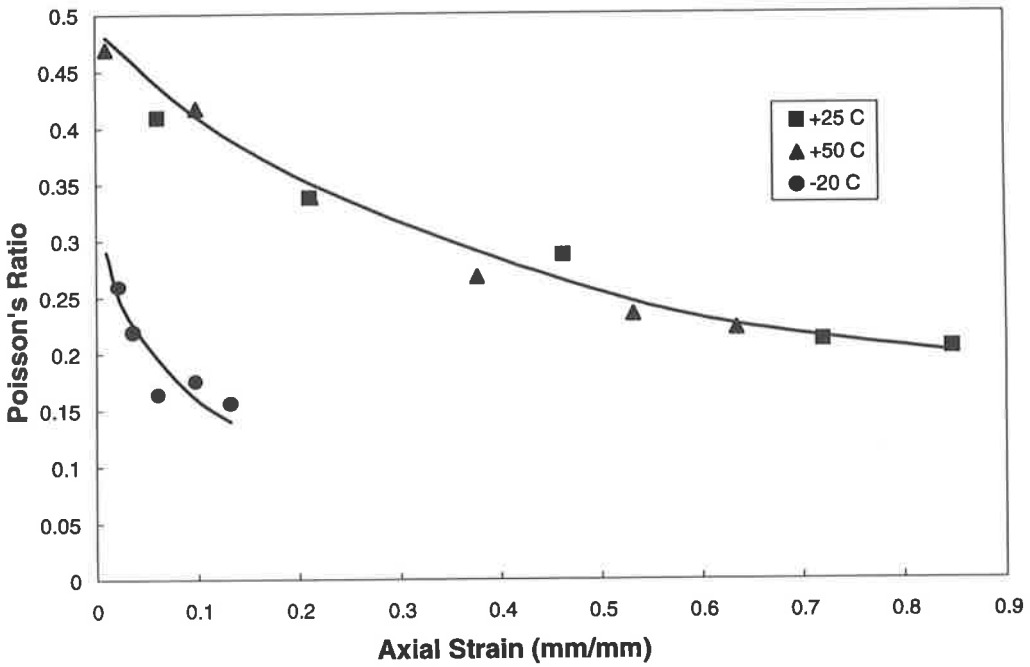

Figure 38 Change in Poisson's ratio with axial strain for inhibitor, T= 25°C

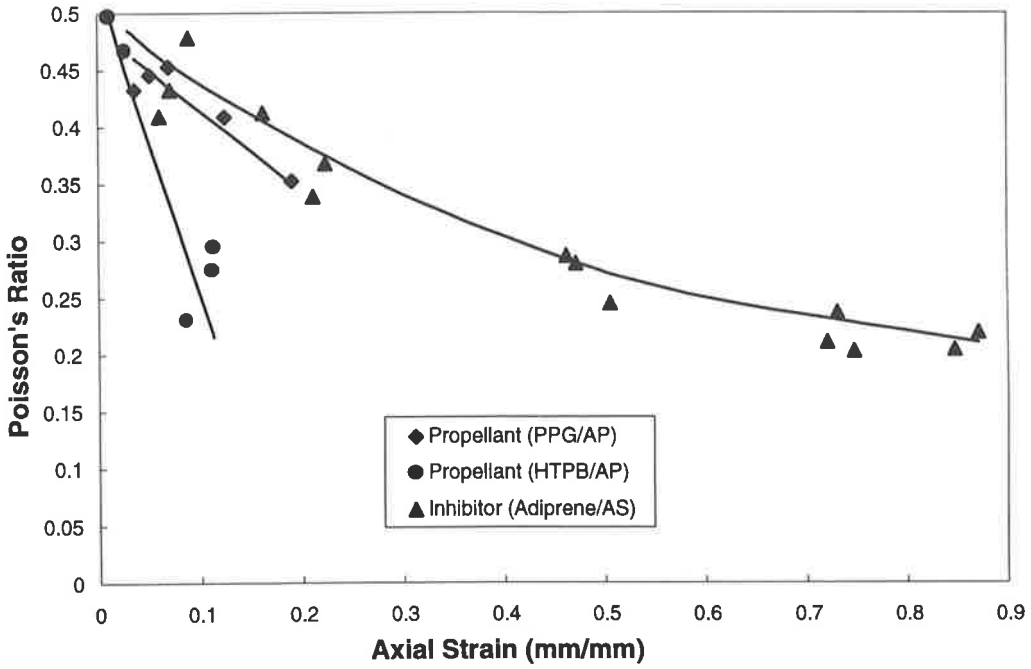

Figure 39 Comparison of Poisson's ratio for different binders and fillers, T= 25°C

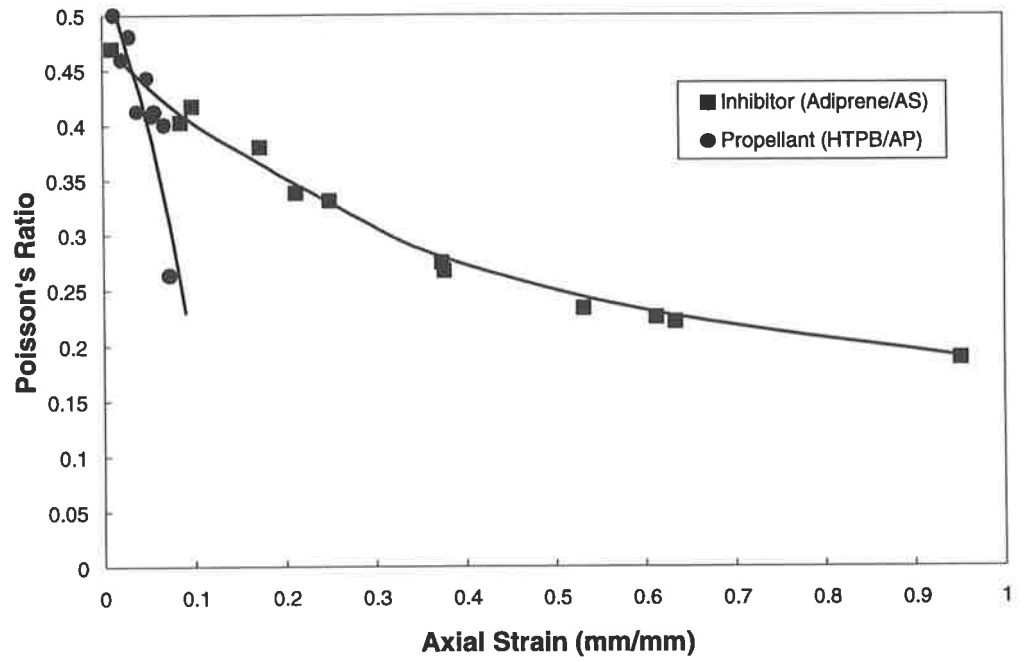

Figure 40 Comparison of Poisson's ratio for different binders and fillers, T= 50°C

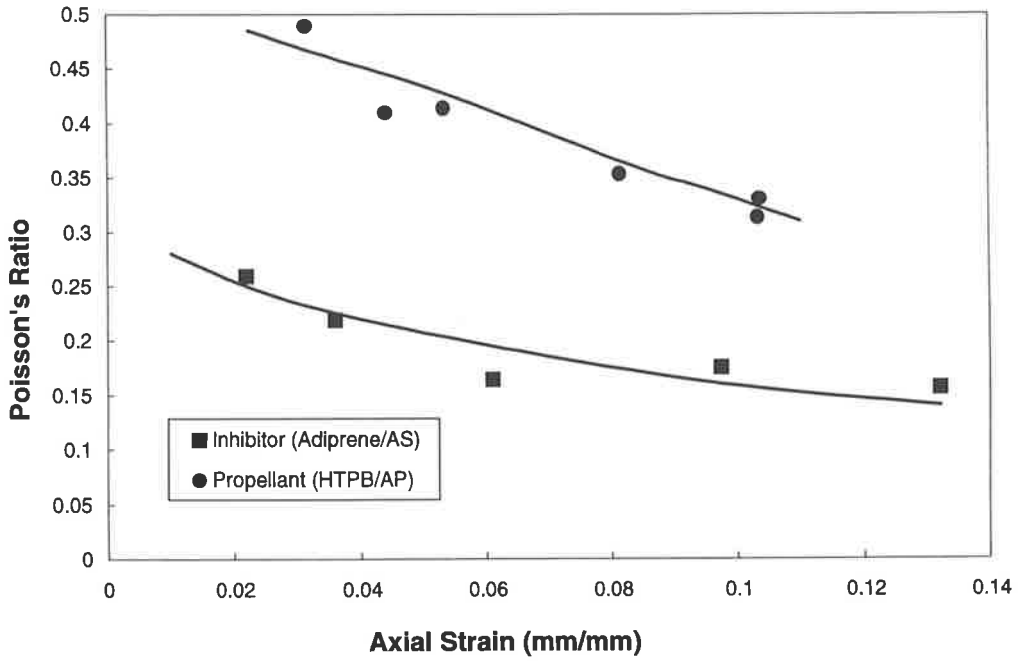

Figure 41 Comparison of Poisson's ratio for different binders and fillers, T= –20°C

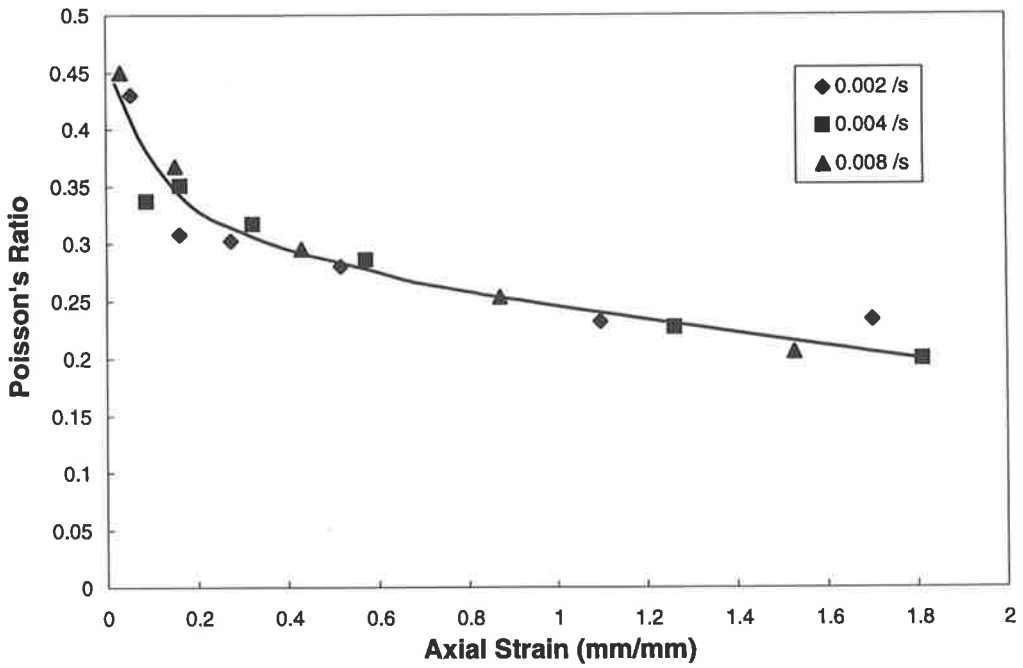

Figure 42 Change in Poisson's ratio with axial strain for insulation, T= 25°C

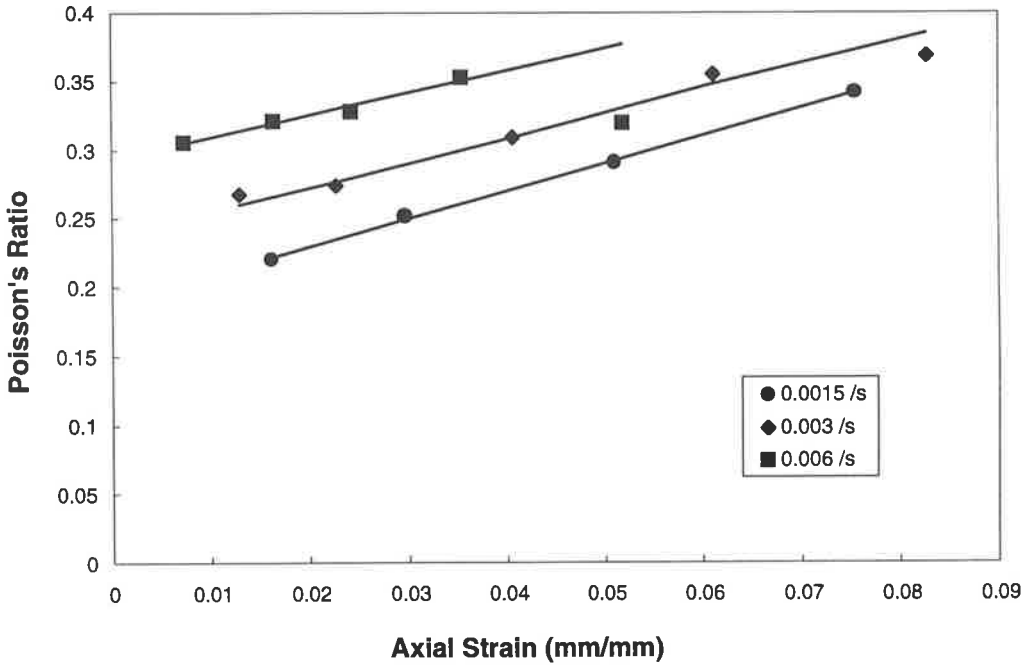

Figure 43 Change in Poisson's ratio with axial strain for epoxy, T= 25°C

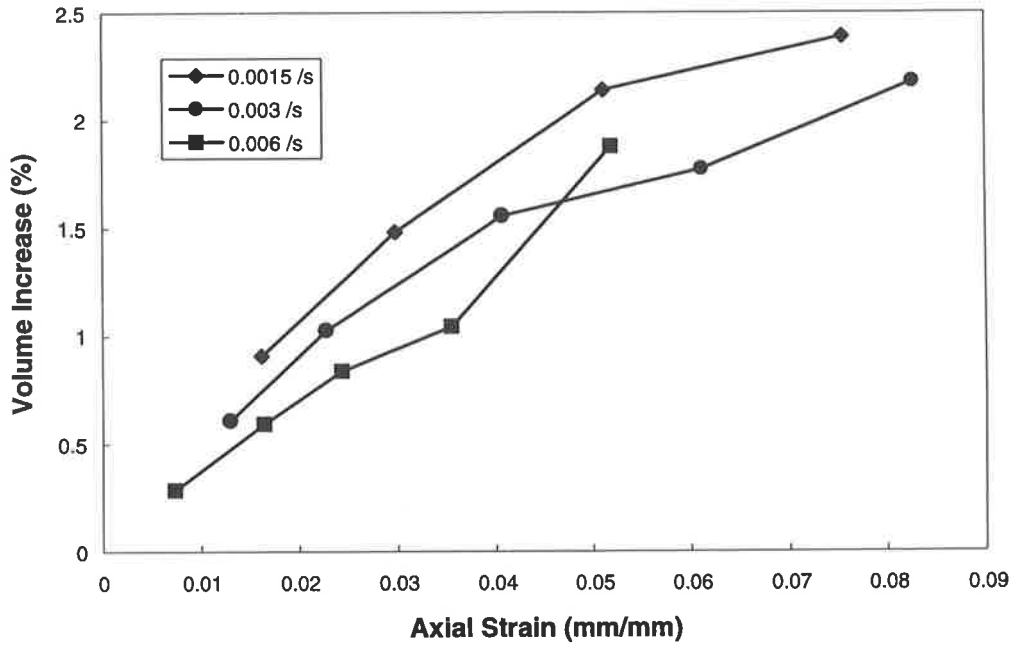

Figure 44 Volume increase with axial strain for epoxy, T= 25°C

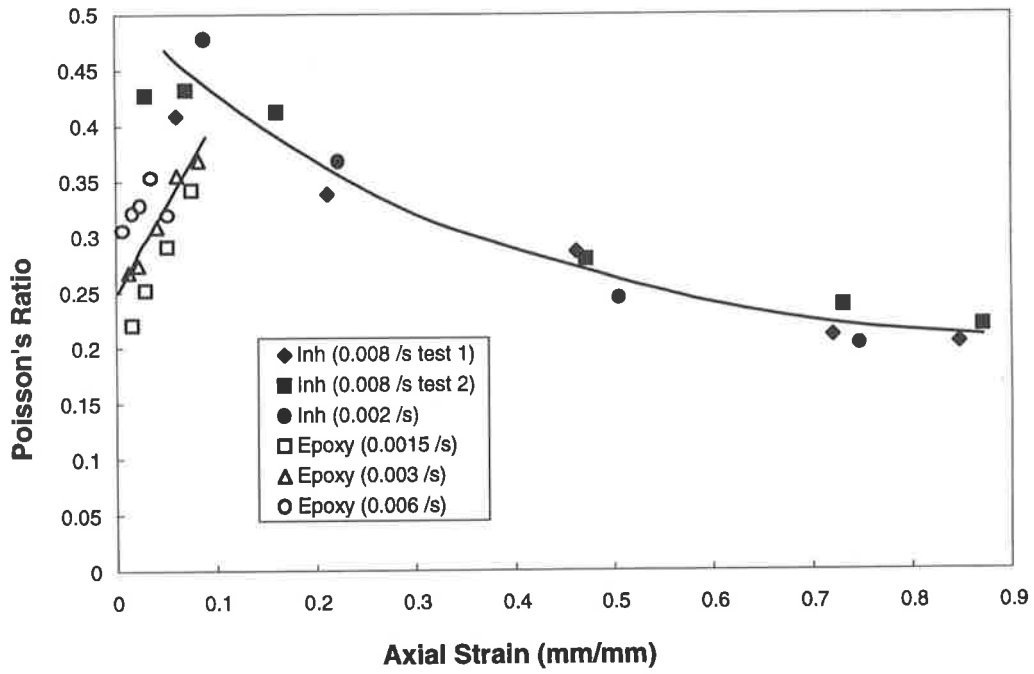

Figure 45 Comparison of Poisson's ratio for inhibitor and epoxy, T= 25°C

HYSTERESIS ENERGY LOSS

The hysteresis cycles contain considerable information on the behaviour of the highly loaded rocket motor materials, measuring the hysteresis energy loss enables the inclusion of viscoelastic material behaviour in the calculation of fracture energy. In this section the hysteresis characteristics of aged and unaged specimens of the propellant, inhibitor and propellant/inhibitor bimaterial employed in the PICTOR rocket motor, at various test temperatures, will be described.

At each strain level the hysteresis loop was repeated three to five times with a 5-10 minute period between each cycle. A typical result for a specimen of propellant can be seen in Figure 46, (Figure 8 shows the load-time curves for the cycling of this specimen) where the additional cycling can be seen to not substantially affect the magnitude of the hysteresis energy losses. This result was consistent for all of the aged and unaged materials tested at each temperature and strain-rate employed. The third hysteresis cycle has been plotted for all figures shown in this section.

As the materials were cyclically loaded to increasingly higher strain levels a gradual decrease in the stress was observed. When strained, damage to the binder matrix and the binder/filler interface results in a loss of reinforcement in the material with a subsequent decrease in its capacity to sustain a load. Whilst the onset of damage is not evident in the hysteresis cycles, it was detected from the change in Poisson's ratio with increasing strain. The hysteresis cycle for each strain level has been plotted and a total stress against strain history for the specimen of propellant is shown in Figure 47. In each successive hysteresis cycle the stress attained as the specimen was elongated was the same for low strains. At higher strains the stress levels

attained decrease as the material undergoes gross deformation prior to fracture. The test was concluded at this point and these hysteresis cycles excluded from the results.

The reproducibility of basic hysteresis loop test results in Figure 48 shows that the data from two different specimens of propellant are almost identical. These hysteresis loops are typical for a viscoelastic material, the various mechanisms causing energy loss result in only a fraction of the applied energy from loading being recovered.[1]

Effect of Temperature on Hysteresis Cycles

The hysteresis loss in specimens of propellant which had been subjected to the various thermal loads was measured at each of the three test temperatures (–40°C, 25°C and 60°C). Figure 49 displays a comparison of the stresses attained from a series of unaged propellant specimens, cyclically loaded to the same maximum strain. The material softens as the temperature increases resulting in a decrease in the stress attained at equivalent values of strain. The hysteresis loops of propellant specimens tested at 25°C and 60°C are quite similar since the specimens are well above the glass transition temperature and behave in a rubbery manner. The response of the propellant specimen tested at –40°C varies considerably as the material temperature is closer to the glass transition (approximately –75.5°C). The material is stiffened, which results in increased stress levels compared to the higher temperatures, at equivalent strains. These trends with temperature were also seen in aged specimens and at all strain-rates.

The hysteresis losses present in specimens of unaged propellant/inhibitor bimaterial tested at each temperature are shown in Figure 50. Again the results shown are typical for the aged specimens and at all strain-rates employed, the stress at the same strain increases as the test temperature decreases. The propellant/inhibitor bimaterial specimens show similar behaviour to

the propellant specimens. The hysteresis loops at 25°C and 60°C are comparable, while that at –40°C is influenced by the increased material stiffness as the temperature approaches the glass transition.

The inhibitor displays quite different responses at each of the three test temperatures (see Figure 51). At 60°C the material has become quite soft and the stress attained is much reduced compared to 25°C, for the same strain. At –40°C the aged and unaged specimens of inhibitor behave in a glass-like manner due to the proximity of the glass transition temperature (approximately –42.7°C for the unaged inhibitor, see Table 1). The stress level attained at an equivalent strain in each hysteresis loop increases as the material temperature decreases. This behaviour corresponds to that observed in the study of the change in Poisson's ratio of the inhibitor specimens with temperature (see Figure 37). The inhibitor exhibits a more glass-like behaviour at –20°C resulting in a large divergence in Poisson's ratio as compared to that at 25°C and 50°C (at these temperatures the behaviour is similar due to the rubbery nature of the material). The strain to failure was also reduced at –20°C due to the more brittle material behaviour.

These results show that the inhibitor is capable of achieving much higher stresses than both the propellant and propellant/inhibitor specimens at each temperature, which is indicative of the stronger bonding between binder and filler particles in the inhibitor. (A comparison of this was made in the section discussing the measurements of Poisson's ratio). In addition to stronger binder/filler bonding, the inhibitor material possesses higher stiffness than the propellant and as a result it has the capacity to sustain higher stress levels at an equivalent strain. The presence of the inhibitor material in the bimaterial specimens contributes to the load capacity in these

specimens. The stresses attained in the propellant/inhibitor bimaterial specimens were slightly greater than those in the specimens of propellant, at the same strain levels.

Effect of Ageing on Hysteresis Cycles

Figure 52 shows a comparison of the hysteresis cycles of unaged propellant and those subjected to accelerated ageing, thermal shock and thermal cycling, tested at 60°C. The data plotted for the unaged, thermally cycled and thermally shocked specimens are for the same level of strain. The accelerated aged material fractured at a much lower strain level than the other three types of material and therefore the hysteresis data plotted is for a lower maximum strain. The significant hardening of the material caused by the accelerated ageing can be compared to the changes in mechanical behaviour resulting from the other thermal loads. Note that the stress level achieved for the accelerated aged material was comparable to that in the other three specimens but at much lower strain. The trends observed in these figures are typical of the hysteresis cycles measured for the aged propellants at each of the three test temperatures and strain-rates.

During the high temperature storage of the accelerated ageing the polymer chains in the binder matrix from additional cross-linking[4] and as a result the propellant hardens.[†] The anti-oxidant added to the propellant at manufacture is gradually consumed during accelerated ageing and as the material oxidises it becomes more brittle.[4] The increased stiffness resulting from the accelerated ageing of the material is evident in the increased stresses seen compared to those present in the unaged material, at an equivalent strain level. The more brittle behaviour also causes the reduced strain to fracture. Both the thermally cycled and thermally shocked materials were subjected to shorter periods of elevated temperatures in their respective thermal

[†] In the context of this study material hardening refers to the ability to sustain an increased stress at an equivalent strain level (see Literature Review, page 11).

loadings and this results in a minor increase in hardening of the material compared to that which occurs in accelerated ageing. The periods of storage at sub-zero temperatures will act to slow the rate of the oxidation and cross-linking.

At –40°C the inhibitor behaved in a glass-like manner and the behaviour of each aged specimen did not vary greatly. It is important to note, however, that some hysteresis energy losses do occur at this low temperature due mainly to dewetting of the filler particles. The effect of temperature on the stiffness of the inhibitor has been discussed, the hysteresis cycles of the inhibitor material at 25°C for specimens subjected to the various thermal loadings are plotted in Figure 53. It can be seen that the hysteresis cycles were not significantly affected by ageing, the material has been only slightly hardened. The more severe the ageing to which the material was subjected, the larger the extent to which the material has deteriorated and become harder. A similar variation in the hysteresis cycles was seen at 60°C, where minor increases in the stress levels were observed with an increased severity of ageing.

The hysteresis behaviour of the propellant/inhibitor bimaterial specimens at the three test temperatures was similar to that of the propellant specimens. The major difference is the higher stress capacity of the propellant/inhibitor specimens due to the presence of the inhibitor material. Figure 54 shows a plot of stress against strain typical for the aged and unaged propellant/inhibitor specimens. The influence of the inhibitor was limited to an overall stiffening of the specimens only. The hysteresis behaviour of the bimaterial specimens was dominated by the propellant material. With a much lower bond strength between the binder and filler in the propellant, the specimen was not subjected to a high enough stress to cause significant hysteresis energy losses in the inhibitor.

As in the case of the propellant specimens, the hardened material resulting from the accelerated ageing has a much higher stiffness than the other aged and unaged materials. The thermally cycled and thermally shocked bimaterial specimens were only slightly affected by the thermal loads with small increases in the stress levels compared to the unaged specimens. These results are also typical for the other strain-rates employed.

Hysteresis Ratios

Changes to the hysteresis ratio with ageing, temperature and strain-rate indicate the effect these factors have on the type and level of irreversible energy loss processes present in a material. A graph of the hysteresis ratios against strain level obtained from tests on propellant is shown in Figure 55. It can be seen that the value of hysteresis ratio was nearly constant up to strain levels at which the material fractures. This behaviour was observed in all of the materials studied, for all temperatures and strain-rates. The hysteresis cycling was conducted over the same range of strain-rates and temperatures as employed in the crack propagation tests.

A table of the hysteresis ratios measured at a strain-rate of 0.0037 s^{-1} is presented below. The values for one strain-rate only are included as the trends were the same at each strain-rate (this behaviour can be seen in the figures of hysteresis ratio against temperature).

Table 2 Values of hysteresis ratio‡, h_r, for $\dot{\varepsilon} = 0.0037\ s^{-1}$

Ageing	T (°C)	Propellant	Inhibitor	Propellant/Inhibitor
Unaged	–40	0.41	0.27	0.52
	25	0.39	0.40	0.50
	60	0.32	0.37	0.45
Shocked	–40	0.41	0.26	0.48
	25	0.37	0.38	0.44
	60	0.29	0.35	0.34
Cycled	–40	0.40	0.25	0.41
	25	0.36	0.37	0.42
	60	0.28	0.36	0.31
Accelerated	–40	0.35	0.23	0.38
	25	0.32	0.35	0.38
	60	0.26	0.31	0.29

‡ see Equation 13.

Figure 56, Figure 57 and Figure 58 show the variation with temperature of the hysteresis ratio for the propellant at each strain-rate. The change in hysteresis ratio with strain-rate for each of the three test temperatures can be seen in Figure 59, Figure 60 and Figure 61. The hysteresis ratio increases with increasing strain-rate at each temperature as expected.

The hysteresis ratio for specimens of propellant subjected to the same thermal loads decreases as the temperature increases. Plastic deformation, binder/filler debonding, microcracking and microvoiding have been described as some of the mechanisms causing hysteresis energy loss.[3] As the temperature of the propellant decreased the material became stiffer and as a result the level of deformation, dewetting and hence the hysteresis energy losses increased. Less energy was recovered as a proportion of that input. In the following section the increased size of the

damage zone ahead of the crack tip with decreasing temperature in fracture tests of propellant, will be discussed.

At each test temperature the unaged material had the highest hysteresis ratio and the accelerated aged propellant the lowest. The accelerated aged propellant attained much higher stresses for the same strain level as compared to the unaged material. During ageing, material is hardened by increased polymer chain cross-linking and can also become more brittle. The level of hysteresis energy losses decreases and as a consequence the hysteresis ratio decreases. In the case of the accelerated aged propellant no damage zone was observed ahead of the crack tip in a fracturing specimen. This indicates that a much lower level of energy losses are present in this type of specimen.

The hysteresis ratio for the thermally cycled and thermally shocked materials lies only slightly below that of the unaged material. These two thermal loadings have little effect on the amount of hysteresis energy losses as compared to unaged material. The thermal cycling and thermal shocking only cause slight hardening of the propellant.

Ho and Tod[3] found that the hysteresis ratio of a naturally aged (from 12 to 85 months) rubbery composite propellant fluctuated with propellant ageing and it was concluded that this was due to the opposing effects of dewetting, rehealing, increased cross-linking and main chain scission.

The hysteresis ratio of the aged and unaged inhibitor specimens is plotted for each of the test temperatures in Figure 62, Figure 63 and Figure 64. Whilst Figure 65, Figure 66 and Figure 67 show that the hysteresis ratio of the inhibitor specimens increases with strain-rate.

In Table 2 the reduced values of hysteresis ratio for the inhibitor at –40°C can be seen. At this temperature the inhibitor specimens behave in an elastic or glass-like manner due to the

proximity of the glass transition. The energy recovered when the specimen was unloaded was high because of this and the magnitude of hysteresis energy losses low (see Figure 51). For perfectly elastic materials there are no hysteresis energy losses and the hysteresis ratio is zero.[1]

When the specimen temperature was increased above the glass transition the material behaved in more rubbery and flexible manner with greater levels of deformation. The material was observed to stress whiten as the strain level increased, whilst no stress whitening was seen at –40°C. The phenomena of stress whitening has been explained as probably due to dewetting and the formation of microvoids or crazes in the composite.[3] Hence, the level of hysteresis losses (and the hysteresis ratio) increase as compared to those temperatures close to the glass transition. On increasing the temperature to 60°C the hysteresis ratios decreased (see Figure 51). The material was further softened, compared to 25°C, by the increase in temperature. The load level capable of being sustained decreased as did the intensity of stress whitening and the hysteresis energy losses. The decrease in hysteresis energy losses as a proportion of the energy input was lower, resulting in decreased hysteresis ratios.

There is limited variation in the hysteresis ratios of the aged inhibitor specimens. It was observed earlier that ageing did not have a pronounced effect on the hysteresis cycles of the inhibitor. The hardening of the inhibitor was minor but increased with the severity of the thermal load. Hence, the hysteresis losses present in the thermally shocked specimens are slightly reduced and the hysteresis ratios are lower than those of unaged specimens. The hysteresis ratios are generally lower again for the thermally cycled specimens. The accelerated aged specimens exhibited the greatest increase in hardness and have the lowest values of hysteresis ratio for all the inhibitor specimens.

The hysteresis ratio for the propellant/inhibitor bimaterial specimens against temperature is plotted in Figure 68, Figure 69 and Figure 70 for each of the three strain-rates employed in these tests. Figure 71, Figure 72 and Figure 73 show the hysteresis ratio of the bimaterial specimens against strain-rate. The hysteresis ratio increases with strain-rate at each test temperature.

The variation in the hysteresis ratios of the bimaterial specimens was dominated by the propellant layer in the specimen. Negligible energy losses occur in the inhibitor as it possesses a much higher stiffness than the propellant. This allows higher stress levels to be sustained than is possible in the wholly propellant specimens at equivalent strain levels but increases the energy losses in the propellant layer of the bimaterial specimen. The result is higher hysteresis ratios than those measured at equivalent strain levels in propellant specimens.

As such the variation of the hysteresis ratios are similar to those found in the wholly propellant specimens (see Table 2), the values decrease as the temperature and severity of the thermal loads increase. The unaged material has the highest value of hysteresis ratio and the accelerated aged specimens the lowest. The hysteresis ratio of the thermally cycled material was generally below that of the thermally shocked specimens.

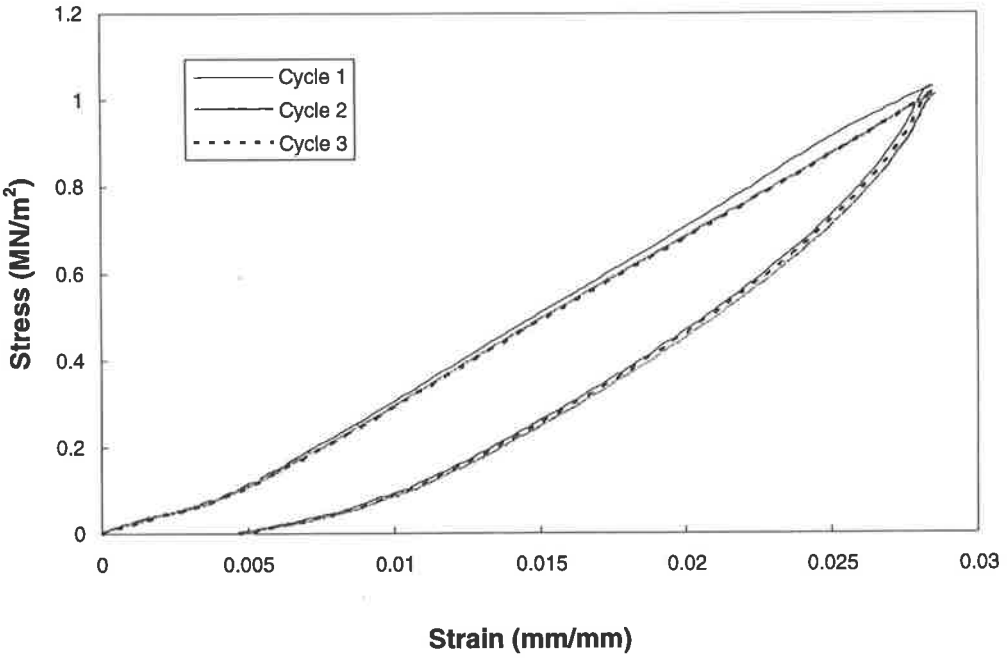

Figure 46 Hysteresis cycles in propellant T= –40°C (unaged, $\dot{\varepsilon} = 0.00077\ s^{-1}$)

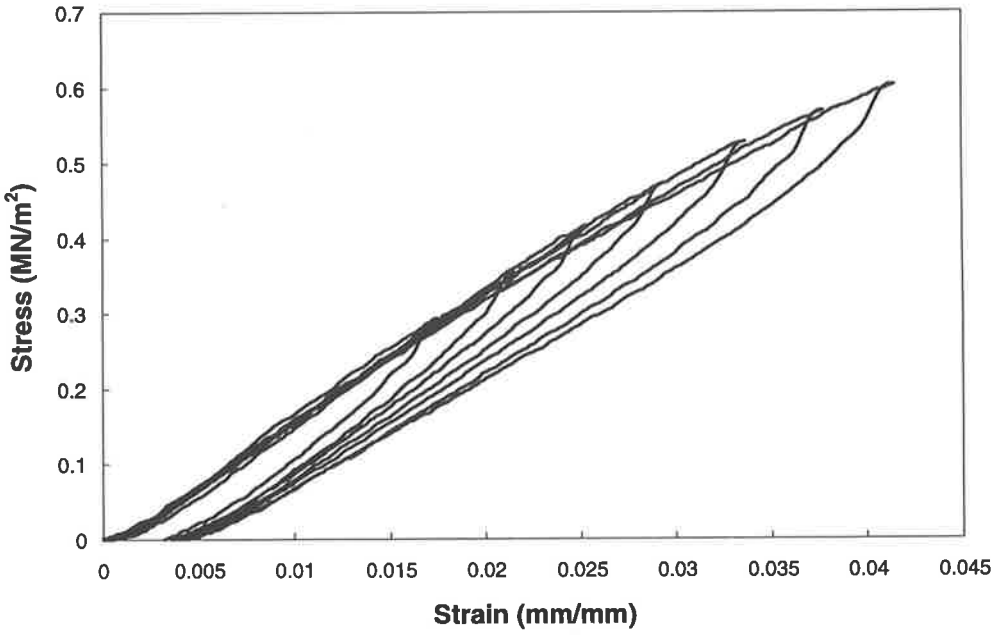

Figure 47 Hysteresis cycles in propellant T= 60°C (unaged, $\dot{\varepsilon} = 0.002\ s^{-1}$)

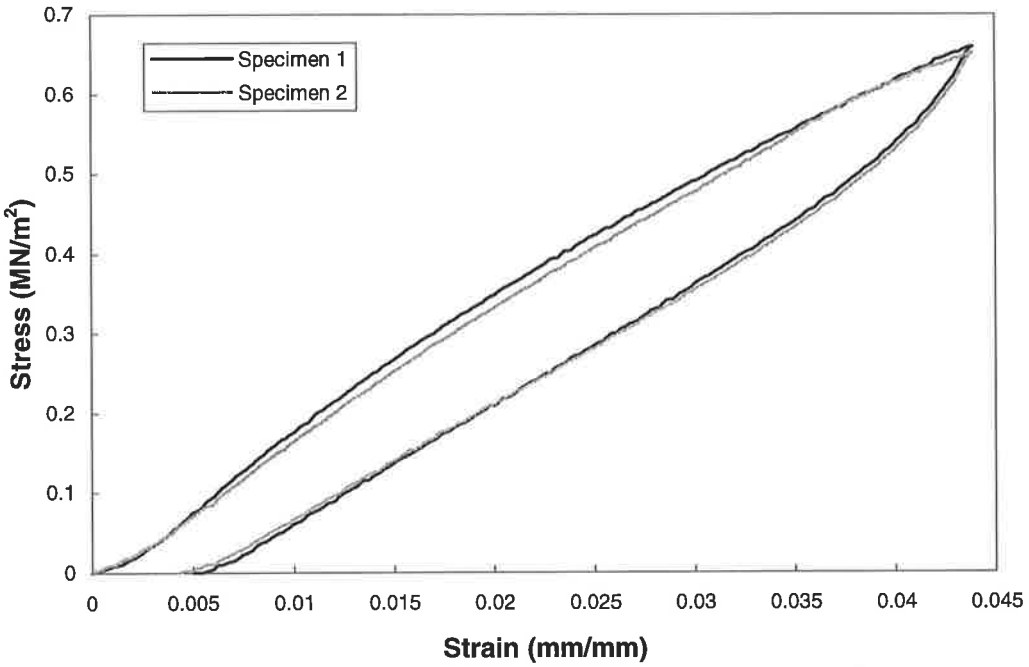

Figure 48 Hysteresis in two tests on propellant T= 25°C (unaged, $\dot{\varepsilon} = 0.00077\ s^{-1}$)

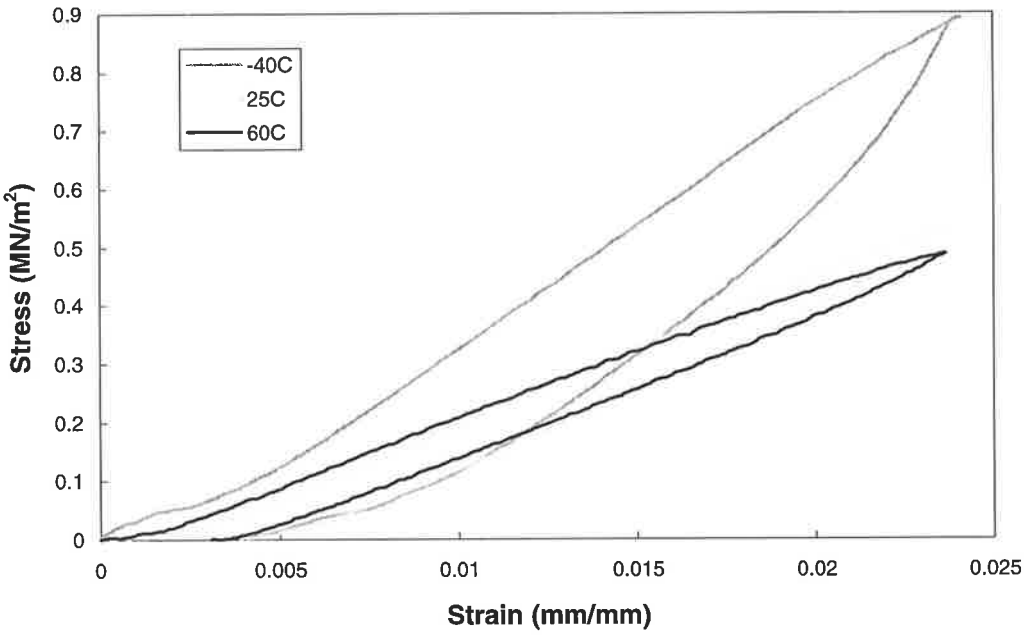

Figure 49 Hysteresis cycles in propellant T= –40, 25 and 60°C (unaged, $\dot{\varepsilon} = 0.00077\ s^{-1}$)

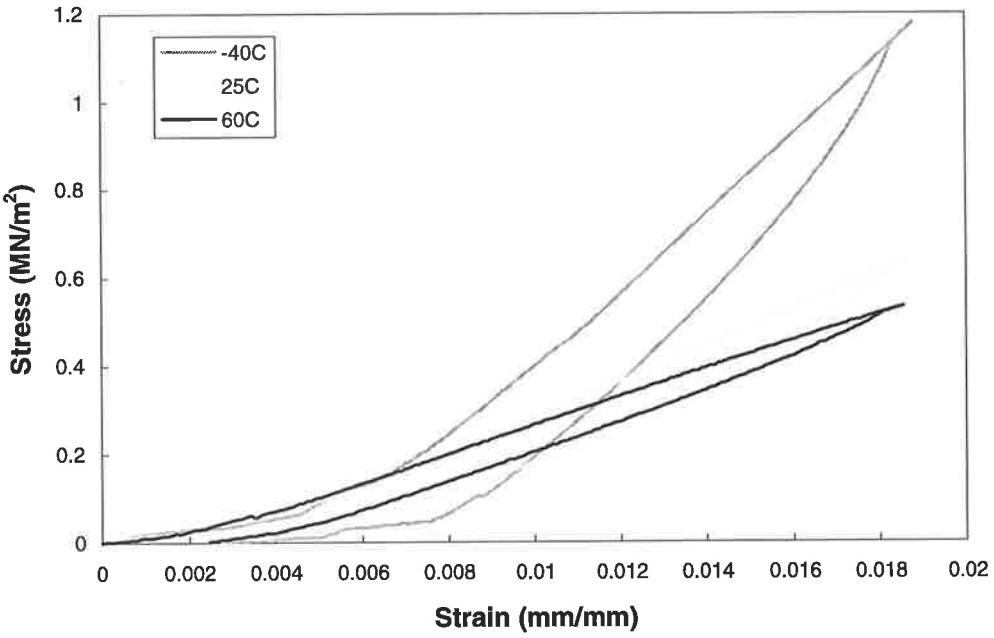

Figure 50 Hysteresis cycles in prop/inhb T= –40, 25 and 60°C (unaged, $\dot{\varepsilon} = 0.00077\ s^{-1}$)

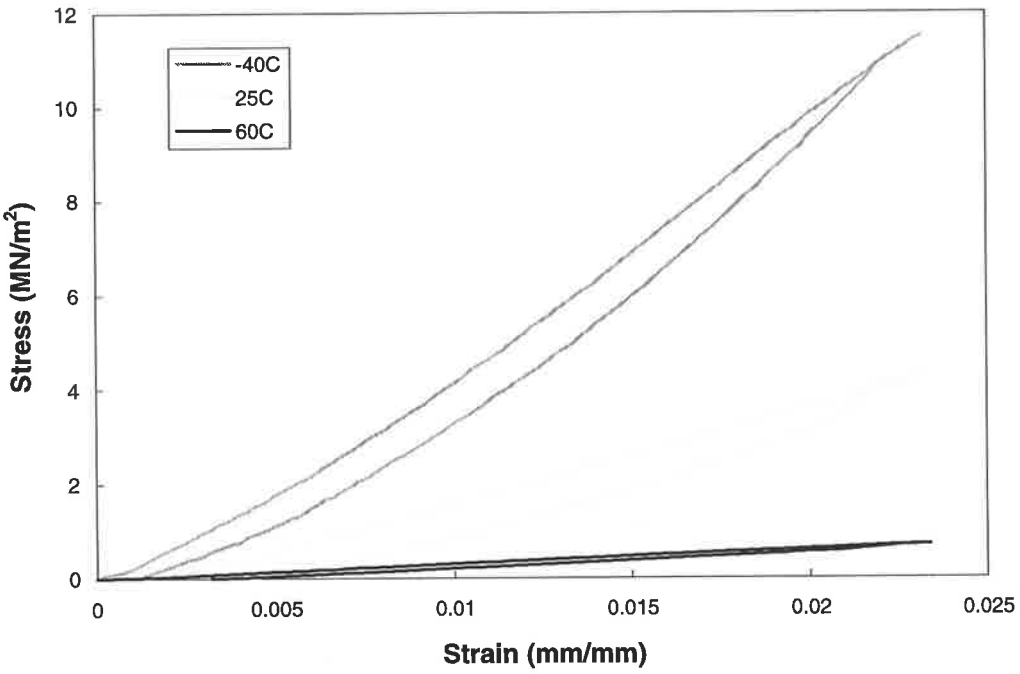

Figure 51 Hysteresis cycles in inhibitor T= –40, 25 and 60°C (unaged, $\dot{\varepsilon} = 0.002\ s^{-1}$)

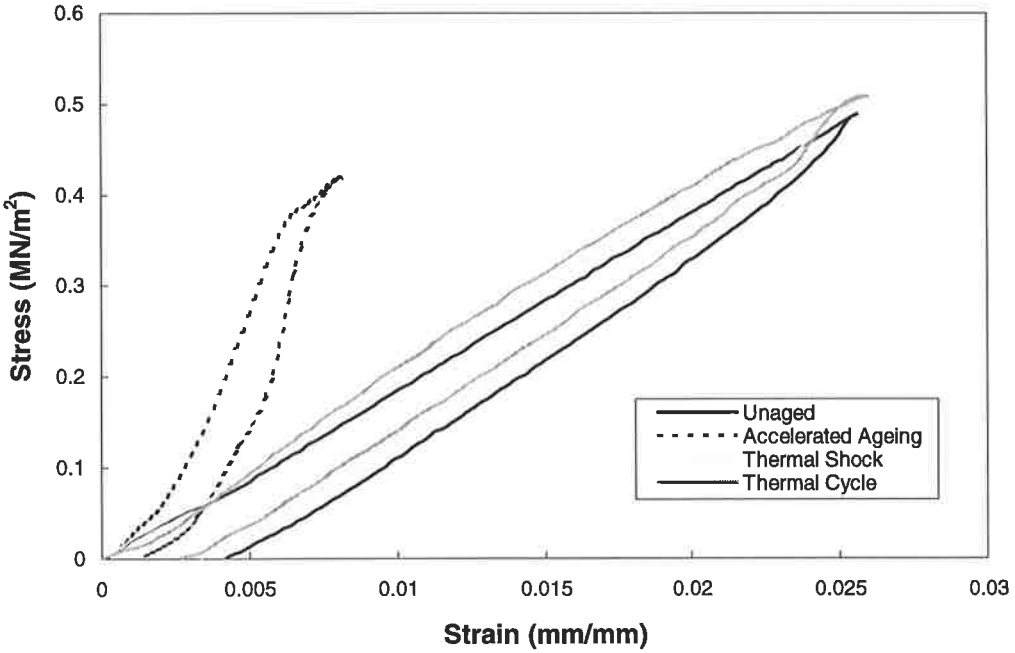

Figure 52 Hysteresis cycles in aged propellant T= 60°C ($\dot{\varepsilon} = 0.002\ s^{-1}$)

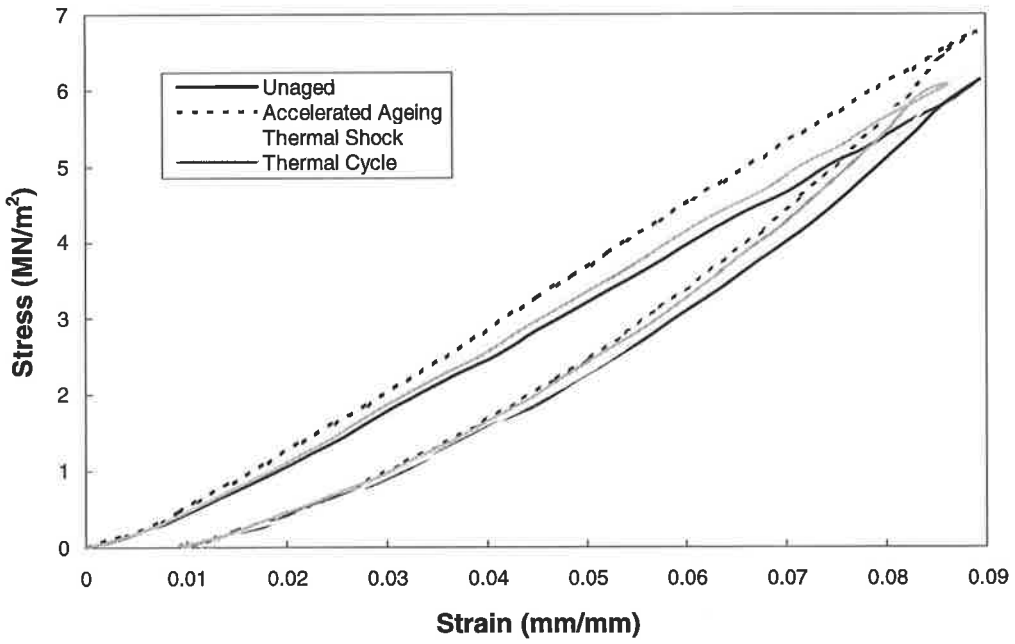

Figure 53 Hysteresis cycles in aged inhibitor T= 25°C ($\dot{\varepsilon} = 0.00077\ s^{-1}$)

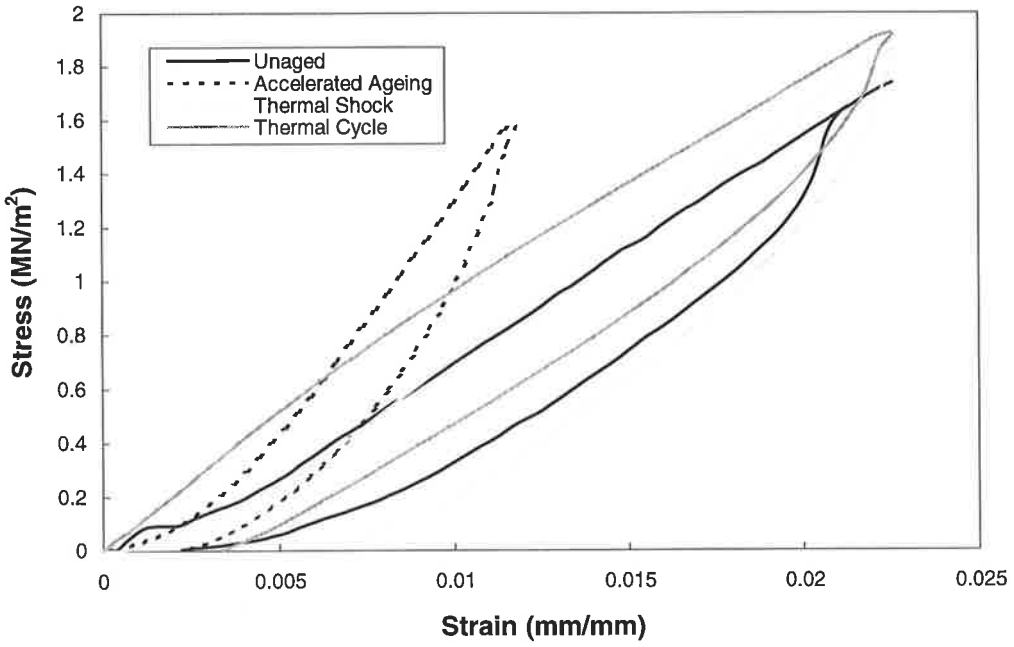

Figure 54 Hysteresis cycles in aged propellant/inhibitor T= –40°C ($\dot{\varepsilon} = 0.0037\ s^{-1}$)

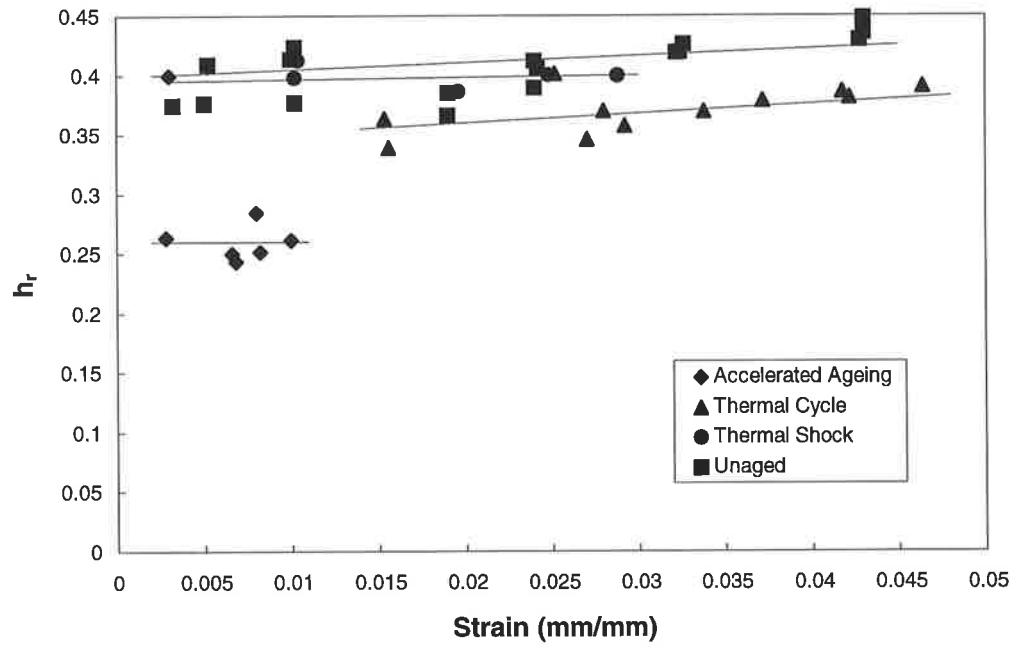

Figure 55 Change in hysteresis ratio for aged propellant T= –40°C ($\dot{\varepsilon} = 0.002\ s^{-1}$)

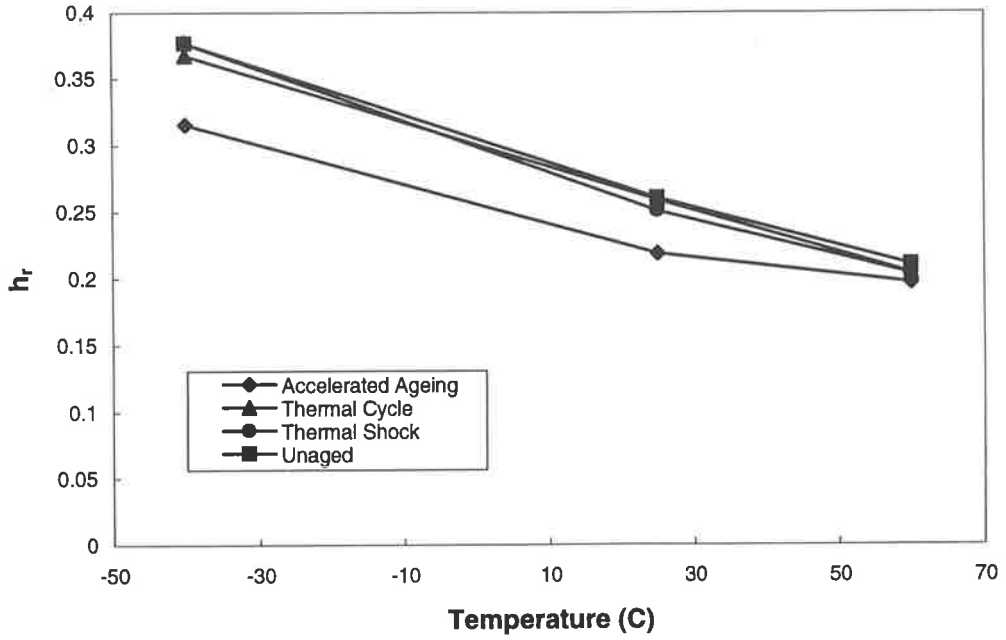

Figure 56 Change in hysteresis ratio with temperature for propellant ($\dot{\varepsilon} = 0.00077\ s^{-1}$)

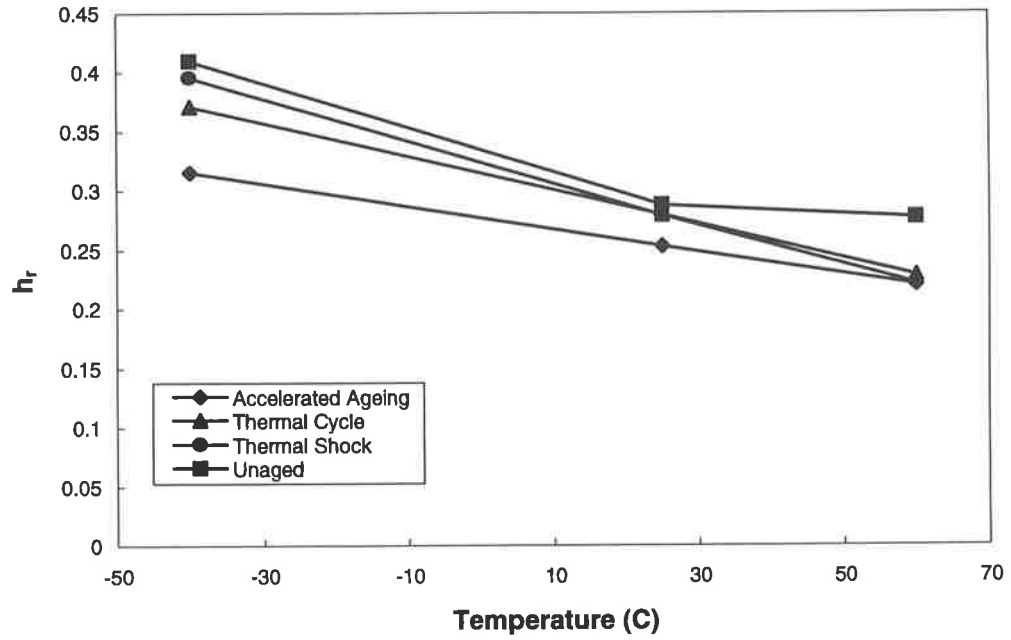

Figure 57 Change in hysteresis ratio with temperature for propellant ($\dot{\varepsilon} = 0.002\ s^{-1}$)

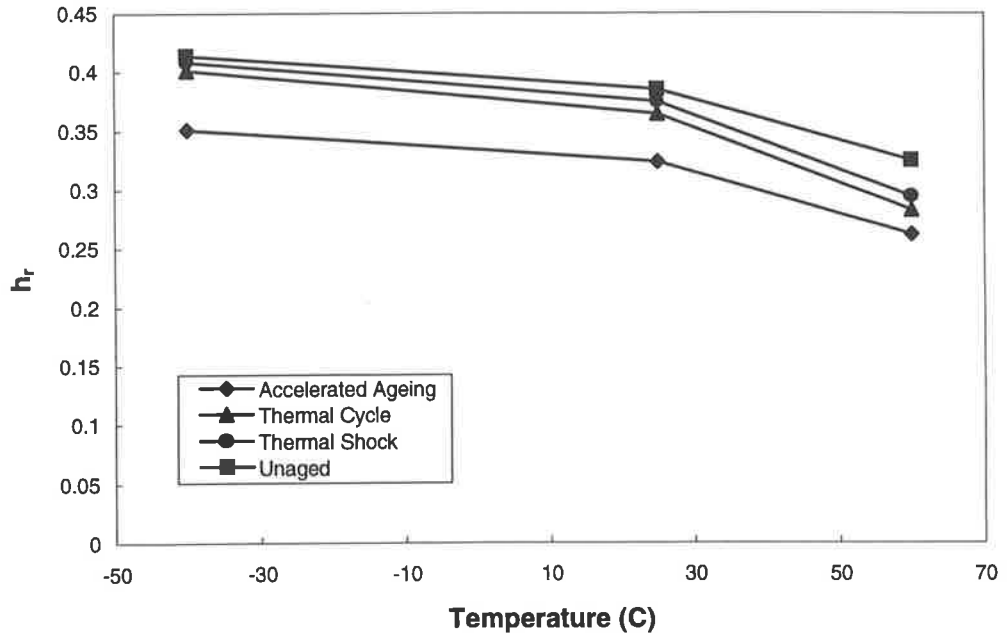

Figure 58 Change in hysteresis ratio with temperature for propellant ($\dot{\varepsilon} = 0.0037\ s^{-1}$)

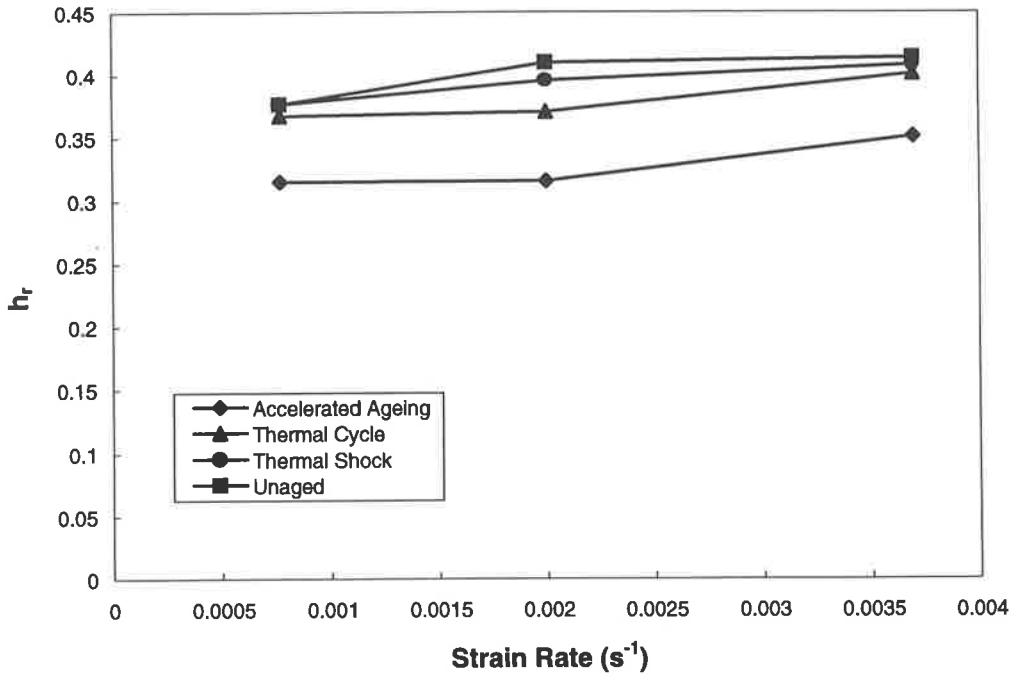

Figure 59 Change in hysteresis ratio with strain-rate for propellant (T= –40°C)

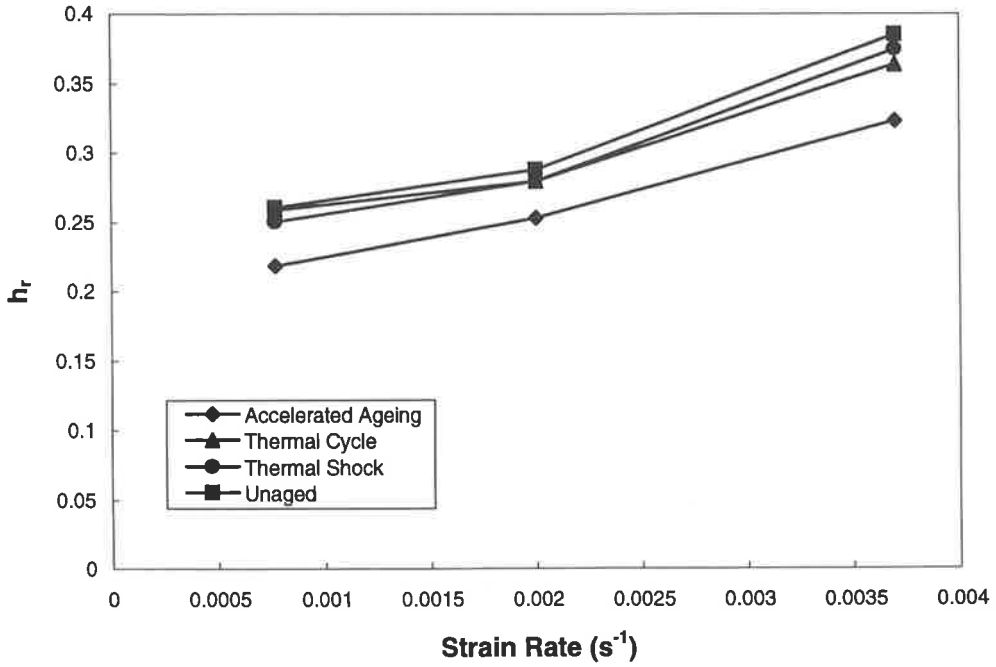

Figure 60 Change in hysteresis ratio with strain-rate for propellant (T= 25°C)

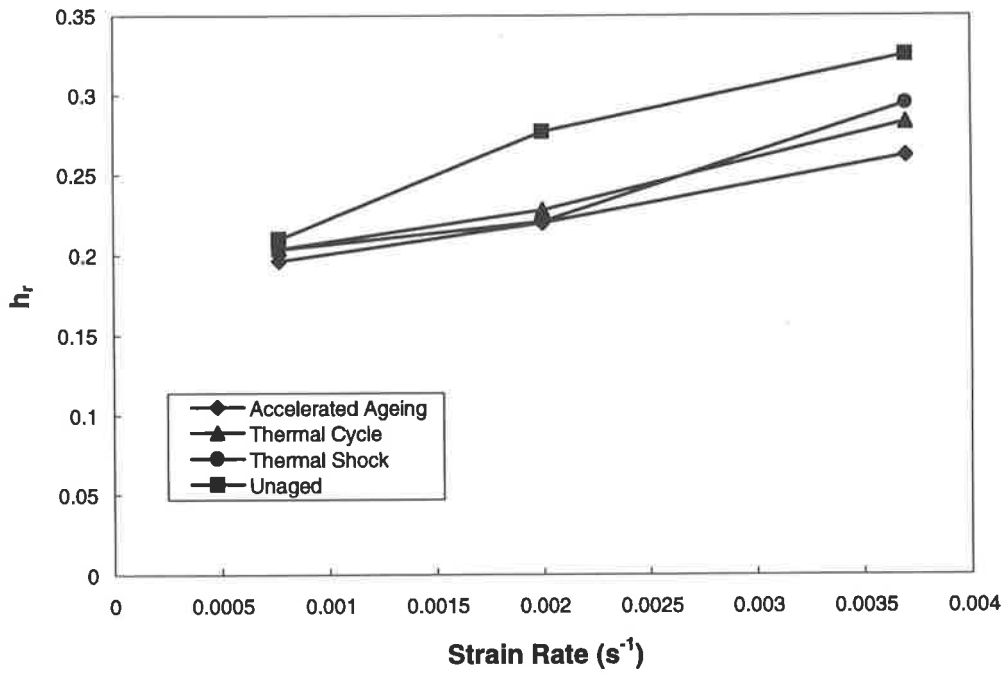

Figure 61 Change in hysteresis ratio with strain-rate for propellant (T= 60°C)

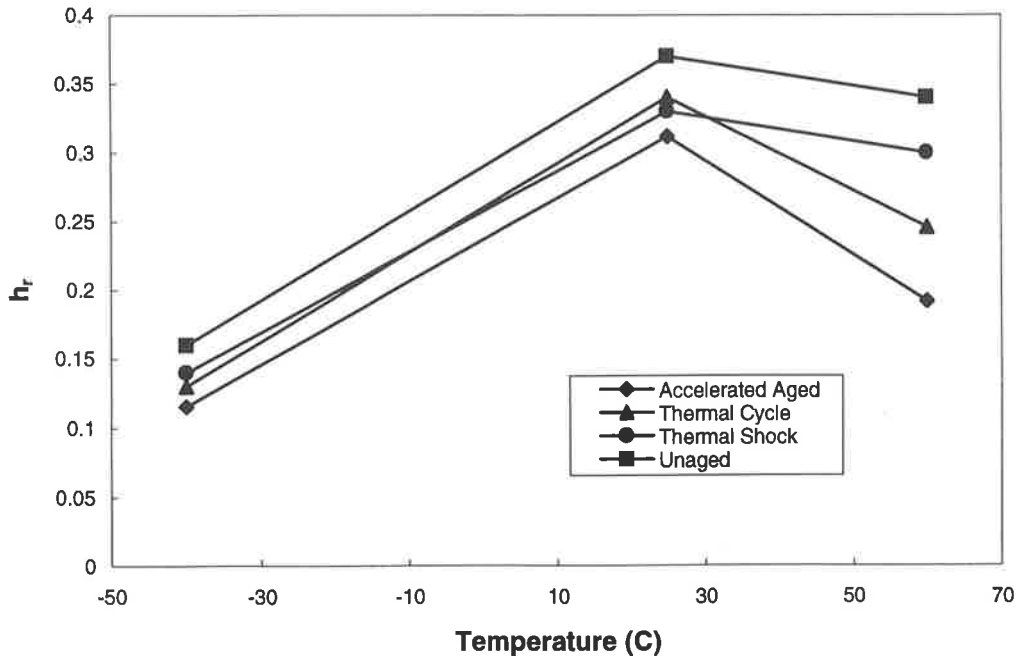

Figure 62 Change in hysteresis ratio with temperature for inhibitor ($\dot{\varepsilon} = 0.00077\ s^{-1}$)

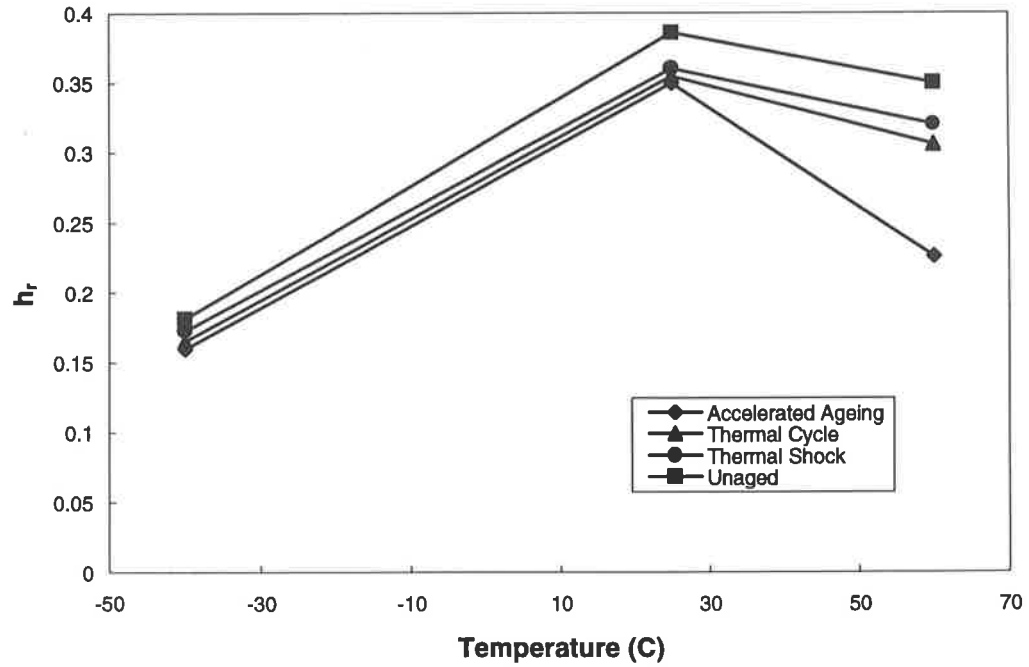

Figure 63 Change in hysteresis ratio with temperature for inhibitor ($\dot{\varepsilon} = 0.002\ s^{-1}$)

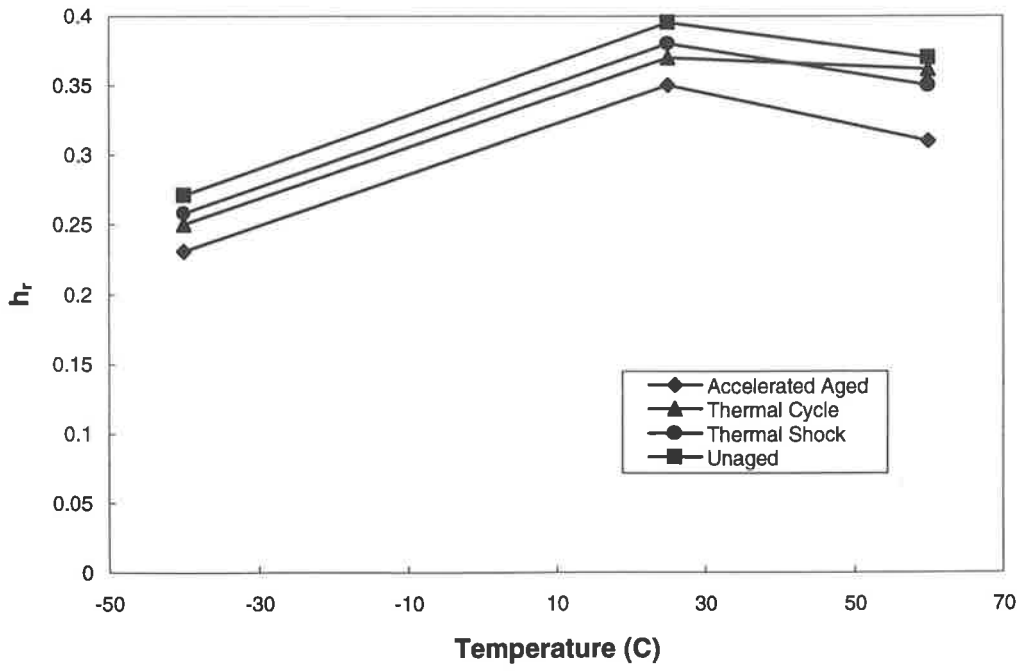

Figure 64 Change in hysteresis ratio with temperature for inhibitor ($\dot{\varepsilon} = 0.0037\ s^{-1}$)

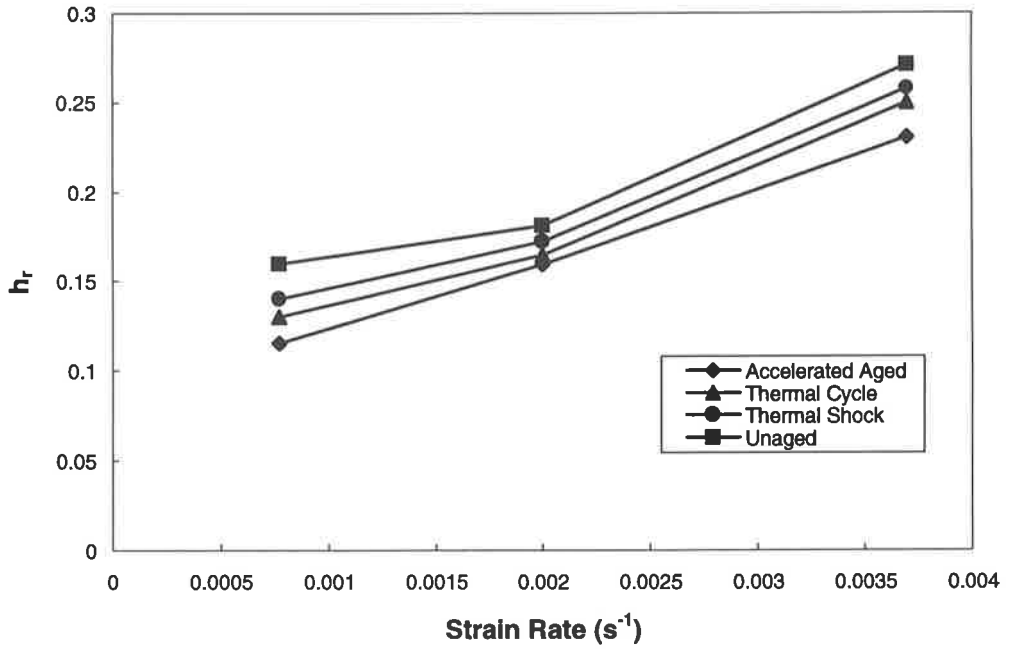

Figure 65 Change in hysteresis ratio with strain-rate for inhibitor (T= –40°C)

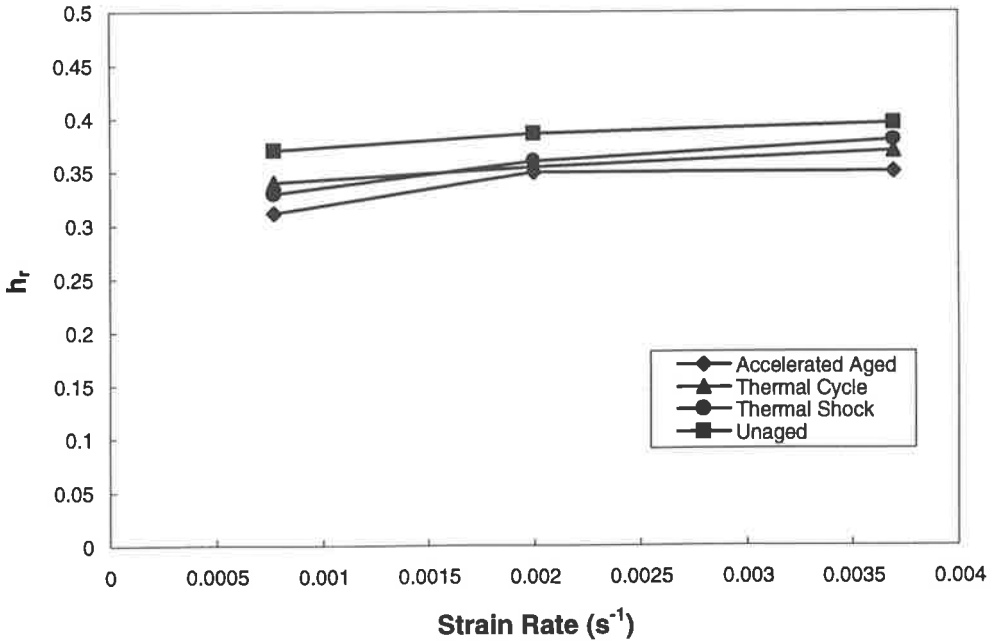

Figure 66 Change in hysteresis ratio with strain-rate for inhibitor (T= 25°C)

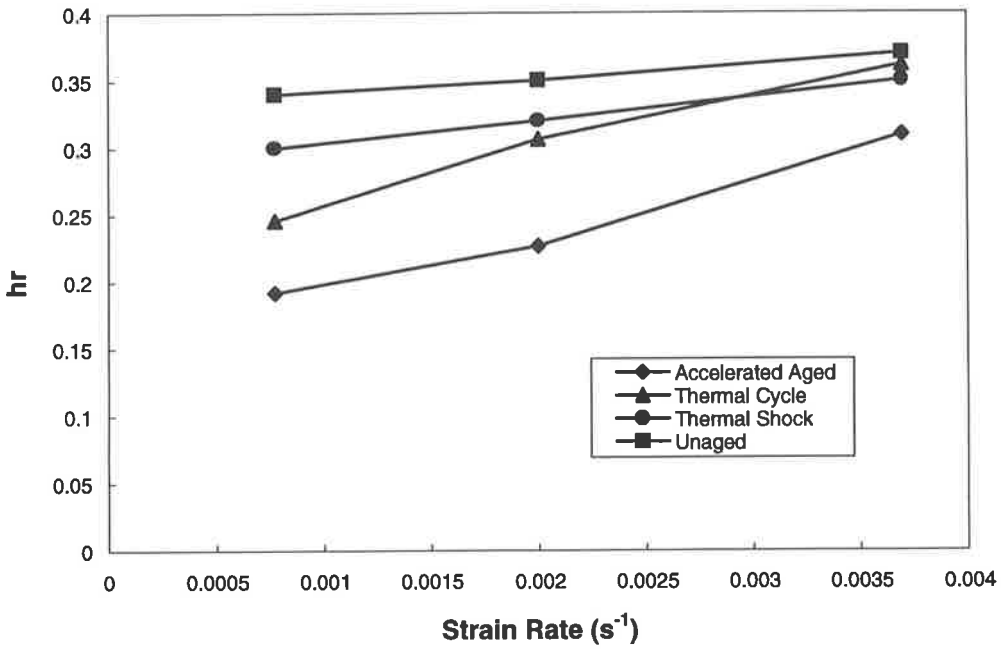

Figure 67 Change in hysteresis ratio with strain-rate for inhibitor (T= 60°C)

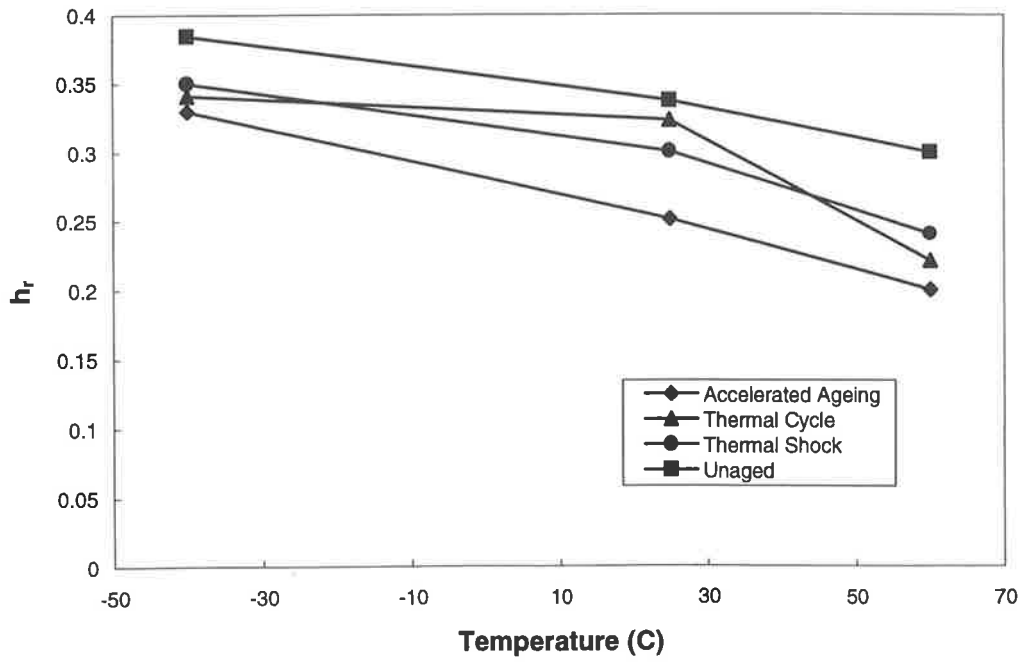

Figure 68 Change in hysteresis ratio with temperature for prop/inhb ($\dot{\varepsilon} = 0.00077\ s^{-1}$)

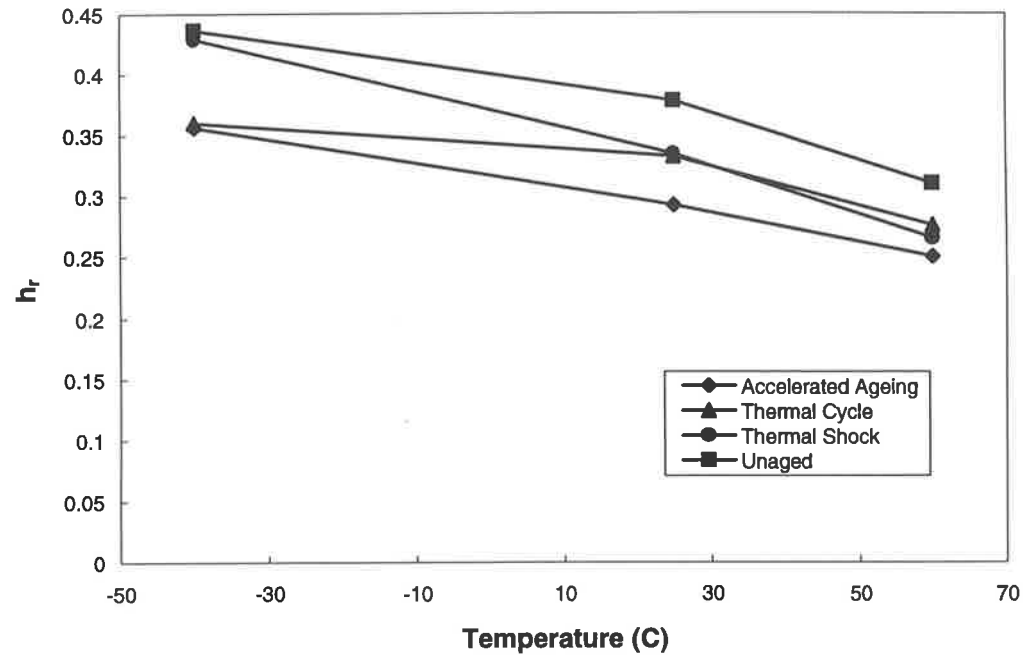

Figure 69 Change in hysteresis ratio with temperature for prop/inhb ($\dot{\varepsilon} = 0.002\ s^{-1}$)

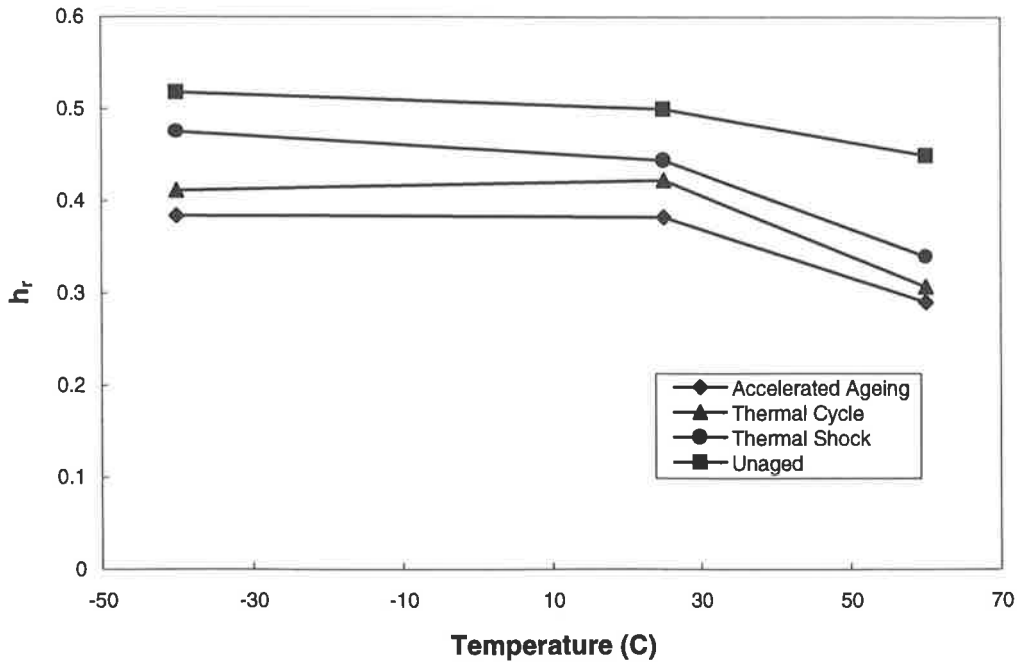

Figure 70 Change in hysteresis ratio with temperature for prop/inhb ($\dot{\varepsilon} = 0.0037\ s^{-1}$)

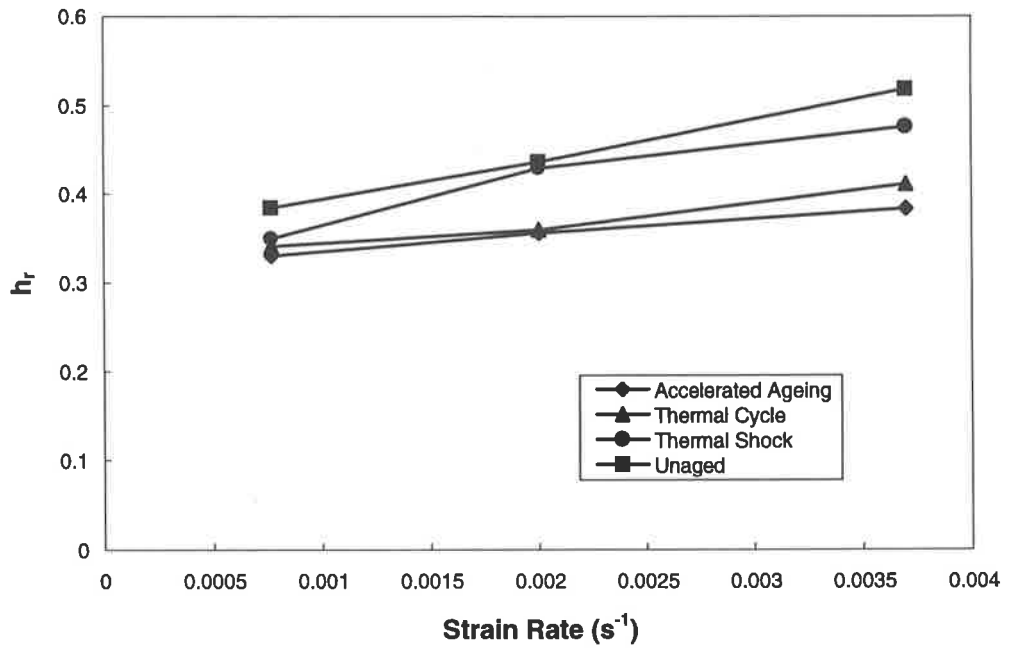

Figure 71 Change in hysteresis ratio with strain-rate for prop/inhb (T= –40°C)

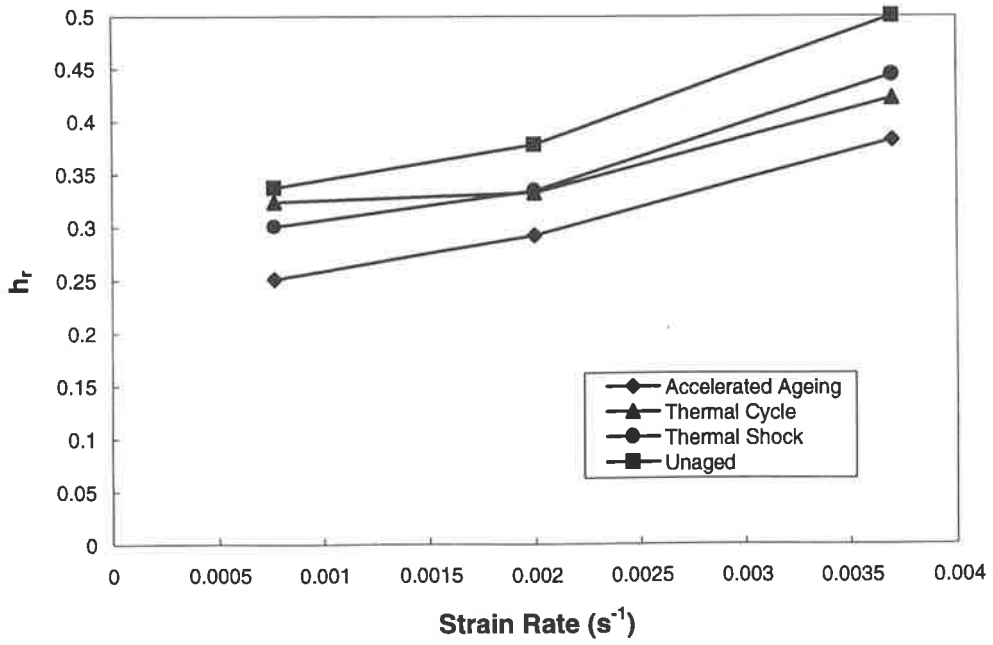

Figure 72 Change in hysteresis ratio with strain-rate for prop/inhb (T= 25°C)

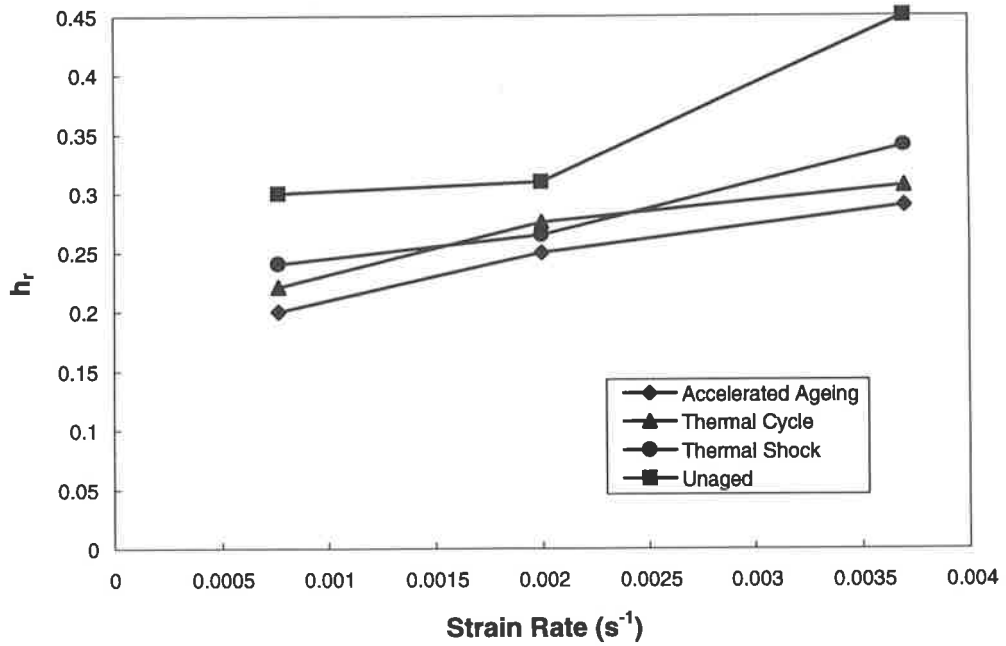

Figure 73 Change in hysteresis ratio with strain-rate for prop/inhb (T= 60°C)

CRACK GROWTH MECHANISM

There are relatively few investigations which have included the effect of temperature, strain-rate and ageing on the crack growth mechanism in a particulate composite. A detailed examination of the effect these variables have on the crack growth mechanism will provide a valuable understanding which can be incorporated into the modelling of the fracture process. The propagation of cracks in aged specimens was recorded to videotape during testing at various temperatures and strain-rates allowing the mechanisms of crack growth to be examined in each case. Images of crack growth captured from the videotape and magnified to highlight the area of interest are presented with the original colour videotape reproduced as 256 levels of grey.

Propellant

The image shown in Figure 74 was captured from the videotape record at a time corresponding to immediately after the application of the load to an unaged propellant specimen. The crack has not yet begun to propagate and the coarse fraction of AP particles are clearly visible in the surface of the propellant as the light grey spherical shaped objects. The initial razor blade cut can be seen as the straight sided area between graticule marks 50 and 66. A concentration of damage in the propellant can be clearly distinguished as a zone containing highly elongated fibrils of HTPB binder and dewetted filler particles, this area is marked on the image. The damage zone forms ahead of the crack whilst the tip itself remains blunt. Smith and Liu[5] observed crack growth in a series of tensile tests on a composite propellant and outlined a mechanism (described in the Literature Review) for the crack propagation. Figure 75(a) shows a schematic of crack tip blunting, the terminology employed by Smith and Liu will be adopted in this study.

The coarse particles of AP next to the tip of the cut were seen to dewet soon after the application of the stress. This behaviour agrees with that seen in the examination of the change in the value of Poisson's ratio with increasing strain. There, the large decrease in Poisson's ratio resulting from dewetting was observed to begin at strain levels greater than approximately 1.5%. The zone of dewetting continues to grow with increasing strain (Figure 75(b) shows a schematic representation of the damage formation in the zone ahead of the crack tip). Small voids surrounding the filler particles form and increase in size as fibrils begin to form from the elongation of dewetted HTPB binder. The small voids coalesce to form larger ones and the cross-sectional area of the fibrils reduces as they are elongated. The damage zone increased to a length of approximately 4.5 mm at which time the crack began to propagate. At this point the fibrils at the crack tip had grown to approximately 1.3 mm in height.

The fibrils in the damage zone rupture at thinned sections of material strained between filler particles or debond at the binder/filler interface. The crack propagates into the damage zone by coalescing with the voids and microcracks as the fibrils fail. Evidence from Scanning Electron Microscopy[55] (SEM) indicates that the particles of AP do not fracture, rather the crack propagates around them via breakage of the fibrils as described above. The crack was observed to extend perpendicular to the direction of the applied load but locally it deviates above and below the particles of AP in a random manner. This is also evident in the surface of the fracture, which was jagged.

Figure 76 shows the shape of the crack tip after it propagated into the damage zone. The crack extended by almost the equivalent of the length of the damage zone. It has resharpened, the few fibrils remaining in the old damage zone will soon fracture. The sharpening of the crack tip is schematically represented in Figure 75(c). A new zone of damage will form in the area ahead

of the crack tip at graticule mark 41. The size of each new damage zone formed during successive periods of crack tip blunting decreased only slightly.

The next picture (Figure 77) shows the crack propagation some time later. The crack tip has blunted and a damage zone is forming ahead of it from graticule marks 49 to 56. The shape of the crack tip as it propagates into the specimen can be described as a continual cycle of blunt-sharp-blunt. The mechanism of crack growth in the unaged propellant can be summarised as initial dewetting in a damage zone ahead of the crack tip, followed by formation of voids and microcracks which increase in size with the strain level. The fibrils of binder reduce in cross-sectional area as they elongate eventually failing at a critical level of strain, whereupon the crack tip propagates (and resharpens) into the damage zone by coalescing with the enlarging voids and microcracks resulting from the breakage of fibrils.

The unique nature of propellant is demonstrated by the distinct crack growth mechanism described above, however, there are comparisons with the mechanism outlined by Broek[59] and Knott[60] for ductile fracture in metals containing particles and inclusions (for example, carbide or nitride well bonded to the matrix). Under the influence of the applied stress the largest particles are loosened or break forming holes which are spaced in a zone ahead of the crack tip. As the stress increases necking between the inclusions may occur with the smallest particles remaining part of the continuous matrix. Eventually voids form around the smaller particles and the crack sharpens by the coalescence of the holes and voids surrounding the particles. The crack becomes blunted as a new zone of particles surrounded by voids commences ahead of the crack tip. The fracture surface is composed of large dimples from extensive inter-inclusion necking around the large particles and finer dimples derived from the smaller particles.

Figure 78 shows the fracture surface near the centre of an unaged specimen of propellant magnified with a Scanning Electron Microscope and Figure 79 shows the surface near the edge of the same specimen. Interpretation of the SEM photographs should be treated with a measure of caution due to the intervening time between performing the fracture test and the microscopy. However, the SEM photographs reveal the highly filled nature of the material with particles of both the coarse and fine fractions of ammonium perchlorate visible in the surface. Circular holes can be seen where AP particles were dislodged and remained in the other fracture surface. As expected the AP particles remained intact, as previously described the crack tip moves over or under particles in the path of the crack. Evidence of particle dewetting can be seen and some of the particles dislodged during this process are loose on the surface. There is no obvious dimpling effect on the surface which is usually the case after fibril breakage. Here the fibrils have relaxed back into the fracture surface. This highlights the importance of the stereo microscope and videotape record which allows details of the crack mechanism not revealed by SEM to be detected. The features left behind at both the edge and centre of the specimen show that the mechanism of crack growth was the same over the width of the specimen.

The damage zone and crack propagation response for an unaged propellant specimen tested at 60°C can be seen in Figure 80. A new damage zone can be seen to be forming after crack propagation extending from the original razor blade cut. It was observed that the crack began to propagate at a level of strain which was less than that for the propellant at 25°C. Just prior to the crack propagating by extension of the original cut, the area of damage that could be clearly distinguished was 2.8 mm in length and the fibrils at the crack tip were 0.83 mm in height. This damage zone is smaller than that measured at 25°C and suggests that the energy losses are less in the propellant at 60°C, a result which is consistent with the value of hysteresis

ratio measured at each temperature. The hysteresis ratio decreased from 0.39 at 25°C to 0.32 at 60°C (at a strain-rate of 0.0037 s^{-1}).

The crack propagated perpendicular to the applied stress as can be seen in Figure 81. The fibrils present in the previous image have failed and the crack tip can be seen to be in a state of temporary arrest while the damage zone increases in size. The size of successive damage zones formed decreases very slightly with crack extension. The mechanism of crack growth appears to be the same as that seen in the tests at 25°C, however, the size of the damaged zone was much reduced and the period between blunting and resharpening also decreased which was reflected in higher crack velocities.

The final picture in this series (Figure 82) shows the resharpened crack tip after propagation into the damage zone. The elongated fibrils of binder visible failed soon after this image was captured and the crack tip began to reblunt as a new damage zone formed. The similarity in the crack growth mechanism at ambient and elevated temperatures has been detailed in the study by Smith, Mouille and Liu.[27] They observed that for test temperatures of 22°C and 74°C the growth mechanism was the same.

Unaged propellant tested at –40°C is shown in Figure 83. The damage zone forms by the same mechanism as outlined previously. However, by comparison with the tests carried out at 25°C and 60°C the damage zone is greatly increased in size for the same level of strain. This correlates with the differences observed in the hysteresis cycles in the propellant at 25°C and 60°C compared to that at –40°C. There it was noted that the behaviour at 25°C and 60°C was similar but that at –40°C the stress level attained was substantially higher at the same strain. The initial razor blade cut can be seen at graticule mark 52 and the crack tip is blunt. Prior to crack propagation the damage zone attained a maximum length of 18.3 mm and the fibrils at

the crack tip were 5.3 mm in height, an area substantially greater than those at temperatures above zero. The strain level for crack propagation was higher than that observed in the tests at elevated temperatures. The higher value of hysteresis ratio (0.41) measured at –40°C reflect the greater energy losses.

At –40°C the propellant is closer to its glass transition and behaves in a much stiffer manner with substantially different mechanical properties (see Figure 49). The increased stiffness of the propellant means that for the same strain the stress level attained was much higher. The fibrils of binder also elongate to greater levels prior to failing, as compared to temperatures substantially above glass transition. This reason for the substantial difference in response of the crack growth was also proposed by Smith, Mouille and Liu[27] who studied crack propagation in a highly filled polymer at –54°C. They concluded that the proximity of the temperature in the material tested to the glass transition caused significant binder stiffening and resulted in much higher stresses to failure than when the material temperature was above zero.

The progress of the crack can be seen in Figure 84 and the model of the crack mechanism shown in Figure 75 remains valid. The crack did not increase in length an amount equal to the size of the damage zone but advanced only a fraction of this distance. Some of the remaining damage is seen between graticule marks 26 to 35. At this point it was observed that multiple damage zones were forming throughout the specimen. These zones contain processes which contribute to the overall irreversible energy losses and are distributed over a wide area. In Figure 85 a large number of the lightly coloured, spherical shaped particles of AP can be seen to have been almost completely dewetted, they are visible clinging to the fibrils of binder in the damage zone. As the strain continued to increase secondary cracks began to propagate. The original crack and secondary cracks connect and eventually the specimen ruptures.

The crack propagation in a specimen of propellant that had been subjected to the accelerated ageing conditions is shown in Figure 86. The test temperature was 25°C. On application of the load the crack propagated very quickly from the edge of the initial cut across the entire specimen. The ageing process has resulted in the binder becoming brittle and hardened with a subsequent reduction in the strain to failure of the propellant. The crack propagates at a strain of 1% as compared to 4% for the unaged material at 25°C and 0.0037 s^{-1}. The crack remained sharp at all times with no evidence of blunting or the formation of a damage zone. The decrease in the irreversible energy loss processes caused by exposure to accelerated ageing was also evident in decreased values of hysteresis ratio (see Table 2). Crack growth in the accelerated aged propellant at 60°C was the same as that observed at 25°C. However, there were measureable differences in the critical stresses and strains present and this will be discussed later (see section entitled Mechanical Properties).

A SEM photograph (see Figure 87) shows the fracture surface of a specimen of accelerated aged propellant. Similar features to those observed in the unaged material can be seen, particles of AP have become dewetted and circular holes remain where others have been removed during the fracture process. A significant difference to the unaged material, however, is the appearance of some fractured particles in the surface. Rather than passing over or under, the crack appears to have propagated via particle fracture. In particular the surface of a large ammonium perchlorate particle which occupies the centre of the image shows evidence of fracturing. When subjected to the accelerated ageing the AP particles oxidise and become more brittle. A damage zone was not detected on the videotape record therefore the large energy losses associated with dewetting and fibril formation were absent. A brittle type of fracture ensued with subsequent low levels of energy loss as a proportion of the energy input. This

result correlates with the low levels of critical stress and strain measured in the accelerated aged specimens.

Figure 88 shows the crack growth at –40°C in an accelerated aged specimen of propellant. The crack has propagated rapidly along the length of the specimen due to the brittle nature of the material. The mechanism of crack growth is similar to that found in the accelerated aged specimens at above zero temperatures, a sharp crack with no visible damage zone. There was, however, a small number of fibrils left in the centre of the specimen which did not fail immediately and their presence suggests that the level of energy losses was greater than that for an accelerated aged specimen tested at 25°C. This is consistent with the higher hysteresis ratio measured for the accelerated aged material at –40°C. The temperature in the material is closer to that of the glass transition and hence the stiffness of the propellant will be increased. The stress level attained increased substantially and the critical strain decreased only slightly, hence the amount of recoverable energy available for crack propagation will be markedly increased.

Crack propagation tests were carried out on specimens of propellant which had been subjected to thermal shock and thermal cycle loadings. The mechanism of crack growth was observed to be the same as that in the unaged propellant and the size of the damage zones were similar in magnitude. However, the stress at crack propagation was greater and the strain lower (the hysteresis ratio was also lower which provides evidence for the effect of ageing on propellant behaviour, other characteristics such as the change in crack velocity will be discussed later). Crack propagation tests were carried out at each of the three strain-rates detailed in the experimental method, a small increase in the size of the damage zone and stress level required for crack growth was observed with increasing strain-rate.

Inhibitor

Figure 89 is an image of the crack tip and surrounds in a specimen of unaged inhibitor 7 seconds after the load was applied. A graticule fixed into the stereo microscope to video camera adaptor can be seen in the top half of the image. Approximately 17 subdivisions on the graticule represents a distance across the image of 10 mm. The straight sides of the initial 10 mm cut, made with the razor blade, can be seen between the graticule marks 49 and 66. The crack tip can be seen between graticule marks 47 to 49 it is wedge shaped and has a rough surface by comparison to the cut portion.

As the load was applied, the area to the left of graticule mark 50 began to change colour, whitening, almost immediately. The intensity of pixels in the images increase with the level of stress. Areas of stress whitening are represented by pixels of high intensity and regions of low stress appear as dark areas. The stress whitening was observed to spread rapidly but unevenly as time progressed and the stress increased. In particular, an intensely whitened circular area can be observed on the image just ahead of the crack tip. The whitening is caused by damage to the material in the form of binder/filler dewetting and crazing.[3] The intensity of the whitening suggests that the amount of dewetting and voiding (and therefore the energy losses) occurring in this concentrated zone of damage is substantially higher than that throughout the rest of the specimen.

As the crack propagated through the specimen its progress across the specimen's surface was tracked by the video camera. Figure 90 shows the crack growth in the same specimen after 17.2 seconds. Overall the crack moves through the specimen perpendicular to the applied stress but locally it deviates up and down as evidenced by the uneven fracture surface. Figure 91 shows a SEM photograph of the fracture surface in the centre of the unaged inhibitor

specimen and Figure 92 is the fracture surface near the edge of the same specimen. The fracture surface contains angular particles of ammonium sulphate which have remained in the surface of the crack and correspondingly shaped holes left behind by the particles carried away in the other fracture surface. The particles remaining do not appear to have been fractured during the crack propagation and many have been dewetted from the binder under the applied stress. Between the particles the polyurethane binder has a smooth appearance with no evidence of fibril formation during the crack propagation. This correlates with the continuously sharp crack tip observed, which is discussed below. The photographs show that the mechanism of crack propagation was the same over the surface of the fracture.

In Figure 90 the tip of the propagating crack has remained relatively sharp. The small fragment of material near the surface of the specimen which has remained attached to both sides of the crack, broke very soon after this image was captured. This behaviour was typical. The propagating crack continues to remain fairly sharp at all times and advances across the specimen without blunting. The mechanisms described above for crack growth in unaged inhibitor define which processes are the major causes of energy loss during fracture. An understanding of the effect of temperature and ageing will aid the modelling of crack propagation in materials exposed to thermal loads. A comparison with those mechanisms present during the crack propagation in propellant and at the propellant/inhibitor interface can be made.

The damage resulting as strain increases has been discussed previously in the section dealing with the variation of Poisson's ratio. For the inhibitor it was observed that the binder/filler bonding was high by comparison to that in the propellant. This stronger resistance to dewetting results in the absence of crack blunting,[27] which is usually associated with crack propagation in propellant. The mechanism of crack growth can be described as one of tip advancement into

the damaged zone by material tearing.[33] It can be seen that the diameter of the intensely whitened damage zone increases with strain. This indicates that the number of microvoids and the dewetting continues to increase with the level of strain. Eventually the damage zone grows to encompass the dimensions of the specimen.

The crack growth mechanism discussed above can be compared to that shown in Figure 93 for which the test temperature was 60°C. Immediately after the load was applied the surface of the specimen to the left of the razor cut was observed to whiten. An intensely whitened damage zone again formed ahead of the crack before it began to propagate. Again the crack tip moved perpendicular to the applied load, however, no local deviations were observed. The tip remained sharp at all times without blunting.

The progress of the crack at a strain level of 13.7% can be seen in Figure 94. It was noted that the crack surfaces have a smoother appearance than those observed in the specimen tested at 25°C. At the elevated temperature the polyurethane binder has been significantly softened, the mechanism of crack growth is the same but the material tears at a much lower stress. In this image the damage zone has extended to the limits of the specimen, the crack continued to propagate without any further intensifying of the stress whitening. At this point the intensity of the pixels in the specimen was less than that in the specimen tested at 25°C indicating a lower level of damage was present. This behaviour correlates with that observed in the hysteresis tests, as the temperature of the material was increased from 25°C to 60°C material softening caused a reduction in the hysteresis ratio measured. The energy losses from binder/filler dewetting, vacuole formation and binder failure decreased as a proportion of the energy input.

A comparison of the size of the damage zone in the unaged specimens of inhibitor at 25°C and 60°C for a strain-rate of 0.002 s^{-1} was performed. At 6% strain and 25°C the diameter of the

roughly circular zone of damage ahead of the crack tip was approximately 5.4 mm, for the test at 60°C the diameter was 0.5 mm. This decrease in the size of the damage zone would again appear to correlate with the reduced energy loss processes measured at 60°C compared to those at 25°C.

All of the aged and unaged specimens of inhibitor tested at –40°C underwent a brittle type of fracture. The glass transition temperature of the inhibitor varied from –42.8°C for the thermally shocked specimens to –40.2°C for the accelerated aged specimens. Hence, at –40°C all of the specimens will approach or behave in a glass-like manner. In all cases, on application of the load, the stress whitening was restricted to a small zone adjacent to the crack tip (see Figure 95). The crack propagated rapidly across the specimen and Figure 96 was captured when the strain level had increased to 2.6%. In the 0.1 second time period that has elapsed between this and the previous image, the material has completely fractured.

At a strain-rate of 0.002 s^{-1} the diameter of the damage zone in the unaged inhibitor reached a maximum of 1.2 mm just prior to specimen failure at 3% strain. These values were typical of the size of the damage zone and strain to failure measured in the inhibitor at –40°C. This is also consistent with the values of hysteresis ratio for specimens of inhibitor at –40°C which were much lower than for specimens tested at 25°C.

The effect of ageing on crack growth is illustrated in the next series of figures discussed. Figure 97 shows the crack propagating in an inhibitor specimen at 25°C which had been subjected to accelerated ageing and Figure 98 the crack propagation in a thermally shocked specimen. The damage zone at 6% strain in the accelerated aged and thermally shocked specimen measured 4.8 mm and 5.2 mm in diameter, respectively. The diameter of the damage zone in a thermally cycled specimen at an equivalent strain was similar in magnitude. In general

the difference between the size of the damage zone in the aged materials and those in the unaged specimens was unable to be determined as it was less than the measurement error. However, the mechanism of crack growth was observed to be the same for all the aged and unaged materials.

Whilst no effect was detectable from image analysis as a result of ageing on the crack growth mechanism at each of the three test temperatures, differences in the extent of damage, were observed in the values of hysteresis ratio measured. At each test temperature the value of hysteresis ratio decreased with the severity of the ageing. Differences were also found to be reflected in the values of crack velocity measured.

A SEM photograph presented in Figure 99 shows the fracture surface at the centre of an accelerated aged specimen of inhibitor. The photograph shows that the crack mechanism had the same characteristics as that in the unaged specimen. No evidence of fibril formation was seen, dewetted particles of ammonium sulphate remain on the surface and the angular holes left by those particles removed with the other surface are obvious. The surface appears to contain more damage, specifically more particles appear to have been dewetted from the binder, when compared to the unaged material. This observation whilst not detected in the videotape record of the crack growth does correlate with the greater critical stress measured for the accelerated aged specimens, which will be discussed in a following section.

A crack propagation test on aged and unaged specimens was carried out at each strain-rate ($0.00077s^{-1}$, $0.002\ s^{-1}$ and $0.0037\ s^{-1}$). No difference was detected by the image analysis in either the mechanism of crack growth or the size of the damage zone at each strain-rate. However, the effect of strain-rate was detected in the values of hysteresis ratio presented and other measures, such as the critical stress.

Propellant/Inhibitor Bimaterial

A description of the mechanism of crack growth at the bondline of the propellant and inhibitor will provide an insight into crack propagation at material interfaces which has not previously been reported. Thus allowing a better interpretation of the effect of ageing and temperature on crack growth for the purposes of FEM. Firstly, cracking in an unaged bimaterial specimen of propellant/inhibitor at 25°C was captured from the videotape record which is shown in Figure 100. Initially the crack was formed by placing a 10 mm piece of teflon tape on the surface of the inhibitor prior to casting the propellant material and this is present in the image from graticule marks 49 to 66. When the load was applied a damage zone began to form in the layer of propellant adjacent to the initial crack and close to the interface of the two materials. No stress whitening of the inhibitor material was evident as expected. The inhibitor has a much higher stiffness relative to that of the propellant and a damage zone does not form in the inhibitor at those strain levels which caused crack propagation in the propellant.

The crack mechanism observed in the propellant/inhibitor bimaterial specimens was similar in most respects to that described above for the propellant specimens. A damage zone consisting of dewetted filler particles and elongated fibrils of binder forms in the layer of propellant ahead of the crack tip. The damage zone increases in size with strain and extends along the bondline in the propellant layer. Prior to crack propagation the concentrated zone of damage measured 9.2 mm in length and the fibrils at the tip of the crack were 0.6 mm in height, which suggests a damage zone that is slightly smaller (by approximating the area of the zone) than for a propellant specimen at the same strain. The strain reaches a critical level where the elongated fibrils of HTPB binder fail between the particles or at the binder/filler interface. The crack propagates into the damage zone and advances in a direction perpendicular to the applied

stress along the interface of the two materials. The fracture of the bimaterial specimen can be regarded as cohesive in the propellant.

Figure 101 shows the crack some time later at a strain level of 3%. The crack has extended a distance equal to only a fraction of the length of the damaged zone. As it advanced into the damaged zone the redistribution of stresses causes a new zone of damage to form ahead of the crack tip whilst it is blunted. The crack growth can be described as blunt-sharp-blunt, the model of this mechanism was presented in Figure 75.

Specimens of propellant/inhibitor were also tested at elevated and sub-zero temperatures. The mechanism of crack growth was observed to be the same process of blunt-sharp-blunt as that at 25°C. The crack shown in Figure 102 is of an unaged propellant/inhibitor specimen at 60°C. The crack has propagated from the initial cut formed by the teflon tape and resharpened by extending a distance equal to the length of the damaged zone in the propellant layer. No damage to the inhibitor layer was detected. A comparison of the damage zone to that in a propellant/inhibitor specimen at 25°C reveals a smaller area measuring a maximum length of 2.7 mm with a fibril height at the crack tip of approximately 0.4 mm just prior to crack propagation. The smaller damage zone corresponds to the value of hysteresis ratio which also decreased with increasing temperature. The binder in the propellant will be softened at the higher temperature and as such the stress at specimen failure will be lower (the corresponding critical strain level increases), however, the amount of recovered strain energy is less than at 25°C.

The crack growth response in unaged propellant/inhibitor bimaterial specimens at –40°C was examined. Figure 103 shows the response of such a specimen soon after the application of the load. The filler particles in the propellant have begun to dewet resulting in a zone of damage

adjacent to the interface of the two materials. Both materials are stiffened as they are closer to their respective glass transition temperatures. The stress and strain at crack propagation for both will be increased compared to temperatures further away from the glass transition. Although the specimens were strained to higher levels in tests at –40°C it was still below that required to cause damage in the stiffened inhibitor material, hence no stress whitening was observed in the inhibitor.

Figure 104 shows the growth of the voids and microcracks in the same specimen at some time later. It can be seen that the crack has not yet begun to propagate and the tip remains blunt. The damage zone (and correspondingly the hysteresis ratio) was substantially greater than those observed when the material temperature was above zero. Prior to the crack propagating the damage zone reached a maximum length of 20.9 mm whilst the fibrils at the crack tip were 1.5 mm in height. The crack extended only a fraction of the length of the damaged zone before a new one began to form. Before the specimen failed a number of secondary damage zones appeared at random positions in other areas of the propellant material these eventually unite with the primary crack causing specimen failure.

The last two images presented are from tests of the propellant/inhibitor specimens that had undergone accelerated ageing. Figure 105 is an image captured from a test conducted at 60°C and Figure 106 from a test at –40°C. In both cases soon after application of the load the crack propagated rapidly across the specimen's length in the propellant at a point immediately adjacent to the bondline. Due to the increased hardening and brittleness of the propellant from the processes occurring during ageing the strain to failure was greatly reduced in these specimens. No damage zone was observed and the crack did not blunt but remained sharp as it propagated. A similar type of crack mechanism was observed in accelerated aged specimens at 25°C. The difference in the crack growth response at each temperature was not visible in the

videotape record but the variation in the mechanism of crack growth observed is important when considering the changes caused by ageing in crack velocity and other mechanical properties such as critical stress, these characteristics will be discussed in the following sections.

Tests were carried out on bimaterial specimens that had been subjected to thermal shock and thermal cycle conditioning. There was no detectable difference in the mechanism of crack growth compared to the unaged specimens. The size of the damage zone for specimens which had been thermally shocked or cycled was measured for tests carried out at the three test temperatures and was found to be similar in magnitude to those observed for the unaged specimens. Again tests for crack propagation were carried out at each of the three strain-rates specified. The mechanism and response of crack growth was observed to be the same for each, however, as expected an increase in the stress required to cause crack propagation with strain-rate was noted.

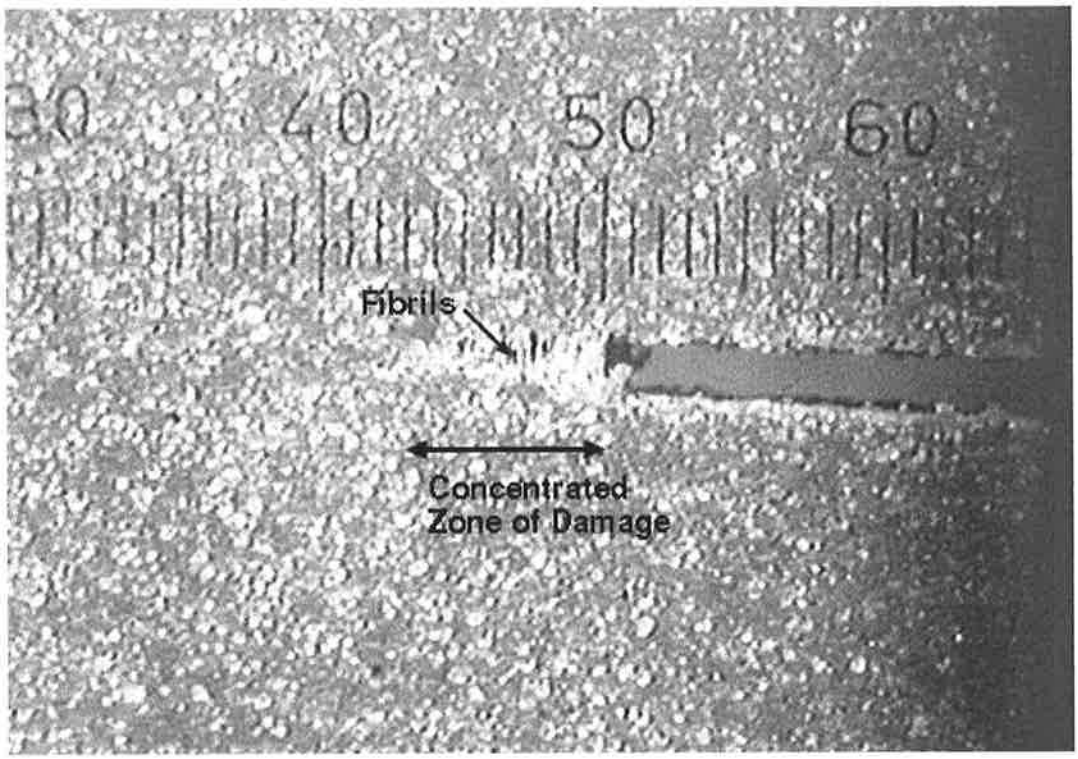

Figure 74 Propellant unaged, T= 25°C, ε= 4.1%

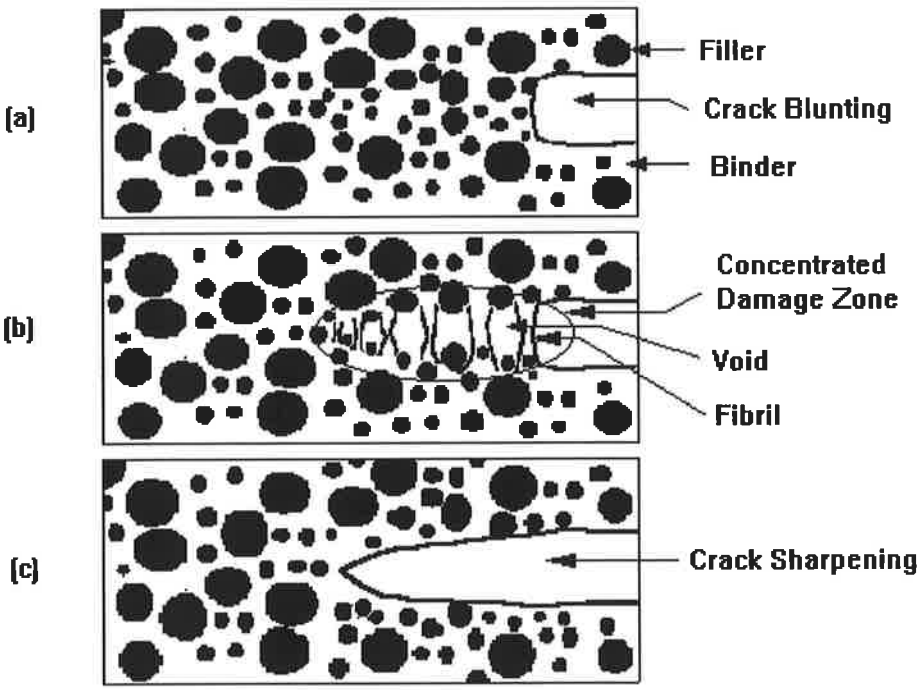

Figure 75 Model of crack propagation mechanism in propellant

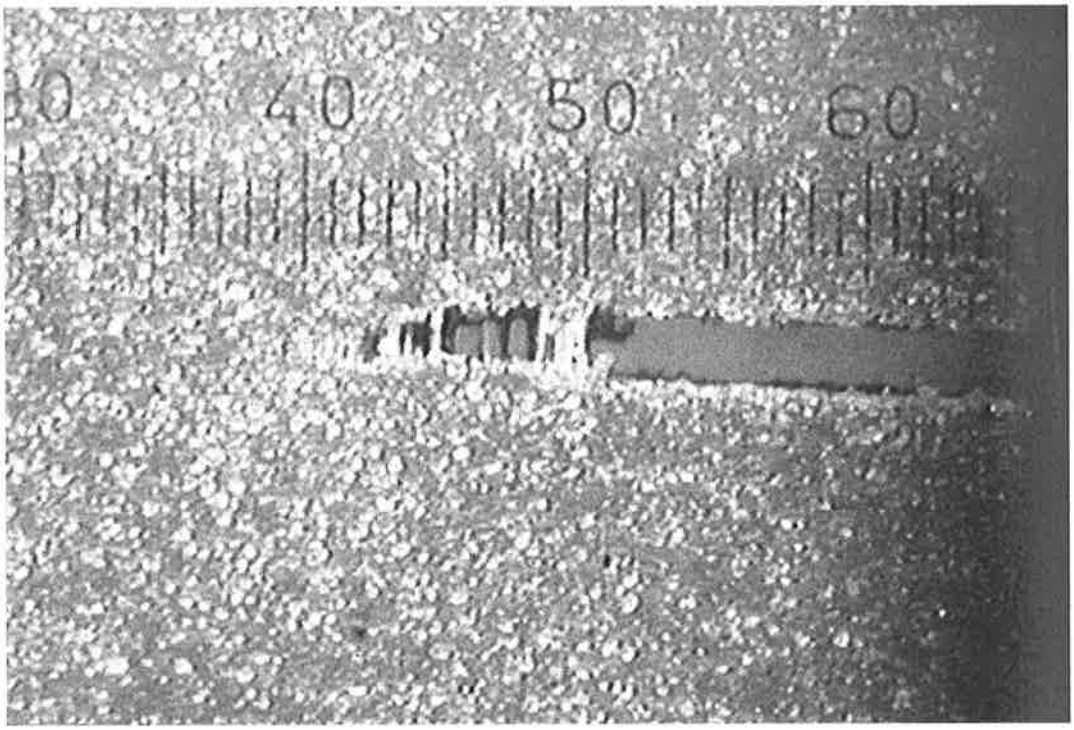

Figure 76 Propellant unaged, T= 25°C, ε= 4.5%

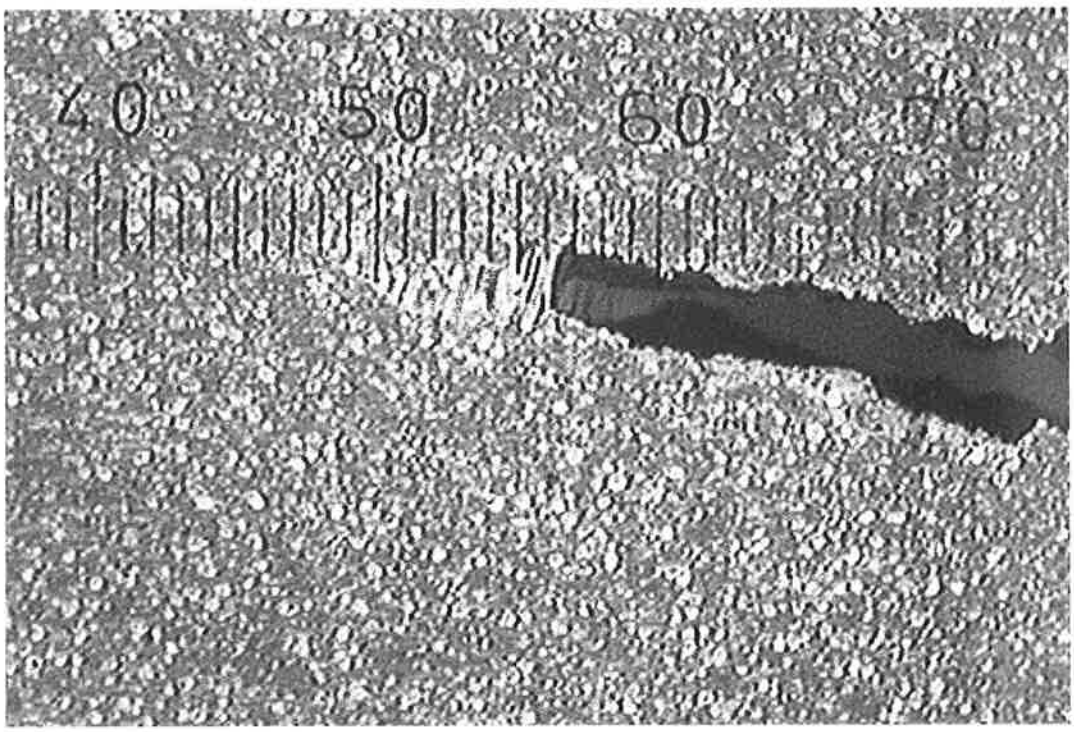

Figure 77 Propellant unaged, T= 25°C, ε= 6.1%

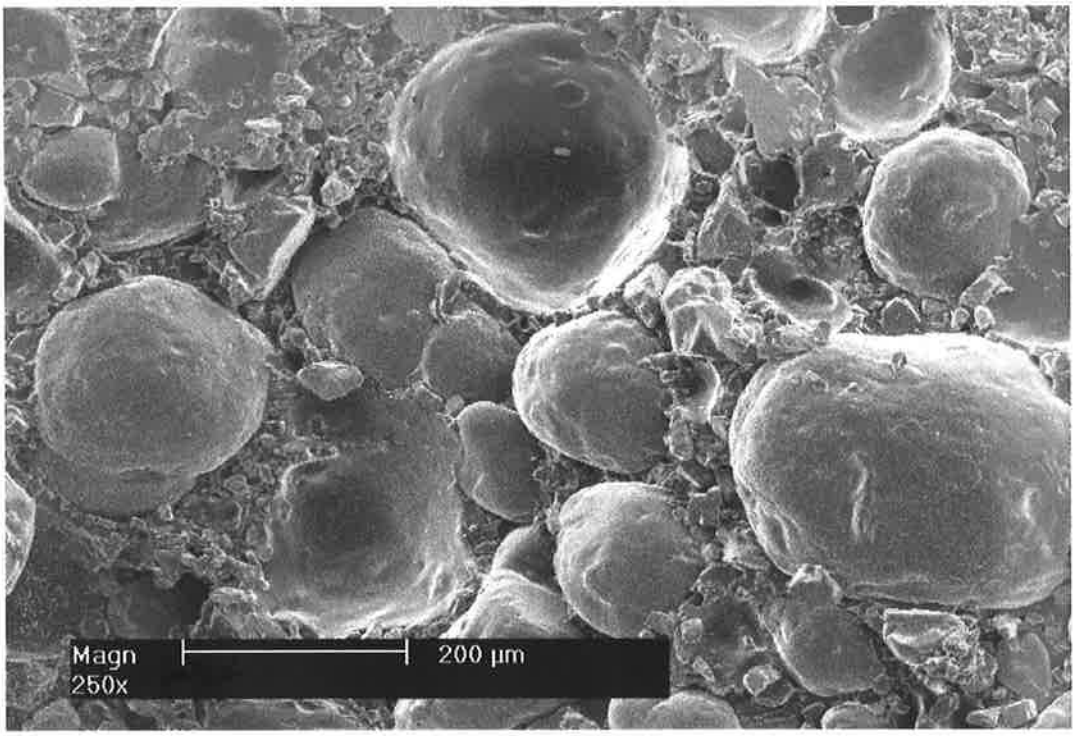

Figure 78 SEM showing centre of fracture surface in unaged propellant, T= 25°C

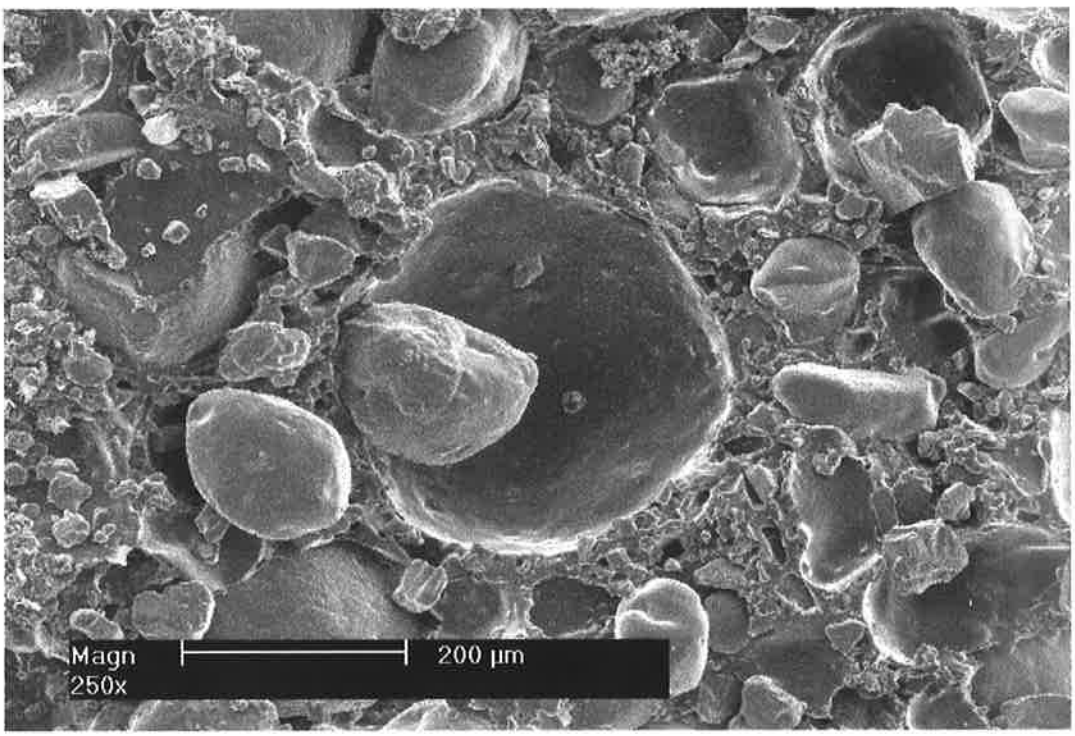

Figure 79 SEM showing edge of fracture surface in unaged propellant, T= 25°C

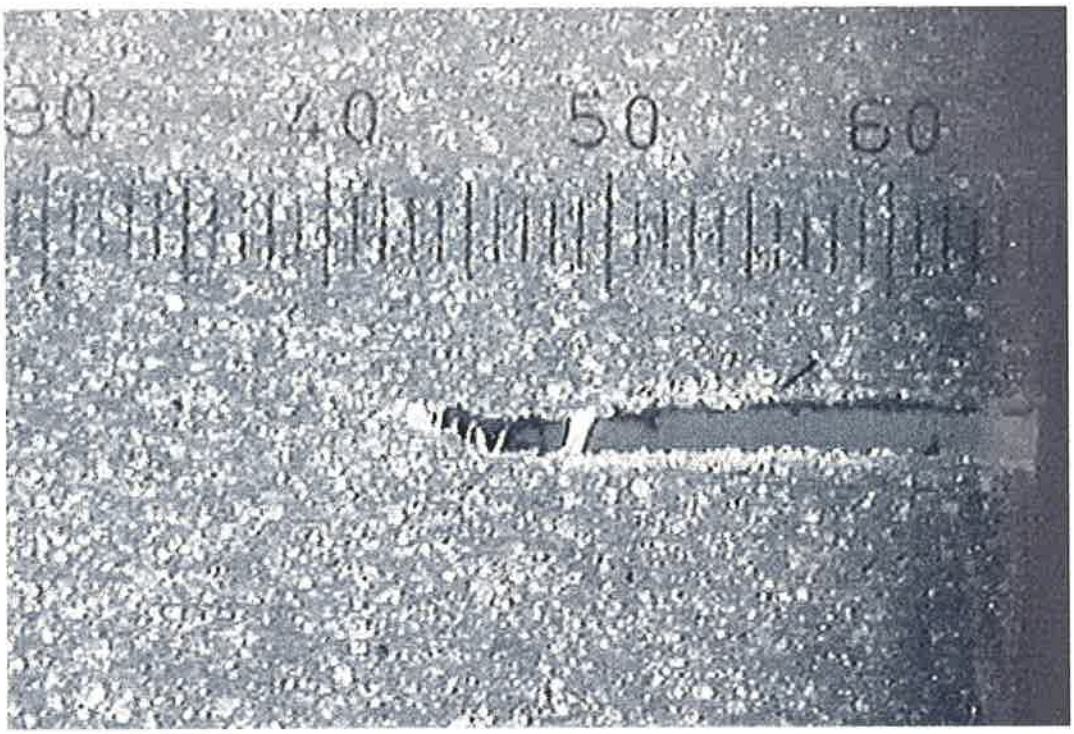

Figure 80 Propellant unaged, T= 60°C, ε= 3.3%

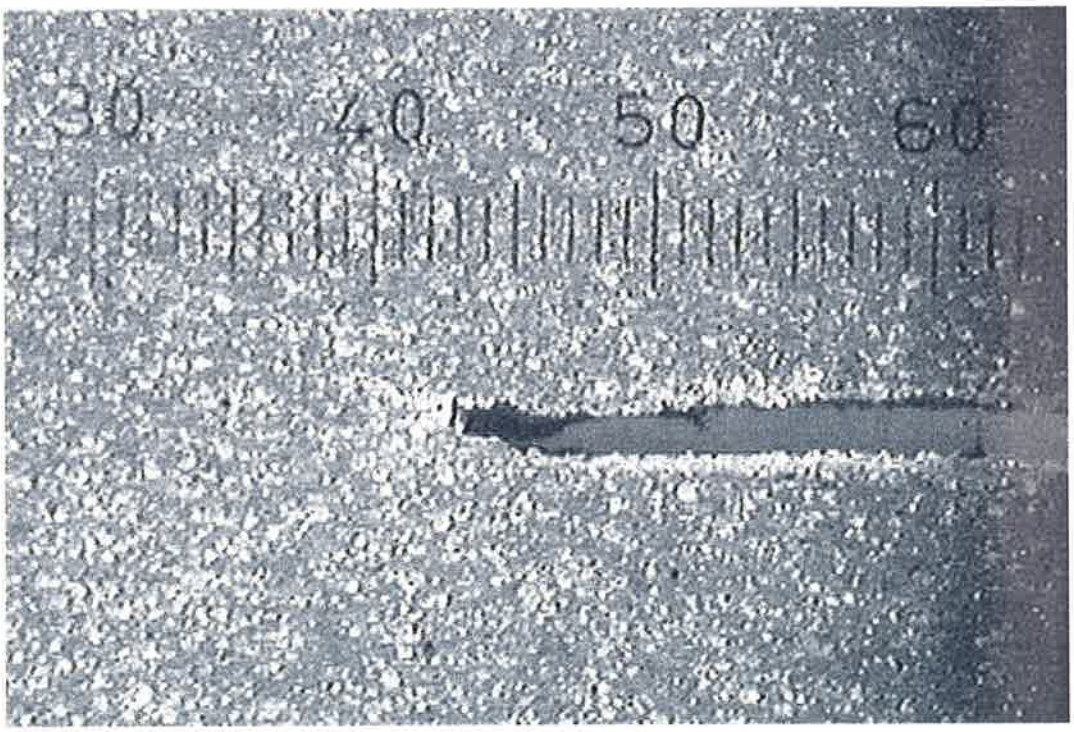

Figure 81 Propellant unaged, T= 60°C, ε= 3.6%

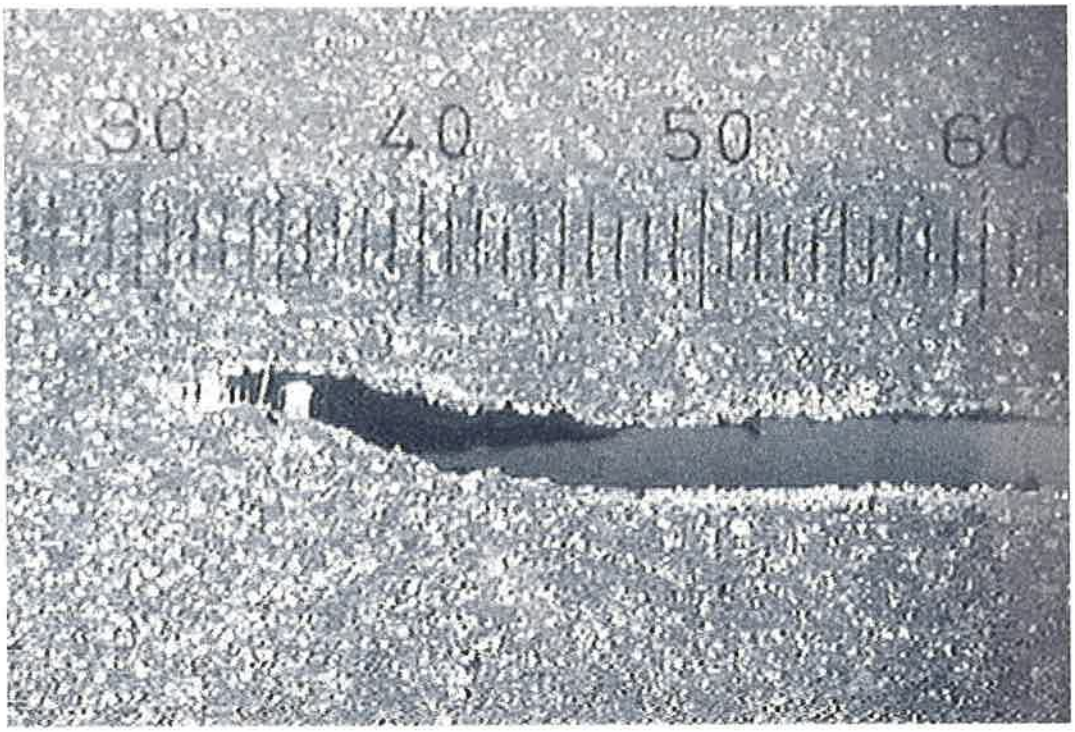

Figure 82 Propellant unaged, T= 60°C, ε= 4.1%

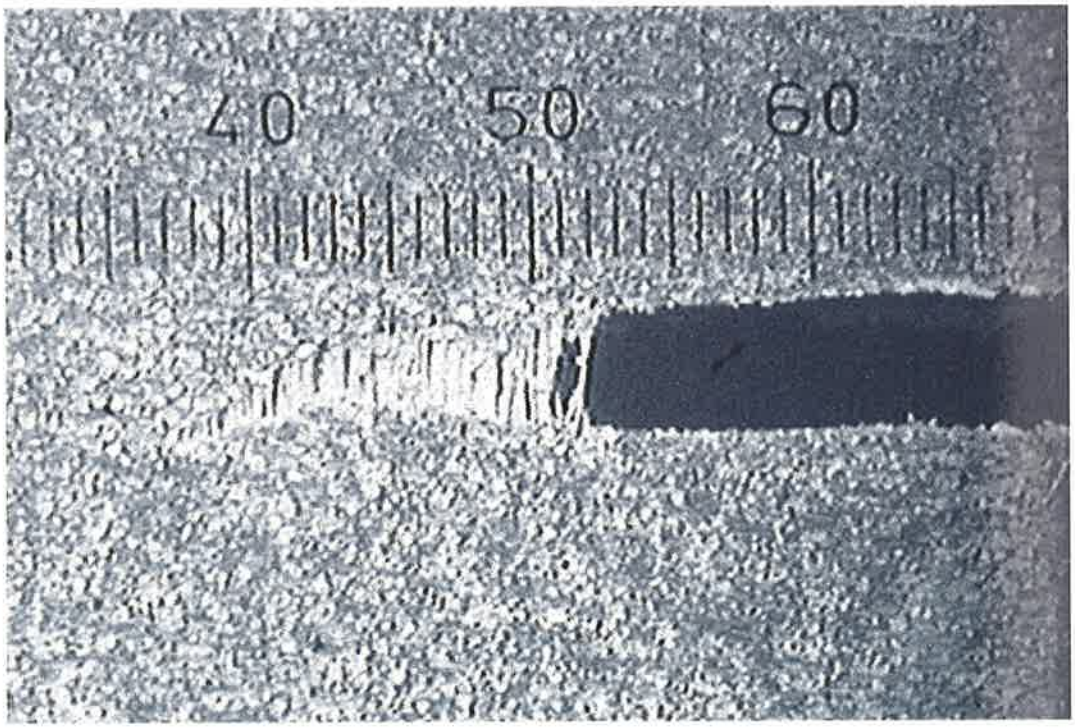

Figure 83 Propellant unaged, T= –40°C, ε= 6.0%

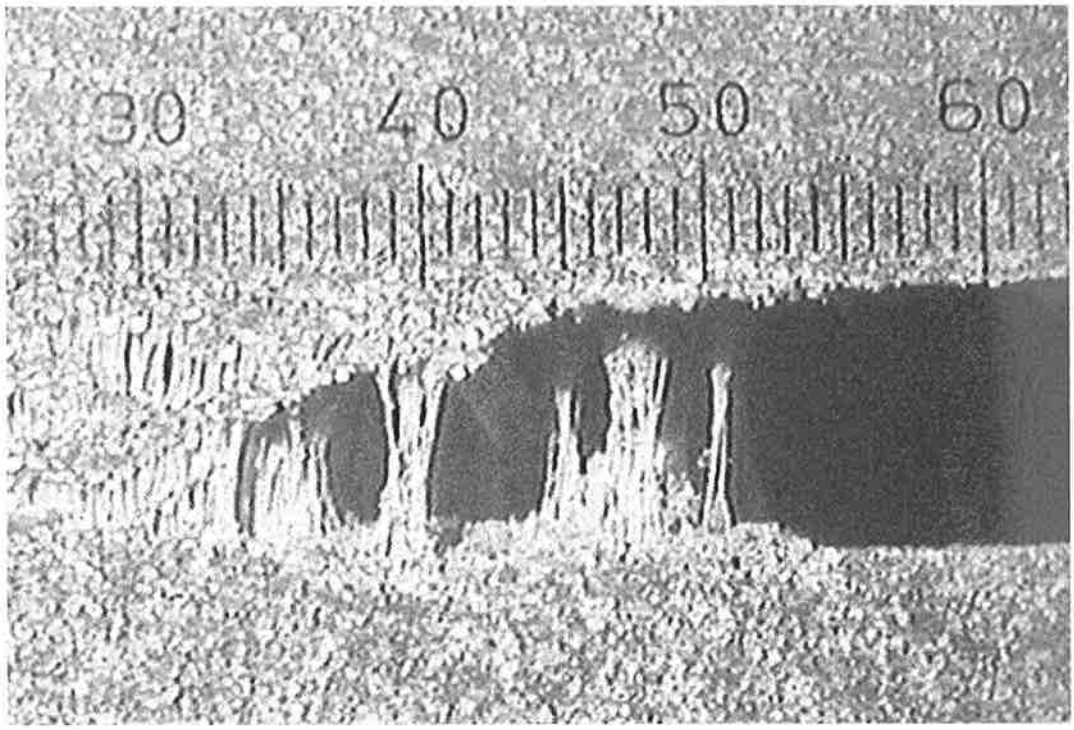

Figure 84 Propellant unaged, T= –40°C, ε= 10.5%

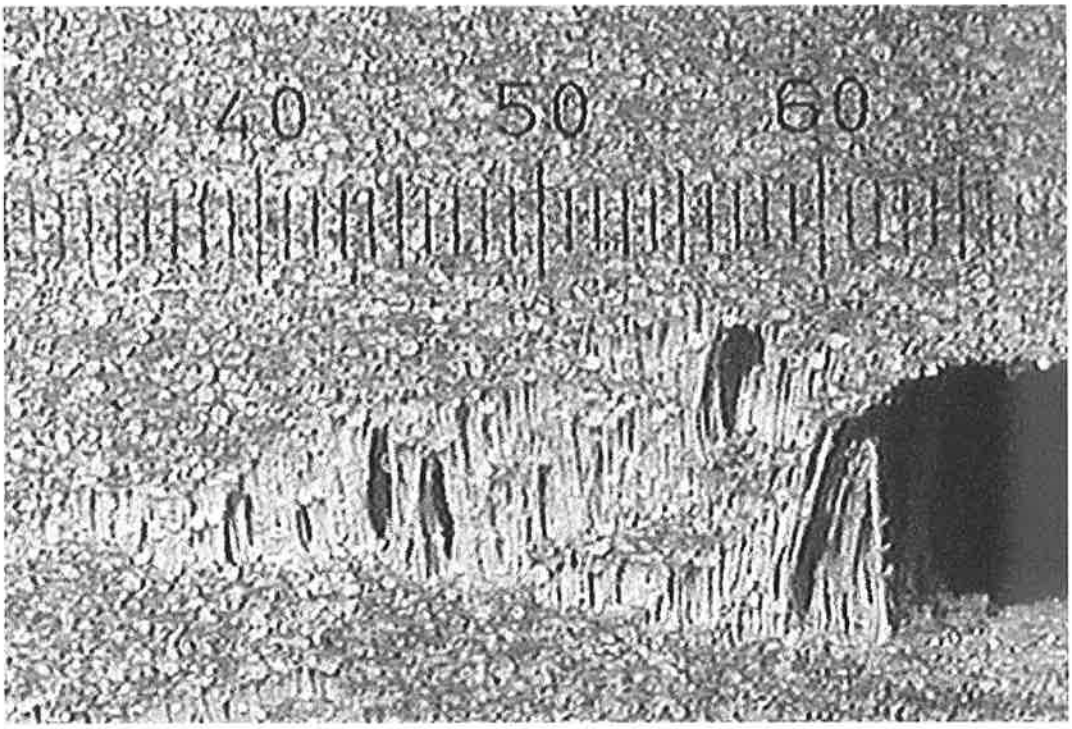

Figure 85 Propellant unaged, T= –40°C, ε= 14.0%

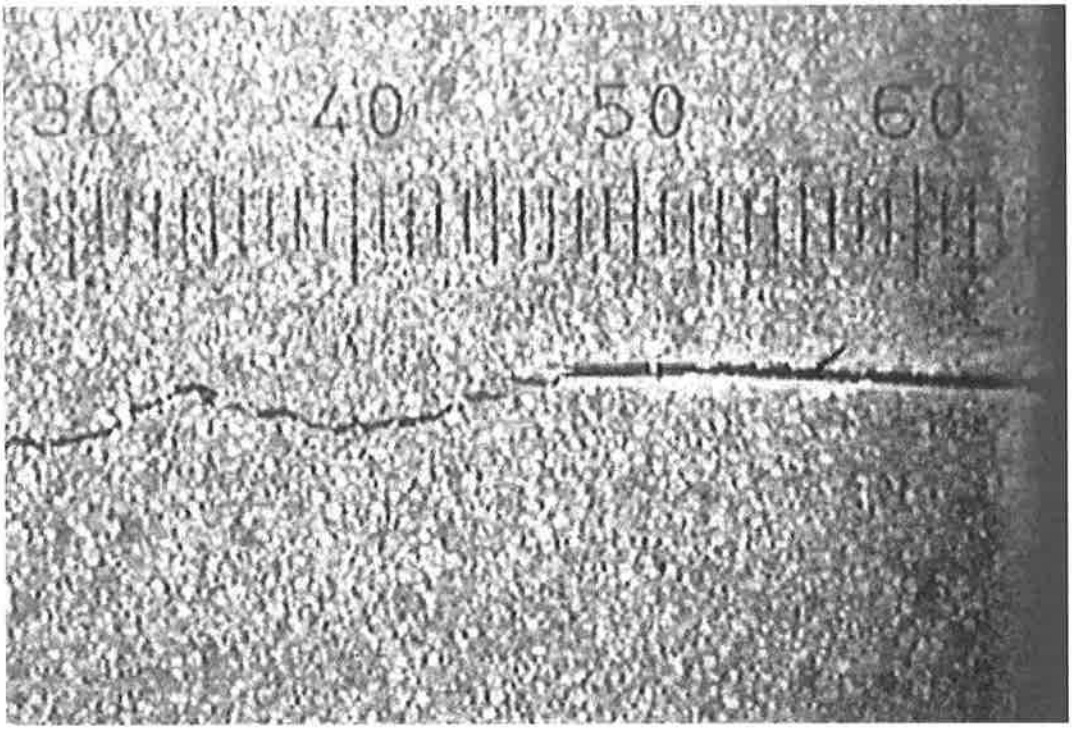

Figure 86 Propellant accelerated aged, T= 25°C, ε= 1.5%

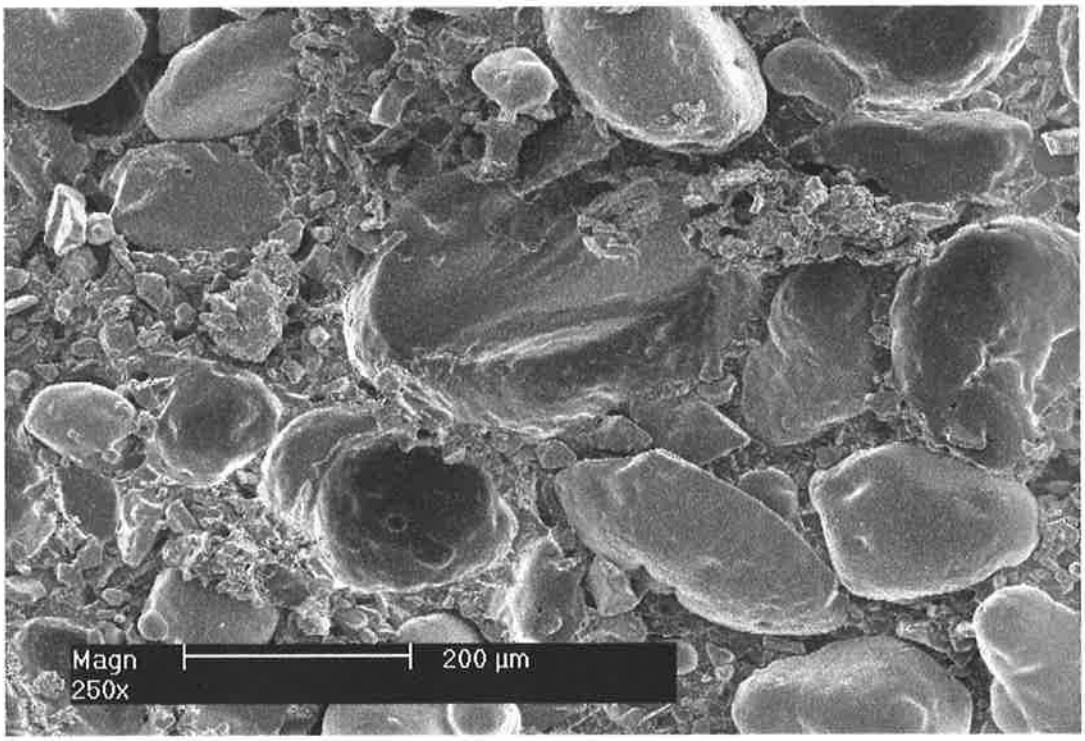

Figure 87 SEM showing fracture surface in accelerated aged propellant, T= 25°C

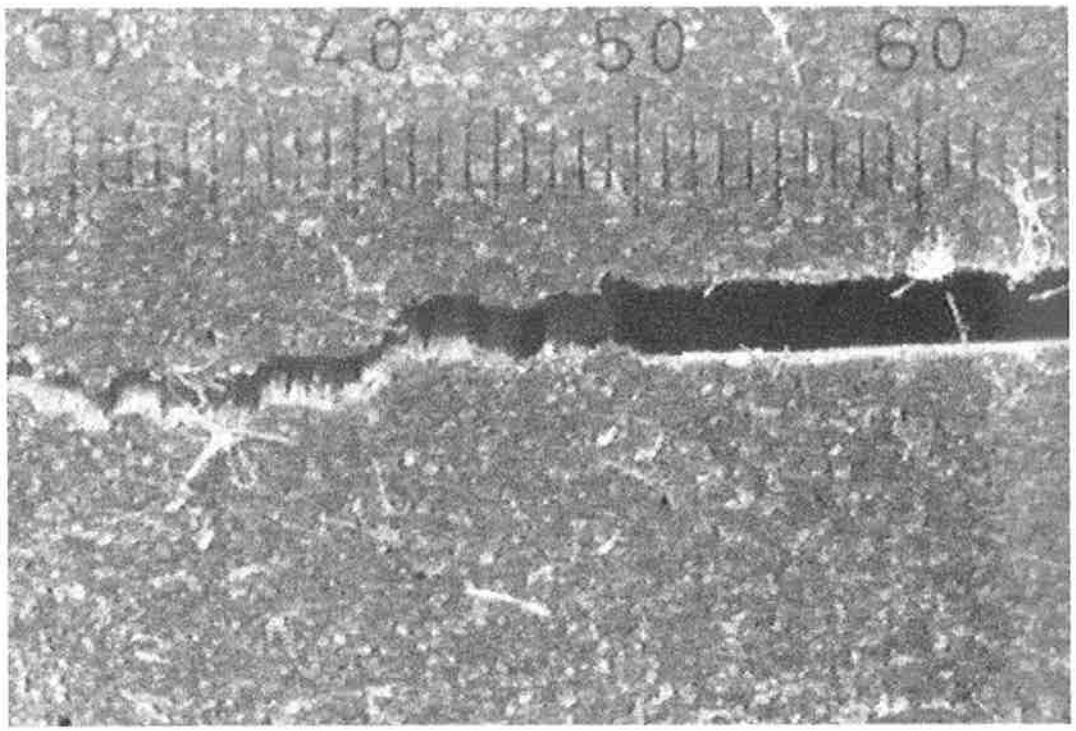

Figure 88 Propellant accelerated aged, T= –40°C, ε= 3.7%

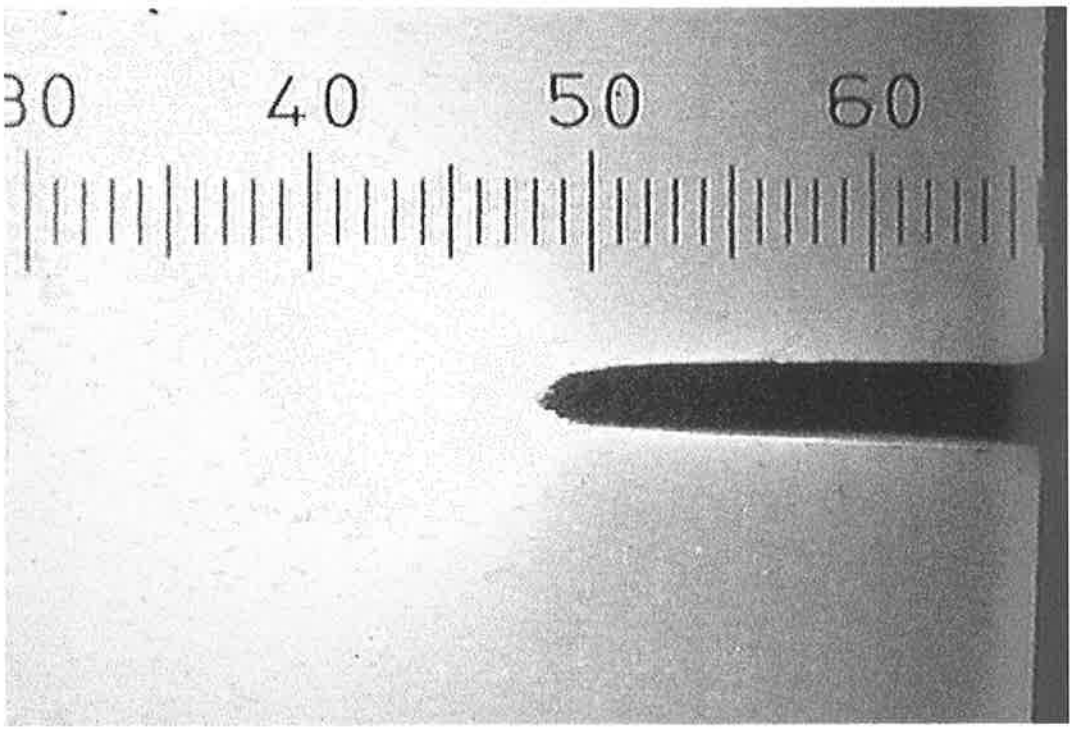

Figure 89 Inhibitor unaged, T= 25°C, ε= 2.6%

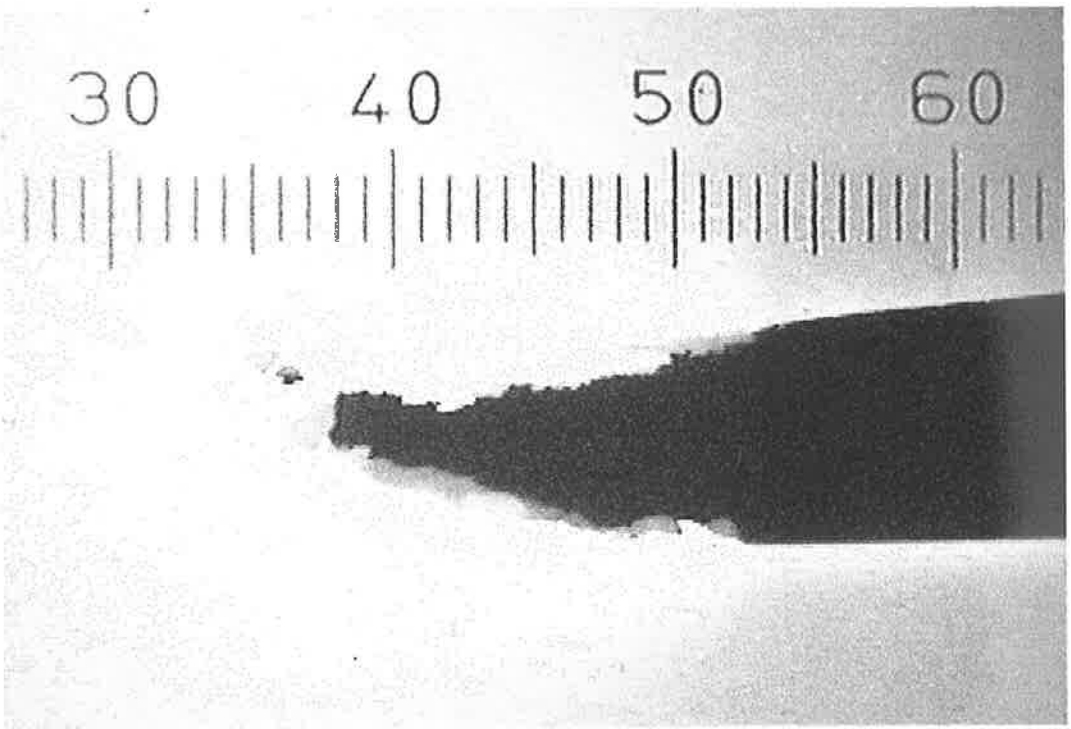

Figure 90 Inhibitor unaged, T= 25°C, ε= 9.0%

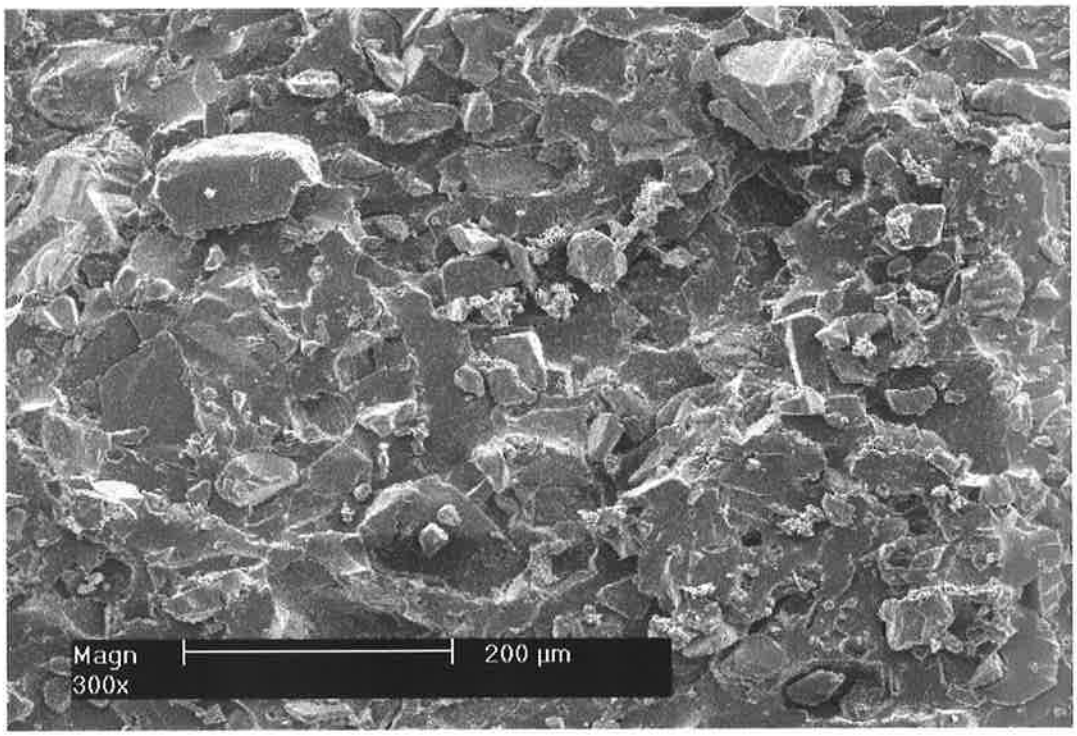

Figure 91 SEM showing centre of fracture surface in unaged inhibitor, T= 25°C

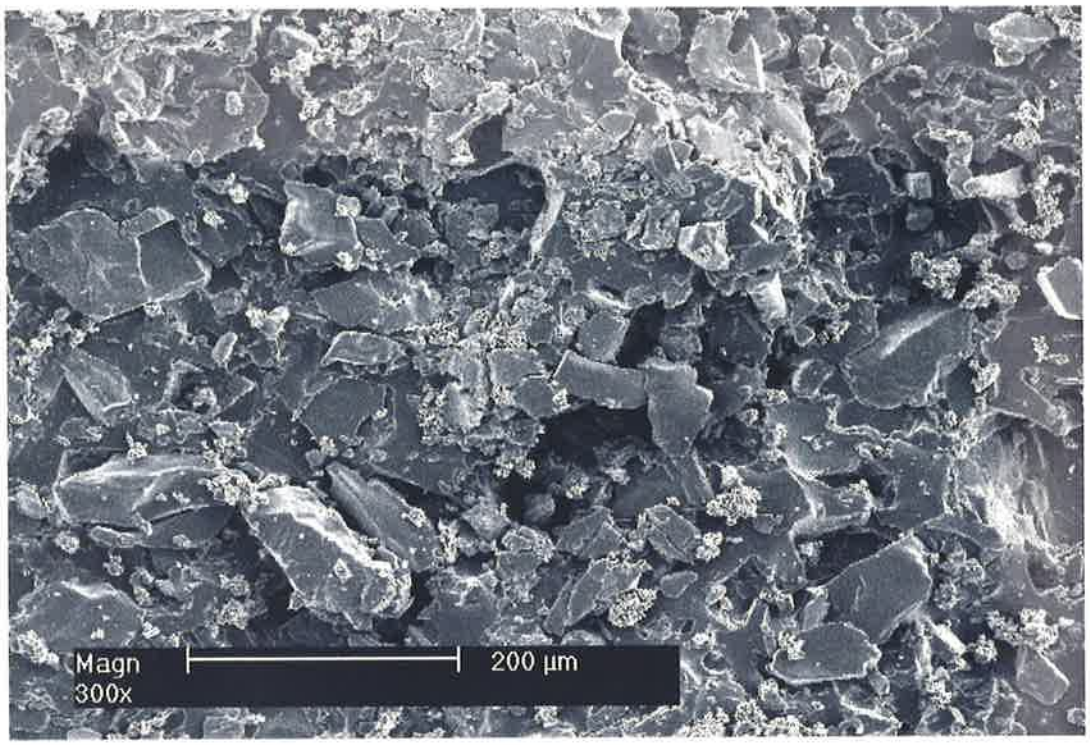

Figure 92 SEM showing edge of fracture surface in unaged inhibitor, T= 25°C

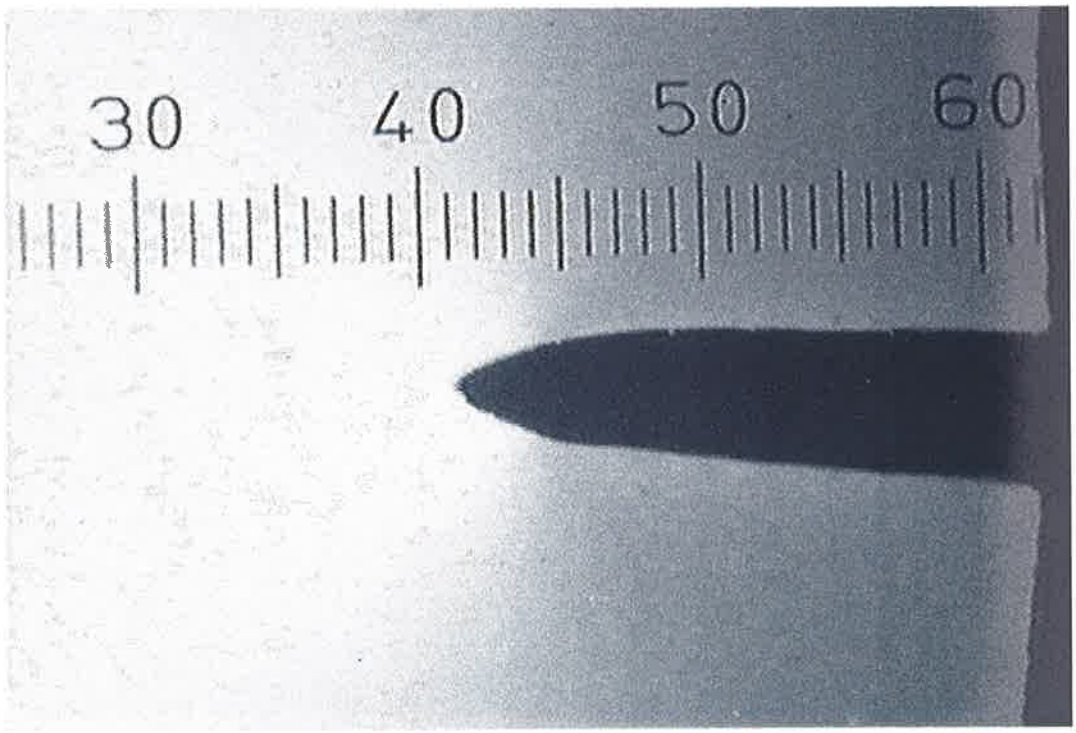

Figure 93 Inhibitor unaged, T= 60°C, ε= 8.4%

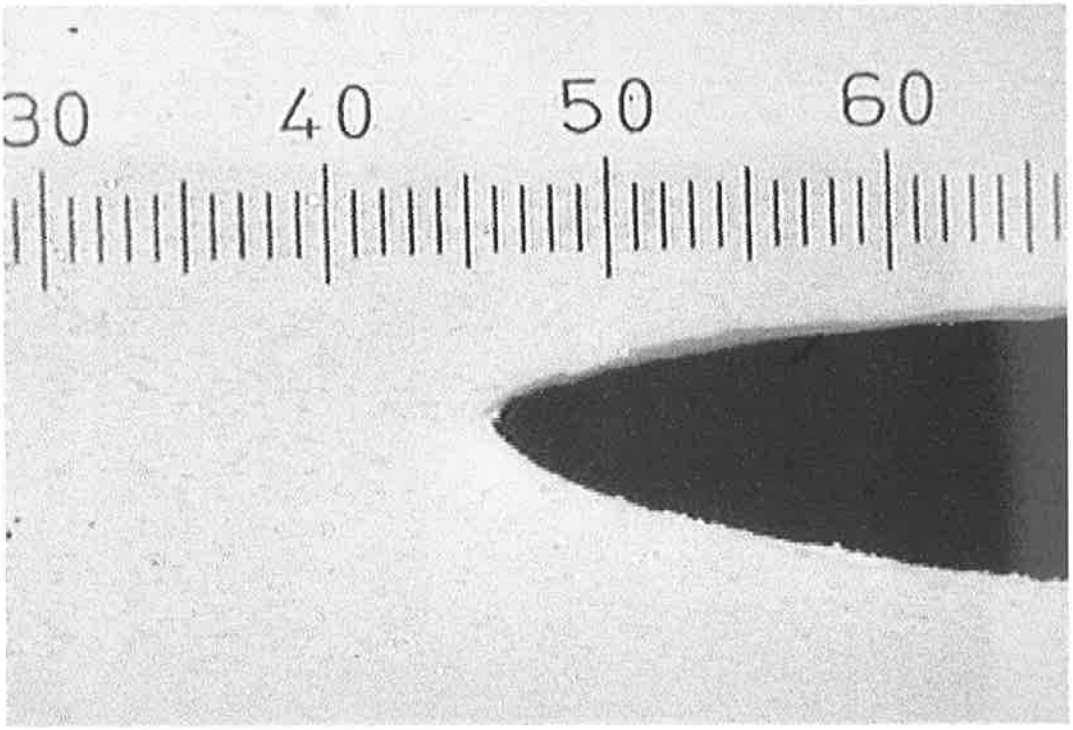

Figure 94 Inhibitor unaged, T= 60°C, ε= 13.7%

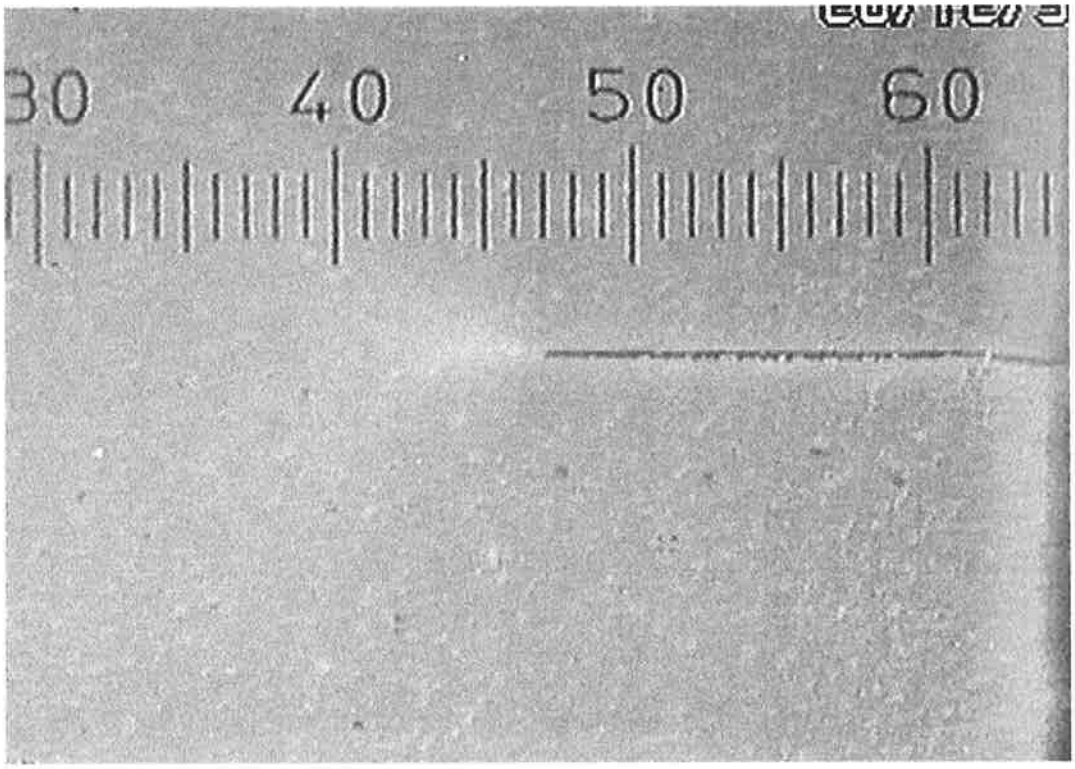

Figure 95 Inhibitor unaged, T= –40°C, ε= 2.55%

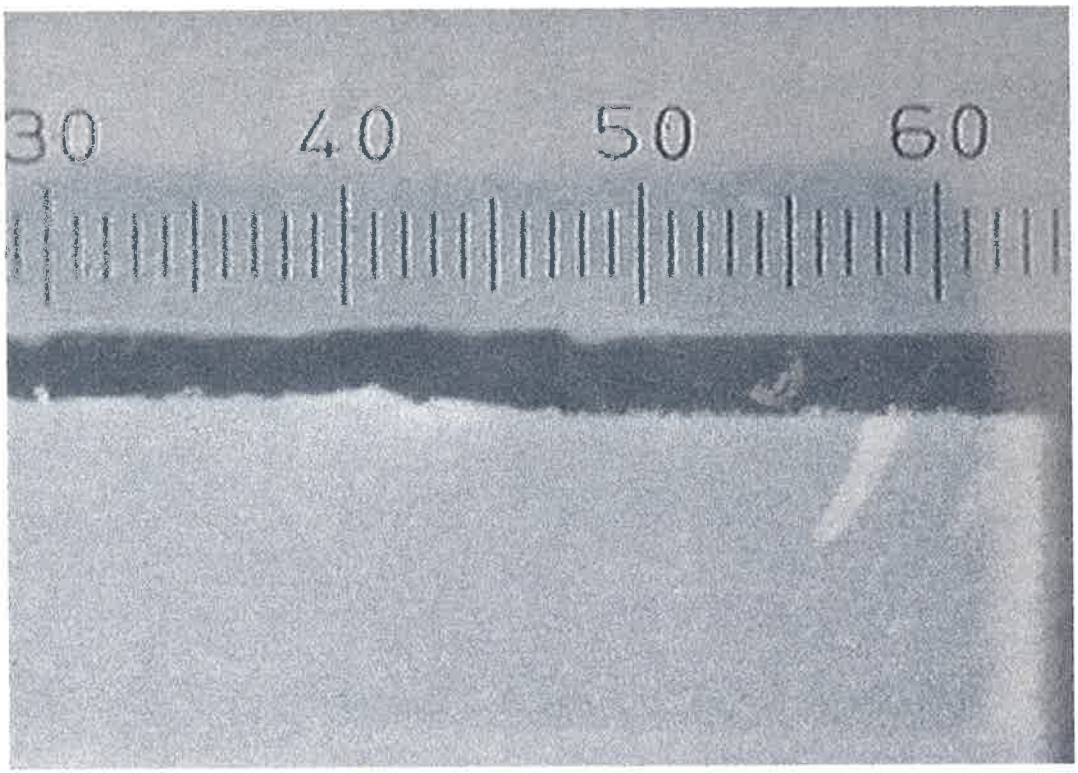

Figure 96 Inhibitor unaged, T= –40°C, ε= 2.6%

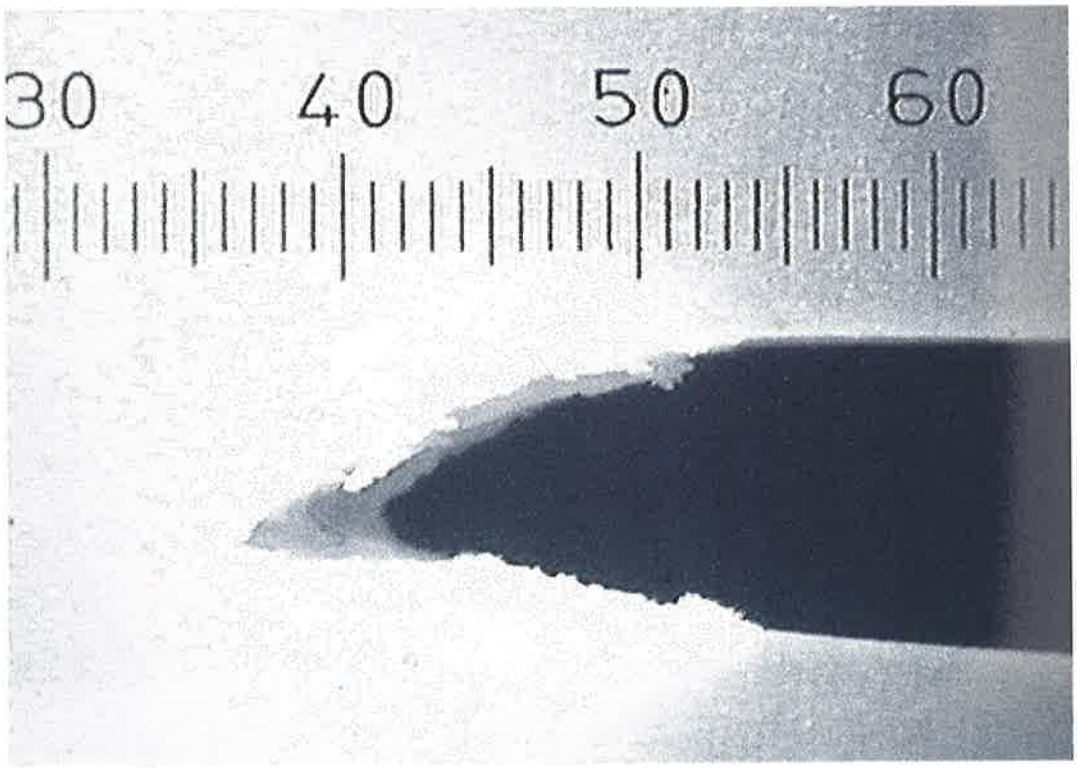

Figure 97 Inhibitor accelerated aged, T= 25°C, ε= 10.1%

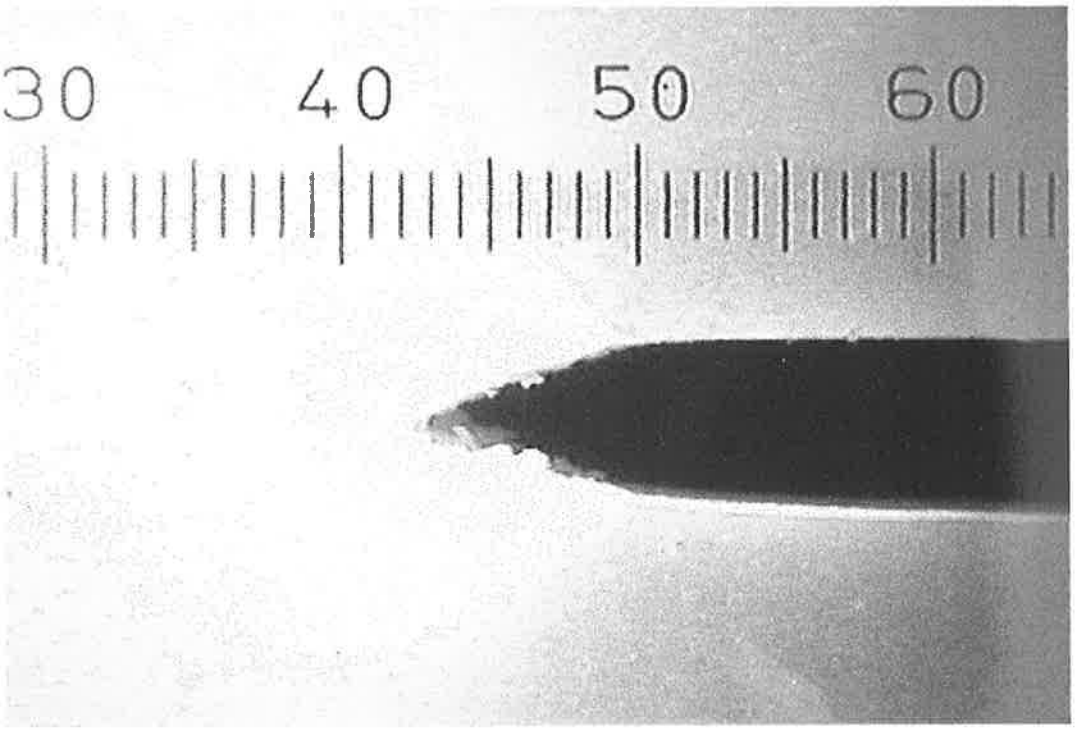

Figure 98 Inhibitor thermally shocked, T= 25°C, ε= 8.9%

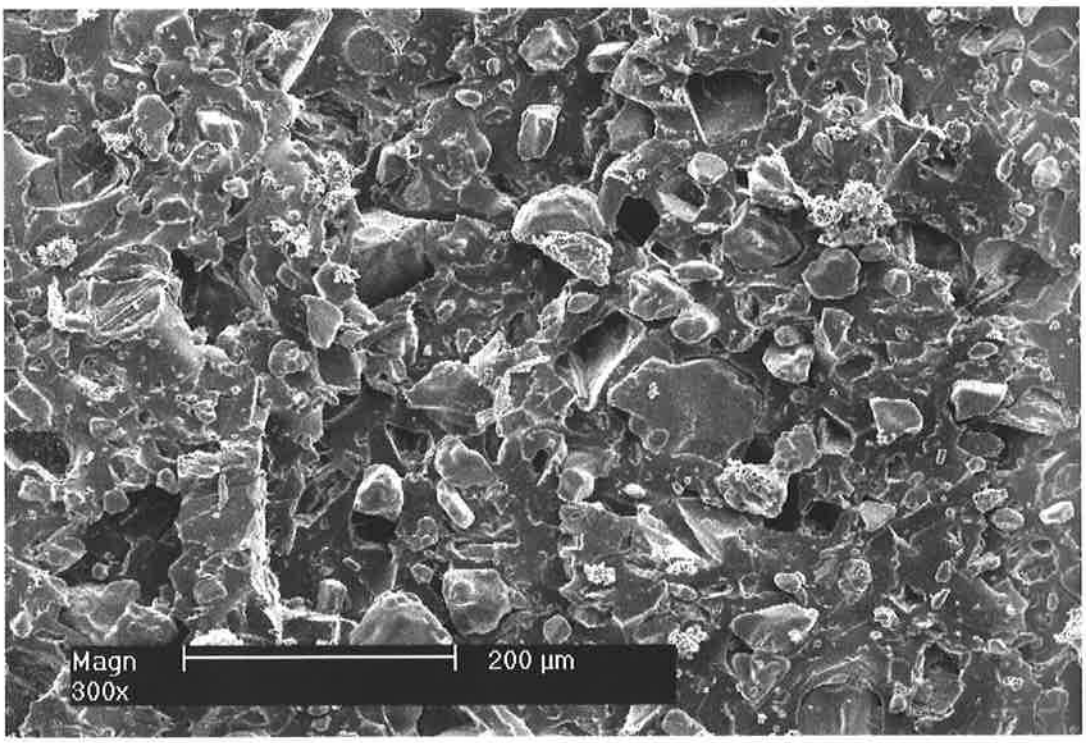

Figure 99 SEM showing fracture surface in accelerated aged inhibitor, T= 25°C

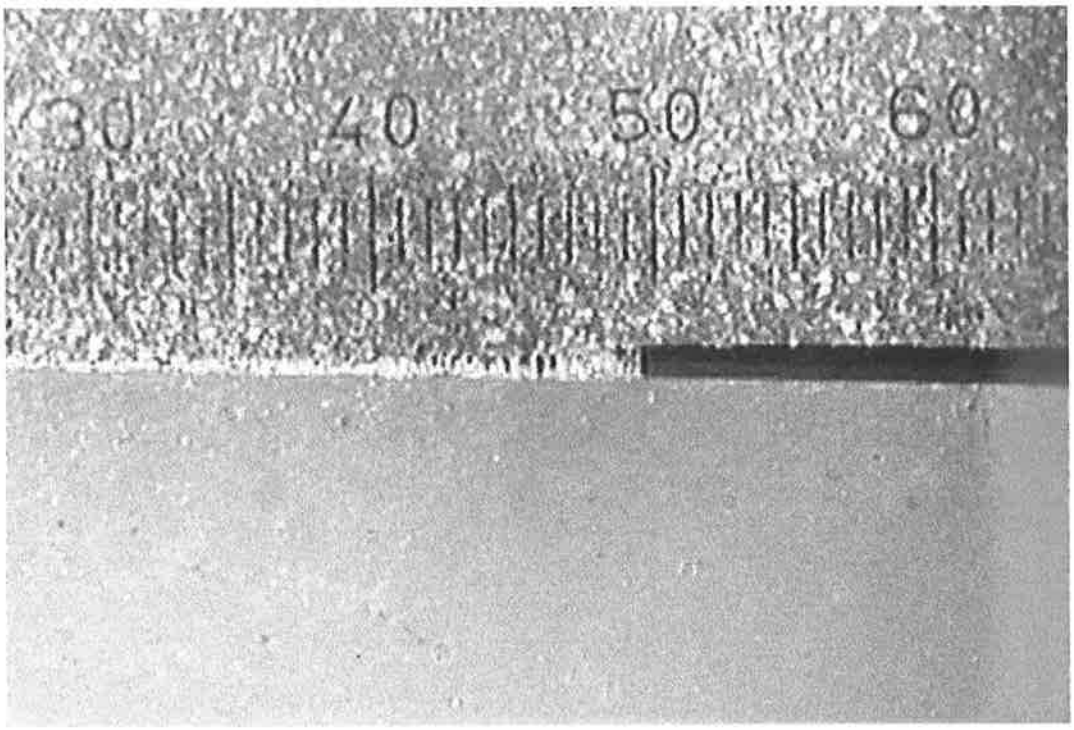

Figure 100 Propellant/inhibitor unaged, T= 25°C, ε= 1.8%

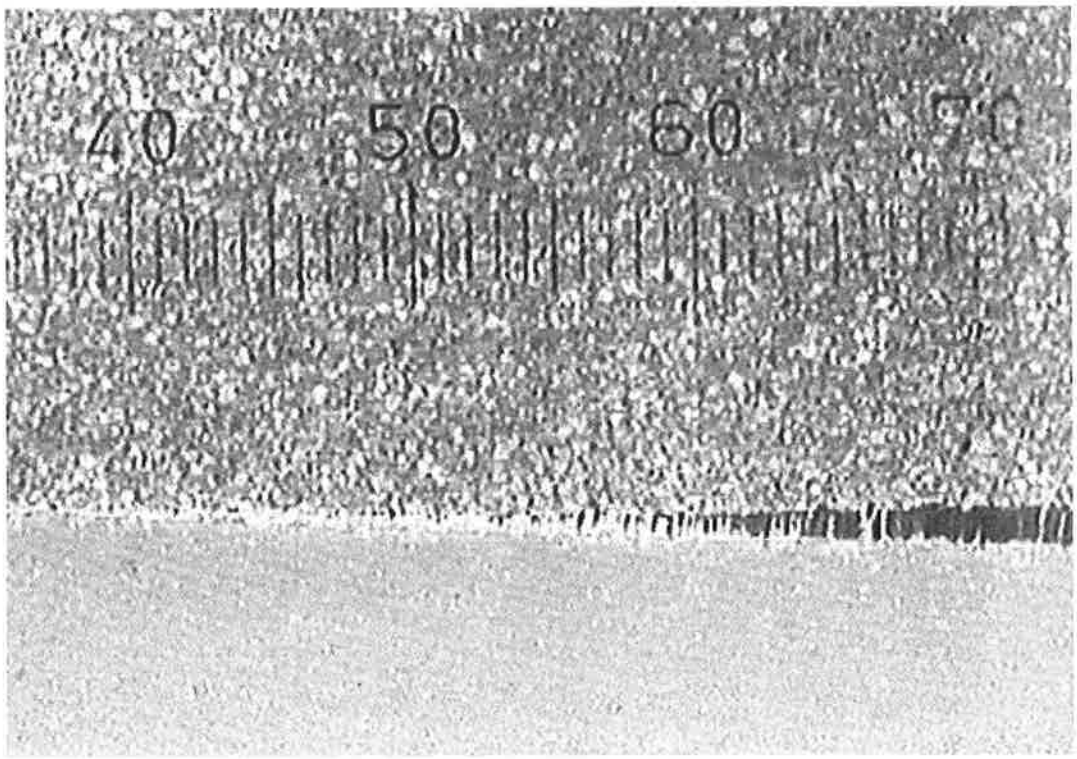

Figure 101 Propellant/inhibitor unaged, T= 25°C, ε= 3.0%

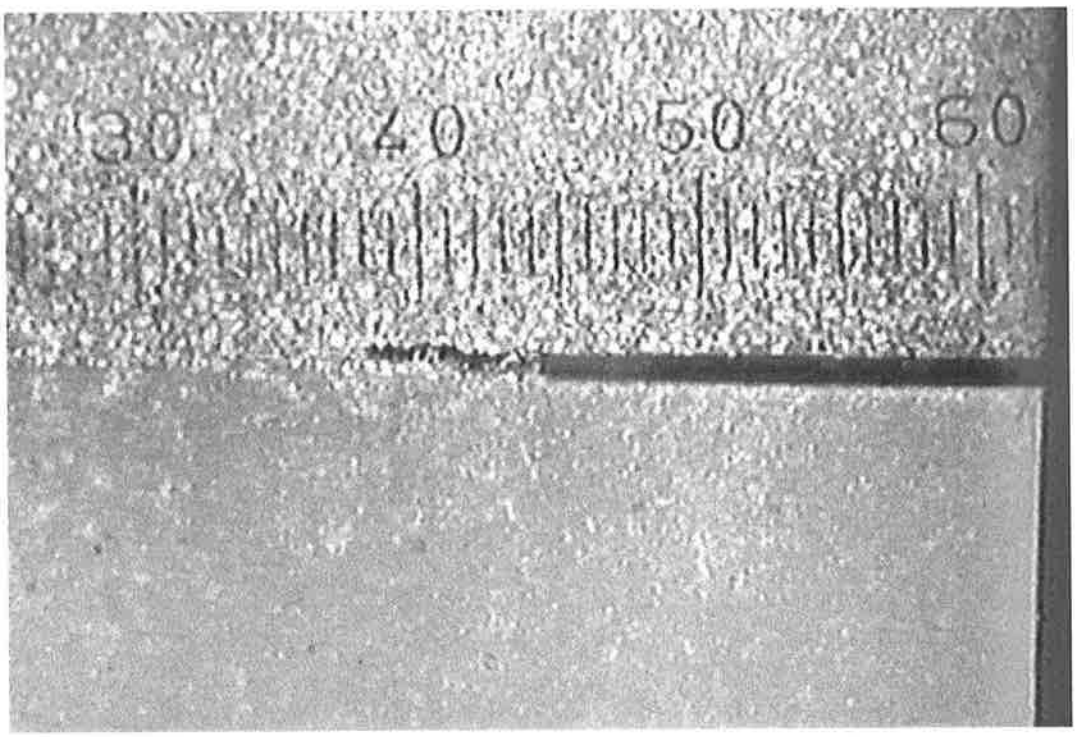

Figure 102 Propellant/inhibitor unaged, T= 60°C, ε= 2.3%

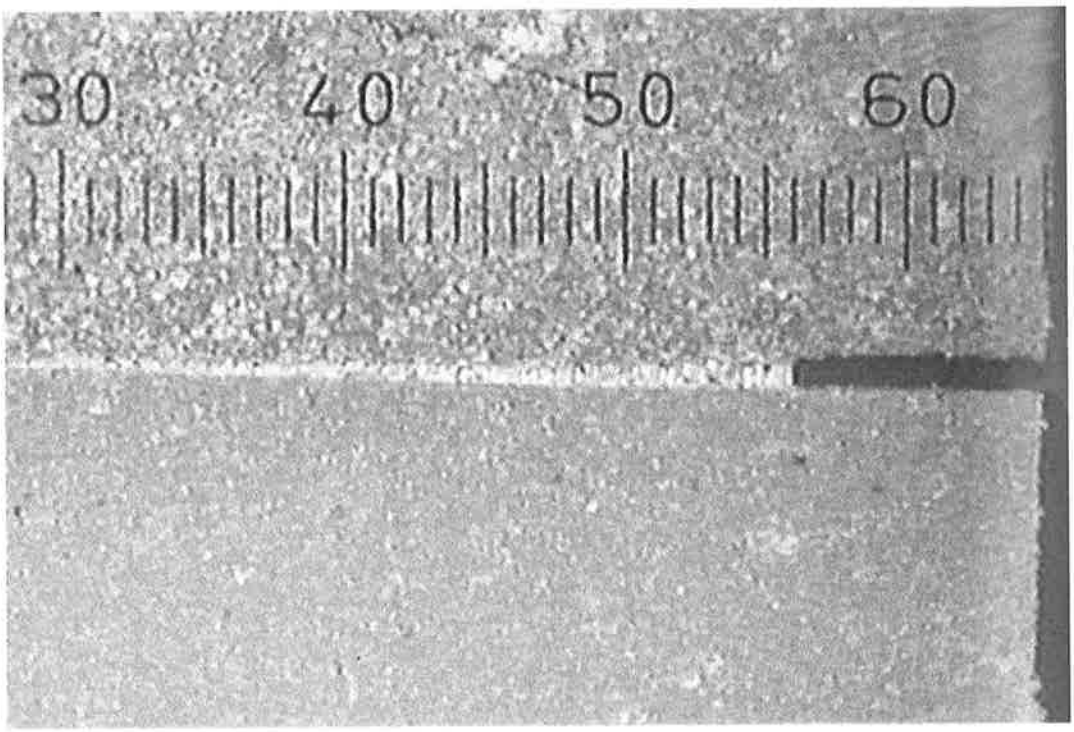

Figure 103 Propellant/inhibitor unaged, T= –40°C, ε= 3.3%

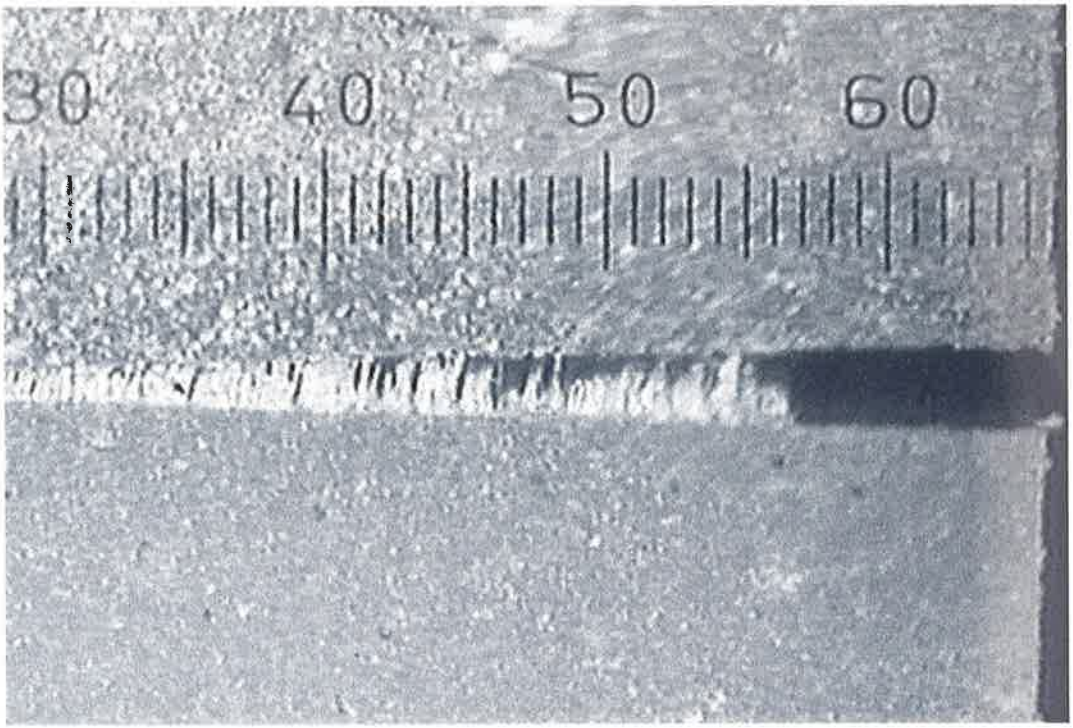

Figure 104 Propellant/inhibitor unaged, T= –40°C, ε= 4.5%

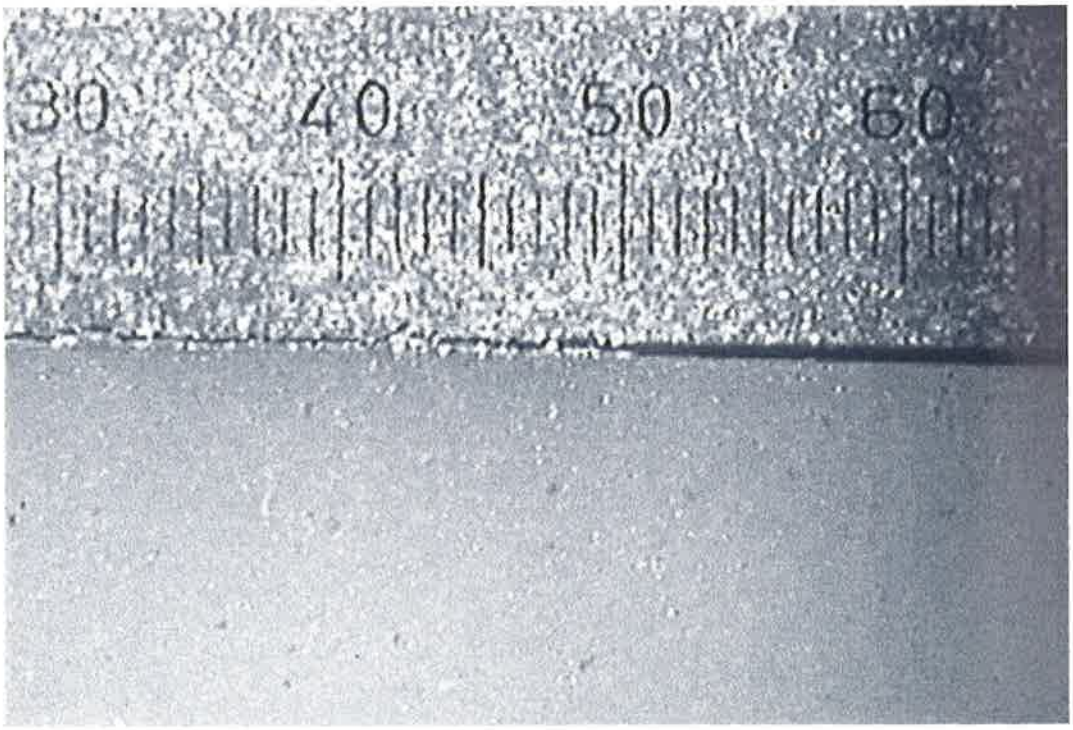

Figure 105 Propellant/inhibitor accelerated aged, T= 60°C, ε= 1.7%

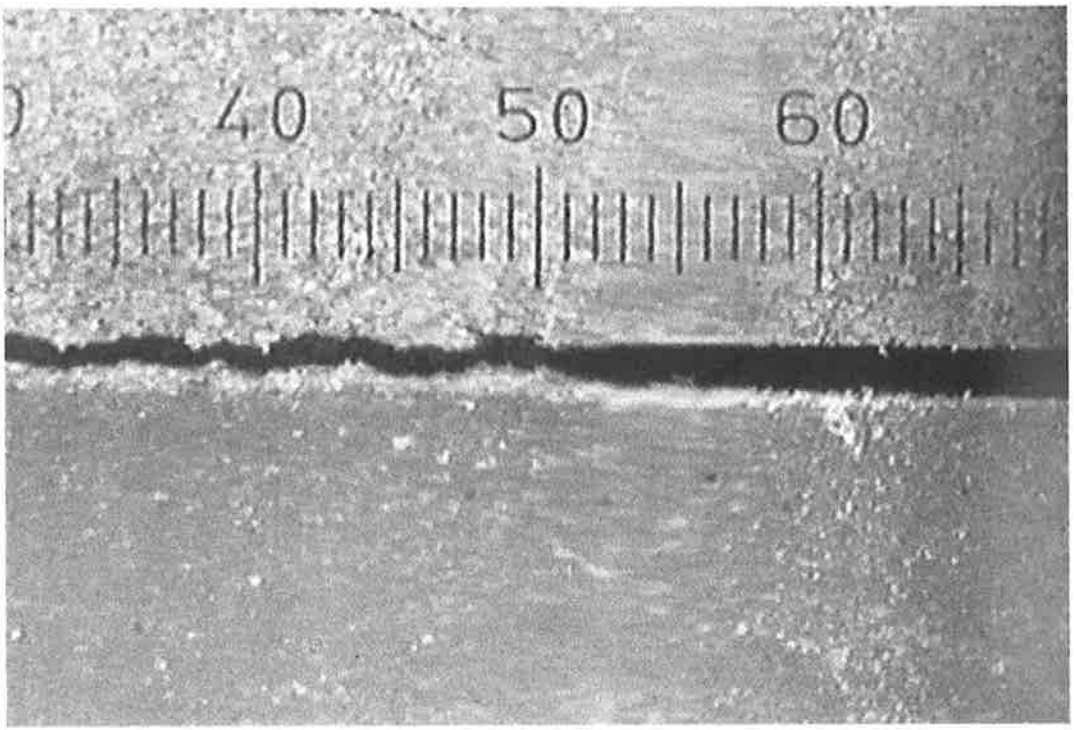

Figure 106 Propellant/inhibitor accelerated aged, T= –40°C, ε= 2.5%

VELOCITY OF CRACK PROPAGATION

Once the criteria for crack initiation and propagation has been attained data describing the rate at which the crack will advance is required for inclusion into the modelling process. The effect of temperature, strain-rate and ageing on the material behaviour and its relationship to the crack velocity in the bulk of the propellant, inhibitor or at the propellant/inhibitor interface has not been adequately reported previously. In this section the velocity of cracks propagating in the various aged and unaged fracture specimens will be discussed.

The mechanism of crack growth in the propellant and propellant/inhibitor bimaterial specimens was one of blunt-sharp-blunt on a local scale, but on a global scale the crack propagated continuously and thus an average velocity was determined from the videotape record. A travelling microscope was employed to track the progress of the crack initiated at the razor blade cut, or teflon tape insert in the case of the propellant/inhibitor bimaterial specimens. Thus, the time for the crack to propagate a known distance across the specimen could be determined.

Propellant

The average velocity of cracks propagating in specimens of propellant subjected to the thermal loads is shown in Figure 107. At a constant temperature, for specimens subjected to the same thermal load the crack velocity increased with strain-rate, this figure shows the average crack velocity at a strain-rate of 0.002 s^{-1}. The mechanism of crack growth was described in the previous section, it was observed that the size of the damage zone increased slightly with the strain-rate and the successive periods of crack blunting and sharpening shortened, this was detected as an increase in the crack velocity.

The magnitude of crack velocity is directly affected by the level of impedance to crack propagation caused by blunting during the blunt-sharp-blunt growth mechanism. As the temperature increases the stress level sustainable by the material decreases which results in smaller damage zones and less impedance to crack propagation. In Figure 107 specimens of propellant subjected to the same ageing conditions exhibited increasing crack velocities with test temperature, correspondingly the size of the damage zone formed ahead of the crack tip decreased. As described in the previous section, at low temperatures (–40°C) the size of the damage zone and the level of crack blunting was substantially higher than that at above zero temperatures. An increase in the crack velocity with temperature supports the model of the crack growth mechanism (which is represented in Figure 75) discussed previously wherein larger damage zones will impede the progress of the crack.

Another contributing factor to the increase in crack velocity with temperature is a decreasing activation energy barrier for crack propagation, which follows from the kinetic approach to fracture.[34] As the material temperature increases the rate at which bonds, for a constant stress, are ruptured increases resulting in higher crack velocities. The variation in crack velocity for the different materials tested in this study is also related to the divergent values of the activation energy for crack propagation each possesses.

In terms of the model of crack growth described, as the material is aged the damage zone gets smaller due to the more brittle type of material behaviour and subsequent lower stress at fibril breakage. The SEM photograph of the fracture surface of an accelerated aged propellant showed evidence of less particle dewetting and the presence of particle fracture in preference to the formation of a zone of damage. Although differences in the size of the damage zone in the unaged propellant specimens and those that had been subjected to thermal cycling and thermal shocking was not detected from image analysis of the crack growth, an indication of

the effect of ageing was given by the variation seen in the values of crack velocity, especially above 25°C. The specimens subjected to the thermal shock had crack velocities slightly greater than that measured in the unaged propellant (2.74 $mm.s^{-1}$ as compared to 2.5 $mm.s^{-1}$ ± 0.02 $mm.s^{-1}$ at 25°C). The crack velocities increased further for the thermally cycled specimens to 3.4 $mm.s^{-1}$. In the case of the accelerated aged specimens, no damage zone was observed during the crack propagation tests, the resulting crack velocity was the maximum for the specimens tested, 3.6 $mm.s^{-1}$. These results imply that the size and/or the rate of formation of the damage zone ahead of the crack tip in specimens subjected to different types of ageing will vary and may be detected in the magnitude of the crack velocity.

The changes to material behaviour caused by ageing can be explained by relating the effect it has on the crack velocity to the blunt-sharp-blunt mechanism of crack growth outlined previously. The unaged specimens will have the largest and slowest forming damage zones causing larger crack blunting and slower crack velocities. The effect of ageing will be to decrease the size of the damage zone ahead of the crack tip which in turn reduces the amount of blunting, resulting in higher crack velocities. The more severe the thermal loading the greater the effect on the properties of the polymer leading to smaller damage zones and increased crack velocities.

Liu[33] reported the effect of pre-damage on the crack velocities in a highly filled polymeric material. Pre-damage can be considered to approximate the effect of ageing and hence the results of Liu's study provide a useful comparison to the those of this investigation. The velocity of a crack propagating in a specimen of dimension 203×51×2.5 mm at two strain-rates (0.0008 s^{-1} and 0.083 s^{-1}) was measured with pre-damage introduced into some test specimens by loading them to 15% strain and unloading prior to crack testing. Liu reported that the effect of pre-damage on the crack growth and velocity was highly dependent on the strain-rate. At

the higher strain-rate there was a negligible difference in the crack growth response for the undamaged and pre-damaged specimens. However, at the low strain-rate the crack velocity in the undamaged specimens was significantly lower than that for pre-damaged specimens. The low strain-rate employed by Liu is comparable to those in this study, the increase in crack velocity detected with more severe material ageing correlates with the difference observed when pre-damage is introduced into a specimen.

The crack velocity was highest at 60°C and lowest at –40°C as the size of the damage zones decreased with temperature. The relative values of crack velocity at each temperature are related to the severity of the ageing, more severe ageing results in smaller damage zones, less blunting and less impedance to crack propagation, which leads to a higher crack velocity. The material that had been accelerated aged exhibited the highest crack velocities and the unaged specimens the lowest.

Inhibitor

A plot showing the crack velocity in the precracked specimens of inhibitor is shown in Figure 108. Note that the crack propagated in an unstable manner in all specimens of inhibitor tested at –40°C. The specimens underwent a brittle type of fracture and the crack propagated rapidly across the length of each specimen. The specimen broke completely within 0.1 seconds and the crack velocity was unable to be accurately determined. A negligible zone of stress whitening ahead of the crack tip was observed prior to crack propagation indicating a very low level of damage was present. The inhibitor material exhibits glass-like behaviour at this temperature due to the proximity of the glass transition. The strain level for crack propagation was very low by comparison to that above the glass transition temperature and only minor plastic deformation was detected on the stress-strain curve prior to fracture.

In the specimens tested above glass transition, the velocity of the crack increases as the test temperature increases from 25°C to 60°C (it also increased with strain-rate as expected). The material is softened by the increase in temperature and fails at lower stresses and higher strains than compared to –40°C. The model of crack growth in the inhibitor material was described in the previous section. Upon application of the load the inhibitor material stress whitened and a dewetted zone of damage ahead of the crack tip formed prior to failure by material tearing, no evidence of fibril formation or crack blunting was found. At 25°C and 60°C, the size of the damage zone increased with the level of strain in the specimen until the entire specimen was stress whitened, however, at an equivalent level of strain the damage zone was smaller and the whitening of the specimen more intense at 25°C than for that measured at 60°C. Therefore, the level of damage occurring in the specimen at 25°C was greater which correlates with the decreased crack velocities detected.

A minor increase of the crack velocity with more severe ageing was also noted which is associated with a decrease in the size of the damage zone present during the crack propagation. Small decreases in the values of hysteresis ratio were also observed as the severity of the ageing increased. At each strain-rate the accelerated aged specimens exhibited the highest crack velocity and the unaged the lowest, however, the crack velocities did not vary greatly. Differences in the size and rate of formation of the damage zone ahead of the crack could not be determined for the unaged and aged specimens from image analysis of the videotape record. However, the level of stress whitening in the unaged specimens was observed to be more intense than that in the accelerated aged specimens indicating that a higher level of damage was present.

Propellant/Inhibitor Bimaterial

The crack velocities measured for the propellant/inhibitor bimaterial specimens were lower than those for the equivalent propellant specimens tested (see Figure 109). The model of crack growth described for the propellant/inhibitor specimens is the same as that for the propellant. On application of the load, damage zones are formed in the propellant layer prior to sharpening of the crack by coalescence with the voids. There was no stress whitening observed in the inhibitor material and the specimen failed by cohesive fracture in the propellant adjacent to the bondline.

The damage zone causes blunting resulting in impedance to the crack propagation, hence, the crack velocity is related to the size of the damage zone and the level of blunting. The crack velocity increased with strain-rate and temperature as expected. At –40°C the damage zones in the propellant were substantial and the period the crack tip was blunted during the blunt-sharp-blunt mechanism was thus greater than that for the higher temperatures. As the temperature increased it was observed that the size of the damage zones decreased resulting in less impedance to the crack and increased velocities.

The size of the damage zones in the unaged specimens and those subjected to the thermal shock and thermal cycle could not be differentiated between on the videotape record whilst no damage zone was detected in the accelerated aged material (the same results were detected for the propellant). The crack velocities presented, however, can be seen to increase with the severity of the ageing (which corresponds to the decrease in hysteresis ratios). At each strain-rate the unaged material exhibited the lowest crack velocities, the thermally shocked material have higher crack velocities, then come the values for thermally cycled material and the accelerated aged material had the highest crack velocities. The unaged material had the largest

damage zone and the highest hysteresis ratio, hence, the greatest energy losses. The greater the effect ageing has on the properties of the polymer the more it will deteriorate, smaller damage zones will be formed with less crack blunting and hence the crack velocity increases.

The velocity of cracks propagating in the inhibitor material ranged from 0.08 to 2.05 $mm.s^{-1}$, in the propellant the velocity ranged from 0.08 to 9 $mm.s^{-1}$ whilst those in the propellant/inhibitor specimens the range was 0.5 to 10.5 $mm.s^{-1}$. The crack velocities in each material are controlled by the rate and size of the damage zones formed. Two factors that determine the rate of formation of the damage zone are the strength of the binder/filler bond and the stiffness of the binder. The results of the Poisson's ratio study showed that the binder/filler bonds in the inhibitor were much stronger than those in the propellant. As a result when dewetting occurs in the inhibitor, the damage zones ahead of the crack tip take longer to form than those in the propellant. The increased impedance of the crack results in decreased crack velocities.

The crack velocities of the propellant were lower than those measured in the propellant/inhibitor specimens. The damage zone ahead of the crack tip observed in the study of the crack mechanism was larger in the propellant as compared to the propellant/inhibitor specimens. This results in more blunting and greater impedance to the crack in the propellant specimens, with a corresponding lower crack velocity.

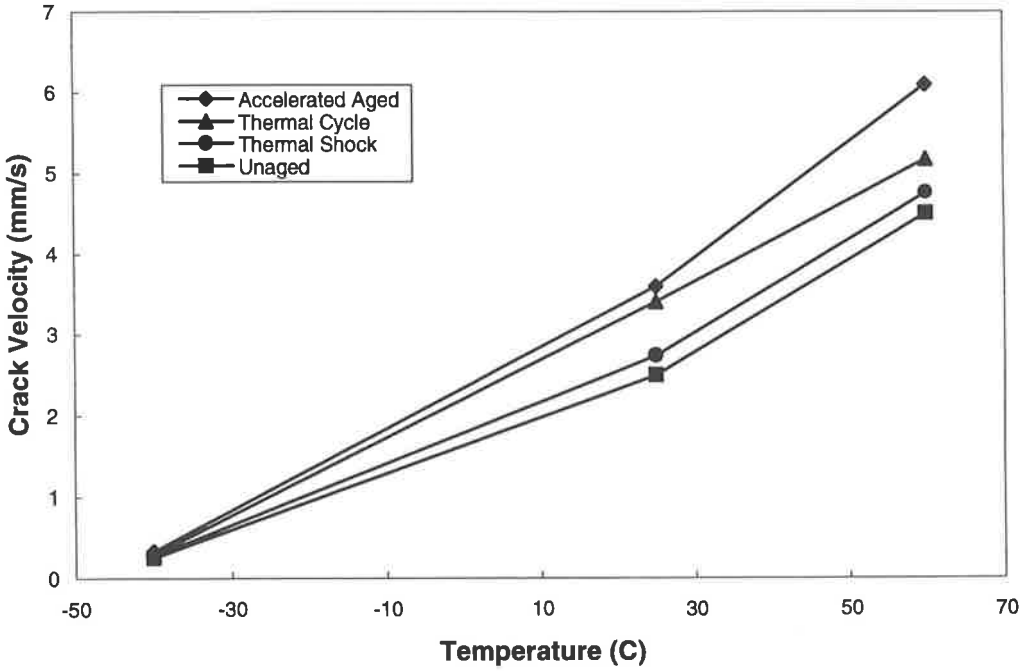

Figure 107 Crack velocity in propellant specimens ($\dot{\varepsilon} = 0.002\ s^{-1}$)

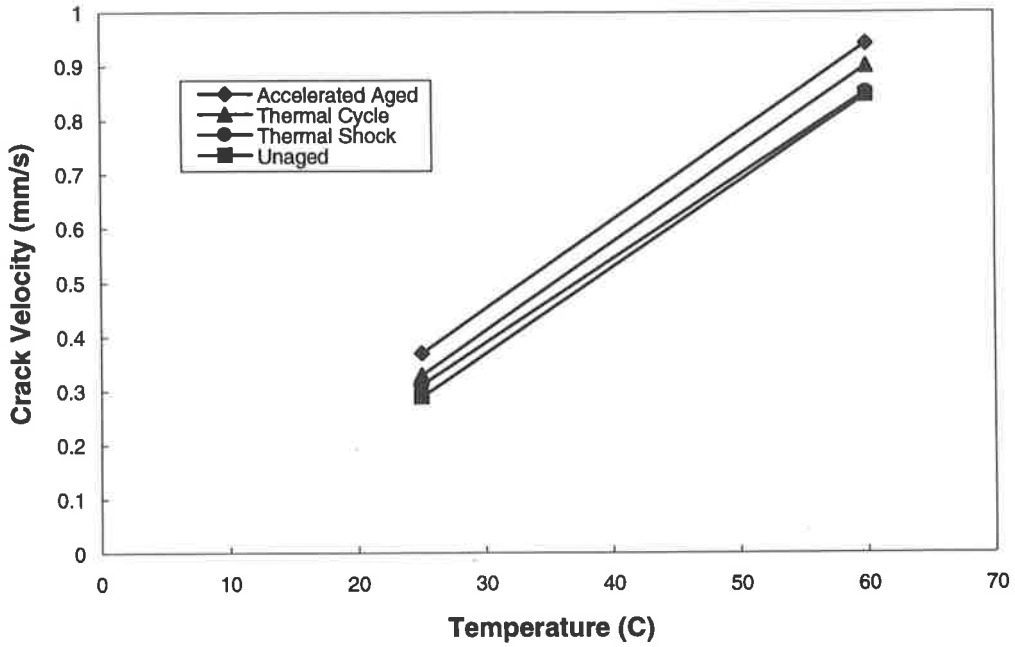

Figure 108 Crack velocity in inhibitor specimens ($\dot{\varepsilon} = 0.002\ s^{-1}$)

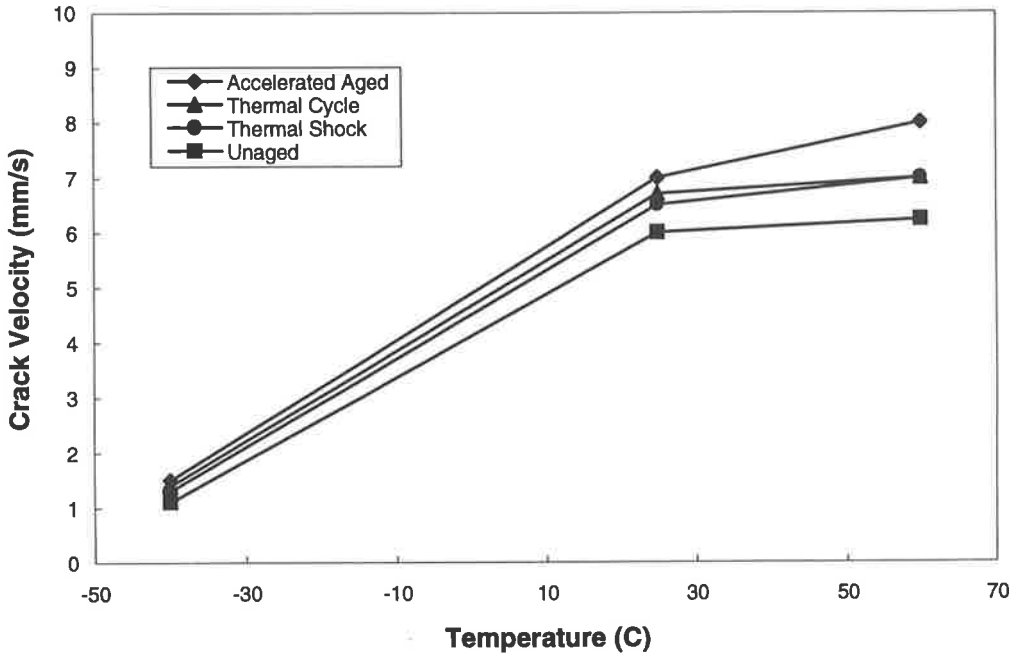

Figure 109 Crack velocity in propellant/inhibitor specimens ($\dot{\varepsilon} = 0.002\ s^{-1}$)

MECHANICAL PROPERTIES

In the preceding sections the effect of temperature and strain-rate on the thermal behaviour, hysteresis energy losses, crack mechanism and crack velocity in aged specimens of the materials employed in a PICTOR rocket motor was reported. The results of these studies are to be incorporated into a service life assessment of the PICTOR rocket motor. Accurate predictions of fracture from finite element analysis requires considerable mechanical property data be obtained from characterisation tests of the rocket motor materials under the conditions of service.

This section will compare the effect of temperature and strain-rate on mechanical properties derived from the crack propagation tests of the "horizontal bar" specimens of aged propellant, inhibitor and a propellant/inhibitor bimaterial. The results of previous sections will be employed to aid the explanation of the change in mechanical properties caused by the various thermal loads.

Propellant

The "horizontal bar" geometry was selected so that the propagation of the crack could proceed over a long centrally located path providing a significant time period to study the crack growth and measure the crack velocity, particularly at the propellant/inhibitor interface. Values of critical strain and stress have been calculated from the data recorded during these crack tests providing a useful comparison of the effect of ageing on mechanical properties.

Stress versus strain curves typical of those obtained from tests conducted on the pre-cracked specimens are presented in Figure 110 and Figure 111. The critical strain (and corresponding critical stress) was identified as the strain level at the instant of crack propagation and is

marked on each curve. Figure 110 is an example of stress against strain recorded during the fracture tests of unaged propellant at 25°C. Varying the strain-rate does not significantly affect the stress against strain data or the critical values; the maximum and critical stresses increase slightly with strain-rate and the critical strain decreases as expected.

Figure 111 shows the stress versus strain data for aged propellants tested at 60°C and a strain-rate of 0.002 s^{-1}. Evidence presented in the previous sections indicated that the accelerated ageing thermal load produces the most severe deterioration in the mechanical behaviour of the propellant (and propellant/inhibitor bimaterial specimens), followed by the thermal cycle and thermal shock respectively. The stiffness of the accelerated aged propellant is markedly higher (at strains > 0.005) and the critical stress and critical strain are greatly reduced by comparison to the other three types of specimens, evidence for a more brittle type of fracture process.

The variation of critical stress for aged propellants calculated from the crack propagation tests is plotted against temperature in Figure 112 for a strain-rate of 0.002 s^{-1}. The propellant that was subjected to accelerated ageing has suffered the most serious degradation. The value of critical stress is lower by comparison to the unaged, thermal cycled and thermal shocked propellants at all temperatures and substantially reduced at –40°C.

Prolonged storage at an elevated temperature during accelerated ageing results in additional cross-linking of the main-chains in the propellant binder.[4] The increased cross-linking leads to hardening of the propellant and an increase in the modulus (see Figure 111) and glass transition temperature[34] (see Table 1 Glass transition temperatures of aged materials). The accelerated aged propellant exhibited the highest crack velocities of all types of propellant specimens tested and no visible damage zone formed at the tip of the crack.

The critical stresses of the thermally cycled specimens of propellant are lower than the unaged material at 25°C but similar at 60°C. During a significant proportion of the thermal cycle the propellant was subjected to an elevated temperature and as a consequence the material undergoes a certain amount of hardening as a result of increased cross-linking, similar to the accelerated aged material. However, at the sub-zero temperature of the thermal cycle the oxidation and cross-linking in the material will be slowed or possibly halted. As a consequence of the less severe thermal load the critical stresses for the thermally cycled propellant are greater than those of the accelerated aged propellant. Further, the mechanical properties of the propellant did not deteriorate as much from the thermal shock as it did for the thermal cycle due to the very limited period at an elevated temperature. The hardening of the thermally shocked material was not as pronounced as that in the other thermal loads and the stress-strain data was very similar to unaged material. As a result the critical stress of the thermally shocked material does not vary greatly from that of the unaged propellant at both 25°C and 60°C.

Both the thermally shocked and thermally cycled materials were hardened by the ageing conditions but did not become more brittle. They are stiffened significantly at –40°C when the material temperature is closer to the glass transition, sustaining greater stresses and higher critical strains (see Figure 113 where the corresponding values of critical strain obtained from the fracture tests are presented). As a result the critical stresses of both were increased significantly above that of the unaged material. The change in material behaviour caused by the thermal cycle and thermal shock at sub-zero temperatures was also observed in the investigation into the thermal behaviour, it was found that these thermal loads caused a reduction in thermal expansion coefficient as compared to the unaged and accelerated aged materials in the temperature range –45°C to 0°C (see Figure 28).

Figure 114 shows the variation in critical strain for each of the aged propellant specimens with strain-rate. As expected the variation is small, an increase in strain-rate results in a decrease in the critical strain and corresponding increase in critical stress. With increasing severity of ageing to which the specimen has been subjected the critical strain decreases.

Inhibitor

Figure 115 shows stress against strain data for the various aged inhibitor specimens at 25°C and a strain-rate of 0.002 s^{-1}. The unaged material exhibits the lowest maximum and critical stress (and the highest critical strain) whilst the accelerated aged material has the highest maximum and critical stress and lowest critical strain. However, the critical strains and stresses have increased only marginally with the severity of the thermal loading, the material becomes slightly stiffer at higher strains with extended ageing but not more brittle.

The stress against strain data for the various aged inhibitor specimens tested at –40°C is presented in Figure 116. The behaviour of the unaged, thermally cycled and thermally shocked specimens can be seen to be similar whilst the accelerated aged material which has an increased critical stress and strain. All of the inhibitor specimens underwent a brittle type of fracture at –40°C, with unstable crack propagation across the length of the specimen. The rapid rupture of the specimens is evidenced by the abrupt decrease in stress at the instant of crack propagation, this prevented a measure of crack velocity being determined.

The variation of critical stress and strain with temperature for the aged and unaged inhibitor material is presented in Figure 117 and Figure 118. It can be seen that the value of critical stress and strain for the aged inhibitor specimens does not vary greatly from those of the unaged material. It was reported above that there was only a slight variation due to ageing of the stress versus strain data for the inhibitor specimens and thus only a slight variation to the

mechanical properties is exhibited. The results of the preceding sections correlate with this. The hysteresis ratios, size of the damage zones observed and the measured values of crack velocity above the glass transition in the various aged inhibitor specimens exhibited minimal variation. The same trends were observed at all strain-rates.

The increase in critical stress of the accelerated aged inhibitor material was more prominent at a test temperature of –40°C. All of the various aged and unaged specimens of inhibitor exhibited glass-like behaviour at –40°C due to the close proximity of the glass transition temperature. Indeed, due to the glass-like behaviour, at –40°C the hysteresis ratios of all the inhibitor specimens were very much lower than those measured above glass transition (see for example Figure 62). In the case of the accelerated aged material the increase in the glass transition temperature was more distinct. The accelerated aged material had a glass transition temperature of –40.2°C (whereas the value ranged from –42.3°C to –42.8°C for the other aged inhibitor specimens). At a test temperature of –40°C the behaviour of the accelerated aged inhibitor will be almost completely glass-like, which in addition to the hardening caused by ageing results in the increased level of stress and strain exhibited.

It can be seen that the accelerated aged material has a higher critical stress than the unaged material at all temperatures over the strain-rates employed in this study (see Figure 119). The mechanism of crack propagation for the inhibitor material was observed to be one of material tearing without crack tip blunting. Due to the increased cross-linking between binder chains in the accelerated aged material it will be harder with increased critical stresses compared to an unaged specimen. This increased stress level will correspond to greater energy input required for crack propagation (and therefore a relatively greater recoverable energy follows from this).

The results of the Poisson's ratio study showed that the bond between binder and filler in the inhibitor was much stronger than that in the propellant. The primary mechanism of energy loss

during ageing of a composite propellant has been found to be the damage caused by debonding at the binder/filler interface.[19] Damage occurring at the binder/filler interface and also in the binder matrix causes a reduction in the mechanical properties of the propellant, the effects of ageing will be much greater in the propellant than the inhibitor for the same ageing conditions. More significant changes to the mechanical properties of the inhibitor will require more severe ageing conditions than those experienced in this study.

Propellant/Inhibitor

The critical stress and strain of the propellant/inhibitor bimaterial specimens measured at a strain-rate of 0.002 s^{-1} are presented in Figure 120 and Figure 121 respectively. In the study of the crack growth mechanism of each material it was observed that for the propellant/inhibitor bimaterial specimens the crack propagated in the layer of propellant material along a path immediately adjacent to the interface. The strain levels attained were not high enough to cause any visible damage in the inhibitor material.

As discussed previously, a reduction in test temperature from 60°C to –40°C will cause the propellant to become stiffer as it is closer to the glass transition. The increase in the stress obtained at an equivalent strain level suggests an increase in the material modulus. A number of other material characteristics are also affected by the decrease in temperature. The hysteresis ratio increased, much larger damage zones ahead of the crack tip were detected and the increase in the level of crack blunting resulted in decreased crack velocities. It follows that the critical stress will increase with decreasing temperature.

The relative levels of critical stress and strain seen in the different types of aged propellant/inhibitor bimaterial specimens correspond to those observed for the propellant specimens, which is to be expected due to the failure of the propellant/inhibitor specimens

occurring in the propellant layer. The greatest deterioration was seen in the accelerated aged material, followed by the thermally cycled material and lastly the thermally shocked propellant/inhibitor. Again only a limited amount of material hardening has occurred in the thermally shocked and thermally cycled specimens due to the reduced period spent at elevated temperature during each of these thermal loads. As a result the specimens are stiffened by a decrease in temperature with higher stress levels attained at the same strain but without any evidence of becoming more brittle. At –40°C the thermally shocked and thermally cycled specimens have higher critical stresses than the unaged material.

Figure 122 shows the effect of strain-rate on the critical stress in the propellant/inhibitor specimens subjected to various ageing. The critical stress increases with strain-rate as expected and the corresponding value of critical strain will decrease.

Fracture Energy

An enhancement to the modelling process being developed by DSTO will be the ability to include crack propagation in the finite element analysis, for which a criterion supplying the propensity for crack propagation is required. The fracture energy of unaged propellant and inhibitor has been calculated using a standard single edge notch[1,3] (SEN) specimen. The hysteresis ratios of each material were measured, hence, the calculated value of the fracture energy includes the viscoelastic material behaviour. The effect of temperature on the fracture energy of propellant and inhibitor has not been reported previously.

The calculation of fracture energy was simplified by Ho and Tod[3] who employed a modified fracture mechanics approach. Specimens are subjected to hysteresis and crack propagation tests from which the hysteresis ratio and input strain energy density are determined respectively, the critical recovered strain energy density is obtained from the expression:

$$W_{rc} = W_i(1 - h_r)$$

The fracture energy is then calculated from the expression:

$$G_c = \frac{2\pi a W_{rc}}{(1+\varepsilon_c)^{1/2}}$$

Figure 123 shows the fracture energy calculated from tests of unaged propellant. The temperature of the SEN fracture tests was varied from –40°C to 60°C at a strain-rate of 0.00077 s^{-1}, (an identical strain-rate as that used in the tests of the "horizontal bar" type specimens). The fracture energy can be seen to increase as temperature decreases. As the temperature decreases towards the glass transition the propellant becomes stiffer. An increase in the stress levels obtained at equivalent strains was observed on the stress-strain curves as the temperature decreased, suggesting that the modulus of the material increases at lower temperatures. A moderate increase in fracture energy results from the decrease in temperature from 60°C to 25°C, the effect of reducing the material temperature from 25°C to –40°C results in a more noticeable change with a substantial increase in the value of fracture energy.

A similar type of change in the material properties with decreasing temperature was reported earlier. The size of the damage zone ahead of the crack increased marginally from 60°C to 25°C and substantially when the temperature decreased from 25°C to –40°C. The increase in impedance to crack propagation resulted in a corresponding decrease in the values of crack velocity calculated. The hysteresis ratio of the SEN specimens follow a similar trend as temperature decreases. The average fracture energy and hysteresis ratios determined from the SEN specimens at each temperature is presented in Table 3 below.

Table 3 Fracture energy and hysteresis ratios for SEN specimens ($\dot{\varepsilon} = 0.00077\ s^{-1}$)

	Propellant*		Inhibitor+	
Temperature (°C)	G_c (J/m^2)	h_r	G_c (J/m^2)	h_r
–40	345	0.37	1650	0.19
25	84	0.26	935	0.45
60	72	0.20	810	0.34

specimen dimensions: * 25×100×5 mm (W×H×T)
+ 25×100×1 mm.

The variation of fracture energy with temperature for unaged inhibitor material is shown in Figure 124. As the test temperature decreases the inhibitor material becomes stiffer resulting in higher critical stresses and an increase in the value of fracture energy. A marked increase in fracture energy resulted from the decrease in temperature from 25°C to –40°C, whilst a more moderate increase in fracture energy was observed when the temperature was reduced from 60°C to 25°C. The inhibitor exhibited glass-like behaviour at –40°C due to the close proximity of the glass transition temperature and underwent a brittle type of fracture with rapid crack propagation across the width of the specimen.

Above the glass transition temperature the increase in fracture energy with decreasing temperature correlates with the mechanical properties measured for the "horizontal bar" specimens of inhibitor. For example, when the temperature decreased from 60°C to 25°C the crack velocity decreased indicating a higher level of impedance to crack propagation. However, close to the glass transition temperature, at –40°C, the velocity of crack propagation was too rapid to be determined from the videotape record. As the test temperature decreases below the glass transition a decrease in fracture energy would be expected.

In Table 3 it can be seen that the hysteresis ratio of the inhibitor specimens at –40°C are lower than those at measured at 25°C, however, the fracture energy is higher. Ho and Tod[3] observed that some hard propellants had high fracture energies and low hysteresis ratios and they concluded that other factors besides mechanisms controlling energy dissipation influenced the fracture behaviour. In the case of the inhibitor material, the glass-like behaviour of the specimens at –40°C results in high critical stress levels and hence the input strain energy required for crack propagation is significantly increased.

As reported earlier, the bond between binder and filler in the inhibitor was much stronger than that in the propellant. The greater level of stress required for crack propagation results in substantially higher values of fracture energy for the inhibitor material in comparison to that for the propellant at all test temperatures. The results show that the inhibitor has significantly less propensity for crack propagation than the propellant.

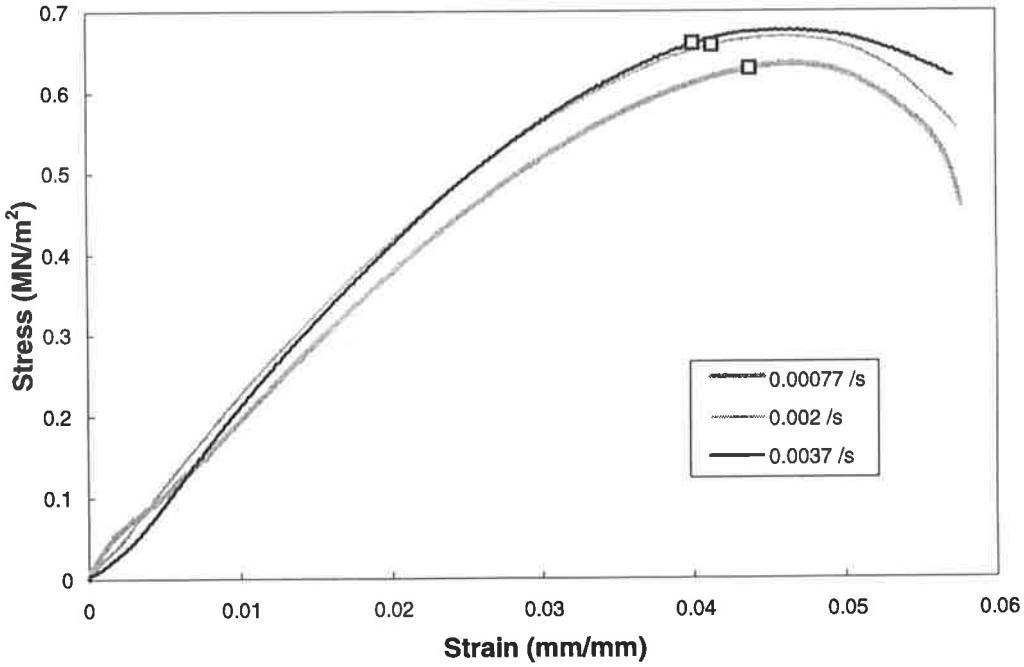

Figure 110 Stress against strain for unaged propellant specimens T= 25°C

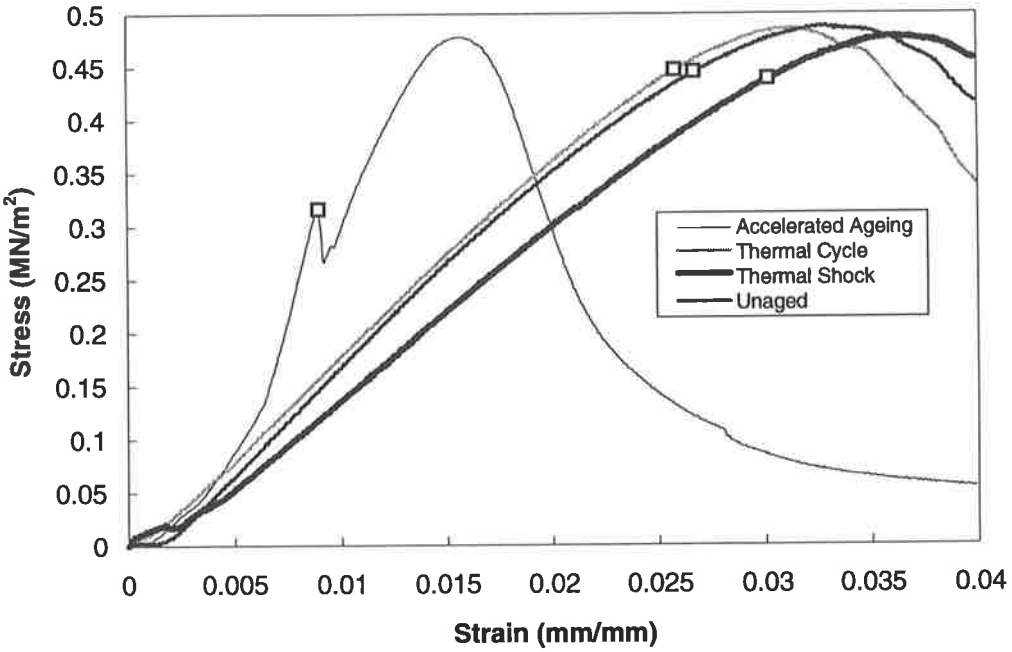

Figure 111 Stress against strain for propellant specimens T= 60°C ($\dot{\varepsilon} = 0.002\ s^{-1}$)

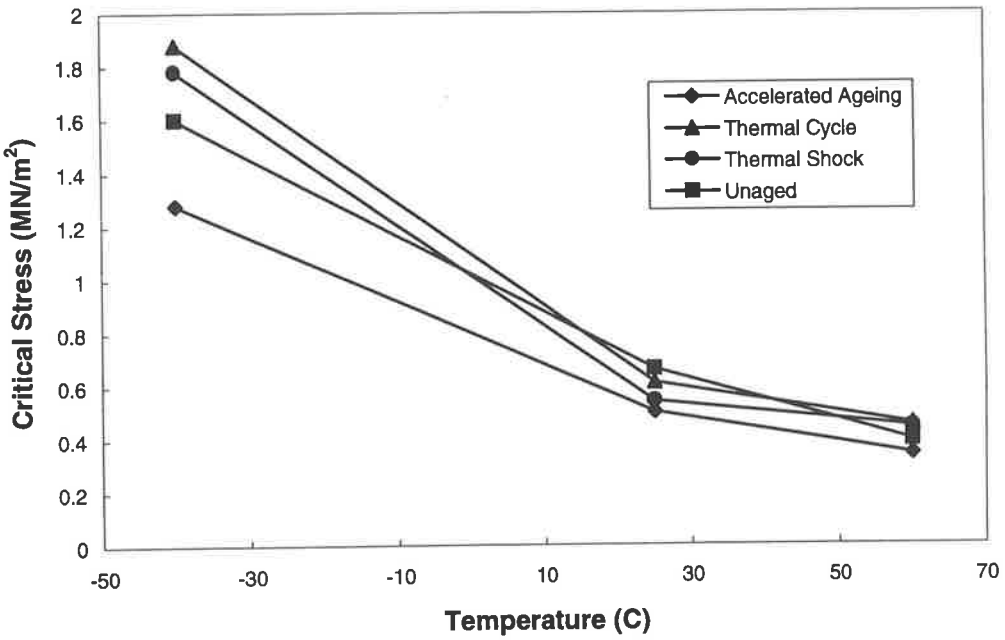

Figure 112 Change in critical stress with temperature for propellant ($\dot{\varepsilon} = 0.002\ s^{-1}$)

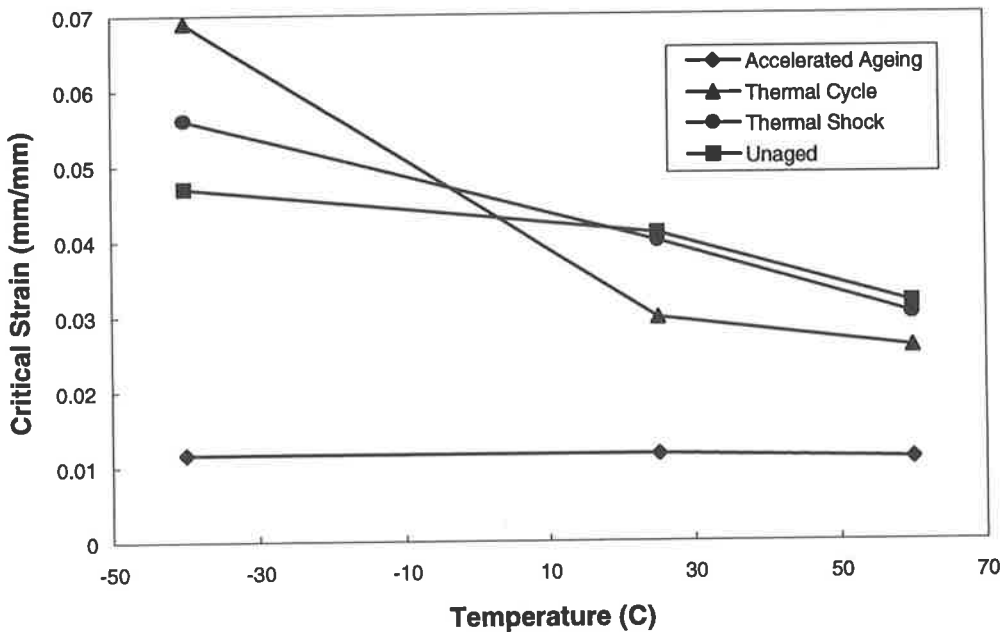

Figure 113 Change in critical strain with temperature for propellant ($\dot{\varepsilon} = 0.002\ s^{-1}$)

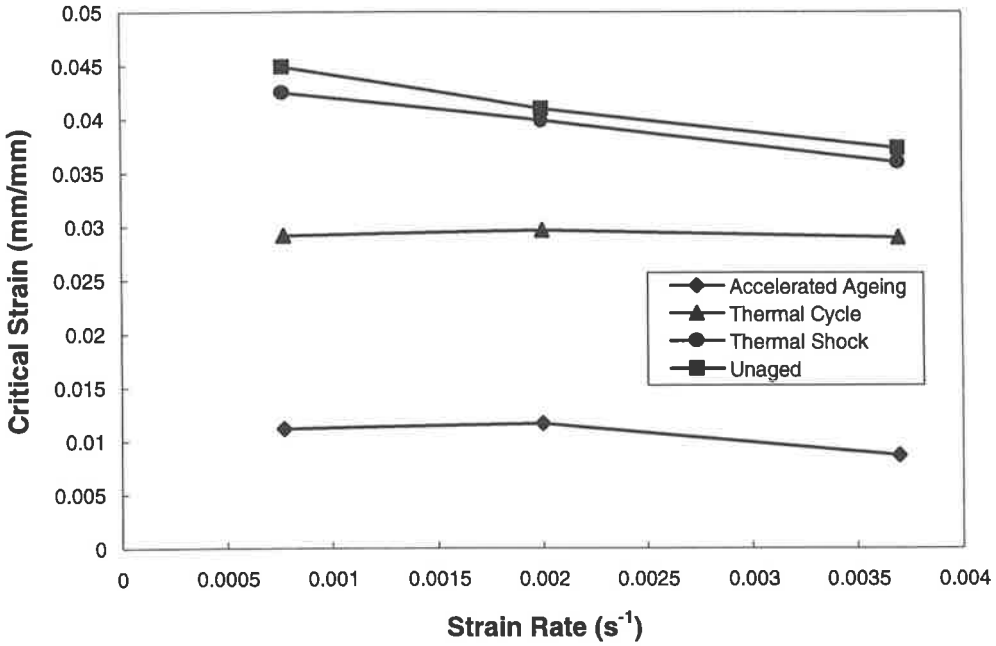

Figure 114 Change in critical strain with strain-rate for propellant (T= 25°C)

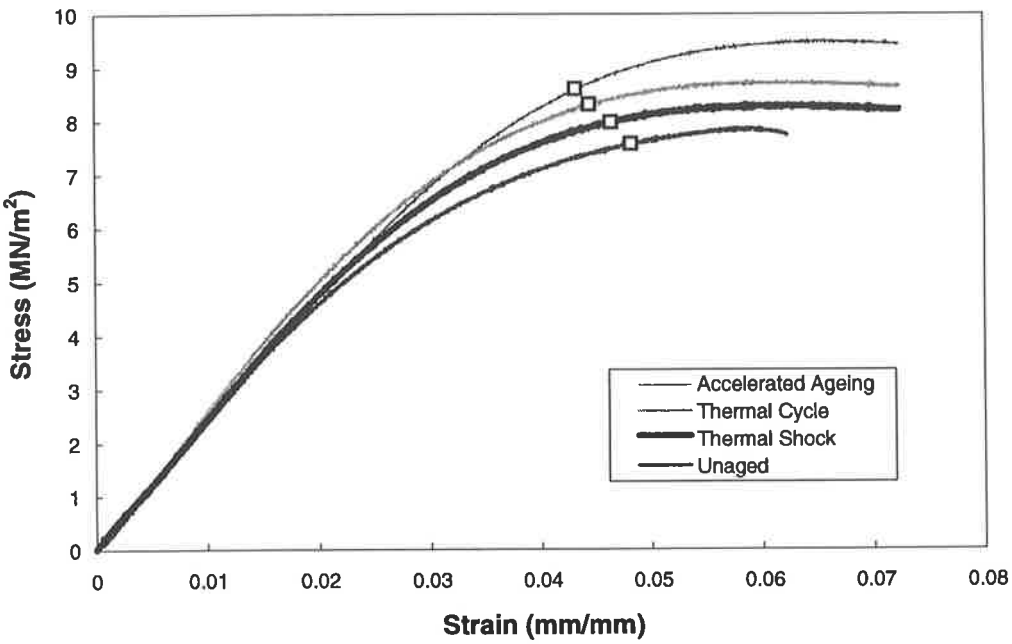

Figure 115 Stress against strain for inhibitor specimens T= 25°C ($\dot{\varepsilon} = 0.002\ s^{-1}$)

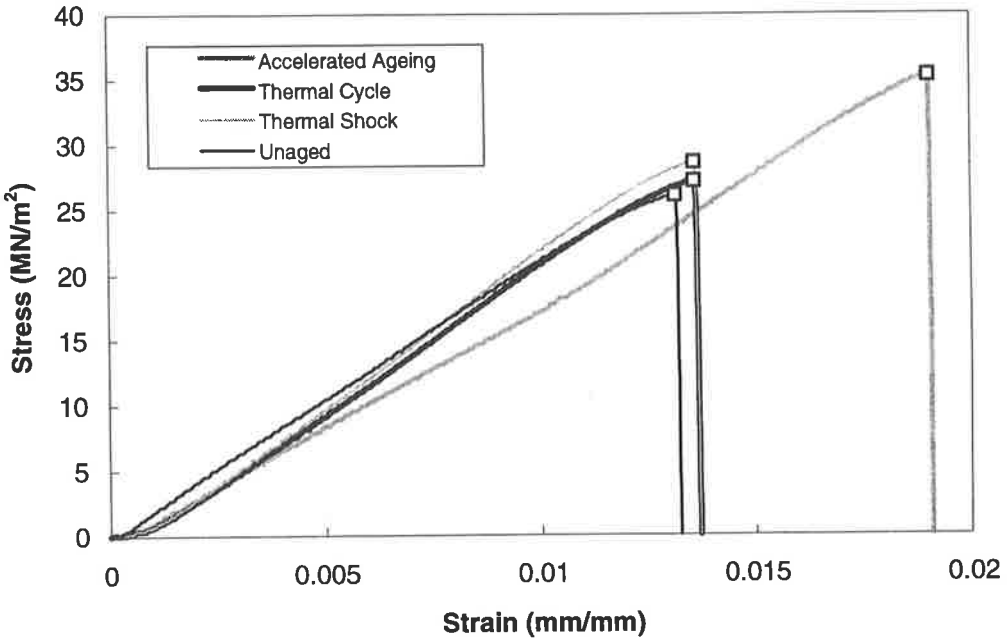

Figure 116 Stress against strain for inhibitor specimens T= –40°C ($\dot{\varepsilon} = 0.002\ s^{-1}$)

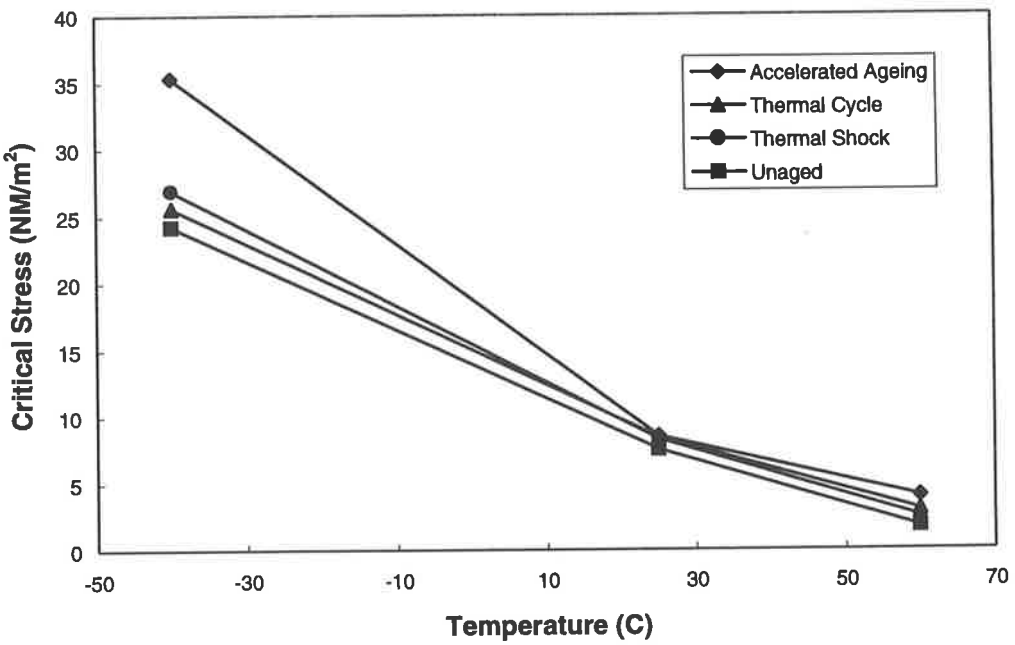

Figure 117 Change in critical stress with temperature for inhibitor ($\dot{\varepsilon} = 0.002\ s^{-1}$)

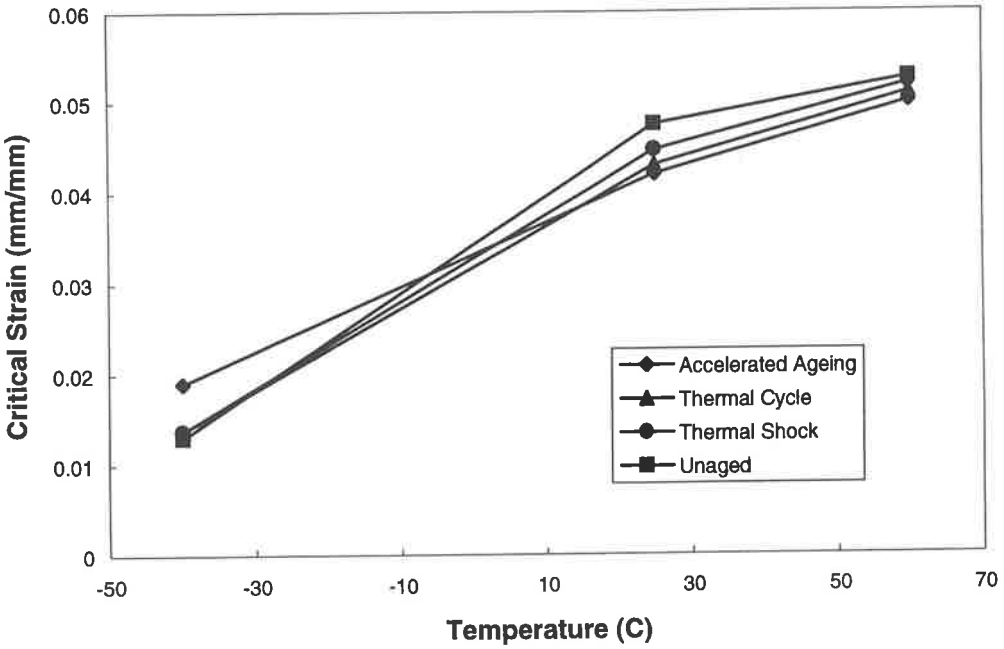

Figure 118 Change in critical strain with temperature for inhibitor ($\dot{\varepsilon} = 0.002\ s^{-1}$)

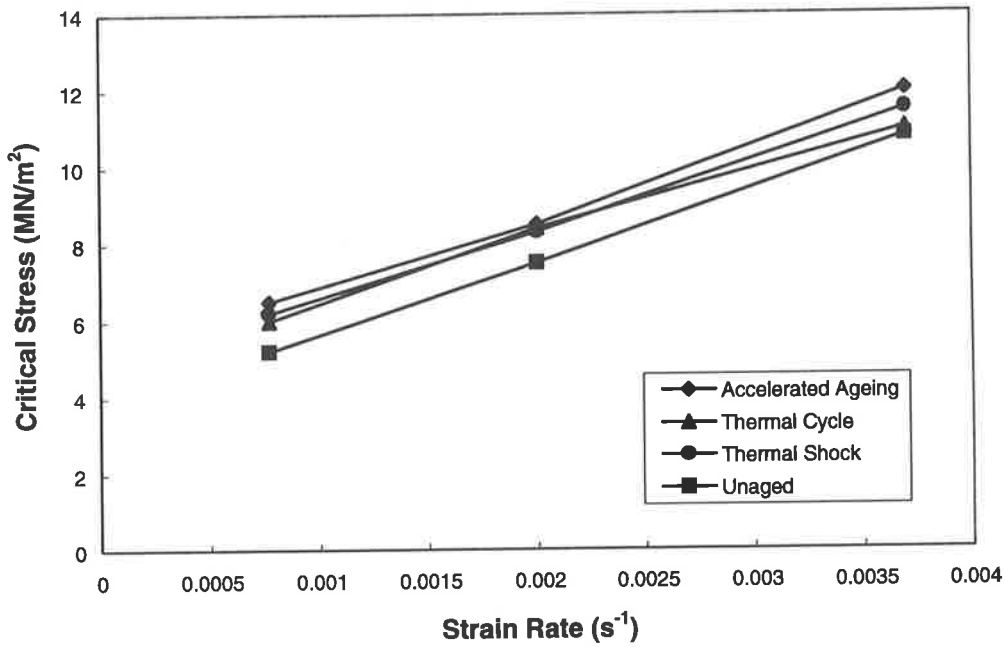

Figure 119 Change in critical stress with strain-rate for inhibitor (T= 25°C)

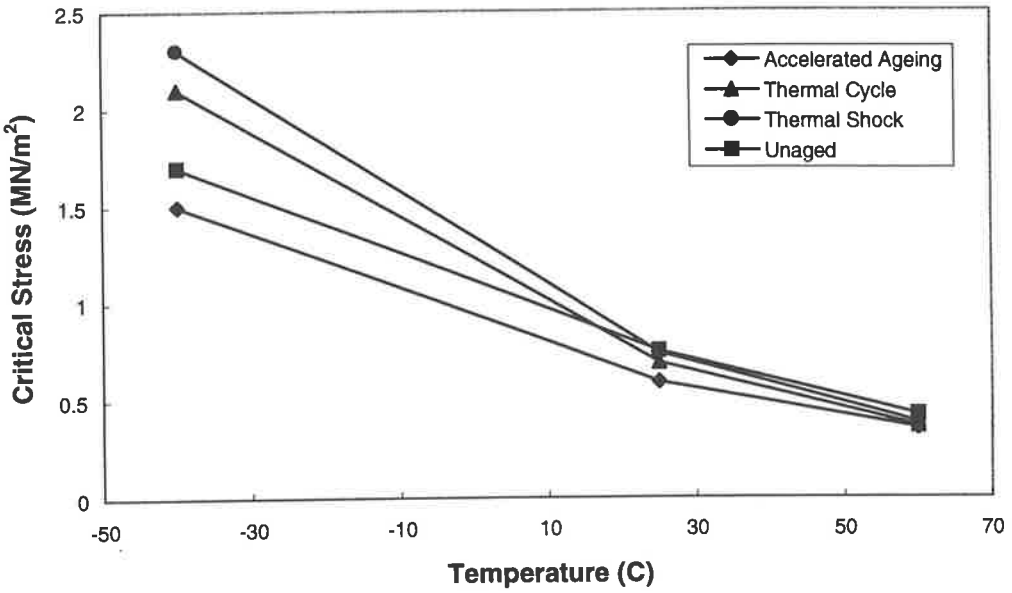

Figure 120 Change in critical stress with temperature for prop/inh ($\dot{\varepsilon} = 0.002\ s^{-1}$)

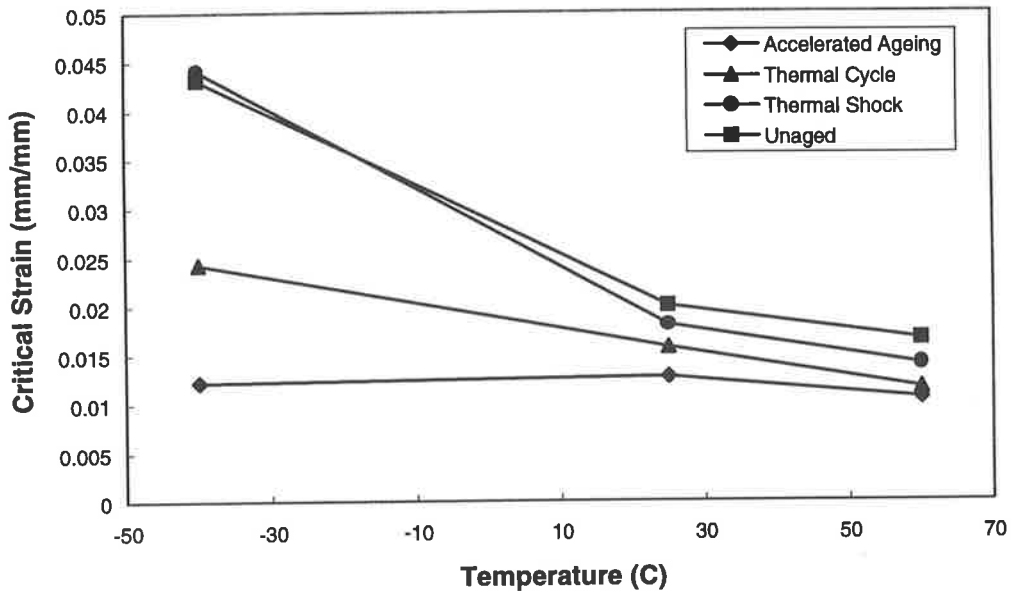

Figure 121 Change in critical strain with temperature for prop/inh ($\dot{\varepsilon} = 0.002\ s^{-1}$)

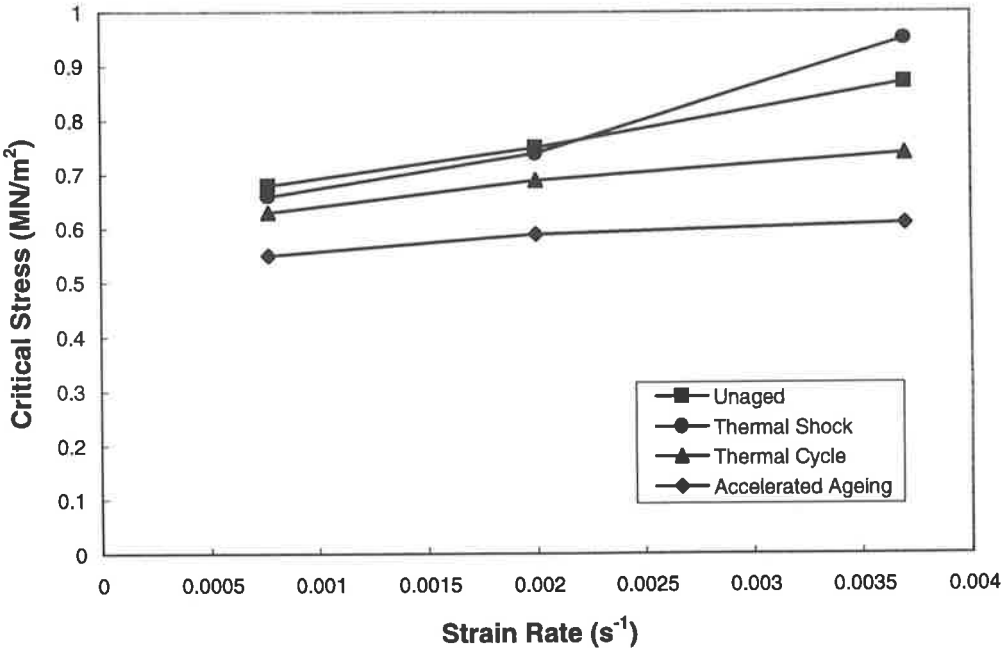

Figure 122 Change in critical stress with strain-rate for prop/inh (T= 25°C)

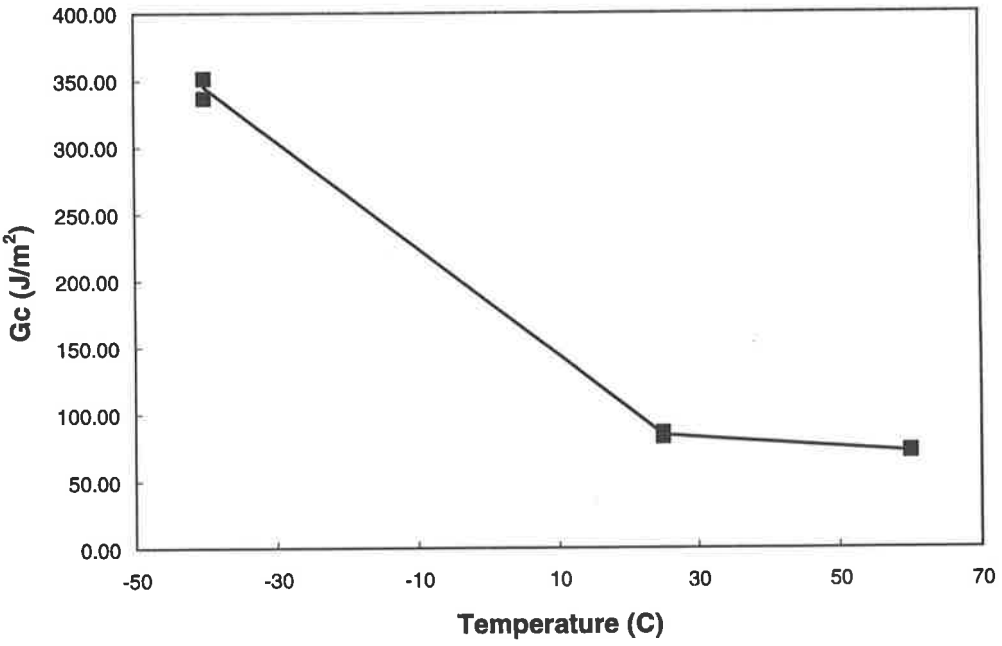

Figure 123 Change in fracture energy with temperature for propellant ($\dot{\varepsilon} = 0.00077\ s^{-1}$)

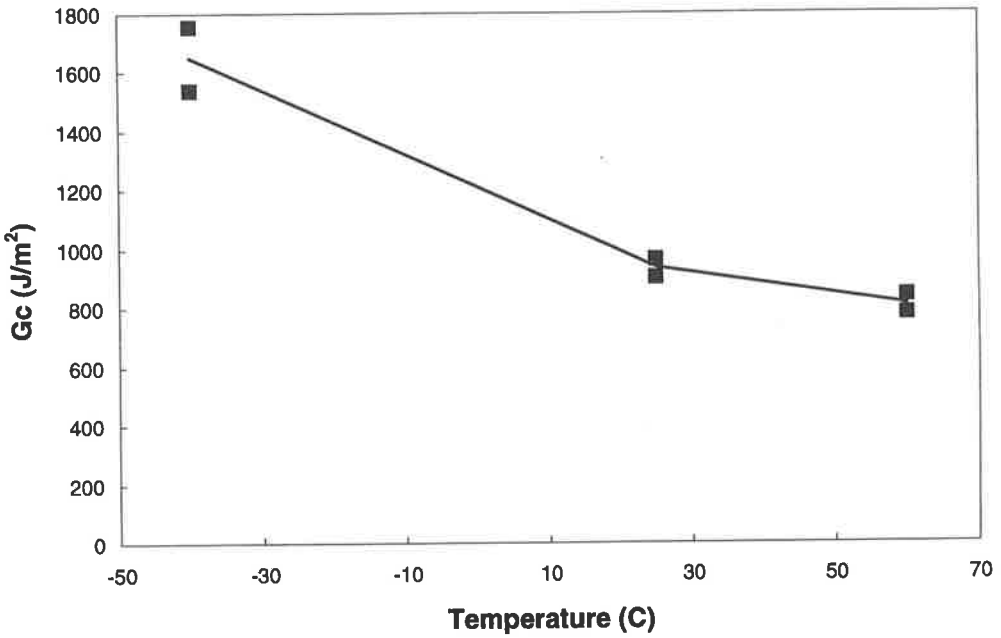

Figure 124 Change in fracture energy with temperature for inhibitor ($\dot{\varepsilon} = 0.00077\ s^{-1}$)

Chapter V
Conclusion

Thermal loads during the service life of a solid propellant rocket motor cause the materials of manufacture to deteriorate due to ageing. This deterioration leads to changes in the ballistic performance of the rocket motor which may result in its failure to operate according to specification. Cracks in the propellant are one reason for the change in ballistic performance. A crack creates extra surface for burning, resulting in the formation of excess combustion gases which may cause overpressurisation of the case leading to catastrophic failure of the rocket motor. It is therefore important to know when the level of deterioration will result in unsafe operation of the rocket motor.

The thermal loads to which the rocket motor is subjected will cause stresses in the componentry of the motor due to their differing values of thermal expansion. The thermally induced stress condition has the potential to cause crack initiation and propagation. Chemical ageing of the rocket motor materials, which has been studied elsewhere, results in degradation of the mechanical properties of the polymers and this affects the propensity for crack initiation and/or propagation in the propellant or at the propellant/inhibitor bondline. Previous studies of the mechanical degradation of rocket motor materials are limited to tests at ambient temperatures of naturally aged propellant or tests on unaged propellant over a range of temperatures. No studies have examined the effect of temperature and strain-rate on thermally shocked or cycled propellant and inhibitor materials or the propellant/inhibitor interface.

A modern approach to the determination of rocket motor service life involves the use of finite element analysis to predict mechanical and fracture behaviour under the conditions of service. A greater understanding of the changes caused by ageing to the mechanical and fracture

properties of the rocket motor materials will allow significant enhancements to the modelling process. The finite element analyis can more precisely model the effect of thermal loads on the fracture behaviour of the rocket motor, leading to more accurate predictions of service life. The aim of this study then was to investigate the effects of ageing on the degradation of mechanical and fracture properties of rocket motor materials. To achieve this all of the polymeric materials employed in a PICTOR rocket motor were subjected to a variety of thermal loads, designed to simulate service life conditions, and the thermal and fracture behaviour of the aged and unaged materials measured at various temperatures and strain-rates.

If a loading condition develops during a transient thermal load which has the potential to cause crack initiation and propagation at the bondline of the inhibitor and epoxy, the charge may cease to be adequately retained within the rocket motor casing. It was found that diverging values for the thermal expansion coefficients of inhibitor and epoxy exist over the range of test temperatures investigated. The inhibitor will contract at a greater rate than the epoxy as the temperature of the rocket motor decreases with the potential for cracking to develop at the bondline.

Of more serious concern is the potential for cracking to occur within the propellant or at the bondline of the propellant and inhibitor. Cracks occurring at these positions will result in an increase in the burning surface of the propellant which may critically affect the performance of the rocket motor. A marked difference in the thermal expansion coefficients of the unaged inhibitor and propellant was apparent in both the sub-zero and elevated ranges of test temperatures. This is significant as differing amounts of expansion and contraction, resulting from transient temperatures during thermal loadings, will lead to the development of stresses in the two materials. Cracks formed in the propellant will result from these stress gradients. The

stress state across the bondline also provides the energy required for crack initiation and/or propagation at the bondline of the propellant and inhibitor.

A change in thermal behaviour resulting from material ageing may lead to a substantial increase in the propensity for crack propagation. Greater divergence in the values of thermal expansion coefficient for the various materials will cause an increase in the stress gradients resulting from thermal loads as compared to those in unaged material. The PICTOR materials subjected to thermal shock, thermal cycling and accelerated ageing exhibited negligible change in the thermal expansion coefficient. Two exceptions were the thermal expansion coefficients of the thermally cycled and thermally shocked propellant, for which a significant decrease was detected in the sub-zero temperature range. As a consequence the difference between the thermal expansion coefficients of the propellant and inhibitor decreased. For example, the difference decreased from 31.3×10^{-6} K^{-1} for unaged specimens to 4.4×10^{-6} K^{-1} (at –45°C) for the aged specimens. Therefore, a rocket motor which has been subjected to thermal shock or thermal cycling during its service life will experience decreased stress gradients across the interface of the propellant and inhibitor at sub-zero temperatures thereby decreasing the likelihood of cracking.

Another thermal property affecting the material behaviour is the glass transition. An increase in glass transition temperature with ageing will lead to a change in material behaviour compared to the unaged material. At temperatures in the region immediately below the transition temperature for the aged material, its behaviour will be glass-like whereas for the unaged material at the same temperature the behaviour would be rubbery. There was negligible variation in the glass transition temperatures of most aged polymers. A slight increase for the accelerated aged specimens resulted from increased cross-linking in the polymer matrix of the propellant, inhibitor and epoxy during prolonged storage at elevated temperature.

The input of more accurate values of the change in Poisson's ratio with strain leads to the calculation of more precise values of lateral stress. The imaging technique was a significant improvement on previous methods, allowing the uniformity of elongation and contraction throughout the specimen to be monitored and eliminating edge effects.

The change in Poisson's ratio with strain illustrated the non-linear material behaviour resulting from the unique nature of highly filled particulate composites. As the strain increases binder/filler debonding results in the formation of vacuoles in the propellant and inhibitor. The strength of the binder/filler bond in the inhibitor was observed to be greater than that in the propellant where strains to specimen rupture were approximately ten times lower than for the inhibitor.

The non-linear material behaviour of the propellant and inhibitor materials will result in only a fraction of the energy supplied from thermal loads being recovered. The irreversible or hysteresis energy losses present must be known so that the inelastic material behaviour can be included in the calculation of the energy of fracture. The hysteresis ratio for unaged and specimens subjected to each of the three thermal loads of propellant, inhibitor and a propellant/inhibitor bimaterial were measured at a variety of temperatures and strain-rates. A marked decrease in hysteresis ratio was detected when the temperature of the propellant specimen was increased and after it had been subjected to accelerated ageing, the hysteresis energy losses present during cyclic loading decrease as a proportion of the energy input. More conclusions relating hysteresis ratio to the fracture properties will be described below.

Image analysis and scanning electron microscopy of fracture and the fracture surface in aged propellant, inhibitor and at the propellant/inhibitor interface has provided an understanding of the mechanism of crack propagation in particulate composites. This study has substantially added to the understanding of the effect of ageing, temperature and strain-rate on fracture in

particulate composites as only limited investigations have been reported previously. The mechanism of crack growth in the propellant can be described as one of blunt-sharp-blunt. A damage zone forms ahead of the crack tip in the periods of blunting. In this zone dewetting of the binder and filler cause vacuoles to be formed which continue to increase in size as the specimen is elongated. Fibrils of dewetted binder material appear which lengthen with increasing strain. The crack sharpens by coalescing with the microvoids and microcracks in the damage zone as the fibrils of binder fail.

The fracture behaviour of the propellant specimens were affected by temperature whilst strain-rate had only a minor effect. It was found that as the material temperature decreased from 25°C to –40°C the stiffening of the propellant caused a significant increase in the size of the damage zone, much higher levels of crack blunting were measured. A small increase in the size of the damage zone was also observed when the material temperature was decreased from 60°C to 25°C.

A crack mechanism affected by ageing, temperature or strain-rate will provide an understanding of the consequences each of these has on the propensity of crack propagation. The most significant change in the mechanism of crack growth was found in the propellant which had been subjected to accelerated ageing. A damage zone was unable to be detected from image analysis of cracks propagating in accelerated aged specimens. The crack remained sharp at all times and propagated across the length of the specimens rapidly, the ageing had produced a change in the material resulting in a more brittle type of fracture. By comparison no difference in the mechanism of crack growth was detected in the thermally shocked and thermally cycled specimens and the damage zone was similar in magnitude.

A distinct correlation was found to exist between the size of the damage zone, hysteresis ratio, crack velocity and the ageing to which the propellant specimen had been subjected. As

discussed above, the severity of the accelerated ageing resulted in no detectable damage zone ahead of the crack tip, whilst the size of the damage zone in the other aged propellant specimens was marginally smaller compared to the unaged material. A decrease in the value of hysteresis ratio corresponding to the increased severity of the thermal loads was found. A substantial decrease in hysteresis ratio for the accelerated aged propellant and more marginal decreases for the thermally cycled and shocked material resulted from progressively lower levels of irreversible energy losses with more severe ageing. Smaller damage zones/lower levels of crack blunting will result in less impedance to the sharpening portion of the crack growth mechanism and consequently higher crack velocities were measured. Not unexpectedly the accelerated aged propellant had the highest crack velocities and the other aged materials had crack velocities in the order (ranked highest to lowest) thermal cycle, thermal shock, unaged.

The mechanism of crack growth in the inhibitor was found to be one of crack propagation by material tearing into a damage zone formed ahead of the crack tip. The crack remained sharp at all times without any evidence of blunting, propagating into an area stress whitened from binder/filler debonding and damage to the polyurethane binder. This can be attributed to much stronger binder/filler bonding existing in the inhibitor as was evident from the substantially higher strain levels at the onset of dewetting and specimen rupture.

The specimen temperature had a significant effect on the mechanical properties of the inhibitor. Plots of stress against strain for the two test temperatures above glass transition showed considerable softening of the material occurred at 60°C with rupture at lower stresses as compared to 25°C. The size of the damage zone is related to the intensity of stress whitening and a correlation was found between this, the roughness of the fracture surface, crack velocity, hysteresis ratio and the behaviour of the material at the two test temperatures. At 25°C the damage zone was larger for an equivalent strain level and the intensity of the stress whitening

greater, a much rougher fracture surface was also observed. Correspondingly, the value of the hysteresis energy losses as a proportion of the input energy (h_r), the size of the damage zone and the amount of material tearing increased as the temperature decreased, the lower crack velocities found at 25°C also correlate with this.

At a test temperature of –40°C all of the inhibitor specimens exhibited glass-like behaviour due to the proximity of the glass transition. The stiffened material ruptures at substantially increased stresses and in a manner typical of brittle materials. The crack propagated across the specimen rapidly with a minute damage zone, this was consistent with the decreased hysteresis ratios measured.

One of the major objectives of this study was to determine the fracture behaviour of inhibitor material subjected to various ageing conditions. From examination of the effect of ageing on the hysteresis ratio, crack mechanism (and the magnitude of the damage zone) and the crack velocity it can be concluded that the inhibitor may be subjected to severe ageing without significant effect. The hysteresis ratios of the aged inhibitor specimens decreased only marginally with ageing. Values for the thermally shocked specimens were similar to and those of the thermally cycled specimens only slightly lower than the unaged material, those for the accelerated aged were the lowest. Negligible differences in the size of the damage zones and crack velocities were found for the specimens subjected to the thermal loads.

Cracks present at the interface of the propellant and inhibitor will form extra surface for burning and thus the inhibitor fails to perform its function of limiting combustion to the end face of the propellant. Examination of the crack growth response for the propellant/inhibitor bimaterial specimens showed that crack propagation occurred in the propellant layer, adjacent to the bondline of the two materials. The fracture was cohesive in the propellant with no damage detected in the layer of inhibitor material. Although the mechanism of crack growth is

similar to that found in the propellant specimens when compared the damage zone was smaller and hence higher crack velocities exist in the propellant/inhibitor bimaterial specimens.

The mechanism of crack growth in the bimaterial specimens was affected by the test temperature but did not vary with strain-rate. As the test temperature was decreased the bimaterial specimens became stiffer with a subsequent increase in the stress level attained at equivalent strains. The size of the damage zone ahead of the crack tip increased markedly when the temperature decreased from 25°C to –40°C, but only marginally when the temperature decreased from 60°C to 25°C. A corresponding increase in hysteresis ratio and decrease in crack velocity was found as the test temperature decreased.

The deterioration in the accelerated aged propellant in the bimaterial specimens was similar to that observed for the propellant specimens. The material fractured rapidly across the length of the specimen without the formation of a damage zone in a manner typical of a brittle material. This thermal load caused hardening of the material with a subsequent lowering of the critical strain. By comparison the thermal shock and thermal cycle did not effect the behaviour of the bimaterial specimens, no difference in the crack mechanism and size of the damage zones compared to the unaged material were detected. The change in the material behaviour of the bimaterial specimens as a result of ageing was detected by variations in the crack velocity. Increased severity of ageing, causing decreased energy losses as a proportion of the energy input (ie., the hysteresis ratio) and a decreased level of crack blunting in the propellant, resulted in higher crack velocities.

Once a crack has been initiated, a criteria for crack propagation describes the conditions for extension of that crack under the influence of the thermal loads. This can be incorporated into a finite element analysis of the rocket motor. The effect of ageing on the mechanical properties of the materials of construction can be included in the analysis of the rocket motor and the

elongation of the crack can be modelled so as to ascertain its effect on the ballistic properties of the rocket motor when fired.

Fracture energy has been successfully applied as a criterion for crack propagation. It is a measure of the energy required for crack propagation which includes bulk inelastic material behaviour when combined with the energy losses associated with hysteresis. There have been relatively few studies which consider the effect of temperature on the propensity for cracking to occur in the propellant and inhibitor. Values of fracture energy have been calculated for unaged specimens and the effect of temperature examined.

A marginal increase in the fracture energy of the propellant was observed when the temperature decreased from 60°C to 25°C. By comparison a more significant increase occurred when the temperature was reduced to –40°C. The fracture energy of the inhibitor exhibited a similar trend. At –40°C the stiffening of both propellant and inhibitor specimens was evident as very much higher stresses at failure and only marginal changes in the critical strain. These combined to give high fracture energies. In the case of the inhibitor a low hysteresis ratio at –40°C and a high value of fracture energy indicates that other factors contribute to the fracture behaviour along with those responsible for the hysteresis energy losses.

The inhibitor consistently exhibited a higher stiffness than the propellant with greater strains to rupture and higher hysteresis ratios. The much stiffer binder in the inhibitor and the increased level of recoverable strain energy resulted in fracture energies of the inhibitor substantially higher than those for the propellant. In some instances the fracture energy of the inhibitor was an order of magnitude greater than that of the propellant for the same conditions, implying that the propensity for crack propagation to occur in the propellant was much higher.

This study of the thermal and fracture behaviour of the various materials employed in the PICTOR rocket motor has provided an insight which will significantly enhance the finite element modelling of rocket motors subjected to thermal loads and allow greater accuracy of model results and service life predictions. It was found that the most severe changes to material mechanical properties occurred under accelerated ageing conditions. The inhibitor was not significantly affected by any of the thermal loads to which it was subjected. However, deterioration of the propellant's mechanical properties was directly related to the severity of the thermal load.

Appendix A
Summary of Rocket Motor Terminology[61]

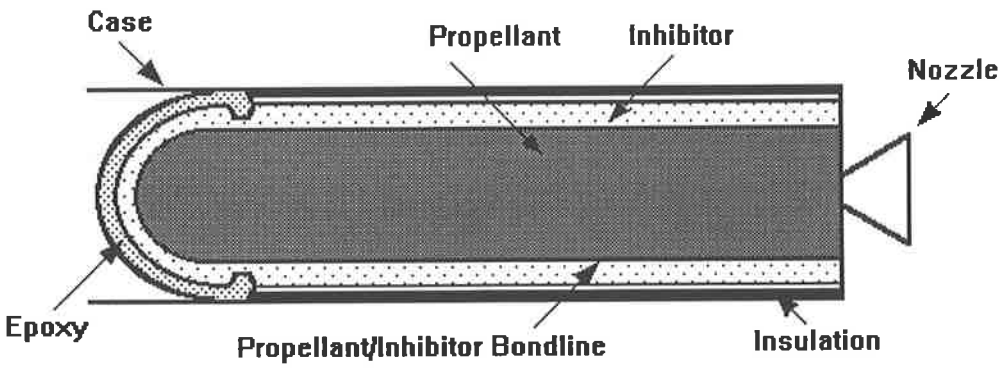

Figure 125 Components of the PICTOR solid propellant rocket motor

Adhesive	epoxy resin which bonds the charge into the case at the head end.
Binder	a synthetic rubber (or plastic) forming a matrix of material which holds the oxidiser particles together, sometimes also acting as a fuel. The PICTOR propellant binder is a hydroxy-terminated polybutadiene.
Case	the rocket motor's outer shell, for PICTOR a maraging steel is employed.
Charge	beaker of inhibitor containing the cast propellant.
Composite propellant	heterogeneous mixture of binder and an energetic filler.
Dewetting	debonding of the binder and filler at the binder/filler interface.
FEA	finite element analysis (also referred to as finite element modelling, FEM) is a tool employed for structural analysis.

Inert propellant	a non-energetic composite which attempts to simulate the live propellant's properties, non-oxidising filler particles are used.
Inhibitor	a composite consisting of a polyurethane and 35% by weight ammonium sulphate filler particles. The inhibitor prevents the combustion spreading away from the end face of the propellant.
Insulation	EPDM rubber providing thermal protection for the rocket motor case.
Keying mechanism	groove in the outer surface of the charge which fills with epoxy resin adhesive, bonding the charge to the head end of the rocket motor case.
Nozzle	expansion of the exhaust gases through the nozzle provides propulsion.
Oxidiser/filler	crystalline ammonium perchlorate particles which is an energetic material constituting 80% by weight of the PICTOR propellant.
Propellant/Inhibitor bondline	adhesive bond at the interface of the propellant and inhibitor.
Service life	that length of time from the date of manufacture that an explosive assembly (eg., propulsion unit) of a missile system will continue to safely and reliably meet all service requirements for storage, performance and operational use.

Bibliography

1. Kinloch, A. J. and Tod, D. A., *"A New Approach to Crack Growth in Rubbery Composite Propellants"*, Propellants, Explosives and Pyrotechnics, Vol 9, 1984, pp 48-55.

2. Oberth, A. E., *"Principles of Solid Propellant Development"*, CPIA Pub 469, Sept. 1987

3. Ho, S.-Y. and Tod, D. A., *"Mechanical Failure Analysis of Rubbery Composite Propellants Using a Modified Fracture Mechanics Approach"*, (Proc) 21st ICT Conference

4. Kishore, K. and Prasad, G., *"Survey of Solid-Propellant Aging Studies"*, Journal of Spacecraft, Vol. 15, No. 5, 1978, pp 261-262.

5. Smith, C. W. and Liu, C. T., *"Global and Near Tip Response of Cracked Solid Propellant"*, Jannaf Propulsion Meeting, Vol. 2, Nov 1993, pp 1-10.

6. Liu, C. T., *"Measurement of Damage in a Solid Propellant by Acoustic Imaging Technique"*, Materials Evaluation, Vol. 47, No. 6, 1989, pp 746-752.

7. Laufer, Z., Diamant, Y., Gill, M. and Fortuna, G., *"A Simple Dilatometric Method for Determining Poisson's Ratio of Nearly Incompressible Elastomers"*, International Journal of Polymeric Materials, Vol 6, 1978, pp 159-174.

8. Urayama, K., Takigawa, T., and Masuda, T., *"Poisson's Ratio of Poly(Vinyl Alcohol) Gels"*, Macromolecules, Vol 23, 1993, pp 3092-3096.

9. Kishore, K., Pai Verneker, V. R. and Prasad, G., *"Mechanism of the Oxidative Degradation of Binder during the Aging of Composite Solid Propellant"*, Journal of Applied Polymer Science, Vol 24, 1979, pp 589-593.

10. Piper, L. B., *"HTPB Propellant Aging"*, CPIA Report CPTR 82-182, 1982.

11. Kishore, K., Pai Verneker, V. R. and Prasad, G., *"Mechanism of Ageing of Composite Solid Propellants"*, Combustion and Flame, Vol 36, 1979, pp 79-85.

12. Perrault, G., Bedard, M., Lavertu, R. R. and Tremblay, M., *"Accelerated Aging of a Composite Explosive"*, Propellants and Explosives, Vol 4, 1979, pp 45-49.

13. Christiansen, A. G., Layton, L. H. and Carpenter, R. L., *"HTPB Propellant Aging"*, Journal of Spacecraft, Vol 18, No 3, 1981, pp 211-215.

14. Layton, L. H., *"Chemical Structural Aging Studies on an HTPB Propellant"*, AFRPL-TR-75-13, Contract F04611-71-C-0049, Morton Thiokol Inc., Brigham City UT (Apr 1975).

15. Gueguen, V., Audouin, L., Pinel, B. and Verdu, J., *"Thermal Oxidation of EPDM Terpolymer and Vulcanisate"*, Polymer Degradation and Stability, Vol 43, 1994, pp 217-223.

16. Guzzo, M. and De Paoli, Marco-A., *"The Photo-oxidation of EPDM rubber: Part V - Mechanical Properties Degradation of Vulcanized Filled Samples"*, Polymer Degradation and Stability, Vol 38, 1992, pp 41-45.

17. Kong, E. S. W. and Adamson, M. J., *"Physical Ageing and its Effect on the Moisture Sorption of Amine-cured Epoxies"*, Polymer Communications, Vol 24, June, 1983, pp 171-173.

18. Neilsen, L. E., Mechanical Properties of Polymers, Vol 2, Marcel Dekker Inc, 1974, p434.

19. Ho, S.-Y. and Tod, D. A., *"Viscoelastic Response and Hysteresis Characteristics of Rubbery Composite and Thermoplastic Elastomer Propellants"*, Propellants, Explosives and Pyrotechnics, Vol

20. Eisele, U., Introduction to Polymer Physics, Springer-Verlag Berlin, 1990.

21. Gent, A. N. and Hwang, Y.-C., Rubber Chem. Techol., Vol 61, 1988, p 630.

22. Smith, T. L., Trans. Soc. Rheol., Vol 3, 1959, p 113.

23. Yilmazer, U. and Farris, R. J., Journal of Applied Polymer Science, Vol. 28, 1983, p 3369.

24. Anderson, L. L. and Farris, R. J., Journal of Applied Polymer Science, Vol. 28, 1983, p 522.

25. Fedors, R. F. and Hong, S. D., *"A New Technique for Measuring Poisson's Ratio"*, Journal Of Polymer Science: Polymer Physics Edition, Vol 20, No. 4, 1982, pp 777-781.

26. Kugler, H. P., Stacer, R. G. and Steimle, C., *"Direct Measurement of Poisson's Ratio in Elastomers"*, Rubber Chemistry Technology, Vol 63, No. 4, 1990, pp 473-487.

27. Smith, C. W., Mouille, H. and Liu, C. T., *"Temperature, Rate and Gradation Effects on the Opening and Growth of Cracks in Particulate Composite Bodies"*, Advances in Experimental Mechanics and Biometrics, W. F. Jones and J. M. Whitney, Eds., ASME AD-V29, AMD-V146, 1992, pp 29-40.

28. Smith, C. W., Wang, L. and Mouille, H., *"Observations of Material and Geometric Effects on Crack Opening and Growth for Particulate Composites"*, Experiments in Micromechanics of Failure Resistant Materials, ASME Applied Mechanics Division, Vol 130, 1991, pp 119-129.

29. Liu, C. T., *"Investigating the Near-Tip Fracture Behaviour and Damage Characteristics in a Particulate Composite Material"*, Fracture Mechanics: Twenty-Third Symposium, ASTM STP 1189, Ravinda Chona, Ed., ASTM, Philadelphia, 1993, pp 668-679.

30. Yeh, H-Y., Le, M. D. and Liu, C. T., *"An Experimental Study of the Loading Rate Effect on the Crack Growth Behaviour in a Composite Solid Propellant"*, Journal of Reinforced Plastics and Composites, Vol. 12, Jan 1993, pp 48-57.

31. Schapery, R. A., *"On a Theory of Crack Growth in Viscoelastic Media"*, Report MM 2763-73-1, Texas A&M University, 1973.

32. Knauss, W. G., *"Delayed Failure - The Griffith Problem for Linearly Viscoelastic Materials"*, International Journal of Fracture Mechanics, Vol. 6, 1970, pp 7-20.

33. Liu, C. T., *"Investigation of the Effect of Predamage on the Crack Growth Behaviour in a Particulate Composite Material"*, AIAA-93-1521-CP.

34. Kinloch, A. J. and Young, R. J., Fracture Behaviour of Polymers, Elsevier Applied Science Publishers, 1985.

35. Langlois, G. and Gonard, R., *"New Law for Crack Propagation in Solid Propellant Material"*, Journal of Spacecraft, Vol. 16, No. 6, Nov-Dec 1979, pp 357-360.

36. Schapery, R. A., *"A Theory of Crack Initiation and Growth in Viscoelastic Media, I. Theoretical Development"*, International Journal of Fracture, Vol. 11, Feb 1975, pp 141-159.

37. Schapery, R. A., *"A Theory of Crack Initiation and Growth in Viscoelastic Media, II. Approximate Methods of Analysis"*, International Journal of Fracture, Vol. 11, Feb 1975, pp 369-388.

38. Schapery, R. A., *"A Theory of Crack Initiation and Growth in Viscoelastic Media, III. Analysis of Continuous Growth"*, International Journal of Fracture, Vol. 11, Aug 1975, pp 549-562.

39. Gledhill, R. A. and Kinloch, A. J., *"A Unique Failure Criterion for Characterising the Fracture of Propellants"*, Propellants and Explosives, Vol. 4, 1979, pp 73-77.

40. Kinloch, A. J. and Gledhill, R. A., *"Propellant Failure: A Fracture Mechanics Approach"*, Journal of Spacecraft, Vol. 18, No. 4, Jul-Aug 1981, pp 333-337.

41. Devereaux, A. S., *"Assessment of Solid Propellant Grain Flaws Through J-Integral Fracture Predictions"*, Paper no. AIAA 94-3288, Proc. 30th AIAA/ASME/SAE/ASEE Joint Propulsion Conference, June 27-29, 1994, Indianapolis, IN.

42. Griffith, A. A., *"The Phenomena of Rupture and Flow in Solids"*, Phil Trans Roy Soc, A, Vol 221, 1921, pp 163-198.

43. Rivlin, R. S. and Thomas, A. G., *"Rupture of Rubber. I. Characteristic Energy for Tearing"*, Journal of Polymer Science, Vol. 10, No. 3, 1953, p291.

44. Marom, G., Harel, H, and Rosner, J., *"Fracture Energies of Composite Propellant"*, Journal or Applied Polymer Science, Vol 21., 1977, pp 1629-1634.

45. ASTM D412, *"Standard Test Methods for Rubber Properties in Tension"*.

46. Tabatabai, A. J. and Mitchell, O. R., *"Edge Location to Subpixel Values in Digital Imagery"*, IEEE Transactions on Pattern Analysis and Machine Intelligence, Vol. PAMI-6, No. 2, March 1984, pp 188-201.

47. Cosandier, D. and Chapman, M. A., *"High Precision Target Location For Industrial Metrology"*, Videometrics, SPIE Vol. 1820, 1992, pp 111-122.

48. De Iasi, R. and Whiteside, J. B., *"Effect of Moisture on Epoxy Resins and Composites"*, ASTM STP 658 (J. R. Vinson Ed.), American Society for Testing and Materials, 1977, pp 2-42.

49. Burton, Bruce L., *"The Effect of Moisture Absorption on a Variety of Cured Epoxy Resins"*, 18th International SAMPE Technical Conference, October 7-9, 1986, pp 124-134.

50. Allen, Charles R., *"Glass Transition Measurement in Wet Polymers and Composites"*, 18th International SAMPE Technical Conference, October 7-9, 1986, pp 583-592.

51. Beyer, R. B., *"Nonlinear Mechanical Behaviour of Solid Propellants"*, Paper No. 65-159, AIAA, 6th Solid Propellant Rocket Conference (proc), Washington DC, Feb 1-3 1965.

52. Stacer, R. G., Hübner, C. and Husband, D. M., *"Binder/Filler Interaction and the Non-Linear Behaviour of Highly-Filled Elastomers"*, Rubber Chemistry and Technology, Vol. 63, Sept-Oct 1990, pp 488-502.

53. Buswell, J. H., Dodds, J. S. and Tod, D. A., *Studies of Composite Propellant Mechanical Properties"*, Paper No. 28, (Proc) Technology Workshop, WTP-4: Energetic Materials and Propulsion Technology, TTCP, DSTO Salisbury, 18-19 April. 1996.

54. Rigbi, Z., *"The Value of Poisson's Ratio of Viscoelastic Materials"*, Applied Polymer Symposia, No. 5, 1967, pp 1-8.

55. Ho, S.-Y. and Fong, C. W., *"Correlation between Fracture Properties and Dynamic Mechanical Relaxations in Composite Propellants"*, Polymer, Vol. 28, 1987, pp 739-744.

56. Ho, S.-Y, and Fong, C. W., *"Temperature Dependence of High Strain-Rate Impact Fracture Behaviour in Highly Filled Polymeric Composite and Plasticised Thermoplastic Propellants"*, Journal of Material Science, Vol. 22, 1987, pp 3023-3031.

57. Eirich, F. R. and Smith, T. L., *"Isothermal Rupture of Elastomers"*, in Fracture; An Advanced Treatise, Volume VII, Fracture of Nonmetals and Composites, Liebowitz, H., (Ed.) Academic Press, 1972.

58. Odom, E. M. and Adams, D. F., *"An Investigation of the Isotropy of Epoxy Polymers"*, J. Mater. Res., Vol. 7, No. 12, Dec 1992, pp 3352-3358.

59. Broek, D., The Practical Use of Fracture Mechanics, Kluwer Academic Publishers (The Netherlands), 1989, p 13.

60. Knott, J. F., Fundamentals of Fracture Mechanic, Butterworth and Co. Ltd. (UK), 1973, p 211.

61. Sutton, G. P., Rocket Propulsion Elements, 5th Ed., 1986, John Wiley & Sons.

Additional References

62. Ahagon, A. and Gent, A. N., *"Threshold Fracture Energies for Elastomers"*, J. Polymer Science, Vol. 13, 1975, pp 1903-1911.

63. Bazhenov, S., Li, J. X. and Baer, E., *"Ductility of Filled Polymers"*, J. Applied Polymer Science, Vol. 52, No. 2, 1994, pp 243-254.

64. Beaumont, P. W. R., *"Micromechanics of Composite Fracture"*, CUED/C-MATS/TR-138, Cambridge University, England, Dept of Engineering, May 1987.

65. Beaumont, P. W. R., *"The Micromechanics of Composite Fracture"*, Materials Forum, Vol. 11, 1987, pp 332-340.

66. Beckwith, S. W. and Wang, D. T., *"Crack Propagation in Double-Base Propellants"*, J. Spacecraft, Vol. 15, No. 6, Nov-Dec 1978, pp 355-361.

67. Britton, S. C., Corley, B. M., Hall, R. L. and Webb, L. D., *"Triaxial Tensile Stress Evaluation of Propellant-to-Case Bond Integrity"*, Solid Propellant Rocket Conference, Palo Alto, Cal., 1964, pp 1-20.

68. Brown, H. R., *"Adhesion Between Polymers"*, IBM J. Res. Develop., Vol. 38, No. 4, July 1994, pp 379-389.

69. Buswell, H. J., *"An Investigation into Mechanical Properties of Composite Propellants"*, Ph D Thesis, March 1975, University of Surrey, England.

70. Christiansen, A. G., Layton, L. H. and Carpenter, R. L., *"HTPB Propellant Aging"*, J. Spacecraft, Vol. 18, No. 3, May-June 1981, pp 211-215.

71. Chu, Y. Z. and Durning, C. J., *"Application of the Blister Test to the Study of Polymer-Polymer Adhesion"*, Journal of Applied Polymer Science, Vol. 45, No. 7, 1992, pp 1151-1164.

72. Erlich, D. C. and Seaman, L., *"Biaxial Strain Deformation and Fracture of Polymers"*, Shock Compression of Condensed Matter (Proc), 7th, 1991, Williamsburg, Va., pp 567-570.

73. Francis, E. C. and Thompson, R. E., *"Nonlinear Structural Modelling of Solid Propellants"*, AIAA-84-1290, 20th Joint Propulsion Meeting, Cincinnati, Oh., 1984, pp 1-5.

74. Fraser, R. A. and Ward, I. M., *"Temperature Dependence of Craze Shape and Fracture in Polycarbonate"*, Polymer, Vol. 19, Feb. 1978, pp 220-224.

75. Guild, F. J. and Young, R. J., *"A Predictive Model for Particulate Filled Composite Materials"*, Part 2: Soft Particles, J Materials Science, Vol. 24, 1989, pp 2454-2460.

76. van Hartingsveldt, E. A. A. and van Aartsen, J. J., *"Strain-rate Dependence of Interfacial Adhesion in Particle-Reinforced Polymers"*, Polymer, Vol. 32, No. 8, 1991, pp 1482-1487.

77. Hashemi, S., Kinloch, A. J. and Williams, G., *"Mixed-Mode Fracture in Fiber-Polymer Composite Laminates"*, Composite Materials: Fatigue and Fracture (Third Volume), ASTM STP 1110, T. K. O'Brien, Ed., Philadelphia, 1991, pp 143-168.

78. Hine, P. J., Duckett, R. A. and Ward, I. M., *"A Study of the Fracture Behaviour of Polyethersulphone"*, Polymer, Vol. 22, Dec. 1981, pp 1745-1753.

79. Hobbs, S. Y. and Bopp, R. C., *"Fracture Toughness of Poly(Butylene Terephthalate)"*, Polymer, Vol. 21, May 1980, pp 559-563.

80. Husband, D. M., *"Use of Dynamic Mechanical Measurements to Determine the Aging Behaviour of Solid Propellant"*, Propellants, Explosives, Pyrotechnics, Vol. 17, 1992, pp 196-201.

81. Hutchinson, J. W., *"Fundamentals of the Phenomenological Theory of Nonlinear Fracture Mechanics"*, Trans. of the ASME, Vol. 50, Dec 1983, pp 1042-1051.

82. Inglis, C. E., *"Stresses in Plates due to the Presence of Cracks and Sharp Corners"*, Trans. Inst. Naval Architects, London, Vol. LV, 1913, pp 219-230.

83. Kelley, F. N., *"Solid Propellant Mechanical Properties Testing, Failure Criteria, and Aging"*, Propellants Manufacture, Hazards, and Testing, 153rd Meeting of the ACS, Miami Beach, Fl., Advances in Chemistry Series 88, 1967, pp 188-243.

84. Kim, K. R., An, J. H., Cho, K. W. and Park, C. E., *"Influence of Microstructure on Dynamic Mechanical Behaviour of Polymer Composites with Inclusions"*, J. Applied Polymer Sci., Vol. 47, 1993, pp 305-322.

85. Lee, W. G., Tsai, J. Y., Bai, G. C. and Chiu, H. S., *"The Environmental Effect on HTPB-AP Propellants Containing a Quaternary Ammonium Salt Modifier"*, Int. Annua. Conf., ICT Environ. Test, Vol. 20, 1989, pp 65/1-65/14.

86. Li, J. X., Silverstein, M., Hiltner, A. and Baer, E., *"The Ductile-to-Quasi-Brittle Transition of Particulate-Filled Thermoplastic Polyester"*, J. Applied Polymer Science, Vol. 52, 1994, pp 255-267.

87. Liechti, K. M. and Liang, Y.-M., *"The Influence of Specimen Geometry on Interfacial Fracture Resistance Measurements"*, AMD-Vol. 130, Experiments in Micromechanics of Failure Resistant Materials, ASME, 1991, pp 1-8.

88. Liqing S., Aklonis, J. J. and Salovey, R., *"Model Filled Polymers. XIV: Effect of Modifications of Filler Composition on Rheology"*, Polymer Engineerin and Science, Vol. 33, No. 20, Oct. 1993, pp 1308-1319.

89. Liu, C. T., *"Numerical Modelling of Crack-Defect Interaction"*, J. Propulsion, Vol. 7, No. 4, August 1991, pp 526-530.

90. Lockett, F. J., Nonlinear Viscoelastic Solids, Academic Press, 1991, London.

91. Mattson, B, Stenberg, B., Gillen, K. T., Clough, R. L. and Östman, E., *"Novel Techniques used to Assess the Ageing of Carbon-Black-Filled Materials"*, Polymer Degradation and Stability, Vol. 41, 1993, pp 211-221.

92. Orowan, E., Fracture and Strength of Solids

93. Parvin, M. and Williams, J. G., *"The effect of Temperature on the Fracture of Polycarbonate"*, J. Mat. Sci., Vol. 10, 1975, pp 1883-1888.

94. Peng, S. T. J., *"Constitutive Equations of Ageing Polymeric Materials"*, J. Materials Science, Vol. 20, 1985, pp 1920-1928.

95. Pitman, G. L. and Ward, I. M., *"Effect of Molecular Weight on Craze Shape and Fracture Toughness in Polycarbonate"*, Polymer, Vol. 20, July 1979, pp 895-902.

96. Sperling, L. H., Klein, A., Sambasivam, M. and Kim, K. D., *"Molecular Basis of Healing and Fracture at Polymer Interfaces"*, Polymers for Advanced Technology, Vol. 5, 1993, pp 453-472.

97. Vollenberg, P. H. T., *"Mechanical Behaviour of Particle Filled Thermoplastics"*, Ph D Thesis, Sep 1987, Technische Hogeschool Eindhoven, Netherlands.

98. Woo, C. W. and Wang, Y. H., *"Analysis of an Edge Crack in a Finite Bi-Material Plate"*, Engineering Fracture Mechanics, Vol. 42, No. 2, 1992, pp 289-297.

99. Xiao, F., Hui, C.-Y. and Kramer, E. J., *"Analysis of a Mixed Mode Fracture Specimen: the Asymmetric Double Cantilever Beam"*, Journal of Materials Science, Vol. 28, 1993, pp. 5620-5629.

100. Yamada, E., Inagaki, S., Okamoto, H. and Furukawa, J., *"Rupture of Filler-Loaded Rubber Vulcanizate"*, J. Applied Polymer Sci.: Applied Polymer Symposium, Vol. 50, 1992, pp 295-307.

101. Yang, A. C.-M., *"Filler-induce Softening Effect in Thermally Aged Polydimethylsiloxane Elastomers"*, Polymer, Vol. 35, No. 15, 1994, pp 3206-3211.

102. Zhang, H. and Berglund, L. A., *"Deformation and Fracture of Glass Bead/CTBN-Rubber/Expoy Composites"*, Polymer Engineering and Science, Vol. 33, No. 2, Jan. 1993, pp 100-107.

103. Zhuk, A. V., Knunyants, N. N., Oshmyan, V. G., Topolkaraev, V. A. and Berlin, A. A., *"Debonding Microprocesses and Interfacial Strength in Particle-Filled Polymer Materials"*, J. Materials Science, Vol. 28, 1993, pp 4595-4606.

List of Publications

1. Ho, S Y., Ide, K. and MacDowell, P., *"Instrumented Service Life Program for the PICTOR Rocket Motor"*, (Proc) NATO/AGARD Propulsion and Energetics Panel, 87th Symposium on Service Life of Solid Propulsion Systems, Athens, Greece, May 1996.

2. Ide, K. M. and Ho, S Y., *"Poisson's Ratio of Elastomers for Thermal Strain Modelling in Rocket Motors"*, The Technical Cooperation Panel, WTP-4, Presented to the 21st Panel meeting, Australia, 1996.

3. Ide, K. M., Ho, S Y. and Williams, D. R. G., *"The Measurement of Poisson's Ratio in Elastomers from an Image Analysis Technique"*, (Proc) First Australasian Congress on Applied Mechanics, Melbourne, Australia, 21-23 February 1996.